Decomposition of Volatile Organic Compounds using Non-Thermal Plasmas

Usman Hassan Dahiru

A thesis presented for the degree of

Doctor of Philosophy

School of Engineering,

Newcastle University, United Kingdom

May 2023

Abstract

Volatile organic compounds (VOCs) are among the most common anthropogenic air pollutants. They have been linked to various human diseases, including cancer, cardiovascular disease, lung, and respiratory diseases. As a result, reducing VOC emissions has become a significant concern and a significant research area worldwide. Non-thermal plasmas (NTPs) are an attractive technique for removing VOC emissions from ambient air. This research concerned the use of a non-thermal plasma dielectric barrier discharge (DBD) method to remove various volatile organic compound emissions from ambient air. The model VOC compounds chosen were hexane, cyclohexane, benzene, and methanol. The principal aim of this research was to improve the performance of a non-thermal plasma DBD reactor on the removal efficiency of VOCs at ambient temperature and atmospheric pressure. The effects of key process parameters such as carrier gases (nitrogen, dry and humidified air), plasma power, oxygen concentrations, residence time and inlet concentration on the removal efficiency, product selectivity and elimination of unwanted by-products were investigated. These investigations showed that the removal efficiencies of the VOCs generally increased with increasing plasma power and residence time, regardless of the carrier gas used. The maximum removal efficiencies of the three 6-carbon hydrocarbons used, hexane (94.4%), cyclohexane (98.2%) and benzene (93.7%), were achieved in humidified air plasma. In contrast, the 96.7% maximum methanol removal efficiency was obtained in dry air plasma. However, the removal efficiency of VOCs decreased with increasing inlet concentration due to the increased number of VOC molecules flowing into the plasma reactor at constant discharge length, plasma power and residence time. It was found that increasing O_2 concentration from 0 to 21% increased the removal efficiency and selectivity to CO_2 due to the increase in the generation of oxygen radicals. The decomposition products were CO_2, CO, H_2, and lower hydrocarbons (C_1-C_5), depending on the model VOC and the carrier gas used. O_3 concentrations were below 10 ppm in dry air plasma for all the studied VOCs, and NO_X was not detected in any carrier gas. To some extent, the hexane, cyclohexane, and benzene decomposed into solid residue due to the oligomerisation of hydrocarbon radicals produced in the DBD plasma system in pure nitrogen and dry air plasma, which would cause arcing and blockage problems after prolonged operation. The effect of water vapour was investigated to determine whether it would reduce the formation of these solid residues in the DBD reactor. Water at RH= 25% (hexane and cyclohexane) and 35% (benzene) significantly increased the removal efficiency and the CO_2 selectivity while eliminating the solid residue and NO_X in the NTP-decomposition of VOCs, probably via the formation of potent OH radicals. Humidification generally improved the removal efficiency and increased the yield of H_2 and

CO_2 selectivity. These results imply that the decomposition of VOCs by non-thermal plasma DBDs is dominated by the effect of OH and O radicals. The addition of water to the decomposition process suppressed O_3 formation and reduced selectivity to CO in all tested conditions. Therefore, the performance of DBD plasmas in removing hexane, cyclohexane, benzene, and perhaps other VOCs would improve when operating in humid conditions or when the inlet gas stream is humidified. In addition, the technique of eliminating solid residue by the addition of water vapour provides a simple solution to a problem that is limiting the application of DBD systems of VOC removal and similar applications.

Dedication

This thesis is dedicated to my parents' endless support, love, and encouragement.

Acknowledgement

My heartfelt gratitude goes to my supervisor, Prof. Adam Harvey, for his supervision, guidance, help, encouragement, friendship, understanding and support throughout my PhD research, without which none would have been possible.

I want to thank my co-supervisor, Dr. Kui Zhang, for his sound advice and insightful discussion throughout my research project. His expertise in plasma processes was invaluable in guiding this research project on the right path. I appreciate his help with the lab equipment, which was unfamiliar. Many thanks to my third supervisor, Dr. Faisal Saleem, for his assistance and support throughout this project. This task would not have been accomplished without his help.

I would also like to thank the Process Intensification Group (PIG) members for their friendship throughout my PhD.

A special thanks must go to my parents, Alhaji Dahiru Hassan Tela and Hajiya Aishatu Dahiru, my brothers (Arch. Aminu, Engr Dr Buhari, Muslim and Salim), my sisters (Maimuna, Rashida, Rayyanatu, Lawiza and Zakiyya), my lovely wife (Fatima), and my son (Muhammad Shaheed), for their love, support, and encouragement, enabled me to complete this work.

Finally, I would like to thank the Petroleum Technology Development Fund (PTDF-Nigeria) and Raw Materials Research Development Council (RMRDC), Federal Ministry of Science and Technology, Abuja, Nigeria, for their financial and technical assistance throughout this research.

List of publications

Published work

1. Usman H. Dahiru, Faisal Saleem, Kui Zhang, Adam Harvey, Removal of cyclohexane as a toxic pollutant from the air using a non-thermal plasma: Influence of different parameters. Journal of Environmental Chemical Engineering. 2021; 9(1) 105023.
2. Usman H. Dahiru, Faisal Saleem, Kui Zhang, and Adam Harvey, Plasma-assisted removal of methanol in N_2, dry and humidified air using a dielectric barrier discharge (DBD) reactor (*RSC Advances*, 2022, 12, 10997 - 11007).
3. Usman H. Dahiru, Faisal Saleem, Farah Talib Al-sudani, Kui Zhang, and Adam Harvey, Decomposition of benzene vapour using non-thermal plasmas: The effect of moisture content on eliminating solid residue. Journal of Environmental Chemical Engineering. 10 (2022) 107767.
4. Usman H. Dahiru, Faisal Saleem, Farah Talib Al-sudani, Kui Zhang, and Adam Harvey, Oxidative removal of hexane from the gas stream by dielectric barrier discharge reactor and effect of gas environment. Chemical Engineering and Processing- Process Intensification. 178 (2022) 109035.

Other publication co-authored during PhD candidature

1. F. Saleem, J. Kennedy, U.H. Dahiru, K. Zhang, A. Harvey, Methane conversion to H_2 and higher hydrocarbons using non-thermal plasma dielectric barrier discharge reactor, Chemical Engineering and Processing-Process Intensification (2019) 107557.

List of conferences

1. "Plasma-assisted decomposition of Cyclohexane in a Dielectric Barrier Discharge Reactor" International Conference on Air Quality and Environmental Health (ICAQEH) London, United Kingdom (22-24th April 2021).
2. "Low-temperature conversion of methanol to higher hydrocarbons using non-thermal plasmas", 17th International Conference on Environmental Science & Technology in Athens, Greece (1-4th September 2021).
3. Results of this work were presented at the School of Engineering Conference in 2018, 2019 and 2020.

Award

1. "Third best prize award in Postgraduate Chemical Engineering Conference 2018".

Table of contents

Abstract i
Dedication iii
Acknowledgement iv
List of publications v
Published work v
Other publication co-authored during PhD candidature v
List of conferences vi
Award vi
Table of contents vii
List of figures x
List of tables xvii
Nomenclature xviii
Abbreviations xix
Chapter 1. Introduction 1
1.1 Volatile organic compounds 1
1.2 Non-thermal Plasmas 3
1.3 Aims and objectives 4
1.4 Thesis structure 4
Chapter 2. Literature review 6
2.1 VOC emissions and their control technologies 6
2.2 VOC treatment technologies 7
2.3 Plasma 11
2.4 Elementary processes in NTPs 13
2.5 Conventional NTP reactors 15
2.5.1 Microwave Plasmas 15
2.5.2 Electron beam plasmas 16
2.5.3 Gliding arc discharge 17
2.5.4 Corona Discharge 18
2.5.5 Dielectric barrier discharge plasma reactor 19
2.6 Fundamental parameters of DBD reactors and their influence on VOC decomposition 22
2.6.1 Dielectric materials for DBD reactor 23
2.6.2 Electrode material 25
2.6.3 Discharge length 25

2.6.4 Discharge gap 26
2.7 Non-thermal plasmas (NTPs) for decomposition of VOCs 27
2.7.1 Hexane 28
2.7.2 Cyclohexane 30
2.7.3 Benzene 31
2.7.4 Methanol 34
2.8 Summary 35
Chapter 3. Materials and methods 39
3.1 Materials and methods 39
3.2 Experimental setup 40
3.3 GC calibration and product analysis 42
3.4 Ozone measurement 44
3.5 Experimental variables 45
3.6 Experimental procedure 46
3.7 Definitions 48
Chapter 4. Oxidative removal of hexane from the gas stream in a dielectric barrier discharge reactor 50
4.1 Introduction 50
4.2 Results and discussion 50
4.2.1 Effect of power and carrier gases 50
4.2.2 Effect of plasma power on DBD reactor wall and downstream gas temperature 54
4.2.3 Hexane decomposition pathways in a DBD plasma system 55
4.2.4 Ozone and NOx formation 57
4.2.5 Effect of oxygen concentration 59
4.2.6 Solid and liquid residues in the DBD reactor 62
4.2.7 Reaction kinetics of hexane decomposition using NTP-plasma 64
4.3 Summary 66
Chapter 5. Removal of cyclohexane as a toxic pollutant from air using a non-thermal plasma: Influence of different parameters 67
5.1 Introduction 67
5.2 Results and discussion 67
5.2.1 Effect of SIE and carrier gas 67
5.2.2 Effect of concentration 72
5.2.3 Effect of residence time 74
5.2.4 Mechanisms of cyclohexane decomposition 77

5.3 Cyclohexane by-products 81
5.3.1 Solid deposit 81
5.3.2 Ozone and NOx formation 82
5.3.3 A semi-empirical model of cyclohexane decomposition 84
5.4 Summary 85
Chapter 6. Decomposition of benzene vapour using non-thermal plasmas: effect of moisture content on eliminating solid residue 87
6.1 Introduction 87
6.2 Results and discussion 87
6.2.1 Effect of power and carrier gases 87
6.2.2 Effect of water vapour 91
6.2.3 Ozone and NOx formation in the DBD reactor 94
6.2.4 Solid residue formation in the dielectric barrier discharge reactor 96
6.2.5 Benzene decomposition pathways in a DBD plasma system 99
6.3 Comparative decomposition of hexane, cyclohexane, and benzene in different carrier gases: understanding the effects of chemical structure 101
6.4 Summary 104
Chapter 7. Plasma-assisted removal of methanol in N_2, dry and humidified air using a dielectric barrier discharge (DBD) reactor 106
7.1 Introduction 106
7.2 Results and Discussion 106
7.2.1 Effect of carrier gases and power 106
7.2.2 Effect of CH_3OH concentration 113
7.2.3 Effect of residence time 116
7.2.4 Mechanisms of methanol decomposition using NTP-plasma 120
7.2.5 Ozone and NOx formation 123
7.3 Summary 125
7.4 Analysis of the overall performance of the DBD reactor 126
Chapter 8. Conclusions and recommendations 131
8.1 Conclusions 131
8.2 Future work 135
8.2.1 Advanced plasma diagnosis of VOC decomposition process 135
8.2.2 Kinetic simulations and scale-up investigation of VOCs decomposition using NTP reactors 135
References 136
Appendices 153

List of figures

Figure 1.1 The NMVOC emissions in the UK: 1970-2020. Reproduced from the Department for Environment Food and Rural Affairs (DEFRA, 2022). 2

Figure 2.1 Classification of VOC removal technologies. 8

Figure 2.2 Examples of naturally produced plasmas (a) lightning, (b) aurora borealis, (c) solar wind, and (d) solar corona. 11

Figure 2.3 An overview of the typical timescale of events in the NTP generation process (Kim, 2004). 14

Figure 2.4 Schematic of a microwave plasma reactor (Urashima *et al.*, 2000). 16

Figure 2.5 Schematic of an electron beam plasma reactor. 16

Figure 2.6 Schematic of the gliding arc discharge plasma reactor (Mutaf-Yardimci *et al.*, 2000). 17

Figure 2.7 Typical configuration of corona discharge (Chen *et al.*, 2014). 18

Figure 2.8 Schematics of basic NTP DBD reactors (Vandenbroucke *et al.*, 2011). 20

Figure 2.9 The first DBD ozone generator of W. Siemens, 1857 (Siemens, 1857). 22

Figure 2.10 Schematic diagram of DBD reactor. 23

Figure 3.1 A schematic of the experimental setup. 40

Figure 3.2 Section of DBD plasma reactor. 41

Figure 3.3. The DBD plasma reactor in a laboratory setup. 42

Figure 3.4 Setup for temperature measurement. 43

Figure 3.5 Schematic setup of the ozone measurement. 44

Figure 4.1 Effect of power and carrier gases on the removal efficiency of hexane (Reaction conditions: temperature = ambient; Inlet concentration of hexane = 350 ppm; Total flow rate = 100 ml/min; Residence time = 2.3 s; SIE = 1.2 – 6 kJ/L). 51

Figure 4.2 Effect of power and carrier gases on energy yield of hexane decomposition (Reaction conditions: Temperature = ambient; inlet concentration of hexane = 350 ppm; Total flow rate = 100 ml/min; Residence time = 2.3 s; SIE = 1.2 – 6 kJ/L). 52

Figure 4.3 Effect of power and carrier gases on selectivity to C_1-C_5 (Reaction conditions: Temperature = ambient; inlet concentration of hexane = 350 ppm; Total flow rate = 100 ml/min; Residence time = 2.3 s; SIE = 1.2 – 6 kJ/L). 52

Figure 4.4 Effect of power and carrier gases (a) on selectivity to CO_2 (b) on selectivity to CO (Reaction conditions: Temperature = ambient; Concentration = 350 ppm; Total flow rate = 100 ml/min; Residence time = 2.3 s; SIE = 1.2 – 6 kJ/L). 54

Figure 4.5 Effect of plasma power on DBD reactor wall and downstream gas temperature (Conditions: Total flow rate = 100 ml/min, Power = 2-10 W, Concentration = 350 ppm)..... 55

Figure 4.6 Ozone formation as function of input power (Reaction conditions: Temperature = ambient; Inlet concentration of hexane = 350 ppm; Total flow rate = 100 ml/min; Residence time = 2.3 s; SIE = 1.2 – 6 kJ/L; Carrier gas = dry air). 58

Figure 4.7 Effect of oxygen concentration on removal efficiency of hexane (Reaction conditions: Temperature = ambient; power = 6 W; Inlet concentration of hexane = 350 ppm; Total flow rate = 100 ml/min; Residence time = 2.3 s; SIE = 3.6 kJ/L). 59

Figure 4.8 Effect of oxygen concentration on CO_2 and CO selectivity (Reaction conditions: Temperature = ambient; Power = 6 W; Total flow rate = 100 ml/min; Residence time = 2.3 s; SIE = 3.6 kJ/L). 61

Figure 4.9 Effect of oxygen concentration on selectivity to C_1-C_5 (Reaction conditions: Temperature = ambient; Power = 6 W; Total flow rate = 100 ml/min; Residence time = 2.3 s; SIE = 3.6 kJ/L). 62

Figure 4.10 Dielectric barrier discharge reactors after hexane decomposition in (a) Nitrogen carrier gas (b) Dry air carrier gas, (c) Humidified air carrier gas. 63

Figure 4.11 Effect of SIE on the remaining fraction of hexane in different carrier gases (Reaction conditions: Temperature = ambient; Inlet concentration of hexane = 350 ppm; Total flow rate = 100 ml/min; Residence time = 2.3 s; Power = 2 – 10 W). 65

Figure 5.1 Effect of SIE on the removal efficiency of cyclohexane in nitrogen, dry and humidified air carrier gas (Reaction conditions: Temperature = ambient; Concentration = 220 ppm; Total flow rate = 100 ml/min; Residence time = 2.3 s). 68

Figure 5.2 Effect of SIE on energy yield of cyclohexane in nitrogen, dry and humidified air carrier gas (Reaction conditions: Temperature = ambient; Concentration = 220 ppm; Total flow rate = 100 ml/min; residence time = 2.3 s). 69

Figure 5.3 Effect of SIE on selectivity to LHC in nitrogen, dry and humidified air carrier gas (Reaction conditions: Temperature = ambient; Concentration = 220 ppm; Total flow rate = 100 ml/min; Residence time = 2.3 s). 70

Figure 5.4 Effect of SIE on yield of H_2 in nitrogen, dry and humidified air carrier gas (Reaction conditions: Temperature = ambient; Concentration = 220 ppm; Total flow rate = 100 ml/min; Residence time = 2.3 s). 70

Figure 5.5 Effect of SIE on selectivity to CO and CO_2 in dry and humidified air carrier gas (Reaction conditions: Temperature = ambient; Concentration = 220 ppm; Total flow rate = 100 ml/min; Residence time = 2.3 s). 71

Figure 5.6 Effect of concentration on removal efficiency of cyclohexane in nitrogen, dry and humidified air carrier gas (Reaction conditions: Temperature = ambient; SIE = 2.4 kJ/L; Total flow rate = 100 ml/min; Residence time = 2.3 s). 72

Figure 5.7 Effect of concentration on selectivity to LHC in nitrogen, dry and humidified air carrier gas (Reaction conditions: Temperature = ambient; SIE = 2.4 kJ/L; Total flow rate = 100 ml/min; Residence time = 2.3 s). 73

Figure 5.8 Effect of concentration on yield of H_2 in nitrogen, dry and humidified air carrier gas (Reaction conditions: Temperature = ambient; SIE = 2.4 kJ/L; Total flow rate = 100 ml/min; Residence time = 2.3 s). 73

Figure 5.9 Effect of concentration on selectivity to CO and CO_2 in dry and humidified air carrier gas (Reaction conditions: Temperature = ambient; SIE = 2.4 kJ/L; Total flow rate = 100 ml/min; Residence time = 2.3 s). 74

Figure 5.10 Effect of residence time on removal efficiency of cyclohexane in nitrogen, dry and humidified air carrier gas (Reaction conditions: Temperature = ambient; Concentration = 220 ppm; Flow rate = 100 -190 ml/min; Power = 4 W). 75

Figure 5.11 Effect of residence time on selectivity to LHC in nitrogen, dry and humidified air carrier gas (Reaction conditions: Temperature = ambient; Concentration = 220 ppm; Flow rate = 100 -190 ml/min; Power = 4 W). 76

Figure 5.12 Effect of residence time on the yield of H_2 in nitrogen, dry and humidified air carrier gas (Reaction conditions: Temperature = ambient; Concentration = 220 ppm; Flow rate = 100 -190 ml/min; Power = 4 W). 76

Figure 5.13 Effect of residence time on selectivity to CO_2 and CO in dry and humidified air carrier gas (Reaction conditions: Temperature = ambient; Concentration = 220 ppm; Flow rate = 100 -190 ml/min; Power = 4 W). 77

Figure 5.14 Proposed cyclohexane decomposition reaction route. 79

Figure 5.15 DBD reactors after cyclohexane decomposition in (a) nitrogen, (b) dry air and (c) humidified air. 81

Figure 5.16 Ozone concentration as function of SIE (Reaction conditions: Temperature = ambient; Concentration = 220 ppm; Total flow rate = 100 ml/min; Residence time = 2.3 s; Carrier gas = dry air). 83

Figure 5.17 Effect of residence time on the remaining fraction of cyclohexane in nitrogen, dry and humidified air (Reaction conditions: Temperature = ambient, power = 4 W, Concentration = 220 ppm, Flow rate = 100 – 190 ml/min). 85

Figure 6.1 Effect of power on the removal efficiency of benzene (Reaction conditions: Temperature = ambient; Concentration = 350 ppm; Total flow rate = 100 ml/min; Residence time = 2.3 s, Relative humidity = 25% at 20℃, SIE = 1.2 – 6 kJ/L). 87

Figure 6.2 Effect of power on energy yield of benzene decomposition (Reaction conditions: Temperature = ambient; Concentration = 350 ppm; Total flow rate = 100 ml/min; Residence time = 2.3 s, Relative humidity = 25% at 20℃, SIE = 1.2 – 6 kJ/L). 88

Figure 6.3 Effect of power on selectivity to (a) CO_2, and (b) CO, (Reaction conditions: Temperature = ambient; Concentration = 350 ppm; Total flow rate = 100 ml/min; Residence time = 2.3 s, Relative humidity = 25% at 20℃, SIE = 1.2 – 6 kJ/L). 89

Figure 6.4 Effect of power on selectivity to C_1-C_5 (Reaction conditions: Temperature = ambient; Concentration = 350 ppm; Total flow rate = 100 ml/min; Residence time = 2.3 s, Relative humidity = 25% at 20℃, SIE = 1.2 – 6 kJ/L). 90

Figure 6.5 Effect of relative humidity on the removal efficiency of benzene (Reaction conditions: Power = 10 W; Temperature = ambient, Concentration = 350 ppm; Total flow rate = 100 ml/min; Residence time = 2.3 s, SIE = 6 kJ/L). 91

Figure 6.6 Effect of relative humidity on selectivity to CO and CO_2 (Reaction conditions: Power = 10 W; Temperature = ambient, Concentration = 350 ppm; Total flow rate = 100 ml/min; Residence time = 2.3 s, SIE = 6 kJ/L). 92

Figure 6.7 Effect of relative humidity on selectivity to C_1-C_5 (Reaction conditions: Power = 10 W; Temperature = ambient, Concentration = 350 ppm; Total flow rate = 100 ml/min; Residence time = 2.3 s; SIE = 6 kJ/L). 93

Figure 6.8 Ozone concentration as a function of relative humidity (Reaction conditions: Power = 10 W; Temperature = ambient; SIE = 6 kJ/L)..... 95

Figure 6.9 Plasma DBD reactors after benzene decomposition in nitrogen, dry and humidified air carrier gases. (a) Nitrogen plasma, (b) Dry air plasma, (c) Humidified air plasma. 97

Figure 6.10 Effect of power and carrier gases on the removal efficiency of HCB (a) nitrogen, (b) dry air, and (c) humidified air (Reaction conditions: Temperature = ambient; Concentration = 350 ppm; Total flow rate = 100 ml/min; Residence time = 2.3 s, Relative humidity 25%). 102

Figure 7.1 Effect of power in different carrier gases as a function of removal efficiency of methanol (Reaction conditions: Temperature = ambient; Concentration = 260 ppm; Total flow rate = 70 ml/min; Residence time = 3.3 s, SIE = 1.7 – 8.6 kJ/L, Relative humidity = 24%, Error bars represent the standard deviation ± σ for 3 measurement results). 107

Figure 7.2 Effect of power and carrier gases on energy yield (Reaction conditions: Temperature = ambient; Concentration = 260 ppm; Total flow rate = 70 ml/min; Residence time = 3.3 s, SIE = 1.7 – 8.6 kJ/L, Relative humidity = 24%, Error bars represent the standard deviation ± σ for 3 measurement results). 108

Figure 7.3 Effect of power in different carrier gases as a function of selectivity to CO_2 (Reaction conditions: Temperature = ambient; Concentration = 260 ppm; Total flow rate = 70 ml/min; Residence time = 3.3 s, SIE = 1.7 – 8.6 kJ/L, Relative humidity = 24%, Error bars represent the standard deviation ± σ for 3 measurement results)..... 109

Figure 7.4 Effect of power in different carrier gases as a function of selectivity to CO (Reaction conditions: Temperature = ambient; Concentration = 260 ppm; Total flow rate = 70 ml/min; Residence time = 3.3 s, SIE =..... 109

Figure 7.5 Effect of power in different carrier gases as a function of selectivity to C_2-C_4 (Reaction conditions: Temperature = ambient; Concentration = 260 ppm; Total flow rate = 70 ml/min; Residence time = 3.3 s, SIE = 1.7 – 8.6 kJ/L, Relative humidity = 24%, Error bars represent the standard deviation ± σ for 3 measurement results). 110

Figure 7.6 Effect of power in different carrier gases as a function of selectivity to CH_4 (Reaction conditions: Temperature = ambient; Concentration = 260 ppm; Total flow rate = 70 ml/min;

Residence time = 3.3 s, SIE = 1.7 – 8.6 kJ/L, Relative humidity = 24%, Error bars represent the standard deviation ± σ for 3 measurement results). 110

Figure 7.7 Effect of carrier gases and power on yield of H_2 (Reaction conditions: Temperature = ambient; Concentration = 260 ppm; Total flow rate = 70 ml/min; Residence time = 3.3 s, SIE = 1.7 – 8.6 kJ/L, Relative humidity = 24%, Error bars represent the standard deviation ± σ for 3 measurement results). 111

Figure 7.8 Effect of concentration on removal efficiency of methanol in N_2, dry and humidified air (Reaction conditions: Temperature = ambient; Power = 6 W; Total flow rate = 70 ml/min; Residence time = 3.3 s, SIE = 5.1 kJ/L, Relative humidity = 24%, Error bars represent the standard deviation ± σ for 3 measurement results). 113

Figure 7.9 Effect of concentration on selectivity to CO_2 in N_2, dry and humidified air (Reaction conditions: Temperature = ambient; Power = 6 W; Total flow rate = 70 ml/min; Residence time = 3.3 s, SIE = 5.1 kJ/L, Relative humidity = 24%, Error bars represent the standard deviation ± σ for 3 measurement results). 114

Figure 7.10 Effect of concentration on selectivity to CO in N_2, dry and humidified air (Reaction conditions: Temperature = ambient; Power = 6 W; Total flow rate = 70 ml/min; Residence time = 3.3 s, SIE = 5.1 kJ/L, Relative humidity = 24%, Error bars represent the standard deviation ± σ for 3 measurement results). 114

Figure 7.11 Effect of concentration on selectivity to CH_4 in N_2, dry and humidified air (Reaction conditions: Temperature = ambient; Power = 6 W; Total flow rate = 70 ml/min; Residence time = 3.3 s, SIE = 5.1 kJ/L, Relative humidity = 24%, Relative humidity = 24%, Error bars represent the standard deviation ± σ for 3 measurement results). 115

Figure 7.12 Effect of concentration on selectivity to C_2-C_4 in N_2, dry and humidified air (Reaction conditions: Temperature = ambient; Power = 6 W; Total flow rate = 70 ml/min; Residence time = 3.3 s, SIE = 5.1 kJ/L, Relative humidity = 24%, Error bars represent the standard deviation ± σ for 3 measurement results). 115

Figure 7.13 Effect of concentration on yield of H_2 in N_2, dry and humidified air (Reaction conditions: Temperature = ambient; Power = 6 W; Total flow rate = 70 ml/min; Residence time = 3.3 s, SIE = 5.1 kJ/L, Relative humidity = 24%, Error bars represent the standard deviation ± σ for 3 measurement results). 116

Figure 7.14 Effect of residence time on the removal efficiency of methanol in N_2, dry and humidified air (Reaction conditions: Temperature = ambient; Concentration = 260 ppm; Flow

rate = 70 -160 ml/min; Power = 6 W, SIE = 2.3 - 5.1 kJ/L, Relative humidity = 24%, Error bars represent the standard deviation ± σ for 3 measurement results). 117

Figure 7.15 Effect of residence time on selectivity to CO_2 in N_2, dry and humidified air (Reaction conditions: Temperature = ambient; Concentration = 260 ppm; Flow rate = 70 -160 ml/min; Power = 6 W, SIE = 2.3 - 5.1 kJ/L, Relative humidity = 24%, Error bars represent the standard deviation ± σ for 3 measurement results). 118

Figure 7.16 Effect of residence time on selectivity to CO in N_2, dry and humidified air (Reaction conditions: Temperature = ambient; Concentration = 260 ppm; Flow rate = 70 -160 ml/min; Power = 6 W, SIE = 2.3 - 5.1 kJ/L, Relative humidity = 24%, Error bars represent the standard deviation ± σ for 3 measurement results). 118

Figure 7.17 Effect of residence time on selectivity to C_2-C_4 in N_2, dry and humidified air (Reaction conditions: Temperature = ambient; Concentration = 260 ppm; Flow rate = 70 -160 ml/min; Power = 6 W, SIE = 2.3 - 5.1 kJ/L, Relative humidity = 24%, Error bars represent the standard deviation ± σ for 3 measurement results). 119

Figure 7.18 Effect of residence time on selectivity to CH_4 in N_2, dry and humidified air (Reaction conditions: Temperature = ambient; Concentration = 260 ppm; Flow rate = 70 -160 ml/min; Power = 6 W, SIE = 2.3 - 5.1 kJ/L, Relative humidity = 24%, Error bars represent the standard deviation ± σ for 3 measurement results). 119

Figure 7.19 Effect of residence time on selectivity to C_2-C_4 in N_2, dry and humidified air (Reaction conditions: Temperature = ambient; Concentration = 260 ppm; Flow rate = 70 -160 ml/min; Power = 6 W, SIE = 2.3 - 5.1 kJ/L, Relative humidity = 24%, Error bars represent the standard deviation ± σ for 3 measurement results). 120

Figure 7.20 Decomposition pathways of methanol. 123

Figure 7.21 Ozone concentration as function of input power (Reaction conditions: Temperature = ambient; Concentration = 260 ppm; Total flow rate = 70 ml/min; Residence time = 3.3 s; SIE = 1.7 – 8.6 kJ/L; Carrier gas = dry and humidified air, Relative humidity = 24%, Error bars represent the standard deviation ± σ for 3 measurement results). 124

List of tables

Table 2.1 Common VOC emission sources and their health hazards (Liotta, 2010; Vandenbroucke *et al.*, 2011).....7

Table 2.2 Common conventional VOC treatment technologies.....10

Table 2.3 Comparison of thermal and non-thermal plasmas (Urashima *et al.*, 2000; Fridman *et al.*, 2004).....13

Table 2.4 An overview of NTP reactions induced by the energetic electrons (Eliasson *et al.*, 1991; Gaens *et al.*, 2013).....14

Table 2.5 Properties of dielectric barrier materials (Xiao *et al.*, 2014).....23

Table 2.6 Common VOCs decomposed by plasma DBD reactor (Li *et al.*, 2020).....28

Table 2.7 An overview of the previous work on VOCs decomposition with NTP.....37

Table 3.1 Materials and chemicals. 39

Table 3.2 List of equipment for the decomposition of VOC.....39

Table 4.1 Decomposition products identified by GC-MS in Nitrogen, dry and humidified air 64

Table 6.1 Overview of benzene removal efficiency and product selectivities. (Conditions: Total flow rate = 100 ml/min, Power = 10 W, Concentration = 350 ppm, SIE = 6 kJ/L, Relative humidity = 35% at 20℃). 94

Table 6.2 Decomposition products identified by GC-MS in dry and humidified air.....98

Table 6.3 Bond dissociation energy of hexane, cyclohexane, and benzene.....103

Table 6.4 Formation of solid residue in different carrier gases.....104

Table 7.1 Overall assessment of the performance of the developed DBD reactor compared with other conventional methods.....127

Table 7.2 Comparison of selected removal efficiency (RE) and energy yield (EY) for this study with previous studies. 129

Nomenclature

eV	Electron volt
T_h	Temperature of heavy specie
T_e	Temperature of electron (eV)
e^-	Electron
V_m	Molar volume of gas
Q	Gas flow rate (ml/min)
P	Power (W)
RE	Removal efficiency (%)
M	Molar mass (g/mole)
ml/min	Millilitre per minute
K_{SIE}	Energy constant (J/L)
n	Reaction order
$[VOC]_{in}$	Initial concentration of VOC
$[VOC]_{out}$	Final concentration of VOC

Abbreviations

CHN	Carbon, hydrogen and nitrogen
DBD	Dielectric barrier discharge
EB	Electron beam
FID	Flame ionisation detector
GAD	Gliding arc discharge
GC	Gas chromatograph
GC-MS	Gas chromatograph mass spectrometry
IARC	International agency for research on cancer
LHC	Lower hydrocarbons
NMVOC	Non-methane volatile organic compounds
NTP	Non-thermal plasma
PCD	Pulsed corona discharge
ppm	Parts per million
RH	Relative humidity
SIE	Specific input energy
TCD	Thermal conductivity detector
TCE	Trichloroethylene
UV	Ultraviolet
VOC	Volatile organic compound
WHO	World health organization

Chapter 1. Introduction

1.1 **Volatile organic compounds**

Volatile organic compounds (VOCs) are generally defined as carbon-based species with boiling points below 260 ℃ at atmospheric pressure. The World Health Organization (WHO) defines VOCs "as organic compounds with boiling points from 50 to 260 ℃ at atmospheric pressure" (WHO, 1989). Scientists have defined VOCs as hydrocarbon compounds that can vaporise and enter the earth`s atmosphere under normal atmospheric conditions (Derwent, 1995; Helmig *et al.*, 2009). Chemically, VOCs are organic compounds consisting of C, H atoms and other atoms (i.e., O, S, N, and halogens), which can be saturated or unsaturated, aromatics or non-aromatics. These compounds are often classified into methane and "non-methane volatile organic compounds" (NMVOC), including volatile and semi-volatile alkanes, cycloalkanes, alkenes, alcohols, aromatic compounds, aldehydes and ketones, as well as oxygenated/halogenated compounds (Jiang *et al.*, 2018). Alkanes and aromatic hydrocarbons constitute the highest percentage of VOCs in the atmosphere (Thevenet *et al.*, 2014).

The emission of VOCs from chemical processing plants, agricultural practices, transportation and consumer products has become a global problem that adversely affects the atmosphere and causes serious human health concerns (Einaga *et al.*, 2008; Liang *et al.*, 2021). According to the Department for Environment Food and Rural Affairs national statistics, NMVOC emissions have decreased by 67% since 1970 to 785,000 tonnes in 2020 in the UK, as shown in Figure 1.1 (DEFRA, 2022). The NMVOCs can pose adverse health and environmental effects. NMVOCs can react with other air pollutants in the presence of sunlight (via ultraviolet radiation) to produce ground-level ozone. Ozone endangers human health by causing inflammation and asthma but also causes oxidative damage to vegetation, including crops (DEFRA, 2022).

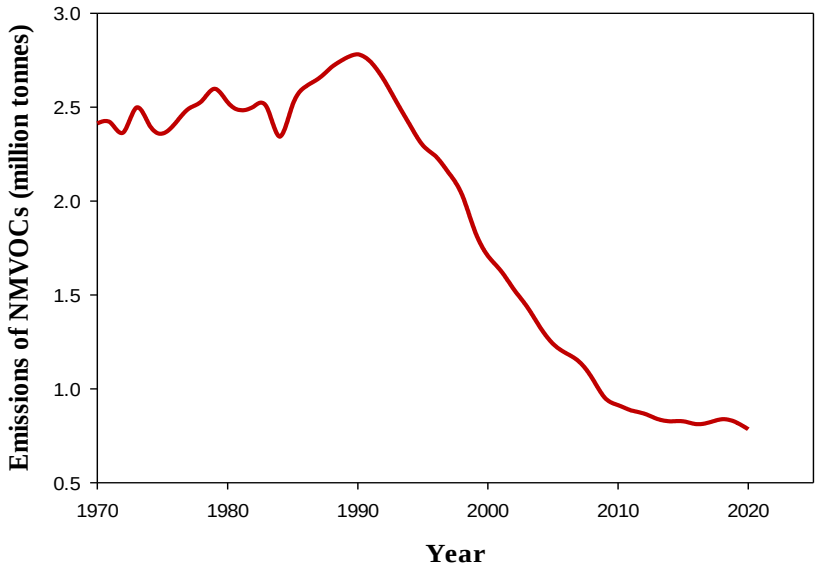

Figure 1.1 The NMVOC emissions in the UK: 1970-2020. Reproduced from the Department for Environment Food and Rural Affairs (DEFRA, 2022).

Climatic studies have revealed that VOCs are precursors to the formation of photochemical smog, organic aerosols, ground-level ozone, and global warming. According to the International Agency for Research on Cancer (IARC), excessive exposure to VOCs such as benzene in the air has increased the risk of developing cancer (IARC, 2017). For example, a link between leukaemia and benzene emission has been established (Hanna *et al.*, 2007). A clear relationship has also been demonstrated between VOC emissions and brain cancer (Boeglin *et al.*, 2006; Karatum *et al.*, 2016). Therefore, increasingly stringent environmental regulations worldwide enforce continuous monitoring and control of VOC emissions.

Currently, VOC remediation technologies, including thermal incineration, condensation, bio-filtration, catalytic and thermal oxidation, adsorption and absorption, are used for controlling VOC emissions (Hu *et al.*, 2015). These techniques have some limitations. For example, condensation has proven effective for treating high VOC concentrations but requires post-treatment and frequent maintenance (Uria-Tellaetxe *et al.*, 2016). Thermal oxidation has the drawback of generating toxic by-products (such as NOx) and requiring additional control equipment for halogenated compounds (Choi *et al.*, 2000). The treatment of biodegradable organic pollutants by bio-filtration and membrane separation has proven effective; however, it takes longer to control biological parameters (Steinberg *et al.*, 2005). Although adsorption is effective for low concentration VOCs, contaminant re-emission is possible (Tian *et al.*, 2016). Catalysts such as metal oxides containing Fe (Lu *et al.*, 2015), Cu (Zheng *et al.*, 2017), Mn (Vandenbroucke *et al.*, 2014), Ni (Liu *et al.*, 2017b) have been widely studied for the

decomposition of VOCs. It is regarded as one of the methods of mitigating secondary emissions (e.g., NOx). Although the addition of a catalyst significantly increases VOC removal, it remains a significant challenge to promote CO_2 selectivity and lower O_3 emission. Due to economic or technical restrictions, these conventional methods were unsuccessful/inefficient in decomposing low concentrations of VOCs from contaminated air streams. Therefore, it is essential to explore/develop an efficient, more economical, and environmentally friendly VOC treatment technology with high removal efficiency and low energy consumption for decomposition of dilute VOCs. A technology based on non-thermal plasma could be a good approach and is receiving significant interest in VOC decomposition because of the following advantages:

1. Operate at ambient temperature and atmospheric pressure
2. It can be combined with a variety of packing materials/catalysts
3. Rapid attainment of a steady-state (seconds to minutes), allowing for fast start-up and shutdown in practice (Thevenet *et al.*, 2014; Bogaerts *et al.*, 2018).

1.2 **Non-thermal Plasmas**

Non-thermal plasma (NTP) is an emerging technology gaining global attention for decomposing VOC emissions. NTPs activate molecules by applying an electric field to the gas molecules rather than with temperature (as in thermal plasmas). In an NTP, the electrons are accelerated by sufficiently strong electric fields. These energetic electrons collide with gas molecules to produce various species, including free radicals, excited atoms, UV photons and ions. The average electron temperature is typically in the range 10000 – 100000 K (corresponding to 1 -10 eV), which is significantly greater than that of the heavy species, which remain between 300 to 1000 K ($T_e \gg T_h$) (Yan *et al.*, 2002). Active species can react with VOC gas molecules and oxidise them into less toxic/more environmentally friendly compounds (Fridman, 2008).

Dielectric barrier discharge (DBD) technology is one of the most studied NTP techniques for removing VOCs among different NTP reactors. It has gained more attention than other methods for treating VOCs because it exhibits many advantages, including flexibility in terms of reactor design, moderate cost, work with mixtures of gases, operating close to room temperature and atmospheric pressure (Subrahmanyam *et al.*, 2006; Bogaerts *et al.*, 2018). In addition, it is easy to scale up for the industrial application, operating at low power, reproducible plasma conditions, and rapid attainment of a steady-state allows for fast start-up and shutdown in practice (Xiao *et al.*, 2014; Bogaerts *et al.*, 2018).

Plasma-only and plasma-catalytic techniques have been tested in the removal of several types of VOCs from a contaminated point source of ambient air streams. Overall, the main limiting factors from the previous studies of NTP decomposition of VOCs include the formation of harmful by-products such as ozone and NO_X (Shang *et al.*, 2020), low product selectivity, high energy consumption, high cost of catalysts, catalyst deactivation and disposal, and formation of solid residue in the DBD reactor due to the complex nature of VOCs as well as lack of control of products. Therefore, to overcome these shortcomings, there is an urgent need to develop an effective and promising VOCs decomposition technique at ambient temperature and atmospheric pressure.

1.3 **Aims and objectives**

The principal aim of this work is to explore and develop an efficient and environmentally friendly technique for the decomposition of main VOCs (i.e., alkanes, aromatics, and alcohols) using NTPs by investigating the effect of key process parameters.

The main objectives of this research are to:

1. Demonstrate the application of NTPs DBD reactor for decomposition of VOCs (using hexane and cyclohexane as a model compound of alkanes, benzene as a model compound of aromatics, and methanol as a model compound of alcohols) at ambient temperature and atmospheric pressure.
2. Investigate the effects of plasma power, carrier gas (nitrogen, dry and humidified air), specific input energy (SIE), oxygen concentrations, inlet concentration, residence time, and moisture content on the removal efficiency of hexane, cyclohexane, benzene, and methanol.
3. Eliminate/reduce the formation of solid residue and unwanted by-products (O_3 and NOx) in the NTP decomposition of hexane, cyclohexane, benzene, and methanol by optimising the reaction parameters.
4. Explore the NTPs VOC decomposition mechanism using different carrier gases and develop a semi-empirical model for removing VOCs from the gas stream at ambient temperature and atmospheric pressure.

1.4 **Thesis structure**

Chapter 2 presents an extensive background of this research.

Chapter 3 presents materials, chemicals, equipment, analytical methods, experimental setups, and the methodology employed in this research.

Chapter 4 presents the oxidative removal of hexane from the gas stream by the DBD reactor and the effect of the gas environment. The role of N_2, dry and humidified air carrier gases are evaluated in terms of removal efficiency, product selectivity and elimination of unwanted by-products. The effect of oxygen concentrations (0 – 21%) on the removal of hexane and product selectivity was also studied at constant plasma power and residence time in an N_2-O_2 mixture for further insight into oxygen's role.

Chapter 5 In this chapter, the removal of cyclohexane as a toxic pollutant from ambient air was investigated in a DBD reactor at ambient temperature and atmospheric pressure. The effects of SIE, carrier gases (nitrogen, dry and humidified air), residence time, and inlet concentration on the removal of cyclohexane, product selectivity and elimination of solid residue in the DBD reactor are evaluated.

Chapter 6 reports an investigation on the decomposition of benzene vapour using NTPs: the effect of moisture content on eliminating solid residue. The effects of plasma power, carrier gases and moisture content on the removal of benzene vapour in a DBD plasma reactor are presented.

Chapter 7 presents the plasma-assisted removal of methanol in N_2, dry and humidified air using a DBD reactor.

Chapter 8: In this chapter, a general summary of this research and results obtained in this work are explained, as well as future work.

Chapter 2. Literature review

This chapter presents an extensive literature research/review into the general definition of VOCs, sources of VOC emissions, and conventional VOC removal/control technologies. The concept of plasma as an emerging technology gaining attention in VOC removal is presented. The significance of this chapter is to review the previous work on the NTP decomposition of VOCs and identify the missing gap in this research area.

2.1 **VOC emissions and their control technologies**

A large number of VOCs are released into the atmosphere from various sources. The most common anthropogenic sources of VOCs include emissions from chemical industries, waste treatment techniques, motor vehicle exhausts, consumer products, household decorative materials etc. (Liotta, 2010). In contrast, biogenic sources include emissions from plants, trees, animals, and natural forest fires (Schiavon *et al.*, 2017). VOCs can react with nitrogen oxides in humidity, sunlight, and low wind to generate ground-level ozone R (2.1) (Wei *et al.*, 2011; Bouchaala, 2012). Several studies have shown a correlation between VOC emissions and the appearance of major environmental problems, such as photochemical smog, secondary aerosols, and ground-level ozone.

$$\mathrm{VOCs} + \mathrm{NO_X} + \mathrm{Sunlight} \rightarrow \mathrm{O_3} + \mathrm{NO_X} + \text{other products} \qquad \text{R (2.1)}$$

Moreover, epidemiologic research has shown that long-term exposure to a VOC-containing atmosphere can cause severe health problems (Liotta, 2010). Table 2.1 lists an overview of common VOC emission sources and their health hazards (Liotta, 2010; Vandenbroucke *et al.*, 2011), and Table 2.6 presents some VOCs decomposed by plasma DBD reactor (Li *et al.*, 2020), as shown in 2.7.

It is impossible to control biogenic sources of VOC emissions, and researchers are focusing their efforts on reducing pollution caused by anthropogenic sources. In order to limit VOC emissions, relevant laws are becoming more stringent. For example, The Gothenburg Protocol (2012) mandates a 50% reduction in maximum VOC emissions in EU member countries by 2020, compared to the baseline year of 2000 (Liotta, 2010).

Table 2.1 Common VOC emission sources and their health hazards (Liotta, 2010; Vandenbroucke *et al.*, 2011).

VOC	Source	Health hazards
Acetaldehyde	Pharmaceutical and petroleum products	Bronchitis, diarrhoea, headache
Acetone	Chemical industries	Carcinogen
Aniline	Leather processing	Kidney and liver diseases
Benzene	Vehicle exhaust gases, combustion	Carcinogen
Cyclohexane	Chemical industries, jet fuel	Nervous system impairment
Formaldehyde	Chemical industries	Carcinogen
Toluene	Paint industries, chemical plants	Nausea, muscle weakness
Xylene	Chemical industries, paint industries	Paralysis of the nerve system
Phenol	Combustion processes	Respiratory diseases
Chlorobenzene	Pharmaceutical and paint industries	Paralysis of the nervous system

Therefore, the removal of VOCs from air streams is critical for air pollution control, since VOCs are one of the most severe environmental issues affecting our quality of life. Process improvements, exhaust treatments, or a combination of both are the most common ways to reduce VOC emissions.

2.2 **VOC treatment technologies**

VOCs are typically removed from gas streams using add-on control technology, namely destruction and recovery processes, as indicated in Figure 2.1 (Khan *et al.*, 2000). Destruction techniques include various oxidation methods such as biofiltration, catalytic oxidation, thermal oxidation, and plasma technology to decompose VOCs (Khan *et al.*, 2000). Recovery techniques include condensation, membrane separation, absorption, and adsorption to remove VOCs from the gas stream (Khan *et al.*, 2000).

Bio-filtration is a cost-effective approach for removing VOCs at high airflows (100 – 100,000 m^3/hr) and low concentrations (< 1000 ppm). The technique has been widely used in removing odorous VOCs (Devinny *et al.*, 1999). The method generally uses micro-organisms (e.g., bacteria) to decompose VOCs to H_2O, CO_2, biomass, and other by-products. The VOC is passed through a porous medium consisting of compost or soil that supports the population of the microbes. In the process, VOCs are initially absorbed from the air feed to the biofilm of the medium. Once absorbed, the bacteria decompose them into CO_2, H_2O, biomass and inorganic by-products (Deshusses *et al.*, 2000).

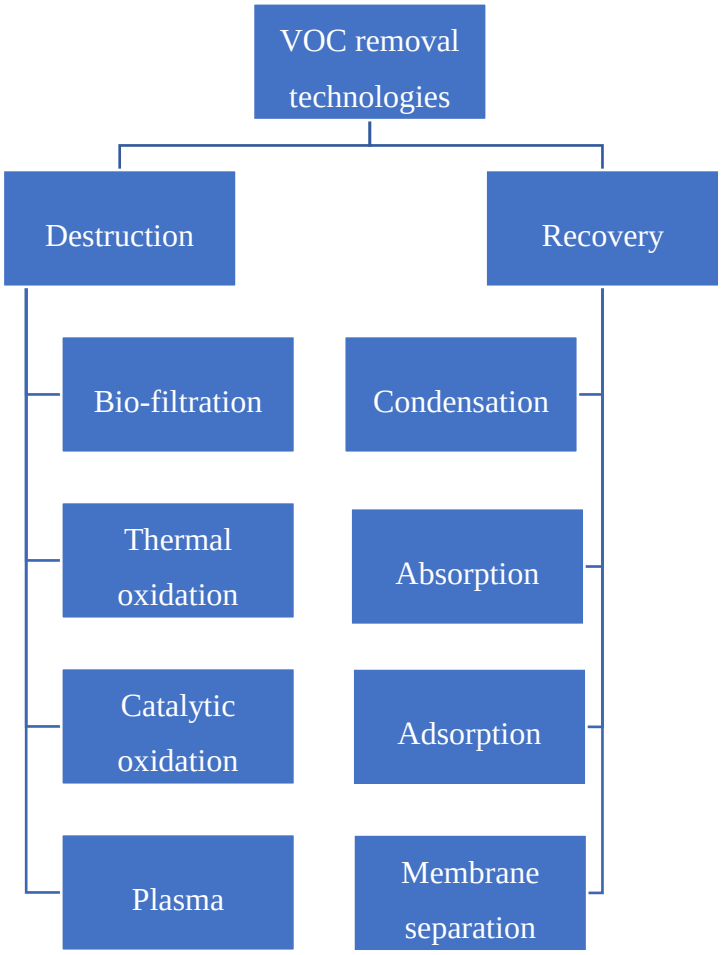

Figure 2.1 Classification of VOC removal technologies.

Previous researchers reported about 99% removal efficiency of toluene was achieved using bio-filters (Deshusses *et al.*, 2000).

Thermal oxidation is a fume incineration technique that typically achieves 95 to 99% removal of 100 to 2,000 ppm VOC concentrations at residence times between 0.5 and 1.0 s. The method can be used in treating all types of VOC emissions. The thermal oxidation system can treat a gas stream at the flow rate of 1,000 to 500,000 cubic feet per minute. The system typically combusts VOCs at temperatures of 704 to 815 ^{0}C, but the specific operating temperature depends on the nature and concentration of the VOC in the gas stream. VOCs at low initial concentrations will require higher heat input and longer residence times to achieve the desired removal efficiency (Parmar *et al.*, 2008).

Catalytic oxidation has been proved to improve the removal efficiency of VOCs at moderate temperatures to address the energy-intensive aspect of the thermal oxidation process (Khan *et al.*, 2000). It involves the incorporation of a catalyst into a thermal oxidation technique to facilitate the oxidation process through the adsorption and reaction of the oxygen molecule and VOCs on the catalyst's surface. The addition of the catalyst in this method can decrease the

reaction temperature to about 320 to 540 ^{0}C. In this technique, various catalysts (binary oxides, supported noble metals, solid solutions of metal oxides, and doped metal oxides) have been developed and used in the treatment of VOCs. Metal oxides are the most common catalyst used in this process. However, catalytic oxidation reactors can treat VOCs with concentrations in the range of 100 to 2000 ppm. This technique is applicable to VOCs with low concentrations. Removal efficiencies of 90 to 95% have been reported in previous work (Ruddy *et al.*, 1993). The main drawback of catalytic oxidation is catalyst deactivation caused by toxic components (halogens and sulphur) in the ambient air stream, including maintenance costs and costs associated with catalyst replacement (Khan *et al.*, 2000).

The condensation method is the most widely used technique for treating highly concentrated VOCs (i.e., > 5,000 ppm). The technique employs a drop in temperature or increase in pressure to cause the VOC in the exhaust stream to condense. In addition, the cleaned air stream is separated from the condensate containing pollutants. However, VOCs with low boiling points can require extensive cooling or pressurization, which is not economical (Khan *et al.*, 2000), and the method is only practical for "high" concentrations. In contrast, many problematic levels of emission are much lower than this.

Absorption is a method of removing VOCs from gas streams by contacting the air pollutant with a liquid medium. The soluble VOCs transfer to the liquid phase. The air stream is effectively scrubbed. This process occurs in an absorber tower designed to provide the liquid vapour contact area required for mass transfer. The liquid and vapour residence times typically range from 1-10 s. Absorption can accomplish 95 to 98% removal efficiency of VOCs (William *et al.*, 1997). In addition, the technique can treat 500 to 5,000 ppm VOC concentrations. Due to start-up time constraints, absorption is unsuitable for cyclic operation. It is, however, suitable for a high humidity stream with a relative humidity of more than 50% (Khan *et al.*, 2000).

VOCs flowing through a solid particle bed are captured by physisorption (rather than chemisorption, with true chemical bonds). The adsorption is employed to remove VOCs from low to medium concentrations, e.g., VOC concentrations of less than 300 ppm gas streams. The adsorptive capacity of the solid tends to increase with VOC concentration, molecular weight and boiling point (Khan *et al.*, 2000). Table 2.2 provides a summary of typical VOC treatment technologies along with their removal efficiencies.

Table 2.2 Common conventional VOC treatment technologies.

Treatment method	Removal efficiency (%)	Comments	References
Biofiltration	60-95	• It necessitates a lower initial investment, produces less non-harmful secondary waste, and is non-hazardous • It requires a big space and a lengthy setup time. • Require more time for control of biological parameters, no material recovery, require selective microbes.	(Steinberg *et al.*, 2005; Wang *et al.*, 2009)
Catalytic oxidation	90-98	• Possible energy recovery of up to 70% • Require catalyst deactivation and disposal. Energy efficiency is highly sensitive to operating parameters.	(Papaefthimiou *et al.*, 1998; Azalim *et al.*, 2011)
Thermal oxidation	95-99	• Possible energy recovery of up to 85% • Additional control equipment may be required for halogenated and other compounds. • Production of toxic by-products (e.g., NO_X)	(Choi *et al.*, 2000)
Condensation	70-85	• Product recovery can offset annual running costs • Require post-treatment and frequent maintenance; not economical, not applicable for VOCs having boiling points above 30℃	(Belaissaoui *et al.*, 2016; Uria-Tellaetxe *et al.*, 2016)
Absorption	90-98	• Product recovery can offset the annual running cost • Not suitable for VOCs having low concentrations, require pre-treatment of the volatile organic compounds, generate wastewater • After absorption, the solution must be discarded • Careful maintenance is needed	(Bay *et al.*, 2006; Jeon *et al.*, 2008)
Adsorption	80-90	• Proven to be efficient for low VOCs and compounds recovery could help offset annual operational costs • risk of pollutants re-emission, and during the desorption process, secondary contamination may occur • Moisture-sensitive; certain compounds, such as aldehydes, ketones, and esters, block pores and reduce treatment efficiency	(Tian *et al.*, 2016; Zhu *et al.*, 2016a)

Among the highlighted VOC treatment methods, thermal oxidation and adsorption are the two most extensively used processes in the industrial sector. However, thermal oxidation consumes a lot of energy because it requires gas heating to reach the reaction temperature. In adsorption, the saturated adsorbents must be regenerated via desorption, which is typically very energy-intensive, and the desorbed gas must be treated further (Kim *et al.*, 2017). Catalytic oxidation has the disadvantages of the high cost of catalyst, rapid deactivation of catalyst by poisoning and sintering, and carbon deposition during the treatment process.

In general, conventional VOC abatement technologies have various restrictions related to economy and technology, particularly for removing diluted VOCs (Subrahmanyam *et al.*, 2007). Therefore, it is essential to explore/develop an efficient, more economical, and environmentally friendly VOC treatment technology with high removal efficiency and low

energy consumption for the decomposition of lower concentration VOCs. NTP could provide some solutions, and it is receiving significant interest in VOC decomposition.

2.3 **Plasma**

Solids, liquids, and gases are the three basic states of matter. As the temperature or energy increases, molecules become more energetic, causing matter to change states in the order of solid, liquid, and then gas. If further energy is added to a gas, the molecules begin to ionise, forming a plasma. Therefore, plasma is often referred to as the fourth state of matter. Plasma is typically a collection of electrons, ions, radicals, excited and neutral molecules, or atoms. Plasmas are approximately estimated to comprise more than 99% of matter in the universe and can occur naturally or artificially (Langmuir, 1928; Fridman *et al.*, 2004; Fridman, 2008). The solar wind, corona, nebula, aurora borealis and lightening are the primary forms of naturally occurring plasmas, as presented in Figure 2.2. Plasmas can be produced artificially in the laboratory or industries for various utilizations such as microwave ovens, plasma TV, fluorescent lamps, and others (Nörtemann, 1999; Fridman *et al.*, 2004; Fridman, 2008).

(a) (b) (c) (d)

Figure 2.2 Examples of naturally produced plasmas (a) lightning, (b) aurora borealis, (c) solar wind, and (d) solar corona.

Plasma has three key characteristics that make it appealing for use in chemistry and chemical engineering fields:

1. Plasma temperatures and energy densities can far exceed those of conventional chemical technologies,
2. Plasmas can produce extremely high concentrations of energetic and chemically active species (e.g., electrons, atoms, radicals, ions, and excited species).
3. Plasma systems can be far from thermodynamic equilibrium, allowing for extremely high concentrations of chemically active species.

These characteristics of plasmas enable considerable intensification of chemical processes, an increase in treatment efficiency, and, in many cases, successful stimulation of chemical reactions that are hard to stimulate in conventional processes (Fridman. A, 2008).

Plasmas can be classified into thermal and non-thermal plasmas (NTPs) depending on the electron temperature (T_e) and temperature of heavy species (T_h) (ions, molecules, radicals, and atoms). In thermal plasma, the electrons and heavy species have the same temperatures ($T_e = T_h \approx 10\,000$ K), so it is regarded as an "equilibrium plasma" (Yang *et al.*, 2005; Fridman, 2008). Thermal plasma systems involve the application of high power and high temperatures in the gas volume, and the increased power is introduced to all plasma particles. Energetic electrons convey the energy in thermal plasmas to the molecules and ions (Schiavon *et al.*, 2016). Industrial thermal plasmas are typically generated by arc and torch plasmas. These thermal plasmas have broader applications in plasma cutting, vapour deposition, material processing, waste material destruction and metal processing (Samal, 2017).

In NTPs, often referred to as "cold" plasmas, the average electron temperature is in the range of 10,000 – 100,000 K (1-10 eV), which is significantly higher than that of the heavier species (atoms, ions etc.), which remain between 300 to 1000 K ($T_e \gg T_h$) (Fridman, 2008). The average energy of the electrons is in the range of 1 -10 eV (Yan *et al.*, 2002). The energy is delivered initially to the electrons rather than imparting kinetic energy to the gas species. The actual gas temperature remains cold, but the electrons have high temperatures. Moreover, as these energetic electrons impact the neutral gas species, leading to ionization, excitation and dissociation, species such as ions, free radicals and molecules are generated, which can result in chemical reactions (Fridman *et al.*, 2004; Fridman, 2008). The generation of highly reactive species in the NTP at ambient temperature and atmospheric pressure has led to a large number of applications of plasma technology in air pollution treatment (e.g. NO_X and VOC destruction) (Dewulf *et al.*, 1999), polymer technology, ozone generation (Harling *et al.*, 2009), sterilization of medical facilities (Bodar *et al.*, 2003) and the hydrogenation of CO_2 (Bunn *et al.*, 2005).

Table 2.3 summarizes the main advantages and disadvantages of thermal and non-thermal plasma techniques for VOCs reduction. The problem of the high energy consumption of thermal plasmas, material costs, as well as the challenges of quick deactivation of catalyst by poisoning and sintering, and carbon deposition in plasma catalytic systems, are prompting more interest in NTP-only systems for the treatment of VOCs (Liu *et al.*, 2017a). NTP technology has also been recognised as having a lower environmental impact than traditional VOC removal technologies, owing to increased removal efficiency and the reduction of unwanted by-products. Another advantage of NTP technology over thermal and catalytic approaches is improved process control. The amount of energy added to the process is easily controlled by controlling the power supply to the plasma-producing electrodes (Fabry *et al.*, 2013).

Table 2.3 Comparison of thermal and non-thermal plasmas (Urashima *et al.*, 2000; Fridman *et al.*, 2004).

Type of plasma	Advantages	Disadvantages
Thermal plasma	• Thermal plasmas are generally more potent than non-thermal plasmas. • Can decompose VOCs with high concentrations in gas streams because of high temperature	• Less cost-effective • Low energy efficiency • Due to the high temperature in the plasma reactor, there is a greater danger of damage to the electrodes or reactor material.
Non-thermal plasma	• It uses an electric field to activate molecules rather than temperature, and the gas temperature remains at room temperature. • Operate at low temperatures and atmospheric pressure • Less expensive than thermal plasmas because most of the electric input goes straight into energizing the electrons rather than heating the entire plasma species • Optimize removal efficiency (conversion) using electrical input instead of temperature • Selective to chemical reactions • Non-thermal plasmas have the potential to enable thermodynamically unfavourable chemical reactions (e.g., CO_2 reduction, VOCs abatement, odour removal) to occur at ambient conditions. • Less risk of electrode damage due to ambient conditions	• Not applicable when treating VOCs with high concentrations in gas streams • Low energy efficiency • Non-thermal plasmas have not been realized in extensive scale processes • Generation of unwanted by-products (solid residue, NO_x and O_3)

2.4 **Elementary processes in NTPs**

The main elementary reactions in NTPs can be classified into two (2): the primary and the secondary processes depending on the timescale of streamer propagation (Kim, 2004). Figure 1.1 presents an overview of the NTP elementary process (Kim, 2004). The typical timescale of the primary processes is 10^{-8} s and the initial stages of the NTP generation in this technique are electron impact ionization, excitation, dissociation, charge transfer and light emission (Kim, 2004). In addition, the efficiency of the primary process is mainly dependent on the characteristics of the energization, such as pulse, AC, AC + pulse or DC, DC+ pulse, frequency, voltage rise-time etc. The subsequent chemical reactions involving the products of primary processes, such as electrons, radicals, ions, and excited molecules, are referred to as secondary processes. In these secondary processes, radical-neutral recombination produces additional radical species and reactive molecules like H_2O_2, O_3, and HO_2 (Kim, 2004).

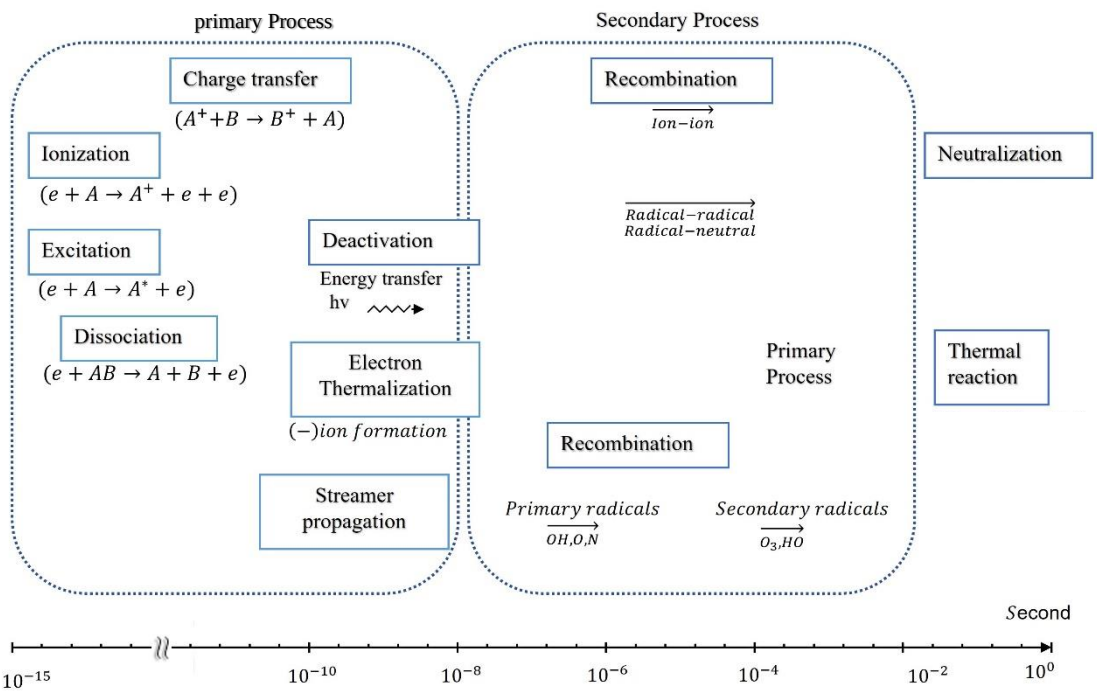

Figure 2.3 An overview of the typical timescale of events in the NTP generation process (Kim, 2004).

In the NTP system, the collision between the energetic electrons and carrier gas (background gas) may lead to molecular and electron reactions resulting in active species such as gas-phase gas-phase radicals and excited and ionic species. These active species may lead to molecular and atomic reactions and decomposition reactions (Eliasson *et al.*, 1991; Gaens *et al.*, 2013). An overview of the chemical reactions initiated by the energetic electrons/electric field in the NTP system at low temperatures and ambient pressure is summarized in Table 2.4. The excitation, dissociation, attachment, and dissociative attachment are the most effective processes under plasma conditions because the techniques need lower average electron energy.

Table 2.4 An overview of NTP reactions induced by the energetic electrons (Eliasson *et al.*, 1991; Gaens *et al.*, 2013).

Electron/molecular reactions in NTP processes		
Excitation	$e + A_2 = A_2^* + e$	R (2.2)
Dissociation	$e + A_2 = 2A + e$	R (2.3)
Attachment	$e + A_2 + M = A_2^- + M$	R (2.4)
Dissociative Attachment	$e + A_2 = A^- + A$	R (2.5)
Ionization	$e + A_2 = A_2^+ + 2e$	R (2.6)
Dissociative Ionization	$e + A_2 = A^+ + A + 2e$	R (2.7)
Recombination	$e + A_2^+ = A_2$	R (2.8)
Detachment	$e + A_2^- = A_2 + 2e$	R (2.9)

Note: e stands for electrons; A and B represent atoms; A_2 and B_2 represent molecules; M stands for a collision specie; the excited species are marked with an asterisk (*); the species marked + or - are ions.

In the NTP process, the outlined reaction channels may contribute to the formation of various reactive intermediates leading to corresponding products depending on the average electron energy that can be described by electron energy distribution function (EEDF). The lower energic electrons can lead to the formation of intermediates by excitation, dissociation, attachment, and dissociative attachment of molecules (A_2). In contrast, the electrons in the higher energy tail of EEDF may contribute to the formation of atomic and molecular ions by ionization and dissociative ionization of molecules (A_2). Furthermore, the molecular ions (A_2+, A_2-) can return to the ground state A_2 molecule by the recombination and detachment reactions (Eliasson *et al.*, 1991; Gaens *et al.*, 2013).

2.5 **Conventional NTP reactors**

There are various types of NTP reactors, including microwave, electron beam, gliding arc discharge, corona discharge, surface discharge, DBD, ferroelectric pellet packed-bed reactor, etc. These NTP techniques are further sub-divided based on the discharge mode, dielectric barrier or catalyst, power supply and geometry, etc.

2.5.1 Microwave Plasmas

As shown in Figure 2.4 (Urashima *et al.*, 2000), microwave discharge is a high-frequency discharge (also known as high-frequency glow discharge). A continuous discharge is formed when the discharge frequency between two electrodes is high enough. This type of travelling wave discharge creates stable plasmas throughout a wide pressure range ($10^{-4} - 10^{1}$Pa) atmospheric pressure, discharge tube diameter (0.5 – 150 mm), frequency (1 MHz – 10 GHz) and high-frequency power (50 – 3000 W)(Arno *et al.*, 1995; Teplý *et al.*, 1995). The microwave plasma can only operate at frequencies greater than 10^{9} Hz.

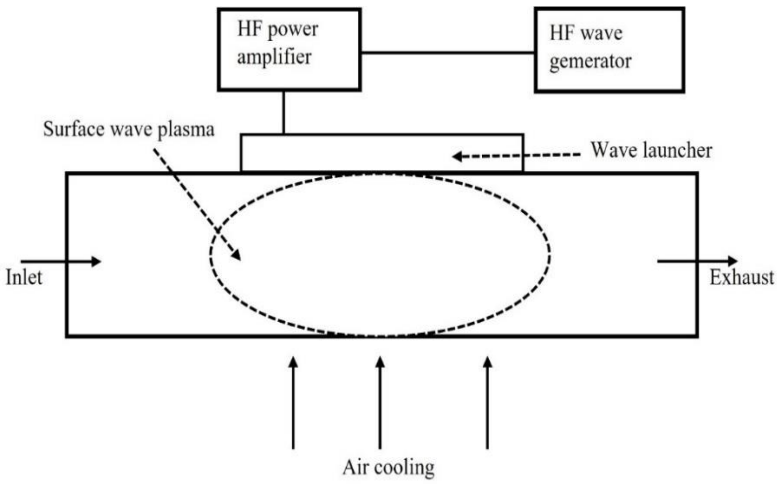

Figure 2.4 Schematic of a microwave plasma reactor (Urashima *et al.*, 2000).

2.5.2 Electron beam plasmas

The electron beam is another method of generating NTPs. It consists of an electron accelerator and a high DC voltage supply system, as shown in

Figure 2.5. The technology operates at a gas flow rate of 10^3 to 10^5 m^3/h and has high plasma densities. The electrons are accelerated by an electric field and a magnetic field in a high vacuum accelerating tube to create a larger plasma zone. The energetic electrons are generated at the outer section of the reaction chamber and subsequently injected into the gas stream via a boron nitride or a thin titanium film. The VOCs can react with the injected electrons through dissociation, dissociative and direct ionization, excitation, dissociative attachment and radiation (Urashima *et al.*, 2000). Hakoda *et al.* (2000) studied the decomposition of trichloroethylene (TCE) using electron beam plasma. The concentration of TCE decreased exponentially when the dose of electrons was increased (air-absorbed energy).

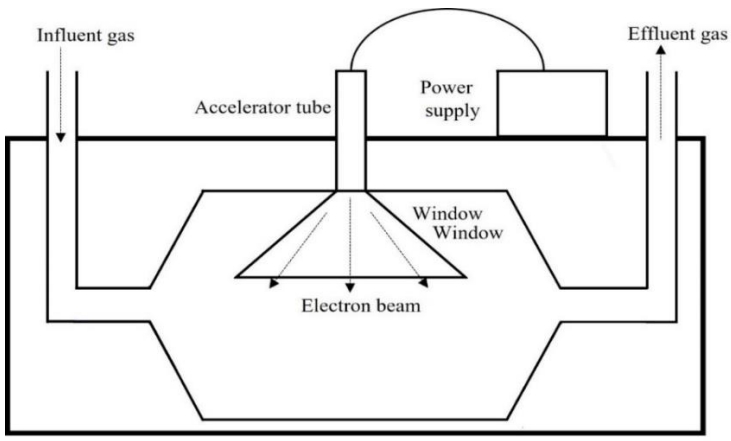

Figure 2.5 Schematic of an electron beam plasma reactor.

For VOCs that require a large number of electrons to decompose, such as the stable carbon tetrachloride, electron beam processing efficiency was found to be remarkably high (Penetrante *et al.*, 1996). Because of their high cost, electron-beam plasma reactor has not been widely used in VOC treatment (Hirota *et al.*, 2004).

2.5.3 Gliding arc discharge

Gliding arc discharge (GAD) is another type of NTP that can produce high plasma density at atmospheric pressure. GAD may have high levels of current, electron density, and power, which are typical of thermal plasmas and low temperatures and a high electric field, which are typical of NTPs (Fridman, 2004). Figure 2.6 Mutaf-Yardimci *et al.* (2000) shows a schematic of a gliding arc plasma reactor.

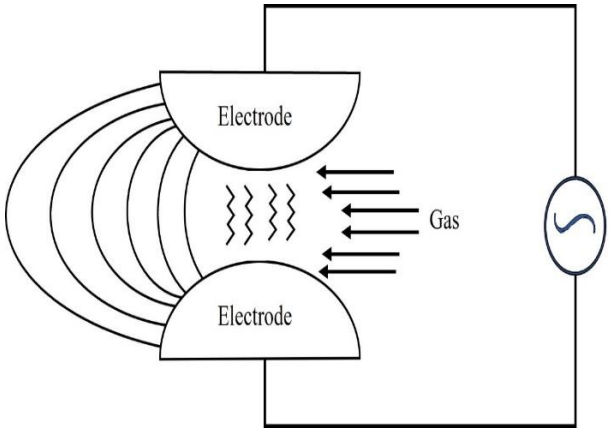

Figure 2.6 Schematic of the gliding arc discharge plasma reactor (Mutaf-Yardimci *et al.*, 2000).

GAD is generated between two or more electrodes positioned in a rapid gas flow. When the applied voltage reaches the breakdown voltage value, for example, ~3 kV/mm in the air at atmospheric pressure, the gliding discharge plasma begins at the shortest distance, 2 – 5 mm, between two diverging electrodes. After the breakdown, a spark channel quickly forms across the gap between the blades. The column is dragged downstream by the gas flow, increasing the length of the plasma column, and as the plasma column reaches its maximum discharge length, it vanishes. A new one begins at the shortest distance between the electrodes (Mutaf-Yardimci *et al.*, 2000). The plasma rapidly cools to a gas temperature of 1000K or less during the transition. The electron temperature rises to 1 eV, the vibrational temperature increases to 3000–5000K, and the electron density remains at the thermal plasma level. In the meantime, the ionisation mechanism can shift from thermal to non-equilibrium, supported by direct electron impact, and up to 75–80% of total power can be wasted in the non-thermal zone (Fridman, 2004). The GAD plasma combines the properties and advantages (and, sadly, occasionally problems) of many other discharges, such as low-temperature glow or corona and

thermal arc discharges. GAD has already found applications in exhaust gas cleaning and waste removal, but high energy consumption limits its application (Fridman, 2004).

2.5.4 Corona Discharge

Corona discharge plasmas are weakly luminous discharges that can be generated at atmospheric pressure. The discharge is generated by strong electric fields near sharp edges, points, needles, or thin diameter wires on an electrode. The typical corona discharge reactor is presented in Figure 2.7.

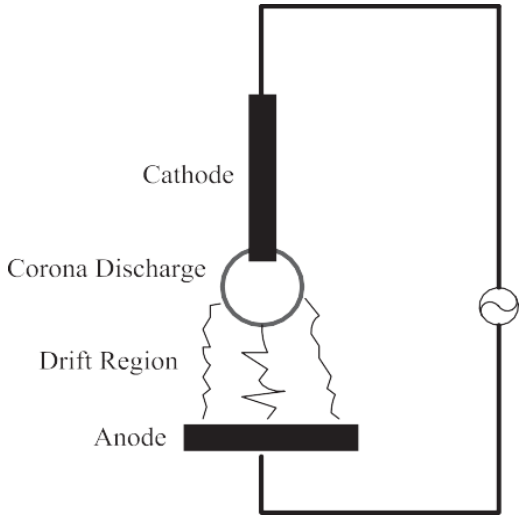

Figure 2.7 Typical configuration of corona discharge (Chen *et al.*, 2014).

The corona discharges are usually non-uniform: a high electric field, brightness and ionisation are all concentrated around one electrode. The weak electric fields drag charged particles from one electrode to another close to an electric circuit. The corona circuit is closed by a displacement current rather than charged particle transport in the early stages of the breakdown.

Pulsed corona discharge (PCD) is another method of generating non-thermal plasmas. The application of the PCD system for VOC treatment was introduced in the 1980s. A typical example of pulsed corona discharge is shown in Figure 2.8 (d). This technique is characterized by a pulsed power supply with a very low voltage rising time of tens of nanoseconds. The voltage level required to energize the discharge process largely depends on VOC composition, pulse duration and the discharge gap between the electrodes (McAdams, 2001). However, the pulsed voltage duration is between 100 – 200 ns to confirm that the spark formation is prevented and that the energy dissipation by ions is minimal. Previous researchers have reported that the electrode configuration of pulsed corona discharge reactors can be either wire-to-plate or wire-to-cylinder (Kim, 2004).

The PCD generally consists of streamers in which the ionization chamber is spread over the entire discharge gap (e.g., 10 cm or more). These are favourable factors for scaling up and reducing pressure drop in the decomposition of VOCs (McAdams, 2001). The most significant disadvantage of a corona discharge reactor is the occurrence of discharge destabilisation in the form of sparks, which causes insulation layer degradation and, as a result, increases energy consumption and lack of homogeneity. Although there has been some research on corona discharge with an emphasis on VOC abatement, the results do not strongly suggest that it is effective for VOC removal due to low energy efficiency and high sensitivity to gas humidity (Schiorlin *et al.*, 2009).

2.5.5 Dielectric barrier discharge plasma reactor

Dielectric barrier discharge (DBD), also known as "silent" discharge, is an NTP technology that has been known for over 165 years. The typical DBD reactor consists of two parallel electrodes, with at least one electrode covered by a dielectric material. An inner electrode is often enclosed by a dielectric tube with a few millimetres gap. The outer electrode is typically a mesh or foil wrapped around the dielectric tube. One of the electrodes is grounded, while the other is connected to a power supply. The gas enters from one side, is gradually activated as it passes across the gap between the inner electrode and the dielectric tube, and then exits from the other side (Bogaerts *et al.*, 2018). DBD reactors are typically used in cylindrical or planar configurations, as presented in Figures 2.8 (a) and (b). One or two dielectric barrier layers are placed either (i) on a powered or a ground electrode, (ii) on two electrodes or (iii) between two metal electrodes.

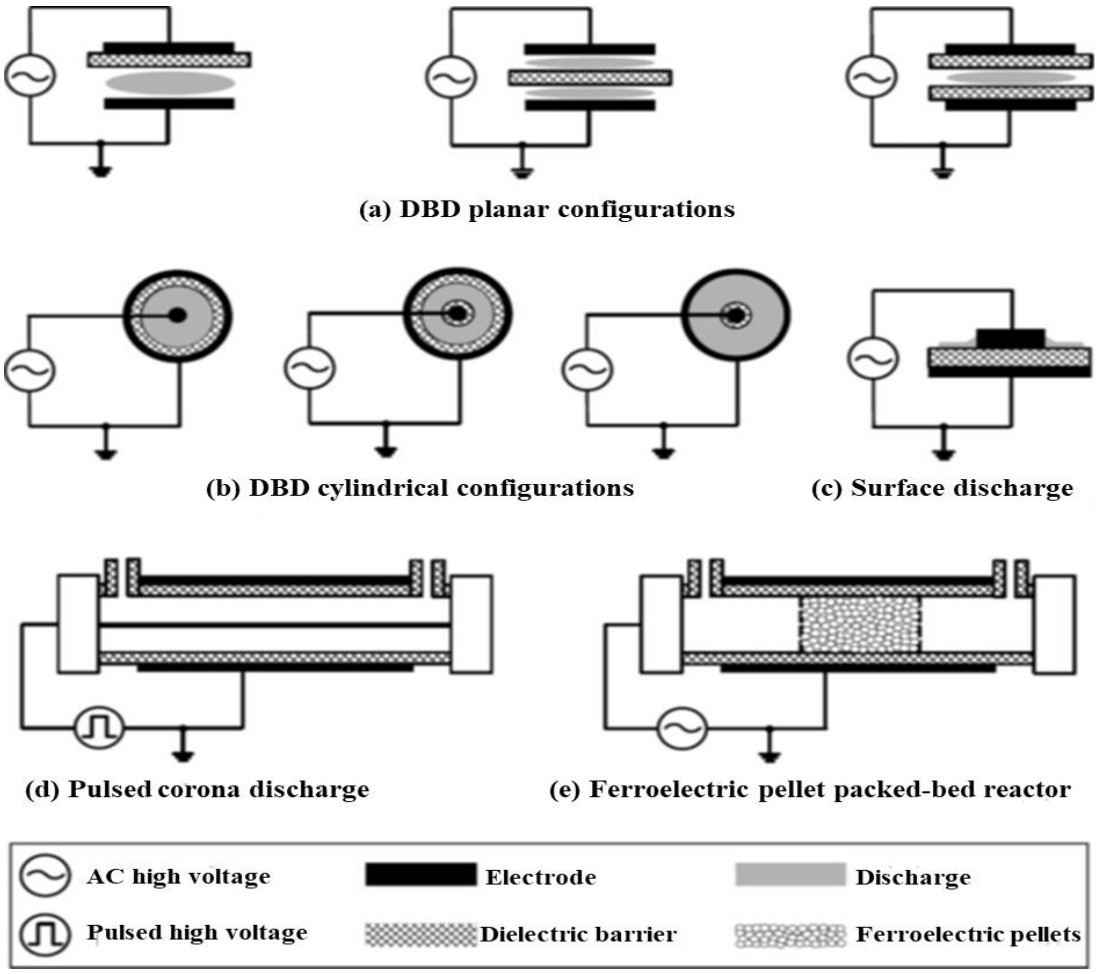

Figure 2.8 Schematics of basic NTP DBD reactors (Vandenbroucke *et al.*, 2011).

The DBD electric discharge mechanism largely depends upon the two electrodes, the discharge gap between the electrodes, the dielectric material, the high power/ strength of the electric field, and the gas flow through the discharge gap. The electric field is generated between the two electrodes. The first electrode is connected to a high voltage power source (cathode), while the second electrode is grounded (anode) (Fridman, 2008).

The plasma is generated by transmitting the electric energy to the electrons rather than gas molecules. The electric field between the two electrodes increases with an increase in applied voltage (usually ranging between 10-30 kV) until the gas breaks down (Yehia, 2016). The energetic electrons within the gap collide with the molecules (atoms), causing ionization, dissociation, and excitation (Fridman, 2008; Schiorlin *et al.*, 2009). Furthermore, the gas temperature remains low, and a voltage of 10-30 kV with high frequencies is required to maintain the plasma discharges (Wang *et al.*, 2012).

The most used dielectric material includes glass, quartz, ceramics, polymer materials, and ferroelectric materials. The dielectric barrier's function is to limit the amounts of charge transferred between both electrodes, thus the electric current preventing the arc discharge

(Kogelschatz, 2003; Bogaerts *et al.*, 2018). However, the discharge characteristics (e.g., density and energy level of various species) in DBD largely depend on the gas composition, dielectric material's nature, and operating parameters of voltage and frequency (Kogelschatz, 2003). In addition, when the electron density in the discharge gap attains a high level, a large amount of separate and short-lived filaments is produced, also known as micro-discharges. Moreover, in some cases, many micro-discharges are formed at a pressure of 10^5 Pa, which is the most favourable pressure range for ozone production and VOC treatment (Kogelschatz, 2003).

Surface discharge (SD) is another way of generating NTPs in a DBD reactor. It is identical to DBD as it uses a dielectric barrier layer. The SD reactor consists of a short and long electrode on a dielectric surface and a lengthy counter-electrode on the bottom side of the dielectric surface (Figure 2.8 (c)). In this type of configuration, a series of strip electrodes can be located on the inner surface of a cylindrical surface discharge reactor. The plasma is generated between the surface of the electrodes and the middle rod electrode (Kogelschatz, 2003).

A ferroelectric pellet packed-bed reactor is shown in Figure 2.8 (e). This is simply a packed-bed reactor filled with ferroelectric material such as barium titanate ($BaTiO_3$), with a dielectric constant between 2 000 and 10,000 (Liang *et al.*, 2009). Other perovskite materials used as ferroelectric materials include $CaTiO_3$, $MgTiO_4$, $PbTiO_3$ (Ogata *et al.*, 1997) etc. There are two major ferroelectric pellet packed-bed reactor configurations: coaxial and parallel-plate configurations. When the ferroelectric material, for example, $BaTiO_3$, is exposed to a strong external electric field, polarization occurs toward the electric field, leading to a high electric field at the points of contact of the pellets. Partial electric discharge occurs in the region of the pallet's contact points. Previous researchers have reported that incorporating ferroelectric pellets packed bed NTP systems with catalysts increase the removal efficiency and reduces the formation of toxic by-products at low energy consumption. For example, when the packing material is placed in the plasma zone of the reactor, the short and long-lived species will interact with the packing material, and the packing material will influence the plasma discharge properties. As a result, radicals, surface discharge, electron- and photon-induced processes, and excited species can contribute to VOC decomposition and suppressed ozone concentration (Li *et al.*, 2020). However, ferroelectric pellets in the discharge region favoured electrical discharge but increased pressure drop over the reactor length (Liang *et al.*, 2013).

The plasma-packed beds/catalyst reactors have many advantages in terms of VOC removal efficiency, CO_2 selectivity, and energy efficiency. Furthermore, optimising a particular system requires a more profound knowledge of the interaction between plasma and packing materials/catalysts.

Among the NTP reactors, the DBD reactor is one of the most studied techniques for removing VOCs. It is gaining more attention than any other method to treat VOC emissions. It exhibits many advantages, including flexibility in reactor design, working with mixtures of gases, and operating close to room temperature and atmospheric pressure. In addition, it operates at low power and close to room temperature, it has reproducible plasma conditions, and rapid attainment of a steady-state allows for fast start-up and shutdown in practice (Xiao *et al.*, 2014; Bogaerts *et al.*, 2018).

2.6 **Fundamental parameters of DBD reactors and their influence on VOC decomposition**

It has been more than 150 years since W. Siemens invented the DBD reactor in 1857 (Siemens, 1857). The original DBD reactor focused on ozone generation, and it was the first time an NTP system was utilised in an environmental application. The device comprises two coaxial cylindrical glass tubes with high voltage and ground electrodes attached to the inner surface of the inner tube and the outer surface of the outer tube, respectively, as shown in Figure 2.9. The discharge occurred when oxygen or air passed through the annular gap between two glass tubes.

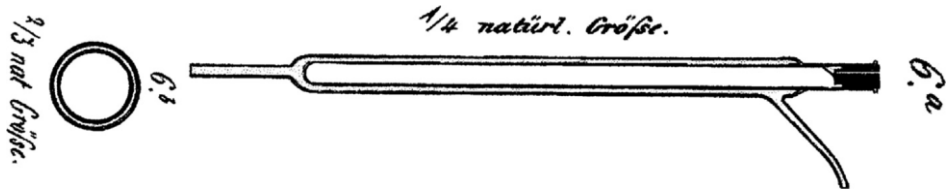

Figure 2.9 The first DBD ozone generator of W. Siemens, 1857 (Siemens, 1857).

Early studies on the application of DBDs to treat VOCs from the contaminated gas stream were reported by Berthelot in 1876 and Schwarz and Kunzer in 1929 (Kogelschatz, 2003).

The full application of DBD reactors for VOC treatment begins from around 1990 because the focus on VOC emissions was realised later than NO_x and SO_2 (Li *et al.*, 2020). Before 2000, most DBD reactors used to decompose VOCs were carried out without packing materials or catalysts, and the removal efficiency was employed as the primary criterion for evaluating reactor performance (Li *et al.*, 2020). Combining the catalyst with DBD opened new avenues for VOC treatment research. Extensive research on plasma catalytic DBD has been conducted over the last two decades, including metal-supported catalysts, packing materials, catalyst placement, etc. Some researchers have focused their attention on improving the configurations and main parameters of the DBD in the treatment of different VOCs (Li *et al.*, 2020). Because unwanted by-products are inevitable in the decomposition of VOCs, CO_2 selectivity, mineralization rate (also known as COx selectivity), and elimination of unwanted by-products

(solid residue and NOx) must be used as an assessment variable rather than only removal efficiency.

The main design parameters of DBD reactors are dielectric materials, electrode materials, discharge length, discharge gap and type of dielectric barrier material, as presented in Figure 2.10. These parameters have a significant influence on the performance of the DBD reactors in terms of removal efficiency, energy efficiency and product selectivity.

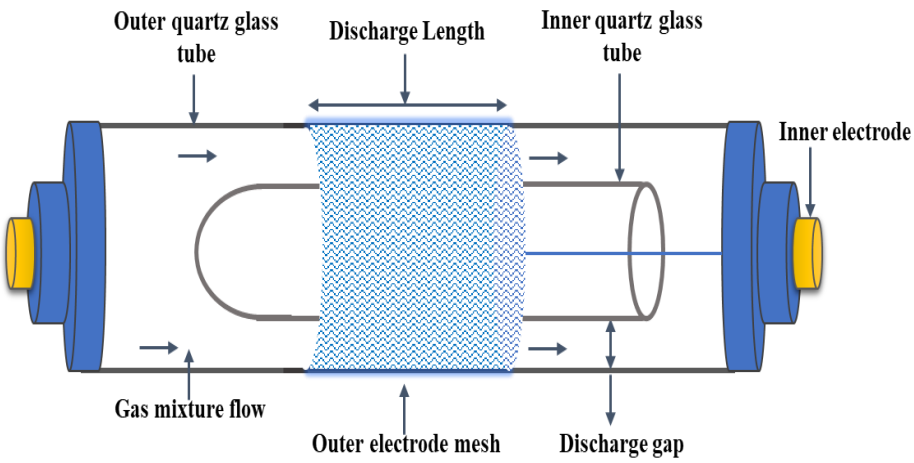

Figure 2.10 Schematic diagram of DBD reactor.

Therefore, reviewing the influence of the fundamental DBD parameters and the operating conditions on the removal of VOCs may provide the basis for improving/optimizing the performance of the DBD reactor. The effects of main DBD parameters are reviewed based on the previous studies on the decomposition of VOCs using DBD reactors.

2.6.1 Dielectric materials for DBD reactor

The dielectric barrier material is one of the most significant discharge parameters in the DBD technique. The dielectric material is an electrically insulating material between the metallic plates of a capacitor that an applied electric field can polarize. The polarization of the dielectric material by the applied electric field increases the capacitor's surface charge for the given electric field strength. Typical dielectric materials include quartz, glass, ceramics, alumina, and ferroelectrics, and they have different dielectric constants, as shown in Table 2.5.

Table 2.5 Properties of dielectric barrier materials (Xiao *et al.*, 2014).

Dielectric material	**Dielectric constant**
Glass	4-6
Quartz	4-7
Aluminium oxides	~10

Ceramics	10s – 10,000s
Ferroelectrics (i.e., $BaTiO_3$)	100s -10,000s
TiO_2	75-150

In most of the previous studies, quartz tubes (Raju. *et al.*, 2013; Chen *et al.*, 2016), silica glass, aluminium oxide (Byeon *et al.*, 2010; Kim *et al.*, 2011) and ceramic materials (Guo *et al.*, 2017) have been used as dielectric barrier materials. Among all the dielectric materials studied, quartz is the most common material used for VOC decomposition in a DBD reactor due to its commercial application and moderate cost. The dielectric material influences the discharge characteristics of the DBD plasma system, which impacts VOC removal efficiency. Since the dielectric and gas gap capacitances in the circuit are connected in series, raising the dielectric capacitance increases the strength of the electric field in the discharge gap, resulting in higher micro-discharge.

Kundu *et al.* (2012) investigated the performance of a double DBD reactor for the decomposition of methane in an argon plasma. They used quartz tubes and alumina as dielectric materials. They found that the DBD reactor with alumina showed a higher removal efficiency (52%) of methane when compared with the quartz DBD reactor (46%) at a constant flow rate (100 ml/min) and 11 kV. The higher removal efficiency in the alumina DBD reactor may be due to the greater dielectric constant of alumina (9.8) compared with the quartz DBD reactor (3.7). Khoja *et al.* (2017) reported a higher methane removal efficiency in an alumina DBD reactor. They reported that alumina dielectric material accelerated the generation of highly energetic electrons due to a stronger electric field. Furthermore, the higher removal efficiency of methane in the alumina DBD reactor may be due to the porosity and roughness of the dielectric material, which increases the residence time in the reactor. As a result of its porous nature, the aluminium reactor's prolonged residence time allowed for more collisions between energetic electrons and gas molecules.

In general, VOC removal efficiency can be increased by using a suitable dielectric material in the DBD reactor. Dielectric materials with a higher dielectric constant can generate a stronger electric field and enhance the ionization of the gas molecules. For example, dielectric material with high dielectric constant, such as ferroelectrics, can be used for industrial applications to treat VOCs from the gas stream. Therefore, there's a growing need to investigate the most efficient dielectric barrier material for higher energy efficiency and effective performance of the DBD system.

2.6.2 Electrode material

The strength of plasmas and their associated discharges is a function of the electrode type. In a DBD reactor, the electrode material plays a significant role in the generation of ions, radicals, and excited species. The intensity of the plasma is directly related to the type of electrode material because different electrode has different electrical properties, e.g., conductivity and resistivity, which can influence plasma discharge. The work function and secondary electron emission of the electrodes directly impact the plasma reactor's discharge current and electric field distribution (Baránková *et al.*, 2010).

Most of the previous studies on VOC decomposition reported the use of metallic rod electrodes, copper, tungsten, sintered metal fibres (SMF), ferroelectric materials and brass wire for the abatement of VOCs in a DBD reactor (Zhang *et al.*, 2015a). Sivachandiran *et al.* (2012) investigated plasma-assisted oxidative removal of chlorobenzene using a silver paste, aluminium foil and copper wire electrodes. At specific input energy ("SIE") of 310 J/L, 90% removal efficiency was achieved in the silver paste electrode DBD reactor, which decreased to 85 and 80% for copper wire and aluminium foil. The product selectivity was also increased using silver paste dielectric material. The formation of "unusual" coronas outside the reactors with aluminium foil and copper electrodes could be the main reason for low removal efficiency compared with silver paste DBD reactor. They concluded that the formation of unusual corona outside the plasma reactors with aluminium foil and copper wire could cause lower removal efficiency than in the silver paste reactor. Corona can form in the gaps between the ground electrode and dielectric barrier due to poor contact. In the reactor with a silver paste electrode, the absence of a gap between the dielectric barrier and electrodes increases maximum energy consumption, resulting in the generation of micro-discharges. In addition, Kim *et al.* (2004) reported similar findings in the packed plasma-assisted benzene decomposition using a silver paste, aluminium tape and copper mesh electrodes.

2.6.3 Discharge length

In a DBD reactor, discharge length refers to the lengths of the discharge zone, high voltage electrode or the reaction region where highly energetic electrons are generated. Some researchers reported the significant impact of discharge length on the removal efficiency of VOCs. Zhang *et al.* (2014) studied the plasma-assisted decomposition of styrene in a DBD reactor with 1.8, 3.6, 5.4 and 7.2 cm discharge lengths. They investigated the effect of the discharge lengths on product selectivity and removal efficiency of styrene at SIE of 170 J/L and 235-ppm styrene inlet concentration. The maximum removal efficiency of styrene was obtained

at 7.2 cm (most extended discharge length), and the minimum was recorded at 1.8 cm (lowest discharge length). They also reported that the maximum CO_2 selectivity (84%) was obtained at 7.2cm, more significant than the minimum selectivity recorded at 1.8 cm discharge length. Khoja *et al.* (2017) evaluated the plasma decomposition of methane using different types of DBD systems. Their results showed that the removal efficiency of methane could be intensified by increasing the length of the discharge length from 10 to 30 cm. It is important to note that increasing the discharge length also increases the residence time of VOCs in the plasma zone, which increases VOC decomposition due to the increased chances of collision between VOC molecules and energetic electrons and other reactive species (Zhang *et al.*, 2014; Khoja *et al.*, 2017).

By increasing the discharge length of the plasma reactor, a low voltage is needed to ignite the plasma. Therefore, increasing the discharge length results in a higher effective electrode surface, leading to more micro-discharges inside the plasma reactor, which increases the likelihood of gas breakdown (Bahri *et al.*, 2016). However, a longer discharge length at a constant input power results in a lower power density due to the expanded plasma zone. Furthermore, increasing the discharge length results in increased energy loss due to dielectric barrier heat dissipation (Wang *et al.*, 2013). The limitation of increasing discharge length is the need to apply more plasma power to accelerate plasma generation, which may lead to higher energy consumption.

2.6.4 Discharge gap

The discharge gap refers to the distance between the inner electrode and dielectric material where plasma reactions are usually taken, as shown in Figure 2.9. DBD reactor designs require a suitable discharge gap to maintain stable plasma conditions. On a laboratory scale, discharge gaps between 1 - 6 mm are applicable for VOC decomposition. For example, several studies have been carried out with a discharge gap between 2-3 mm in the plasma-assisted decomposition of VOCs (Karuppiah *et al.*, 2013). Mustafa *et al.* (2018) investigated the decomposition of benzene in a DBD reactor consisting of two cylindrical dielectric inner tubes with discharge gaps of 3mm (reactor A) and 6mm (reactor B). It was found that the maximum removal efficiency of benzene (94.6%) was obtained in the reactor with a shorter discharge gap (reactor A) compared to (85.5%) for the reactor with a more significant discharge gap (reactor B). This is because a short discharge gap can increase the mean electric field strength in the discharge region, which may increase removal efficiency. However, if the discharge gap is too small, an arc or spark discharge may occur, and the interaction between the target VOC

molecule and the active species may be limited due to a short residence time. As a result, to achieve an effective DBD performance for VOC decomposition, both the discharge gap and the residence time must be considered. The solid residue was formed in the DBD reactor, which can cause operation problems over time. In addition, Magureanu *et al.* (2007) reported similar findings on the plasma-assisted decomposition of trichloroethylene in a DBD reactor with discharge gaps between 1-5 mm. It was found that DBD reactors with a discharge gap between 1-3 mm have the maximum removal efficiency of trichloroethylene. The enhancement of the removal efficiency of VOCs with smaller discharge gaps could be due to two reasons:

(i) The decrease in the discharge gap between the reactor electrodes and dielectric material can significantly increase the electrical field strength, improving the energy of generated electrons reacting with VOC molecules in the plasma reaction zone, and significantly increasing removal efficiency (Ma *et al.*, 2015).

(ii) The shorter discharge gap facilitates the formation of energetic electrons and active radicals, such as $OH^{\cdot}$, $O^{\cdot}$ and $N^{\cdot}$ in the discharge zone, which can increase the chances of collision between the VOC model compounds and the active radicals during the decomposition process. Furthermore, a short discharge gap can limit the mobility of highly energetic electrons in the discharge region, giving way to the increased collision capabilities (Sultana *et al.*, 2015).

However, an increase in the discharge gap causes a significant decrease in the power density, known as the discharge power per volume at fixed plasma power, due to the rise in plasma volume. Moreover, an increase in the discharge gap may lead to partial plasma discharge instead of full discharge (Mei *et al.*, 2017).

Even though the geometry of the DBD reactor is simple, its design variables are diverse. For example, various plasma DBD reactors design variables, such as reactor configuration, discharge gap and length, electrode material, dielectric material and thickness, and many dielectrics, will influence plasma discharge characteristics and, thus, the removal efficiency of VOC. In most cases, optimising the plasma reactor design variables will result in an increased electric field or discharge current, which will increase the removal efficiency of VOC and CO_2 selectivity.

2.7 **Non-thermal plasmas (NTPs) for decomposition of VOCs**

There are hundreds of types of VOCs released from a wide range of industrial processes, making VOC abatement complex. These VOCs are aromatics, ketones, aldehydes, alcohols, esters, alkanes, alkenes, halocarbons etc. The chemical structure, weight of hydrogen (mass

percentage) and ionisation potential of distinct VOCs can all influence how difficult they are to decompose in DBD. In recent years, many studies have been conducted to identify the best possible operating conditions for removing different types of VOCs from an ambient air gas stream using NTPs. Table 2.6 illustrates common VOCs treated by a plasma DBD reactor.

Table 2.6 Common VOCs decomposed by plasma DBD reactor (Li *et al.*, 2020).

Classification	**Target VOC**
Alkanes	Propane, Ethylene, Methane
Aromatics	Toluene, Xylene, Styrene, Benzene
Esters	Ethyl acetate
Ketones	Acetone
Alcohols	Methanol, Ethanol
Aldehydes	Acetaldehyde, Formaldehyde
Halocarbons	Chlorobenzene, Dichloromethane, Trifluoromethane, Tetrachloromethane, Trichloroethylene

Typical VOCs from industrial streams, waste treatment plants and consumer products are branched and cyclic alkanes, aromatic hydrocarbons, alcohols, and aldehydes (Mustafa *et al.*, 2017). Alkanes and aromatics are more easily emitted in the environment than any other VOC class and are typically volatile to quickly enter the earth's atmosphere (Vandenbroucke *et al.*, 2011). Furthermore, alkane and aromatic hydrocarbons constitute the most common anthropogenic VOCs in the atmosphere (Thevenet *et al.*, 2014).

This research focussed on hexane, cyclohexane, benzene, and methanol. Hence, the NTP decomposition of hexane, cyclohexane, benzene, and methanol are reviewed in the next few sections.

2.7.1 Hexane

Hexane is one of the most used saturated aliphatic hydrocarbons. It is classified as a highly volatile VOC because of its relatively low boiling point (69℃). It is very stable due to its saturation and non-polarised nature (Son *et al.*, 2021). It has many adverse effects on both the environment and human health. Therefore, the EPA classified hexane as a hazardous air pollutant under the Clean Air Act (EPA, 1990). It is widely used as a solvent in cleaning and extraction processes and significantly in the gasoline, ink, and glue industries (Bouchard *et al.*, 2008; Lee *et al.*, 2010). Large amounts of hexane from service stations, automobile exhaust, food and chemical processing industries pollute the environment and pose serious health hazards to humans (Spigno *et al.*, 2005). Chronic exposure to hexane in the air is linked to polyneuropathy in humans, blurred vision, headache, and dermatitis (Sarigiannis *et al.*, 2011).

Previous studies have been carried out into applying NTP techniques such as gliding arc discharge, corona discharge and packed dielectric reactor for the decomposition of alkanes. Hill *et al.* (2007) studied the decomposition of propane in a packed dielectric reactor using an air carrier gas. They observed that increasing the specific input energy resulted in higher removal efficiencies. The primary decomposition by-products were CO_2 and CO, and no hydrocarbon products such as methanol, ethane, ethanol, or acetylene could be detected. However, they reported high concentrations of NOx as the by-products. Oxygen plays an essential role in the decomposition of VOCs in the DBD reactor. The O_2 content of the discharge gas has a significant impact on the removal efficiency. Jin *et al.* (2016) investigated the decomposition of n-hexane in 15% O_2 (N_2 balance) using an NTP-DBD reactor filled with quartz, porous alumina balls and fewer alumina balls. They found that CO, CO_2 and liquid products (3-hexanone and 2-hexanone) were the main decomposition by-products. However, high O_3 concentrations were observed during the decomposition process (Jin *et al.*, 2016).

VOCs are decomposed by collisions with the energetic electrons, excited and metastable nitrogen species in the pure nitrogen carrier gas. After introducing O_2 to the DBD plasma, the oxygen molecules, atoms, and OH radicals contribute to the decomposition of the VOC, thereby increasing the removal efficiency. When the O_2 concentration increases over a certain level, however, the generation of O_3 and NOx begins to appear, consuming a considerable number of reactive species generated from O_2 and N_2, leading to a decreased removal efficiency (Li *et al.*, 2020). Marotta *et al.* (2007) studied the decomposition of n-hexane and 2,2,4-trimethylpentane in a DC corona discharge. They reported that oxygen radicals directly oxidise alkane radicals to ketones. However, solid black deposits were formed in the reactor, which may cause damage and loss of activity over time. Yan *et al.* (2007) investigated the decomposition of hexane using a gliding arc discharge plasma at different oxygen concentrations. They found that increasing the oxygen concentration in the background gas increases the removal efficiency but results in a high NOx concentration. The selectivity to CO_2 is higher when compared with CO selectivity due to fast oxidation of CO to CO_2 by O radicals.

Overall, the main drawbacks of the previous research on the application of NTP for removing alkanes from waste gas streams are low selectivity and the formation of unwanted by-products such as NOx, O_3, and solid residue in the DBD reactor. The formation of solid residue may eventually foul the NTP reactor. Though some researchers applied plasma catalytic systems to decompose VOCs, the major limitations of the catalytic systems were the high cost of catalysts, catalyst deactivation and disposal, and carbon deposition due to the complex nature of VOCs. Furthermore, there is still a knowledge gap on the optimal oxygen concentration for the

decomposition of alkanes. To address these problems, there is an urgent need to optimise the non-catalytic plasma system for the abatement of VOCs by improving removal efficiency, product selectivity, and the elimination of unwanted by-products. In addition, the influence of water vapour on the decomposition of VOCs in DBD is not negligible since industrial oxidation processes can release exhaust gases containing water vapours (Liotta, 2010). Hence, water vapour's role in hexane decomposition must be investigated.

2.7.2 Cyclohexane

Cyclohexane plays a significant role in the modern world due to its presence in consumer products such as diesel fuels, jet fuels, and chemical solvents. Cyclohexane is one of the most common cycloalkanes and is classified as a highly volatile organic compound. It is produced industrially from the hydrogenation of benzene. Recent research shows that producers of cyclohexane account for 11.4% of the global demand for benzene (Salamanca *et al.*, 2017). In addition, cyclohexane is one of the most used non-polar solvents globally and is an intermediate in the production of nylon 6, 6. About 55% of the global use of cyclohexane is in the synthesis of adipic acid, and ~26 % for caprolactam production. In 2013, about 3.5 Mt of adipic acid were produced worldwide, and nearly 95% of the global production of adipic acid was achieved through the oxidation of cyclohexane (between 125 and 165℃). This has significantly increased cyclohexane emission to the ambient air (Kuo *et al.*, 2014). Other sources of cyclohexane emission include spills from petroleum products, solvent usage, and rubber industries.

Młotek *et al.* (2015) investigated the removal of cyclohexane from ambient air using a 3-phase gliding arc plasma reactor. The study evaluated the effect of plasma power, inlet concentration and gas flow rates on cyclohexane removal efficiency in synthetic air carrier gas over Ni/cordierite and Ni_3Al catalyst. It was reported that the removal efficiency of cyclohexane increased with power at constant concentration due to the increase in electric field strength. The removal efficiency increased with residence time due to more significant contact between the cyclohexane molecules and highly energetic electrons in the plasma zone. Furthermore, the selectivity to CO_2 increased with plasma power and residence time, while the selectivity to lower hydrocarbons decreased. At “high” concentrations, i.e., the removal efficiency remained the same when the cyclohexane concentration was above 0.5% vol. Carbon dioxide, water, acetylene, methane and solid deposits was identified as the main products of cyclohexane decomposition (Młotek *et al.*, 2015). In addition, the selectivity to LHC was very low: only traces of C_1-C_3 hydrocarbons were detected at high power, although after the experiments, the deposition of electrode material and soot was observed. In another study, Raju *et al.* (2013)

studied plasma catalytic decomposition of a mixture of cyclohexane (75 ppm), n-hexane (100 ppm) and p-xylene (75 ppm) in a DBD reactor (over sintered metal fibres-made of Fe-Cr alloy) SMF, CoO_X/SMF, MnO_x/SMF catalyst using dry and humid air (2.3 vol% humidity) carrier gases at 298K respectively. It was reported that the removal efficiency of cyclohexane increased with increasing specific input energy. It was also observed that the presence of $OH^{\cdot}$ radicals in the water vapour resulted in higher removal efficiency of cyclohexane at given specific input energy over a MnO_X/SMF catalyst. The major limiting factors from previous studies of cyclohexane decomposition include the formation of toxic by-products such as ozone and NO_X. Furthermore, the formation of solid deposits in the reactor may cause fouling problems after prolonged operation, high energy consumption and low selectivity.

2.7.3 Benzene

Benzene is one of the most common aromatic VOCs widely used in chemical processing industries, and its emission is problematic due to its high toxicity (Ye *et al.*, 2008). According to the International Agency for Research on Cancer (IARC), excessive exposure to VOCs such as benzene in the air has increased the risk of developing cancer (IARC, 2017). For example, leukaemia can be caused by benzene emissions (Hanna *et al.*, 2007), and there is a clear relationship between VOC emissions and brain cancer (Boeglin *et al.*, 2006; Karatum *et al.*, 2016). In recent years, various attempts have been made to remove benzene emissions from ambient air using NTP-DBD systems. Ye *et al.* (2008) studied the removal of benzene in a DBD reactor using air (RH= 70%). They reported that the removal efficiency of benzene significantly increased with increasing plasma power at a constant initial concentration. They also obtained a maximum removal efficiency of about 45% at higher power (112 W). They also observed that the removal efficiency decreased with increasing inlet concentrations of benzene. However, a brown polymeric residue was formed on the reactor's inner wall, which might eventually lead to the mechanical breakdown of the dielectric owing to thermal energy build-up. Cal *et al.* (2001) studied the removal of benzene in a planar DBD reactor as a function of relative humidity (RH). They found that about >99.9% benzene was removed in both dry and humidified air gas streams. However, the degree of mineralization in humidified plasma increased compared to dry air plasma. Unfortunately, high relative humidity causes a polymeric residue to form on the dielectric plates, which reduces the removal of benzene over time. Kim *et al.* (2008) studied the effect of oxygen concentration and discovered that a 3–5% O_2 concentration was optimal for benzene decomposition using a DBD plasma. The removal efficiency was substantially reduced when the oxygen content rises. They believe that the contribution of N radicals and excited N_2 molecules to higher benzene degradation at lower O_2

partial pressure is due to the contribution of N radicals and excited N_2 molecules. Lee *et al.* (2004) investigated benzene decomposition (100 ppm) in a DBD reactor using air. They reported that O radicals from O_2 react with benzene to produce H_2O and CO_2. The final decomposition products were not complete oxidation of H_2O and CO_2. However, benzene was also converted into secondary products such as phenol, benzenediol and benzaldehyde. From their findings, it was expected that the hydrocarbon radicals formed can react with other reaction intermediates in the oxidation stage to produce higher aromatics compounds which are undesired by-products that can limit the application of DBD reactors. Some researchers also reported that the optimum amount of humidity to achieve the maximum benzene degradation was between 30% and 40% relative humidity (Jiang *et al.*, 2016; Ma *et al.*, 2016). For example, Ma *et al.* (2016) investigated the influence of relative humidity (RH = 0 – 83%) on benzene decomposition using DBD non-thermal plasma reactor. They observed the maximum removal efficiency of benzene at a relative humidity of 40%, which significantly decreased with increasing the relative humidity. The removal efficiency of benzene increased as a result of the formation of OH radicals when water vapour was introduced to the DBD system. However, the removal efficiency decreased to 69% when the relative humidity increased to 80%. In another study, Jiang *et al.* (2016) investigated the influence of water vapour (relative humidity 0 to 80%) on the plasma-assisted decomposition of benzene. They reported that the removal efficiency and CO_2 selectivity increased when the relative humidity increased from 0 to 30%. They obtained the maximum removal efficiency of benzene at 30% relative humidity, which significantly decreased when relative humidity increased above 30%. However, solid residue was accumulated in the reactor. Saleem *et al.* (2019g) investigated benzene decomposition in H_2 and CO_2 carrier gases using a DBD reactor. They reported almost complete removal of benzene in both H_2 and CO_2 carrier gases. They found that the removal efficiency of benzene increased with plasma power and residence time. However, solid residues were formed in both carrier gases. These solid residues are undesired by-products of the NTP decomposition of VOCs and may cause operational problems.

The formation of high concentrations of O_3 and NO_X during benzene decomposition has been reported in previous studies of plasma DBD decomposition of benzene (Jiang *et al.*, 2016; Ma *et al.*, 2016). The generation of O_3 and NO_X is inevitable during plasma discharge of the DBD reactors, which are serious air pollutants. Solid residue formation and poor product selectivity are the main drawbacks limiting the application of the NTP-DBD system for VOC reduction. The solid residues must be eliminated to optimize the performance of the NTP reactors in

practical applications. Therefore, the complete removal of benzene into less toxic by-products is essential.

Water vapour is an important parameter in VOC decomposition in NTP-DBD reactors. Determination of the role of H_2O vapour is of great interest because most of the emissions from chemical processing industries contain water vapour in the gas streams under fluctuating conditions (Vandenbroucke *et al.*, 2011). The H_2O molecule has electronegative properties, and it can be transformed into OH and H radicals in a DBD reactor through an electron-impacted reaction, as reported by (Vandenbroucke *et al.*, 2011; Abdelaziz *et al.*, 2018), as shown in R(2.10) – R(2.13).

$$e + H_2O \rightarrow e + OH^{\cdot} + H^{\cdot} \qquad R(2.10)$$

$$N_2(A^3\sum_u{}^+) + H_2O \rightarrow N_2 + OH^{\cdot} + H^{\cdot} \qquad R(2.11)$$

$$e + O_2 \rightarrow e + O(^1D) + O(^3P) \qquad R(2.12)$$

$$O(^1D) + H_2O \rightarrow 2OH^{\cdot} \qquad R(2.13)$$

Previous studies on the decomposition of benzene under the influence of humidity indicated that water vapour could influence benzene decomposition in the following ways;

(i) the addition of a small amount of water vapour is thought to substantially impact the formation of active species. The concentrations of OH and H radicals could be increased by the presence of water vapour, leading to an increased number of reactive species in the plasma, resulting in higher removal efficiencies and CO_2 selectivity (Jiang *et al.*, 2016; Ma *et al.*, 2016).

(ii) excess water vapour has a negative impact on benzene removal because of its electronegative properties, which limit electron density and quench active radicals (Jiang *et al.*, 2016; Ma *et al.*, 2016).

(iii) In addition, water vapour can also alter the properties of the discharge. When water vapour accumulated on the dielectric surface, the surface resistance decreased. The effective dielectric capacity decreased, decreasing the total current and the number of energetic electrons in the system (Falkenstein *et al.*, 1997).

Thus, understanding the influence of water vapour in the decomposition of VOCs must be thoroughly investigated. In addition, a better understanding of the benzene decomposition pathways in an NTP system using dry and wet air would be beneficial in developing an efficient DBD technique involving various plasma species with optimized removal efficiency.

2.7.4 Methanol

Methanol is one of the most common alcohols and is a key product in the chemical industry. It is mainly used to produce other chemicals, such as acetic acid, formaldehyde, and polymers (Irena and methanol institute, 2021). Methanol is classified as a "highly volatile" alcohol that has been widely used as a solvent in the chemical processing industries (Zhu *et al.*, 2016b). Recent research shows that methanol production has nearly doubled in the past decade. Under the current situation, the production rate could rise to about 500 Mt per annum by 2050, leading to increased methanol emissions (Irena and methanol institute, 2021). Long-term exposure to methanol can cause nausea, headaches, blurred vision and neurological damage (Zhu *et al.*, 2016b).

Previous researchers have studied the use of DBD plasma reactors to decompose odorous VOCs such as methanol. Sato *et al.* (2005) investigated methanol decomposition in a DBD reactor at a 16-20 kV voltage using an air carrier gas. Although a high removal efficiency was achieved, they did not report the product's composition. The hydrogen concentration and yield were not reported in their studies. Wang *et al.* (2016) reported the direct conversion of methanol into value-added chemicals and fuels in a DBD reactor using an N_2 carrier gas. They studied the influence of processing parameters such as plasma power (20 – 50 W), methanol inlet concentration and pre-heating temperature (80 ℃) using a DBD reactor consisting of stainless-steel mesh, discharge length of 100 mm, discharge gap of 2 mm, frequency of about 8-12 kHz and peak voltage of 30 kV. They reported a removal efficiency of 74% at 50 W and a constant concentration of CH_3OH in N_2 flow rate of 250 ml/min. It was demonstrated that increasing the power increased the methanol removal efficiency and product selectivity to n-C_4H_{10}, H_2, and CO. Therefore, optimizing plasma power could be an efficient way of reducing the generation of CO. Wang *et al.* (2019) studied methanol oxidation in a DBD reactor using an air carrier gas. They reported that for an NTP-only system, the removal efficiency of methanol increased from 14.1% to 43.9% when the input power increased from 0.3 to 0.9 W. Their findings showed the formation of a high concentration of O_3 (about 773 ppm), which is an undesirable by-product that can limit the usage of NTP-DBD reactors. Futamura *et al.* (2004) observed relatively low methanol conversions (between 8-26%) at 1-mol % inlet concentration and a gas flow rate of 100 ml/min using N_2 in two different configurations of the DBD reactor. In another study, Shuji Tanabe (2000) used a DBD reactor to decompose methanol to hydrogen using argon carrier gas at a low voltage of 2-6 kV. They obtained a maximum removal efficiency of 80%, and the yield of H_2 increased with increasing plasma power in the absence of humidity. They reported a significant increase in the yield of H_2 when H_2O was introduced to the DBD system. CO or

CO_2 was the other main product. They also reported that, in addition to methanol decomposition to H_2 and CO, the reaction between CH_3OH and H_2O produced H_2 and CO_2 simultaneously. Their findings explained the influence of H_2O in converting CH_3OH to H_2 and CO_2. In humid plasma, H and OH radicals can be generated through electron impact dissociation of H_2O molecules. OH is an important radical in the NTP system, which can oxidise CO and hydrocarbons intermediates resulting to the formation of high CO_2. Norsic *et al.* (2018) investigated methanol oxidation using dry and humidified air carrier gases. They reported a removal efficiency of 60% in dry air plasma, which decreased to 43% when water vapour with a relative humidity of 35% was introduced to the DBD system. Their findings showed that high humidity had an inhibitive influence on methanol decomposition and hindered the formation of secondary products such as formaldehyde, methylal and methyl formate. They reported that the presence of water vapour with very low humidity enhances the OH radical concentration which can increase the chemical reactivity. The affinity of formaldehyde (HCOH) to H_2O would promote its conversion into CO_2 instead of CO. In addition, the complete oxidation of methylal and methyl formate under the influence of water vapour can also increase selectivity to CO_2.

Compared to catalytic oxidation processes, treatment with NTP-only systems successfully reduced low methanol concentrations with minimal energy usage. However, the process is adversely affected by high humidity, and because it is non-selective, it produces undesired by-products such as O_3 and NOx. In addition, the features of the plasma discharge characteristic and the chemistry of the plasma are influenced by the water vapour in the gas stream, which has a substantial impact on the removal efficiency. High humidities reduced the current at constant applied voltage due to the dielectric's surface resistance alteration and lowered the transferred charges between the electrodes, limiting the plasma volume (Falkenstein *et al.*, 1997). Solid residue formation can cause fouling problems for the DBD reactors over a long operation. Rico et al. (2010) reported the formation of coke during the conversion of CH_3OH into CO and H_2 using a DBD reactor.

2.8 **Summary**

Despite numerous previous efforts to remove various VOCs from ambient air gas streams using NTPs, various problems persist, including low removal efficiency, low selectivity, high ozone generation, and the formation of unwanted by-products such as NO_x and solid deposition. The formation of solid deposits in the reactor will cause arcing and blockage problems after prolonged operation. The solid residue can change the dielectric constant of the quartz tube and interfere with the overall performance of the plasma DBD reactor. Therefore, it is necessary to

optimize the performance of NTP-only systems by systematically investigating the effect of various carrier gases, oxygen concentrations, plasma power, residence time, VOC inlet concentrations and moisture content on the removal efficiency, product selectivity and elimination of the solid residue in the DBD reactor. Furthermore, understanding the VOC decomposition pathways in the plasma-only system using different carrier gases is necessary for the full application/scale-up of NTP-DBD technology. Since most of the emissions from the chemical processing industries contain water vapour in the gas streams at fluctuating conditions, the inclusion of dry and humidified air carrier gases will allow the role of H_2O-derived radicals to be explored.

Table 2.7 give an overview of the previous studies on VOC decomposition using NTPs.

Table 2.7 An overview of the previous work on VOCs decomposition with NTP

VOCs	Type of NTP reactor	Carrier gas	C_{in} (ppm)	Flow rate (ml/min)	RE (%)	Energy yield (g/kWh)	Main by-products	References
Toluene	DBD	Air	95.0	6600	74.0	2.60	Benzoic acid crystals	(Karatum *et al.*, 2016)
Toluene	DBD	Nitrogen	400	2000	21.1	4.70	Brown solid deposits	(Ognier *et al.*, 2007)
		Dry air			23.0	5.20		
Toluene	DBD	Air	1000	200	70.0	32.2	Benzoic acid residue	(Ban *et al.*, 2006)
Toluene	DBD	Humid air (RH = 55%)	100	1000	46.0	0.30		
Propane	DBD	Air	100	2000	17.4	1.41	NOx	(Hill *et al.*, 2007)
Propane	PCD	Air	14000	500	68.1	4.50	n.d	(Jarrige *et al.*, 2006)
Hexane	DBD	Air 15% O_2 (N_2 balance)	367	500	78.2	0.81	O_3, 3-hexanone and 2-hexanone	(Jin *et al.*, 2016)
Hexane	CD	Air	500	800	57.1	-	O_3, Black solid deposits	(Marotta *et al.*, 2007)
Hexane	GAD	Air	968	1170	81.3	-	NOx	(Yan *et al.*, 2007)
		Nitrogen			57.1			
		Argon			56.0			
Cyclohexane	GAD	Air	0.5, 1% vol.	3333	92.5	-	Solid residue	(Młotek *et al.*, 2015)
Benzene	DBD	Humid air (RH =70%)	276	10^4	45.4	3.90	Brown polymeric residue	(Ye *et al.*, 2008)
Benzene	DBD	Dry air	200	4000-5000	75.2	5.70	O_3	(Kim *et al.*, 2008)
		(5% O_2)						
Benzene	DBD	Air	500-2700	500-2000	>99.9	-	Polymeric residue	(Cal *et al.*, 2001)

		(RH = 0-90%)						
Benzene	DBD	Dry air	100	200	90.0	1.50	Benzoic nitric and phenol	(Lee *et al.*, 2004)
Benzene	DBD	Air	95.0	6600	58.0	0.50	Solid residue	(Karatum *et al.*, 2016)
Benzene	DBD	Humid air	500	1400	75.1	15.2	NOx, O_3, Phenol derivative	(Ma *et al.*, 2016)
Benzene	Hybrid surface/packed-bed discharge (HSPBD)	Air	400	500	65.0	-	Solid residue, NOx, O_3, formic acid	(Jiang *et al.*, 2016)
Methanol	DBD	Nitrogen	18.0 mol%	250	74.0	5.00	1,5-heptadien-3-yne	(Wang *et al.*, 2016)
Methanol	DBD	Nitrogen/Air	446	1000	44.0	1.30	O_3, HCHO and HCOOH	(Wang *et al.*, 2019)
Methanol	SDBD	Dry air	50.0	5000	60.0	0.16	O_3, HCOH	(Norsic *et al.*, 2018)
		Humid air (RH= 35%)			43.1	0.12		

Chapter 3. Materials and methods

3.1 Materials and methods

This chapter describes the materials, equipment, experimental setup, and methodology used for this research. The materials and chemicals used for this research and their specifications are presented in Table 3.1. Table 3.2 shows the lists of the equipment used for the decomposition of hexane, cyclohexane, benzene, and methanol. Methanol (≥ 99.9%), hexane (95%), cyclohexane (99.5%), and benzene (99.8%) were purchased from Sigma Aldrich. Pure nitrogen (≥ 99.9%), dry air (zero grade) consisting of 80% N_2, 20% O_2, and oxygen (>99.9%) were purchased from BOC industrial gases (UK). The purity of hexane is 95% because it consists of typical impurities such as non-volatile matter, sulphur compounds, aromatic hydrocarbons (C_6H_6), thiophene and water. The presence of impurities cannot affect the findings because the hexane purity is 95.0% which is the minimum assay for plasma/GC analysis.

Table 3.1 Materials and chemicals.

Material	Product	Model/Purity
Methanol	Sigma-Aldrich	≥ 99.9%
Hexane	Sigma-Aldrich	95%
Cyclohexane	Sigma-Aldrich	99.5%
Benzene	Sigma-Aldrich	99.8%
Nitrogen gas	BOC	≥ 99.9%
Dry air gas	BOC	Zero grade
Oxygen gas	BOC	>99.9%

Table 3.2 List of equipment for the decomposition of VOC.

Equipment	Uses/Product	Availability/Model
DBD reactor	Decomposition of VOC	PI-Laboratory SCEAM
Gas Chromatography	Varian/Agilent	Varian 450 – GC
Digital Weighing Balance	RADWAG	AS 220/C/2
Digital Flowmeter	Agilent Technologies	Optiflow 570
Gastec Detector Tube	Gastec	GV-100
Mass Flow Controller	Bronkhorst	F201
GC-MS system	Agilent Technologies	Agilent 8890 GC/5977B MSD

3.2 **Experimental setup**

A schematic of the experimental setup is shown in Figure 3.1 below:

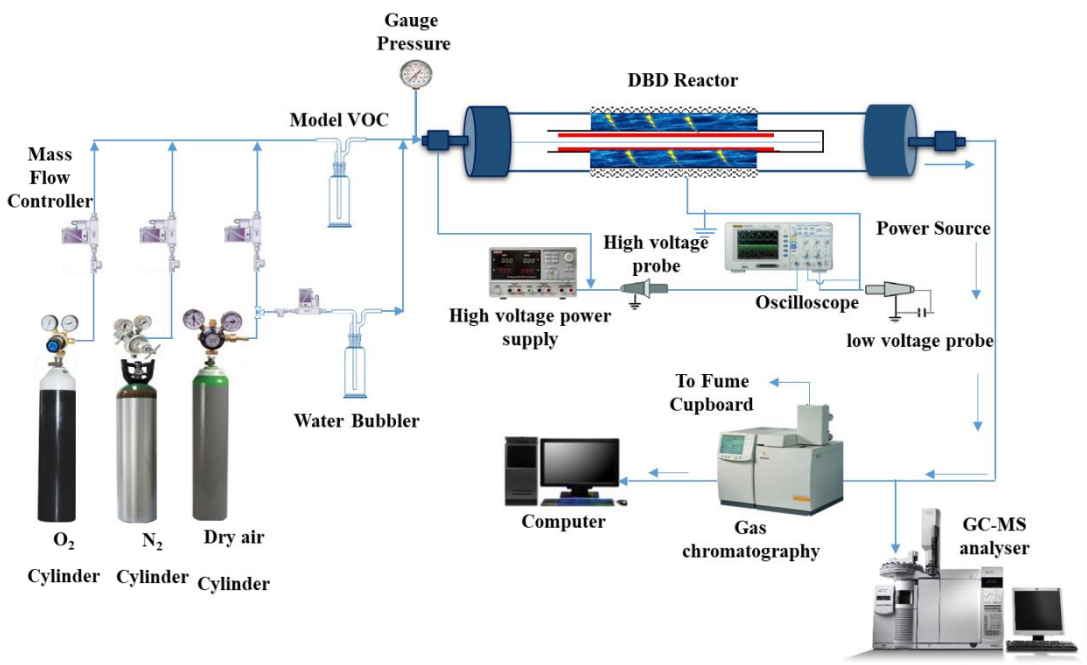

Figure 3.1 A schematic of the experimental setup.

The dielectric barrier discharge (DBD) reactor comprises two coaxial quartz tubes, the smaller one in the inner and the larger one outside. There were two 316 stainless steel metal electrodes: a mesh (60 mm) on the outside of a cylindrical quartz tube (330 mm long, 15 mm internal diameter, and 18 mm external diameter) and the other, a sheet within the inner quartz tube (12 mm outer diameter). One end of the inner quartz tube was closed to allow the gas to pass through the annular gap. The discharge gap was 1.5 mm, and the inner tube was secured with quartz wool to keep the discharge gap consistent. Therefore, the plasma was formed in the space between these coaxial quartz tubes. The discharge zone was 60 mm long (i.e., the length of the exterior mesh), resulting in a discharge volume of 3.82 cm^3. In the current experimental setup, the discharge zone is where the two electrodes overlap. The residence time was calculated based on this volume. The cross-section of the DBD reactor is shown in Figure 3.2.

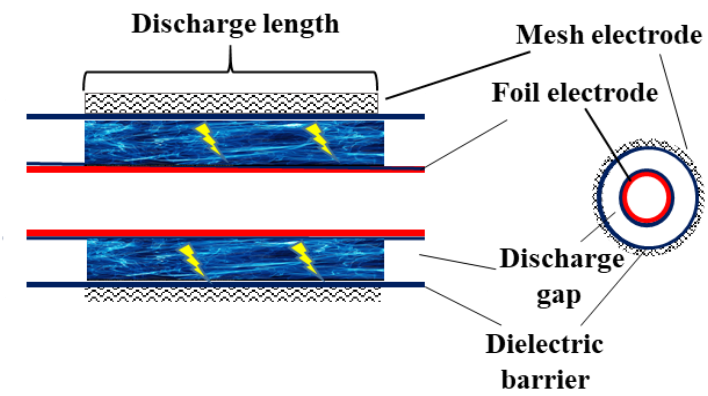

Figure 3.2 Section of DBD plasma reactor.

The plasma generator supplies the power to the dielectric barrier discharge (DBD) system at about 20 kHz. The power source unit of the plasma could provide 0-100 W by regulating the amplitude of the applied voltage. In this work, an alternating sinusoidal high voltage of about 20 kV amplitude (peak-to-peak) and frequency of 20 kHz was applied to the two stainless steel mesh electrodes of the DBD reactor. In addition, a variac AC transformer was used to regulate the power supplied to the reactor from the plasma power source. A P6015A high voltage probe was used to monitor the voltage signal/waveform applied to the plasma DBD reactor, and a PEM CWT003X/B current probe was used to determine the plasma current signal/waveform.

Furthermore, the voltage and current signals were recorded by a TPS 2014 four-channel digital storage oscilloscope (Tektronix). The discharge power was determined by integrating the current signal I(t) and the voltage (U(t)) recorded by the oscilloscope.

$$P = \frac{1}{T}\int_0^T U(t)I(t)dt \qquad (3.1)$$

Nitrogen and dry air (zero grade) were purchased from BOC industrial gases U.K. As shown in Fig. 1, Bronkhorst F201 mass flow controllers (MFC) were used to control the flow rate of the carrier gases (70-190 ml/min). The carrier gases pass through the model VOC bubbler to be saturated with the desired amount of the VOC (hexane, cyclohexane, benzene, and methanol), respectively. The mixture of the VOC vapour and carrier gas then passed through the DBD reactor. To investigate the influence of O_2 concentration, the flow rates of N_2 (MFC-1) and O_2 (MFC-2) were changed proportionally, but the total flow rate was maintained at 100 ml/min.

In addition, for humidified air experiments, water vapour of relative humidity in the range of 0 – 25% (at 20℃ and atmospheric pressure) was introduced into the non-thermal plasma DBD reactor by passing dry air through a conventional water bubbler kept in a standard water bath (20℃). The relative humidity of the carrier gas (humidified air) was controlled using a humidity

regulator, which was a jacketed Dreschel bottle containing a deionized water. The relative humidity was regulated by varying the flow rate of the dry air passing through the water bubbler using MFC. A Grant LTC1 Water Recycler kept the Dreschel's temperature constant at 20℃. The relative humidity of the humidified air exiting the Dreschel bottle was measured using a calibrated PCE-PCO 1 humidity meter.

To study the effect of moisture content on the reaction of the benzene decomposition, water vapour with RH in the range of 0, 15, 25, 35 and 40% (at 1 atmosphere and 20℃) was supplied to the DBD system through a water bubbler kept in a standard water bath (20℃).

Figure 3.3 shows the DBD plasma reactor used in a laboratory setup for this research.

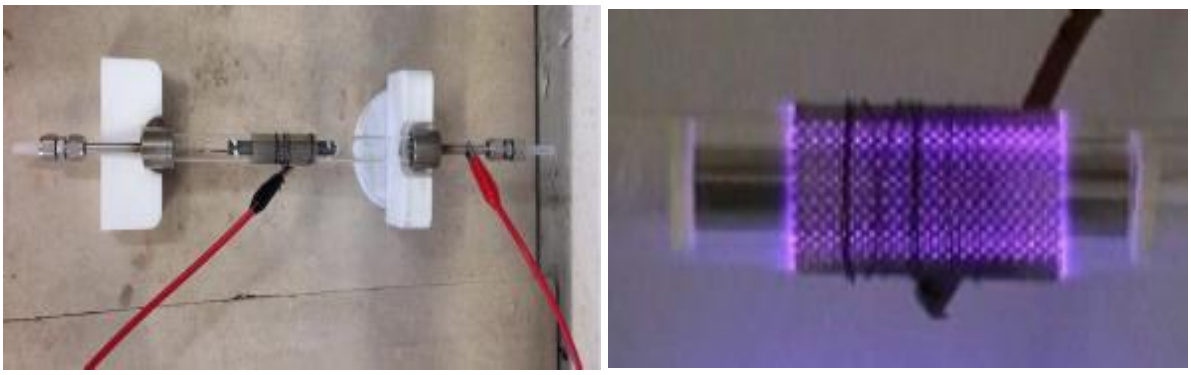

Figure 3.3. The DBD plasma reactor in a laboratory setup.

3.3 GC calibration and product analysis

The Varian 450 gas chromatograph was calibrated for each model VOC. To determine the peak areas, known concentrations of hexane, cyclohexane, benzene, and methanol were injected into the gas chromatograph. A calibration curve was then developed by plotting the peak areas obtained as a function of concentrations. All tests were carried out under controlled reaction settings of standard temperature and pressure (STP) and were repeated three times.

The inlet and outlet concentration of the model VOC and the product gas composition were determined by a Varian 450-GC equipped with a thermal conductivity detector (TCD) and a flame ionization detector (FID). The TCD detector was used for measuring methane, carbon dioxide, hydrogen, oxygen, nitrogen and carbon monoxide and the FID for measuring the concentrations of the model VOC and lower hydrocarbons (LHC- C_1-C_5).

The concentrations of NO + NO_2 at the reactor outlet when working at a steady-state were analysed with the aid of GV-100 Gastec tube detectors (detection limit = 0.01 ppm and accuracy = $\pm$0.05 ppm). The gas samples were collected from the reactor outlet in a gas sampling bag. A freshly sealed NO_x detector tube was inserted into the pump. The tips of the fresh detector

tubes were broken with the aid of the tube tip breaker in the Gastec pump. The tube was inserted into the pump inlet with the arrow on the tube pointed toward the pump. The guide marks on the pump body aligned with the handle's guide marks. The detector tube was connected to the gas sampling bag. The handle of the Gastec pump was pulled all the way out until it was locked at one pump stroke (100 ml), and two minutes were allowed to complete and confirm the sampling. The concentration levels of NO_x at the interface where the stained reagent meets the unstained reagent were measured.

The plasma zone wall temperature was measured by FLIR TG165 imaging IR thermometer, and the downstream gas temperature was measured using RS-PRO digital thermometer, as shown in Figure 3.4. The thermocouple was used to measure the gas temperature at different plasma power (2 – 10 W), and the plasma zone wall temperatures were also recorded.

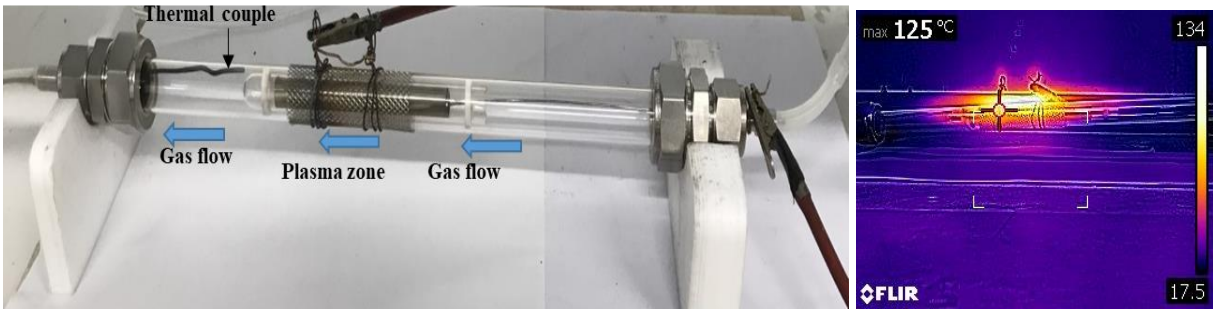

Figure 3.4 Setup for temperature measurement

The mass of the residue formed in the DBD reactor was determined by the simple weighing method. The DBD reactor was weighed before and after the experimental runs. The hexane was used to dissolve collected solid residue and filtered by a 0.22- µm organic phase needle-filter and analysed with a GC-MS analyser (Models Agilent 8890GC/5977B MSD single quadrupole MS with Electron Impact (EI) ionisation source). The GC-MS analyser is equipped with capillary column Rtx 1701: 0.25 mm ID × 0.25 µm film thickness × 60 m length. The injection volume was 1 µL, and the inlet temperature was 250 °C. The sample analysis was performed using the MS scan mode, which was qualitatively evaluated based on peak areas and retention times. The data analysis was conducted using Agilent mass hunter software. In addition, a cooling trap was used to collect the condensable products of benzene decomposition in the gas stream from the outlet of the plasma DBD reactor. The condensable products were continuously collected using hexane (purity 95% anhydrous, Sigma-Aldrich) at a relative humidity of 35%, at 20°C, 10 W, 350 ppm and 2.3 s for 8 hours. The collected liquid sample was analysed using GC-MS and qualitatively identified using the mass spectral library of the National Institutes of Standards and Technology (NIST).

3.4 **Ozone measurement**

Ozone concentrations from the outlet of the DBD reactor were measured using the standard potassium iodide (KI) titration technique (U Chasanah, 2019; Yulianto *et al.*, 2019).

Figure 3.5 shows the schematic setup of ozone measurement.

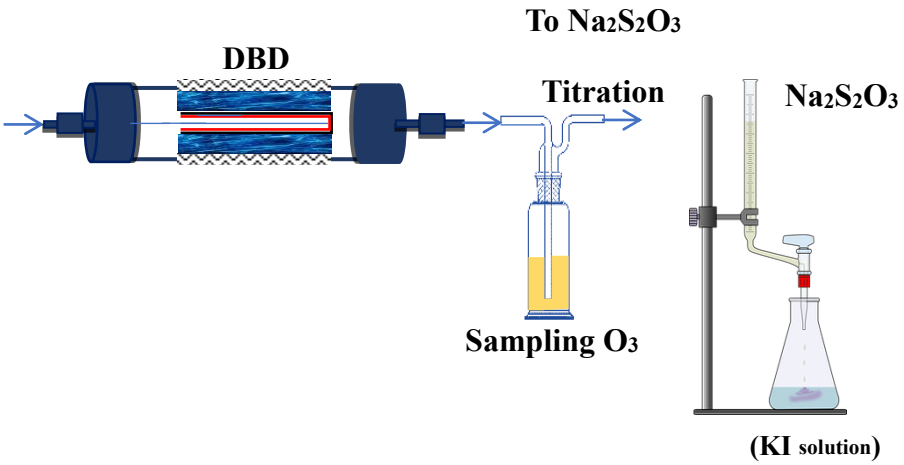

Figure 3.5 Schematic setup of the ozone measurement.

The amount of ozone produced was determined by passing the gas stream through a 0.2M KI trap with a known volume of at least 100 mL and an exposure time of about 10 minutes. The colour of the KI solution was changed from clear to yellow-brown showing ozone oxidised KI solution. The O_3 was calculated using the reaction of I^- with O_3, which produced I_2. The I_2 was formed through oxidation reaction R(3.2).

$$O_3 + 2I^- + H_2O \rightarrow I_2 + 2OH^- + O_2 \qquad \text{R(3.2)}$$

Titrations were performed using 0.005N sodium thiosulfate and 5 mL of 2N H_2SO_4 as an indicator until the yellow iodine colour disappeared. In this work, 1 - 2 mL of starch indicator solution was added, which turned the solution blue. Titrations were performed until the amount of I_2 was proportional to the amount of sodium thiosulfate, as indicated by a change in colour from brownish-yellow to clear and colourless. The number of moles of O_3 was equal to half the number of moles of iodine, according to the chemical equation R(3.3).

$$I_2 + 2Na_2S_2O_3 \rightarrow 2NaI + Na_2S_4O_6 \qquad \text{R(3.3)}$$

Therefore, O_3 concentration can be calculated using equation 3.4.

$$O_3(\text{ppm}) = \frac{R \times V_t \times M \times 1000}{Q \times t} \qquad \text{R(3.4)}$$

where O_3 is the ozone concentration in ppm, V_t is the total volume of titrant (sodium thiosulfate) in litres, R is the gas constant, M is the molarity of titrant (sodium thiosulfate) in mol/L, Q is the total flow rate in ml/min and t is the time of exposure of ozone to the KI solution.

3.5 **Experimental variables**

The experimental variables studied were:

1. Model VOCs:
    a. hexane (C_6H_{14})
    b. cyclohexane (C_6H_{12})
    c. benzene (C_6H_6)
    d. methanol (CH_3OH)

The model VOCs were chosen because alkanes (including cycloalkanes), aromatics, and alcohol hydrocarbons constitute the most common anthropogenic VOCs in the atmosphere. Hexane, cyclohexane, benzene, and methanol are more easily emitted into the environment than any other VOC and are typically volatile, allowing them to enter the earth's atmosphere quickly (Vandenbroucke *et al.*, 2011). Furthermore, hexane, cyclohexane, and benzene have been chosen to represent the C_6 sequence to explore the plasma-assisted decomposition differences between straight-chain, ring, and aromatic compounds. Methanol was also chosen when a specific industrial problem with a local industrial partner (confidential) was identified. The dry air, humidified air, and nitrogen were chosen because they are usually present in the air in most pollution sources. The selection of dry and humidified air allowed the role of water derived radicals to be investigated. They can help develop the mechanism of VOC decomposition.

2. Concentration: 220 – 520 ppm.

The concentration of VOCs was chosen based on the permissible exposure limit (PEL). VOC concentrations below and above the PEL were selected to study the concentration's effect on the removal efficiency.

3. Plasma power: 2 -10 W.

The plasma power is an important parameter in the plasma system. It was hoped that an optimal plasma power could be discovered to allow for satisfactory VOC decomposition while keeping the process's operating costs to a minimum. In the current laboratory setup, the maximum power the plasma could be subjected to was around 100 W. The plasma power in the range of 2 to 10 W was chosen based on the previous findings. The performance of the DBD reactor at 10 W would be evaluated in terms of removal efficiency, and if necessary, a higher plasma power

would be explored. It was also decided that testing five levels of plasma power, with increments of 2 W, would provide a sufficient body of data for the study.

4. Residence time:

The residence time within the plasma region of the DBD reactor was investigated to determine how it affected the VOC decomposition in the gas stream. The residence time was changed by changing the flow of nitrogen and dry air gases using a Bronkhorst mass flow controller. The different levels of gas flow rate were chosen to generate a good amount of data to evaluate the impact of residence time on the VOC decomposition. The flow rate levels were set at 70, 100, 130, 160 and 190 ml/min. The VOC removal efficiency using the chosen flow rates was to be evaluated, and if necessary, the flow rates were decreased or increased to get the desired range of VOC conversion. A "plasma volume" of 3.82 cm^3 was used to convert the flow rates into respective residence times of 3.3, 2.3, 1.8, 1.4 and 1.2 s.

3.6 Experimental procedure

1. The DBD reactor was placed inside the fume cupboard. The clips of the power source unit were attached to the plasma device, one with the central metallic mesh around the quartz tube and the other to the top end of the reactor cap, as shown in Figure 3.3.
2. The carrier gas cylinder (N_2 or dry air) was opened, and the flow streams were connected to the bubbler with the aid of Bronkhorst F201 mass flow controllers. The gas was bubbled through the VOC bubbler at a specified flow rate, which entrained the model VOC before flowing into the plasma DBD reactor. An online Varian 450 gas chromatography was connected to the exit of the DBD reactor to measure the concentration of the gaseous products.
3. The dielectric barrier discharge reactor was continually purged (for 30 minutes) by the selected carrier gas (N_2 or dry air) to remove air from the system once all connections were made (confirmed by GC analysis). A computer-controlled mass flow controller was then used to determine the flow rate of a specific gas. After stabilising the flow, a digital bubbler flow meter was used to check the actual flow rate.
4. After stabilising the flow rate, blank (no plasma) runs were completed to determine the initial peak areas of hexane, cyclohexane, benzene, and methanol using nitrogen, dry and humidified air. In the blank run, the plasma power was turned off to determine the inlet concentrations of hexane, cyclohexane, benzene, and methanol in the absence of any reaction. The blank run also aided in detecting any noise in the GC interface. Before

each run of experiments, the blank run was tested at least two times after obtaining a stable reading.

5. For determining the steady state before final measurements, the peak area of the initial concentration of the model VOC, conversion and product selectivity were analysed by a GC every 20 minutes. It was noticed from the stability test that the experiments ran in a stable way under plasma conditions after 20 minutes. The peak area of the model VOCs was compared with the peak area of the standards at the same residence time.
6. After obtaining a consistent VOC inlet concentration reading, the power source unit of the plasma systems was turned on and set at a specific wattage using a variac of the HV-plasma controller for at least 10 minutes to remove power variations. An energy meter was used to continuously check the power delivered to the reactor. When the power measurement on the energy metre was stable, the sample was injected into the Varian 450-gas chromatograph.
7. After four minutes of sample injection into the GC, the plasma power was turned off. The GC chromatogram was obtained after 15 minutes.
8. When a considerable amount (visible) of solid residues were formed inside the DBD reactor, it was replaced with a clean/new reactor and steps 3–6 were repeated. The used reactor was cleaned in the furnace for 4 hours at 680-700 ℃.
9. For studying the effect of concentrations, the output stream from the bubbler was diluted with the same carrier gas to alter the concentration of hexane, cyclohexane, benzene, and methanol in the DBD reactor. In addition, a Varian 450-GC was used to measure the variations in VOC inlet concentration.
10. The experimental runs were carried out by altering the level of plasma power, VOC inlet concentrations, residence time, oxygen concentration and relative humidity. All measurements were repeated three times.
11. The amount of the solid/viscous residues formed in the decomposition of VOC (hexane, cyclohexane, and benzene) was determined by a simple weighing method. The dielectric barrier discharge reactor was weighed before and after the experiment, and the solid/viscous residue was analysed using a GC-MS analyser.
12. After the experiment was completed, the plasma system was switched off, and the flow from the control system was lowered to zero. Gas cylinders were closed, and all the connections between the Varian 450 gas chromatography and the DBD reactor were disconnected.

3.7 Definitions

The removal efficiency of volatile organic compounds (VOCs) was defined as:

$$\text{Removal efficiency (\%)} = \frac{[\text{VOC}]_{\text{in}} - [\text{VOC}]_{\text{out}}}{[\text{VOC}]_{\text{in}}} \times 100$$

where $[\text{VOC}]_{\text{in}}$ is the initial concentration of VOC introduced in the reactor and $[\text{VOC}]_{\text{out}}$ is the outlet concentration (ppm).

The specific input energy (SIE) was defined as:

$$\text{Specific input energy (J/L)} = \frac{\text{P(W)}/1000}{\text{Q(L/min)}} \times 60$$

$$\text{Energy yield (EY)} \left(\frac{\text{g}}{\text{kWh}}\right) = \frac{\text{RE.}\,[\text{VOC}]_{\text{in}}.\,\text{M} \times 0.15}{\text{SIE.}\,\text{V}_{\text{m}}}$$

where M is the molecular weight of the VOC in g/mol.c

The hexane removal efficiency was defined as:

$$\text{Removal efficiency (\%)} = \frac{[\text{C}_6\text{H}_{14}]_{\text{in}} - [\text{C}_6\text{H}_{14}]_{\text{out}}}{[\text{C}_6\text{H}_{14}]_{\text{in}}} \times 100$$

The selectivity of different gas products was evaluated using the following equations:

$$\text{LHC selectivity (\%)} = \frac{\sum \text{moles of LHC produced} \times \text{m (mol/min)}}{6 \times \text{moles of C}_6\text{H}_{14}\text{ converted (mol/min)}} \times 100$$

Where LHC: lighter hydrocarbon products (C_1-C_5), m is the number of carbon atoms in the molecules respectively.

$$\text{CO}_2\text{ selectivity (\%)} = \frac{\text{moles of CO}_2\text{ produced}}{6 \times \text{moles of C}_6\text{H}_{14}\text{ converted}} \times 100$$

$$\text{CO selectivity (\%)} = \frac{\text{moles of CO produced}}{6 \times \text{moles of C}_6\text{H}_{14}\text{ converted}} \times 100$$

The cyclohexane removal efficiency was defined as:

$$\text{Removal efficiency (\%)} = \frac{[\text{C}_6\text{H}_{12}]_{\text{in}} - [\text{C}_6\text{H}_{12}]_{\text{out}}}{[\text{C}_6\text{H}_{12}]_{\text{in}}} \times 100$$

$$\text{LHC selectivity (\%)} = \frac{\sum \text{moles of LHC} \times \text{m (mol/min)}}{6 \times \text{moles of converted cyclohexane (mol/min)}} \times 100$$

$$\text{CO}_2\text{ selectivity (\%)} = \frac{\text{moles of CO}_2\text{ produced}}{6 \times \text{moles of converted cyclohexane}} \times 100$$

$$H_2 \text{ yield } (\%) = \frac{\text{moles of } H_2 \text{ produced}}{6 \times \text{moles of } [C_6H_{12}]_{in}} \times 100$$

In humid air carrier gas:

$$H_2 \text{ yield } (\%) = \frac{\text{moles of } H_2 \text{ produced}}{(6 \times \text{moles of } [C_6H_{12}]_{in}) + \text{moles of } H_2O \text{ in}} \times 100$$

The removal efficiency of benzene was defined as:

$$\text{Removal efficiency } (\%) = \frac{[C_6H_6]_{in} - [C_6H_6]_{out}}{[C_6H_6]_{in}} \times 100$$

The selectivity of different gas products was evaluated using the following equations:

$$\text{LHC selectivity } (\%) = \frac{\sum \text{moles of LHC produced} \times m \text{ (mol/min)}}{6 \times \text{moles of } C_6H_6 \text{ converted (mol/min)}} \times 100$$

$$CO_2 \text{ selectivity } (\%) = \frac{\text{moles of } CO_2 \text{ produced}}{6 \times \text{moles of } C_6H_6 \text{ converted}} \times 100$$

$$\text{CO selectivity } (\%) = \frac{\text{moles of CO produced}}{6 \times \text{moles of } C_6H_6 \text{ converted}} \times 100$$

The removal efficiency of methanol was defined as:

$$\text{Removal efficiency } (\%) = \frac{[CH_3OH]_{in} - [CH_3OH]_{out}}{[CH_3OH]_{in}} \times 100$$

The following formulae were used to determine the selectivity of different gas products:

$$C_mH_n \text{ selectivity } (\%) = \frac{\sum \text{moles of } C_mH_n \text{ produced} \times m \text{ (mol/min)}}{\text{moles of } CH_3OH \text{ converted (mol/min)}} \times 100$$

$$CO_2 \text{ selectivity } (\%) = \frac{\text{moles of } CO_2 \text{ produced}}{\text{moles of } [CH_3OH] \text{ converted}} \times 100$$

$$\text{CO selectivity } (\%) = \frac{\text{moles of CO produced}}{\text{moles of } [CH_3OH] \text{ converted}} \times 100$$

The yield of hydrogen was defined as:

$$H_2 \text{ yield } (\%) = \frac{\text{moles of } H_2 \text{ produced}}{2 \times \text{moles of } [CH_3OH]_{in} + \text{moles of } H_2O \text{ In}} \times 100$$

$$\text{Carbon balance (CB)} = \frac{\sum C_{out}}{\sum C_{in}} \times 100$$

Chapter 4. Oxidative removal of hexane from the gas stream in a dielectric barrier discharge reactor

4.1 **Introduction**

In this chapter, the removal of hexane from a gas stream using a dielectric barrier discharge (DBD) reactor was investigated at ambient temperature and atmospheric pressure. The roles of N_2, dry and humidified air carrier gases were studied in terms of removal efficiency, product selectivity and elimination of unwanted by-products. The oxygen concentration was also varied over 0 – 21% at constant power and residence time in an N_2-O_2 mixture for further insight into oxygen's role. The effect of plasma power on the plasma zone wall and the downstream gas temperature was also investigated.

4.2 **Results and discussion**

4.2.1 Effect of power and carrier gases

The influence of plasma power on the removal efficiency of hexane in N_2, dry and humidified air carrier gases are presented in Figure 4.1. In this study, the influence of the carrier gases: N_2, dry and humidified air, was studied at constant inlet concentration and residence time. The input power of the plasma reactor was varied over the range of 2-10 W at ambient temperature and atmospheric pressure. It was observed that the removal efficiency of hexane increased proportionally with increasing plasma power regardless of the carrier used. The higher plasma power could increase the numbers and the mean energy of the energetic electrons, thereby increasing the amounts of reactive species due to collision between the energetic electrons and gas molecules (Zhu *et al.*, 2015). The collision probability between hexane molecules and reactive species increased accordingly. As a result, the hexane removal efficiency was increased.

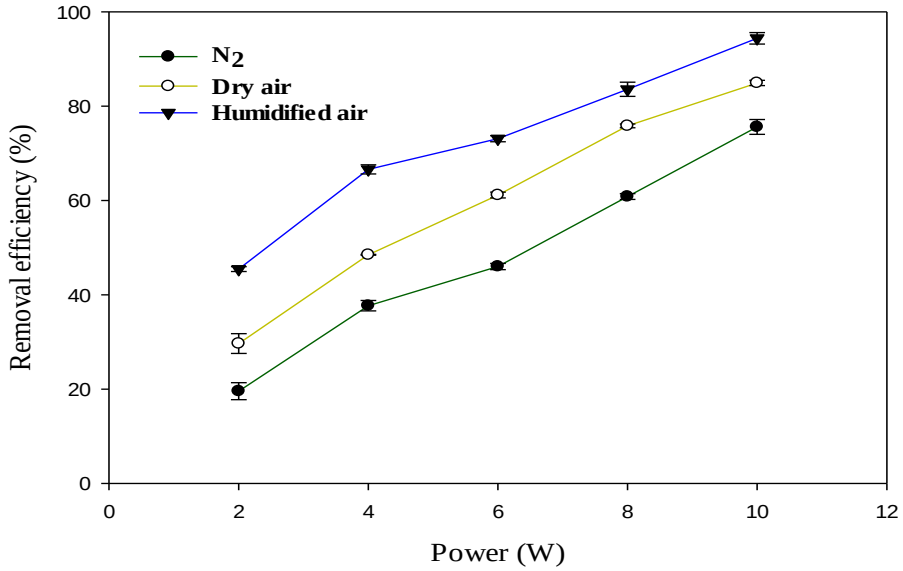

Figure 4.1 Effect of power and carrier gases on the removal efficiency of hexane (Reaction conditions: temperature = ambient; Inlet concentration of hexane = 350 ppm; Total flow rate = 100 ml/min; Residence time = 2.3 s; SIE = 1.2 – 6 kJ/L).

Increasing the plasma power at constant inlet concentration and residence time would increase the number of energetic electrons and reactive species in the plasma reactor. As the power increased, the probability of the collision between the reactive species and VOC molecules in the plasma discharge zone increased, which enhanced the removal efficiency (Karatum *et al.*, 2016). The removal efficiency of hexane increased from 19.6 (N_2), 29.7% (dry air), 45.5% (humidified air) to 75.6%, 84.9% and 94.4% when the power increased from 2 to 10 W, respectively.

Humidified air carrier gas showed the highest removal efficiency of 94.4%, followed by dry air (84.9%) and nitrogen (75.6%). This is probably due to the formation of O and OH radicals in dry and humidified air carrier gases. It has been reported that the oxidation power of OH radicals is higher than excited O_2 species or other radicals generated in non-thermal plasma reactors (Sun *et al.*, 1997). Relative humidities of 25% and 30% have been reported to increase cyclohexane and benzene's removal efficiency due to the influence of OH in the plasma decomposition process (Kim *et al.*, 2003).

Figure 4.2 presents the system's energy yield as a function of power. The energy yield was determined and analyzed at a constant initial concentration and fixed residence time at ambient temperature and atmospheric pressure. It was observed that the energy yield decreased with increasing plasma power in all the carrier gases, even though the removal efficiency of hexane increased. This may be partially due to energy loss to vibration and electronic excitation of

carrier gas molecules, resulting in decreased input energy (Mustafa *et al.*, 2018). In addition, there are "diminishing returns" as the plasma input power increases (Saleem *et al.*, 2019f).

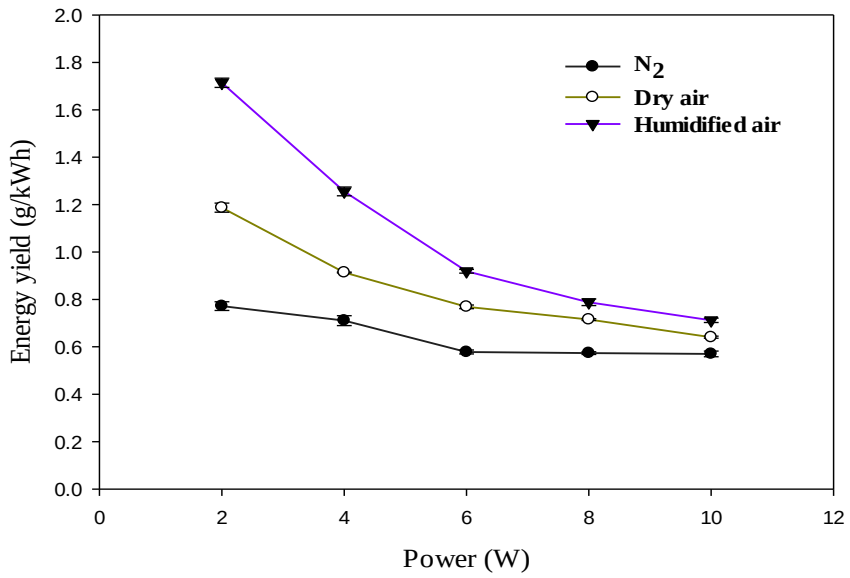

Figure 4.2 Effect of power and carrier gases on the energy yield of hexane decomposition (Reaction conditions: Temperature = ambient; inlet concentration of hexane = 350 ppm; Total flow rate = 100 ml/min; Residence time = 2.3 s; SIE = 1.2 – 6 kJ/L).

Figure 4.3 shows the selectivity to lower hydrocarbons (C_1-C_5) as a function of carrier gases and plasma power.

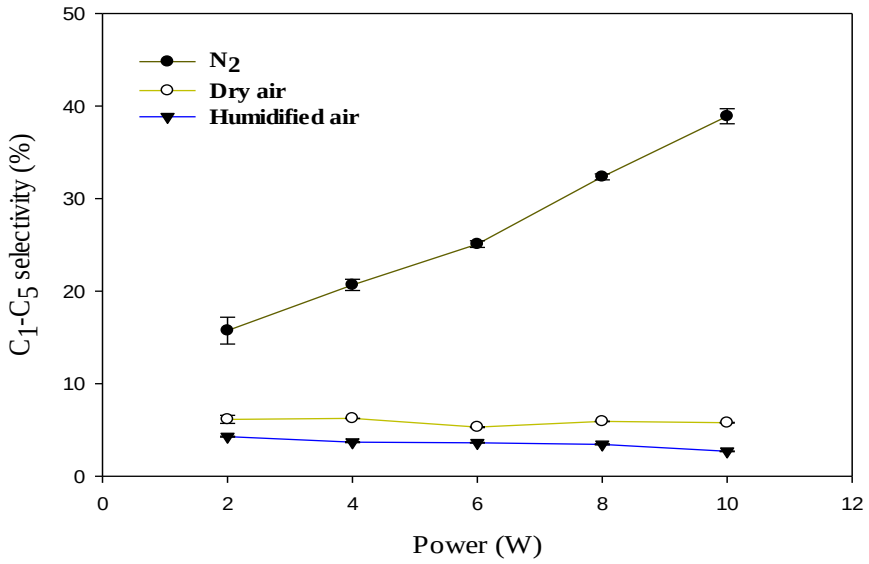

Figure 4.3 Effect of power and carrier gases on selectivity to C_1-C_5 (Reaction conditions: Temperature = ambient; inlet concentration of hexane = 350 ppm; Total flow rate = 100 ml/min; Residence time = 2.3 s; SIE = 1.2 – 6 kJ/L).

The selectivity to lower hydrocarbons significantly increased with increasing plasma power in pure N_2 but decreased in humidified and dry air carrier gases, as shown in Fig. 4.2. For instance, selectivity to lower hydrocarbons increased from 15.7% to 38.9% in N_2 and decreased from 4.3% to 2.7% in humidified air when the plasma power increased from 2W to 10 W. The increase in selectivity to lower hydrocarbons in N_2 plasma could be due to the absence of oxygen in nitrogen plasmas. Therefore, nitrogen excited species such as N_2, $N_2(A)$, $N_2(A^3\sum_u^+)$ and highly energetic electrons favoured decomposition to lower hydrocarbons and solid residue. However, the decrease in lower hydrocarbon selectivity in humidified and dry air carrier gases is probably due to the presence of O_2 and H_2O in the decomposition process, which promotes the formation of CO_2 and CO. Furthermore, the selectivity to lower hydrocarbons (C_1-C_5) decreases as the O_2 concentration in the carrier gases increases. Similar findings have been previously reported in the non-thermal plasma decomposition of hexane (Yan *et al.*, 2007; Ağıral *et al.*, 2010). The presence of H_2O vapour in the plasma-assisted decomposition of VOCs has been shown to reduce the selectivity to lower hydrocarbons and improve selectivity to CO_2 (Trushkin *et al.*, 2013).

The effect of power and carrier gases on selectivity to CO_2 and CO are presented in Figure 4.4 (a) and (b).

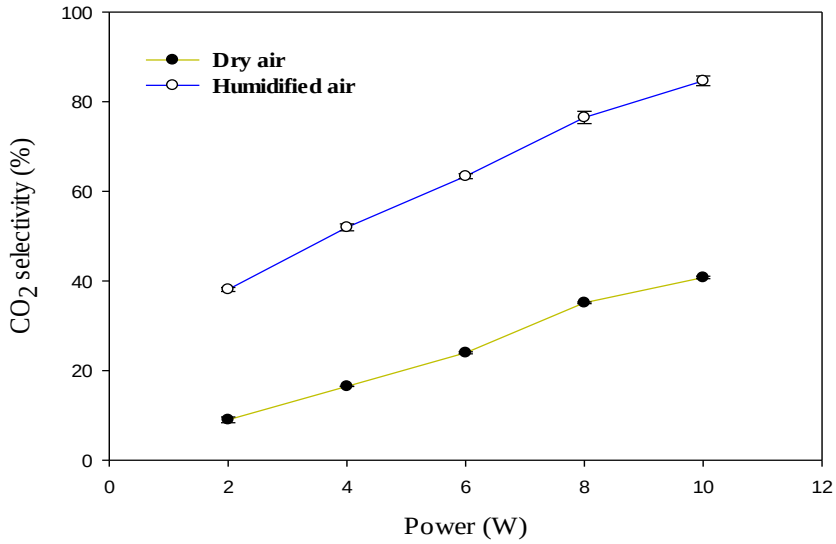

(a)

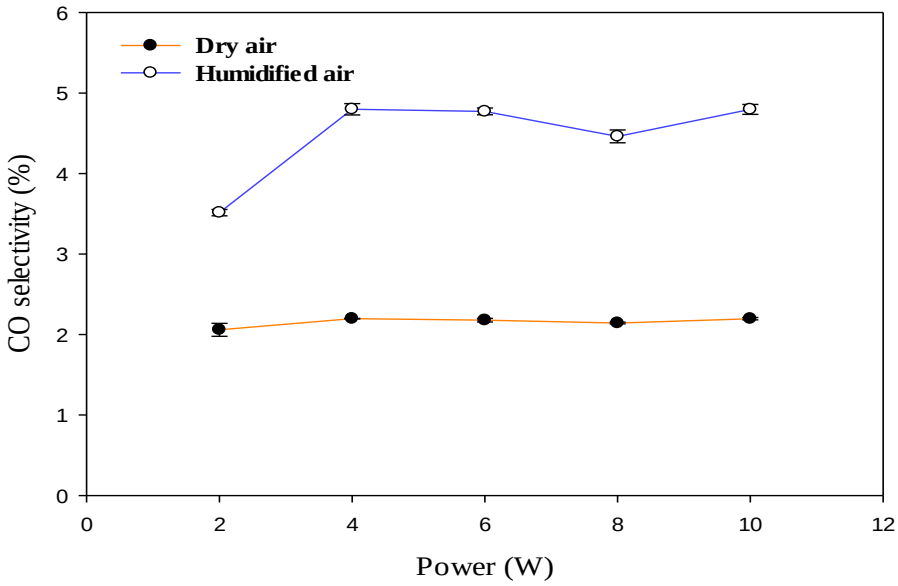

(b)

Figure 4.4 Effect of power and carrier gases (a) on selectivity to CO_2 (b) on selectivity to CO (Reaction conditions: Temperature = ambient; Concentration = 350 ppm; Total flow rate = 100 ml/min; Residence time = 2.3 s; SIE = 1.2 – 6 kJ/L).

The selectivity to CO_2 can be observed to increase significantly with increasing plasma power in dry and humidified air. It was observed that selectivity to CO_2 increased from 9% (dry air) and 38.1% (humidified air) to 40.8% and 84.7% when the plasma power increased from 2 to 10 W. The increase in selectivity to CO_2 must be due to the presence of OH and O radicals in humidified and dry air carrier gases (Raju *et al.*, 2013). The number of reactive species (e.g. O and OH) increased as the input energy increased, which would increase the likelihood of oxidation of intermediate products into final decomposition products, resulting in higher selectivity of CO_2 and CO (Ma *et al.*, 2016). However, the selectivity to CO remained constant in dry air as the plasma power increased, but CO selectivity initially increased when power increased from 2 to 4 W in humidified air plasma.

4.2.2 Effect of plasma power on DBD reactor wall and downstream gas temperature

The influence of the plasma power on the DBD reactor wall and downstream gas temperature on the reaction performance was also examined, as shown in Figure 4.5.

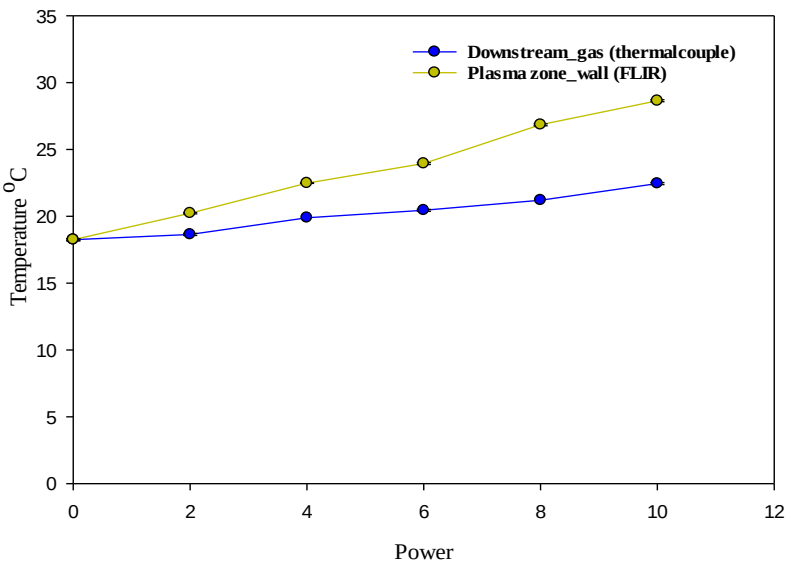

Figure 4.5 Effect of plasma power on DBD reactor wall and downstream gas temperature (Conditions: Total flow rate = 100 ml/min, Power = 2-10 W, Concentration = 350 ppm).

It was observed that both the DBD reactor wall and downstream gas temperature increased with the power. The maximum removal efficiency of hexane was achieved at maximum plasma zone wall temperature and downstream gas temperature respectively. Increasing the plasma power at constant residence time and fixed initial hexane concentration would increase the number of energetic electrons and reactive species in the plasma reactor. In addition, the increase in plasma power increased the molecules internal energy and gas temperature in the plasma DBD reactor, which is beneficial to the conversion of VOC (Wang *et al.*, 2016).

4.2.3 Hexane decomposition pathways in a DBD plasma system

Dielectric barrier discharge NTPs consist of reactive species such as energetic electrons, atoms, ions, and molecules. The highly energetic electrons generate excited species and gas-phase radicals, with average electron energies from 1-10 eV (Petitpas *et al.*, 2007). The energetic electrons can react with VOCs (e.g., hexane) to decompose them into various products such as LHCs, CO_2 and H_2O (Lee *et al.*, 2004; Hoseini *et al.*, 2019). Moreover, the energetic electrons can generate more reactive species through electron impact dissociation, ionization and excitation of the VOC molecules and the carrier gases, which can trigger VOC decomposition.

In this study, the NTP decomposition of hexane can take place through the following major pathways:

(i) direct: electron impact decomposition

(ii) indirect: collisions with reactive species (excited species and gas-phase radicals).

The two major pathways can initiate hexane decomposition.

The proposed hexane decomposition pathways in N_2, dry and humidified air carrier gases are presented in R(4.1)-R(4.3):

$$C_6H_{14}/N_2 \xrightarrow{e,\ N_2^*,\ N_2(A),\ \ N_2(A^3\sum_u{}^+),} LHC\ (C_1-C_5), solid\ residue \qquad R(4.1)$$

$$C_6H_{14}/Air \xrightarrow{e,\ N_2^*,\ N_2(A), O_2^*\ \ O(^3P),\ \ O(^1D),} CO_2, CO, LHC\ (C_1-C_5), O_3, solid\ residue \qquad R(4.2)$$

$$C_6H_{14}/Air + H_2O \xrightarrow{e,\ \ H^{\cdot}, O(^1D), OH^{\cdot}} CO_2, CO, LHC\ (C_1-C_5), H_2O \qquad R(4.3)$$

R(4.3) is the most important reaction; it is the primary source of gas-phase radicals, such as $H^{\cdot}, O(^1D), OH^{\cdot}$ that promoted hexane decomposition, product selectivity, and elimination of unwanted by-products such as ozone and solid residue.

In hexane molecules, the bond dissociation energy of the C-C is 3.74 eV and 4.25 eV for the C-H bonds (Luo, 2004). Thus, it is more likely that the initial step of hexane decomposition can occur by breaking the C-C bond than the stronger C–H bond.

In the N_2 plasma, the removal efficiency increased with plasma power due to the increased concentration of excited nitrogen species such as N_2, $N_2(A)$ and metastable $N_2(A^3\sum_u{}^+)$. The N_2 molecules become energised and change to a higher energy state after collision with highly energetic electrons. The average electron temperature of pure nitrogen is 3.85 eV (Luo, 2004). Nitrogen's excited species $N_2(A)$ and nitrogen metastable state $N_2(A^3\sum_u{}^+)$ with mean electron energies above 3.74 eV can break the C-C bond in hexane, leading to the formation of intermediates, which are converted to C_1-C_5 hydrocarbons and solid residues (probably of longer chain hydrocarbons). Initially, the excited N_2 species collide with hexane molecules, reducing C_6H_{14} to $C_6H_{13}{}^{\cdot}$ and $H^{\cdot}$ which then decompose further into lower hydrocarbons. Previous studies reported that the excited species of N_2 has played an important role in the non-thermal plasma decomposition of VOCs (Bityurin *et al.*, 2009). Probably, the energetic electrons and the excited species of N_2 colliding with hexane molecules convert the C_6H_{14} to lower hydrocarbons (C_1-C_5) and solid residue through dissociation by electron impact, the reaction between hexane ions and radicals and recombination reactions, as has been suggested before (Yan *et al.*, 2007; Son *et al.*, 2021).

The additional presence of O_2 in dry air plasma can lead to the generation of O radicals, excited O_2 atoms and molecules. These species can increase the removal efficiency of VOCs and change product selectivity. The decomposition of hexane can occur through hydrogen abstraction by O_2 molecules, forming hexyl radicals and HO_2. The hexyl radicals can react with

O_2 species and O radicals to form various products, such as C_1-C_5: (CH_4, C_2H_4, C_3H_8, C_4H_8, C_5H_{10} and C_5H_{12}).

The oxidation of hydrocarbons using non-thermal plasmas causes the formation of CO_2, H_2O, and CO (Marotta *et al.*, 2007; Karatum *et al.*, 2016). In this study, it was observed that the presence of O_2 increased the removal efficiency of hexane whilst increasing the production of CO_2 and CO. The probable route is that the decomposition process was initiated by energetic electrons, converting hexane into lower hydrocarbons. Excited O_2 species and O radicals could oxidize the lower hydrocarbons to generate CO_2 and CO, as shown in R(4.1).

The introduction of H_2O vapour to the DBD system changed the outcomes further due to the formation of different reactive species, such as $OH^{\cdot}, O^{\cdot}, O_2^*, H^{\cdot}$ as shown in R(4.3). The OH and H radicals were generated by the direct collision of energetic electrons with H_2O (Karuppiah *et al.*, 2012). The electrons have sufficient energy to produce chemically reactive species from H_2O via dissociation, ionization and excitation (Liu *et al.*, 2017a). The reactive species, such as $OH^{\cdot}, O^{\cdot}, O_2^*$, can oxidize the hydrocarbon products to produce CO_2, CO and H_2O. It has been reported that water vapour increases the selectivity of CO_X and suppresses the formation of lower hydrocarbons (Trushkin *et al.*, 2013).

The selectivity is also affected by varying the power. The main products identified in this study were lower hydrocarbons C_1-C_5: (CH_4, C_2H_4, C_3H_8, C_4H_8, C_5H_{10} and C_5H_{12}), CO_2, CO, and H_2O. Furthermore, yellow solid/viscous deposits were also formed in the DBD reactor in nitrogen and dry air carrier gases, and in dry air (only), O_3 was also observed.

4.2.4 Ozone and NOx formation

Ozone and NOx generation are inevitable by-products in the NTP decomposition of volatile organic compounds in dry air plasmas. Here, the DBD reactor outlet O_3 concentrations were measured using standard KI solution techniques, as described in section 3.4.

Figure 4.6 shows O_3 formation as a function of plasma power in the dry air carrier gas.

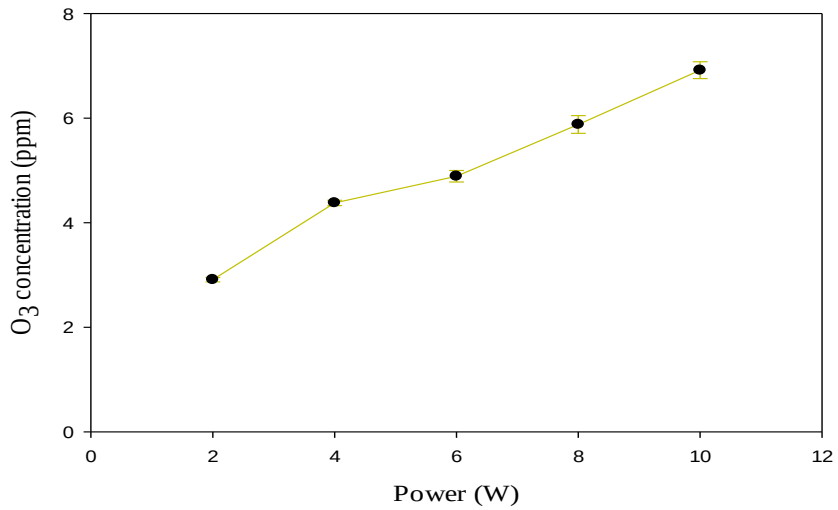

Figure 4.6 Ozone formation as a function of input power (Reaction conditions: Temperature = ambient; Inlet concentration of hexane = 350 ppm; Total flow rate = 100 ml/min; Residence time = 2.3 s; SIE = 1.2 – 6 kJ/L; Carrier gas = dry air).

The O_3 concentration increased from 2.9 to 6.9 ppm when power increased from 2 to 10 W. The formation of ozone is initiated via a collision with highly energetic electrons, which splits the oxygen molecules into atomic oxygen as shown in R(4.4)-R(4.5) (Gudmundsson *et al.*, 2013):

$$e + O_2 \rightarrow O(^3P) + O(^3P) + e\ (6.1\ eV) \qquad R(4.4)$$

$$e + O_2 \rightarrow O(^3P) + O(^1D) + e\ (8.4\ eV) \qquad R(4.5)$$

In the presence of a third body molecule M (M = N_2, O_2, reactor wall or the surface of the dielectric), atomic oxygen will then react with oxygen molecules to generate O_3 as shown in R(4.6) (Atkinson *et al.*, 1997):

$$O + O_2 + M \rightarrow O_3 + M \qquad R(4.6)$$

In humidified air, O_3 was not detected. This is because the intermediate products generated in the plasma react with OH and O radicals, leading to the formation of oxidized hydrocarbons, such as ethyl acetate and acetic acid (Appendix A-4.1) and $OH^{\cdot}$ which decomposes O_3.

However, NOx formation is a serious problem in the non-thermal plasma-assisted abatement of VOCs because its formation can reduce the performance of the NTP reactors (Subrahmanyam *et al.*, 2006; Karatum *et al.*, 2016). NOx has a wide range of environmental and health effects. It can cause can infiltrate through the lung's alveolar cells (epithelium) and surrounding capillary capillaries, disrupting alveolar architecture and their function. NOx is generated from reactions between atomic or excited nitrogen and excited oxygen. In this study,

Gastec Detector Tubes (detection limit =0.1 ppm) were used to measure the NOx concentrations in the DBD outlet. NOx was not detected in the effluent of the DBD reactor used in this study. This could be due to the impact of low flow rates, low plasma power, and composition of the pollutants. It is important to note that operating a DBD reactor at very flow rates and low plasma power can increase both the specific input energy and residence time, and both can suppress the formation of O_3 and NOx. Furthermore, the presence of H_2O in the plasma discharge zone leads to more OH radicals, leading to the rapid oxidation of NOx to HNO_2 in the decomposition of VOCs (Zheng *et al.*, 2013).

4.2.5 Effect of oxygen concentration

The effect of O_2 concentration on removal efficiency and product selectivity was investigated using mixtures of N_2 and O_2 at constant power and residence time. The O_2 concentration in the gas mixture was set at 0, 5, 10, 15 or 21% (to match ambient air).

Figure 4.7 shows the influence of increasing O_2 concentrations on the removal efficiency of hexane.

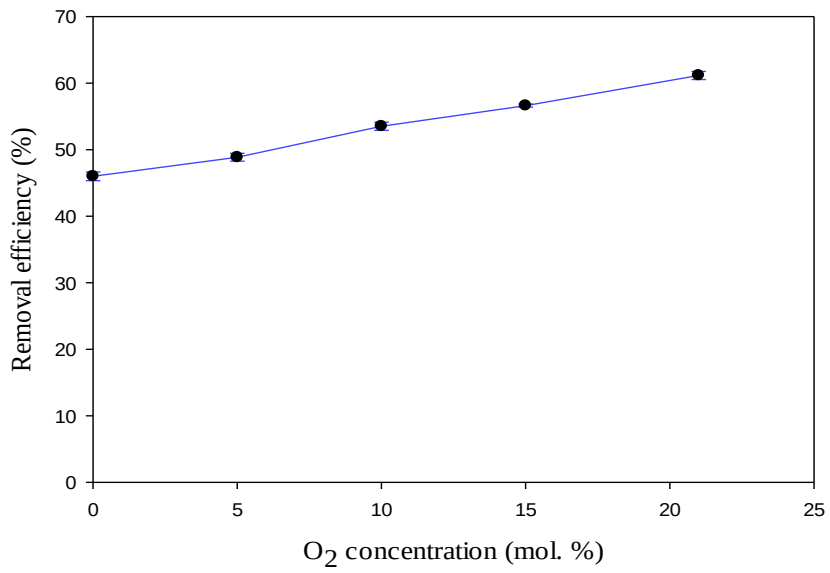

Figure 4.7 Effect of oxygen concentration on removal efficiency of hexane (Reaction conditions: Temperature = ambient; power = 6 W; Inlet concentration of hexane = 350 ppm; Total flow rate = 100 ml/min; Residence time = 2.3 s; SIE = 3.6 kJ/L).

The removal efficiency of hexane increased with increasing O_2 concentration, from 48.9% to 61.1%, as the O_2 concentration increased from 5% to 21%. The increase in removal efficiency is probably due to the formation of more excited O_2 species and O radicals in the plasma DBD, which are proportional to the oxygen concentration at a constant power (Yao *et al.*, 2015). It

has been reported that O_2 is an important parameter that promotes the NTP decomposition of alkanes (Jiang *et al.*, 2020). The initial step in non-thermal plasma DBD decomposition of hexane is the electron impact excitation of molecular O_2 producing atomic O radicals in the excited $O(^1D)$ and ground $O(^3P)$ states. The $O(^1D)$ and $O(^3P)$ species can break the C-H bond in alkanes (Zhang *et al.*, 2004). The mechanism of the formation of excited $O(^1D)$ and ground $O(^3P)$ states by electron impact in DBD plasma is described in R(4.7) – R(4.8):

$$e + O_2 \rightarrow O_2(A^3\sum_u{}^+) \rightarrow e + O(^3P) + O(^3P) \qquad R(4.7)$$ (Kudryashov *et al.*, 2018)

$$e + O_2 \rightarrow O_2(B^3\sum_u{}^-) \rightarrow e + O(^3P) + O(^1D) \qquad R(4.8)$$

The hexane decomposition occurs when $O(^1D)$ and $O(^3P)$ abstract hydrogen from C_6H_{14}, which leads to the formation of OH and hexyl radicals. The hexyl radical formed in the discharge zone in the presence of molecular O_2 is then transformed into a product mixture of CO, CO_2 and C_1-C_5 hydrocarbons through reactions as shown in R(4.9)-R(4.12).

$$C_6H_{14} + O(^3P) \rightarrow OH^{\cdot} + C_6H_{13}^{\cdot} \qquad R(4.9)$$

$$C_6H_{14} + O(^1D) \rightarrow OH^{\cdot} + C_6H_{13}^{\cdot} \qquad R(4.10)$$

$$C_6H_{13}^{\cdot} + O(^1D) \rightarrow \text{products } (CO, CO_2, C_1 - C_5) \qquad R(4.11)$$

$$C_6H_{13}^{\cdot} + O(^3P) \rightarrow \text{products } (CO, CO_2, C_1 - C_5) \qquad R(4.12)$$

Therefore, adding oxygen to the plasma DBD system facilitates the generation of free oxygen radicals to initiate or replace the chain initiation and propagation stage through faster processes involving electron impact on O_2 molecules. This resulted in a significant increase in the removal efficiency of hexane and selectivity to CO_2.

Figure 4.8 illustrates the effect of O_2 concentration on selectivity to CO_2 and CO.

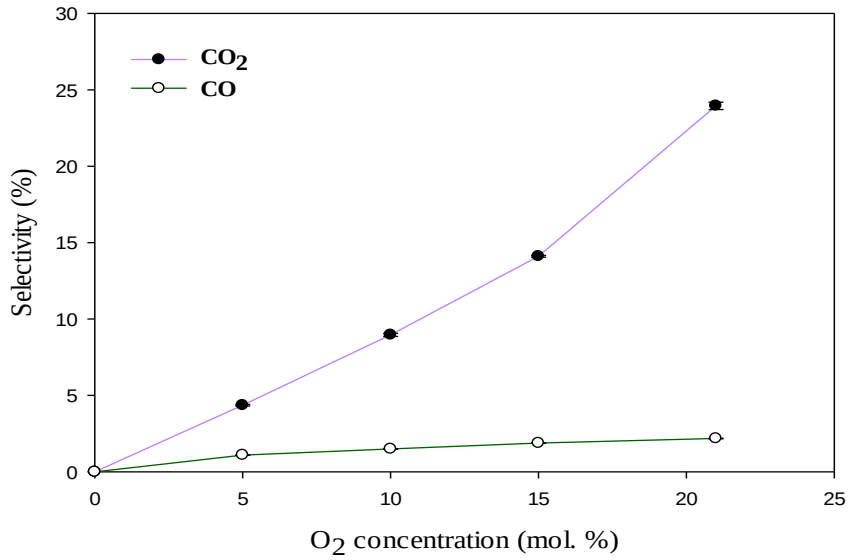

Figure 4.8 Effect of oxygen concentration on CO_2 and CO selectivity (Reaction conditions: Temperature = ambient; Power = 6 W; Total flow rate = 100 ml/min; Residence time = 2.3 s; SIE = 3.6 kJ/L).

It was observed that selectivity to CO_2 increased with increasing O_2 concentration at constant power. It was also noted that selectivity to CO slightly increases when O_2 concentration increases to 5%, then remains constant when O_2 increases from 5 to 21%. The selectivity to CO_2 is much higher than the CO selectivity as the O_2 concentration increases, increasing from 4.4% to 23.9% when O_2 increases from 5 to 21%. The relatively small increase in CO with increasing power is due to the rapid oxidation of CO to CO_2 by O radicals, which become more available as the input O_2 concentration increases (Yan *et al.*, 2007). Marotta *et al.* (2007) also reported that the oxidation of hydrocarbons using non-thermal plasma results in the formation of CO_2 and minimal amounts of CO.

Figure 4.9 shows the effect of O_2 concentration on selectivity to lower hydrocarbons. It was observed that selectivity to lower hydrocarbons significantly decreased with increasing O_2 concentration. This is due to the increase in oxygen reactive species, which oxidized the fragments of hexane to CO and CO_2 at the expense of C_1-C_5 products.

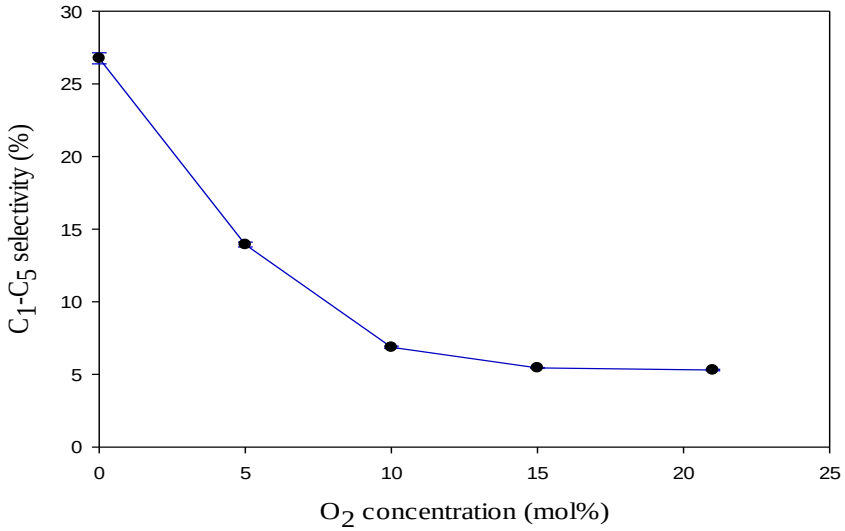

Figure 4.9 Effect of oxygen concentration on selectivity to C_1-C_5 (Reaction conditions: Temperature = ambient; Power = 6 W; Total flow rate = 100 ml/min; Residence time = 2.3 s; SIE = 3.6 kJ/L).

4.2.6 Solid and liquid residues in the DBD reactor

In the DBD technique, some undesired by-products may form during complex chemical processes in the plasma reactor (Mustafa *et al.*, 2018; Wenjing Lu, 2019). The undesired by-products can be solid residue or gaseous emissions (Wenjing Lu, 2019). Solid residues have previously been observed during the plasma-assisted decomposition of VOCs, such as ethylbenzene and toluene (Karatum *et al.*, 2016) and benzene (Saleem *et al.*, 2019g). The solid deposition is a challenge in the application of plasma in various VOC decomposition processes because their formation can eventually foul the dielectric barrier discharge reactor (Saleem *et al.*, 2019f). Furthermore, the solid residues can alter the quartz's dielectric constant, causing thermal energy to accumulate, which can cause mechanical failure of the dielectric barrier (Wenjing Lu, 2019).

In this study, significant amounts of solid/viscous liquid residues were deposited on the inner tube's external surface and the DBD reactor's inner wall in N_2 and dry air plasmas, as shown in Figure 4.10 (a) and 4.8 (b). However, as shown in Figure 4.10 (c), no deposit was observed when the air was humidified.

(a) Nitrogen carrier gas.

(b) Dry air carrier gas.

(c) Humidified air carrier gas.

Figure 4.10 Dielectric barrier discharge reactors after hexane decomposition in (a) Nitrogen carrier gas (b) Dry air carrier gas, (c) Humidified air carrier gas.

The mass of solid residue was determined by weighing the reactor before and afterwards. The solid deposits accounted for 36% and 31% of the total carbon in the decomposition reaction of hexane in N_2 and dry air, respectively. To determine the composition of the solid, the residue was dissolved in n-decane and analysed by GCMS. In nitrogen and humidified air plasmas, the GCMS showed that the solid residue consisted of cyclohexane, hexane, 3-methyl, heptane, 3-methyl, octane, and toluene, as shown in Table 4.1 and Appendix A-4.6. However, ethyl acetate and acetic acid were observed in humidified air plasmas.

Table 4.1 Decomposition products identified by GC-MS in Nitrogen, dry and humidified air

Name of compound	Chemical formula	Chemical structure	Nitrogen	Dry air	Humidified air
Cyclohexane	C_6H_{12}		+	−	+
Hexane, 3-methyl	C_7H_{16}	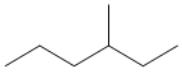	+	−	+
Heptane, 3-methyl	C_8H_{18}	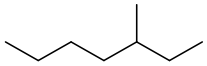	+	−	+
Octane	C_8H_{18}	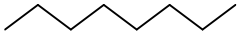	+	−	+
Toluene	C_7H_8	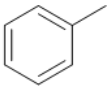	+	−	+
Ethyl acetate	$C_4H_8O_2$	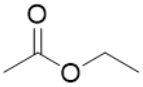	−	−	+
Acetic acid	CH_3COOH	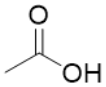	−	−	+

" − ": not detected and " + " : detected

These solid deposits are undesired, as their formation may foul the DBD reactor over prolonged operation. For novel DBD plasma technology to address this drawback, the formation of solid deposits must therefore be eliminated or reduced. In this study, H_2O vapour with a RH of 25% (absolute humidity = 0.004 kg/m^3) at 20 ℃ was used as a carrier gas at similar experimental conditions (N_2 and dry air) to eliminate the formation of solid deposits in the DBD reactor. The solid deposits were prevented, as shown in Figure 4.8 (c), so there is a relatively simple solution to this problem. The elimination of the deposit in the humidified stream was due to the formation of OH radicals, which provided sufficient OH and O_2 to the DBD system. The OH, H and O radicals generated in the plasma reactor can convert hexane and its intermediates to CO, CO_2, and H_2O, resulting in the elimination of solid residue in the DBD reactor.

4.2.7 Reaction kinetics of hexane decomposition using NTP-plasma

In the determination and prediction of the performance of DBD plasma reactors, the development of VOC abatement models is important. A previous study by Yu *et al.* (2012) showed that the decomposition of a compound in a non-thermal plasma system was energy-dependent. In this study, a previously published 1st order kinetic model was used to evaluate the NTP decomposition process (Anderson *et al.*, 1999; Zhang *et al.*, 2011). The model equations R (4.13) and R (4.14) are semi-empirical and do not explain the complex decomposition

reaction in the plasma reactor. The model combined the decomposition processes into a simple equation, which gives the overall kinetic relationship.

$$X^{\cdot} + [C_6H_{14}] \xrightarrow{k_{SIE}} \text{Products} \qquad \text{R (4.13)}$$

Therefore, the equation of NTP decomposition of the model compound with respect to specific input energy (SIE) can be written in the general form (Yu *et al.*, 2012):

$$r = {}^{-1}/_{n} \times {}^{d[C_6H_{14}]}/_{dSIE} = k_{SIE}[C_6H_{14}]^n \qquad \text{R(4.14)}$$

where k_{SIE} represents the energy constant (L/kJ), and n is the reaction order.

Figure 4.11 is a plot of natural logarithms of the remaining hexane fraction as a function of SIE. Based on this graph, the decomposition of hexane in N_2, dry and humidified air can be represented by equation 4.15.

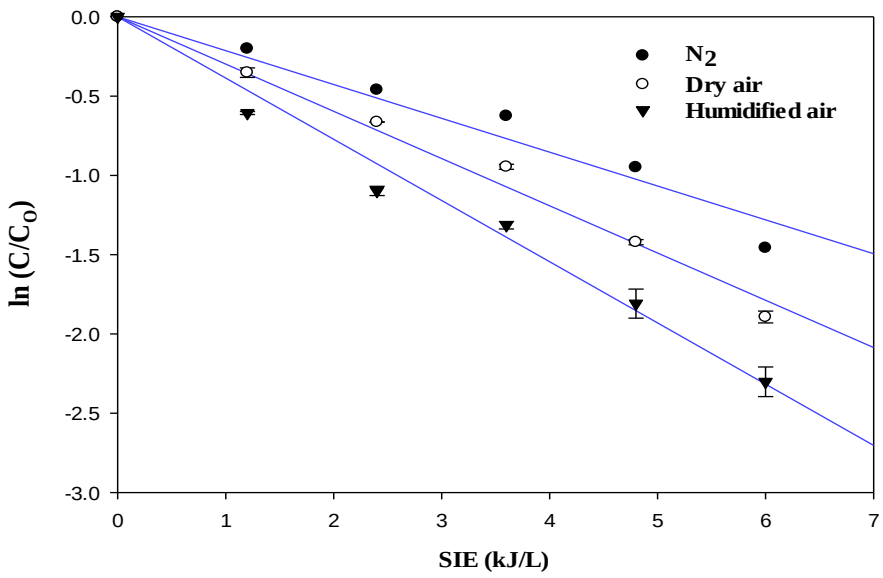

Figure 4.11 Effect of SIE on the remaining fraction of hexane in different carrier gases (Reaction conditions: Temperature = ambient; Inlet concentration of hexane = 350 ppm; Total flow rate = 100 ml/min; Residence time = 2.3 s; Power = 2 – 10 W).

$$\ln \frac{[C_6H_{14}]}{[C_6H_{14}]_0} = -k_{SIE} \times SIE \qquad (4.15)$$

The overall energy constant k_{SIE} on the decomposition process can be determined from the slope of the fitting curves. The plot of $\ln \frac{[C_6H_{14}]}{[C_6H_{14}]_0}$ as a function of SIE exhibits a straight line in all the carrier gases. Therefore, the decomposition of hexane in a DBD reactor as a function of specific input energy (SIE) shows first-order kinetics. Similar findings have been reported in

the plasma-assisted decomposition of toluene (Saleem *et al.*, 2019f; Saleem *et al.*, 2021b) and benzene (Saleem *et al.*, 2019g). The electron impact plays a significant role in the non-thermal plasma decomposition of VOCs.

4.3 **Summary**

In this study, the decomposition of hexane in a non-thermal plasma dielectric barrier discharge (DBD) system was investigated. The experiments were carried out using three different carrier gases (N_2, dry and humidified air) at plasma powers across the range of 2-10 W. The effect of oxygen was also investigated via experiments with N_2/O_2 mixtures at concentrations between 0 and 21%. The hexane removal efficiencies were shown to increase with increasing power and O_2 concentration. Hexane mainly decomposed to lower hydrocarbons (C_1-C_5), CO, CO_2, and solid/viscous residues. In N_2, hexane is mainly decomposed to C_1-C_5 and solid deposit. In N_2, the NTP exhibited the lowest removal efficiency. The removal efficiency in air and humidified air was higher due to the formation of O and OH radicals. CO, CO_2, C_1-C_5, O_3 and solid residue were the main products in dry air. In both N_2 and dry air, the deposits formed would create fouling and other problems, such as arcing, over time. However, the introduction of water vapour (RH= 25%) significantly increased the removal efficiency and the selectivity to CO_2, while preventing the formation of solid residue and O_3, probably due to the formation of potent OH radicals. Furthermore, the maximum removal efficiency achieved in this parameter space, 94.4%, and the maximum CO_2 selectivity, 84.7%, was achieved in humidified air.

Increasing the O_2 concentration was shown to increase both the removal efficiency and the CO_2 selectivity, probably due to the generation of more reactive oxygen radicals. As O_2 concentration increased from 5 to 21%, the product formation shifted toward CO_2, and the production of lower hydrocarbons decreased. A simple first-order reaction model was shown to be consistent with the non-thermal plasma decomposition of hexane in all three atmospheres investigated. Rate constants ("energy constants") were derived for all three atmospheres. This would be vital information for reactor design and scale-up of this technology.

The key finding of this work is the role of H_2O and OH radicals: these results indicate that high hexane removal efficiencies can be achieved in humid air (or by humidifying dry air streams) at low powers (10W or less) without residue formation or NOx or ozone formation.

Chapter 5. Removal of cyclohexane as a toxic pollutant from air using a non-thermal plasma: Influence of different parameters

5.1 Introduction

In this chapter, the removal of cyclohexane as a toxic pollutant from ambient air was investigated in a dielectric barrier discharge (DBD) reactor at ambient temperature and atmospheric pressure. The effects of specific input energy (SIE) (1.2–3 kJ/L), carrier gases, residence time (1.2–2.3 s) and concentration (220–520 ppm) were evaluated to investigate the performance of the DBD reactor in terms of removal efficiency, product selectivity and elimination of solid residue. The carrier gases were chosen because they can aid in developing the pathways of VOCs abatement using NTPs. The dry and humidified air carrier gases could help in the treatment of actual waste gases containing VOCs because they are usually present in the air in most industrial pollution exhausts.

5.2 Results and discussion

5.2.1 Effect of SIE and carrier gas

Specific input energy (SIE) is an important factor influencing VOC decomposition in dielectric barrier discharge (DBD) reactor, and it is directly associated with the plasma input power of the system in this study. The SIE of the plasma reactor was varied over the range of 1.2-3.0 kJ/L by increasing the plasma power at a fixed flow rate of 100 mL/min. The effect of SIE on the removal efficiency of cyclohexane in nitrogen, dry and humidified air plasmas is shown in Figure 5.1.

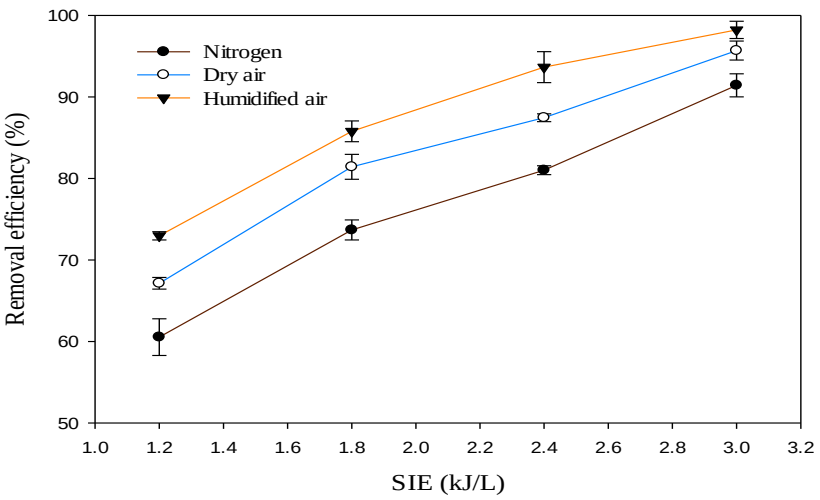

Figure 5.1 Effect of SIE on the removal efficiency of cyclohexane in nitrogen, dry and humidified air carrier gas (Reaction conditions: Temperature = ambient; Concentration = 220 ppm; Total flow rate = 100 ml/min; Residence time = 2.3 s).

The SIE was increased by increasing the plasma input power (2-5 W) at constant inlet concentration (220 ppm) and residence time (2.3 s). In all cases, the removal efficiency of cyclohexane increased with increasing SIE. The maximum removal efficiency of cyclohexane (98.2%) was achieved at 3.0 kJ/L (5 W) in humidified air. In this study, the increase in SIE was realized by increasing the voltage (peak to peak). Hence, the increase in SIE led to an increase in the reduced electric field, hence the average electron energy, meaning that the concentration of energetic electrons increases. Clearly, increasing the SIE at constant concentration and flow rate increased the number of highly energetic electrons and active species in the DBD reactor in all the carrier gases. Młotek *et al.* (2015) reported that an increase in plasma power at constant inlet concentration increased the electron density, which increased the rate of collision between cyclohexane molecules and the energetic electrons, which led to higher conversion of cyclohexane in gliding arc plasma reactor. Similar findings have been reported on the effect of SIE in the decomposition of hexane, toluene and benzene in an NTP DBD reactor (Karatum *et al.*, 2016; Saleem *et al.*, 2019g). Moreover, in addition to the direct electron impact decomposition of cyclohexane, increasing the SIE produces more chemically reactive species such as $OH^{\cdot}$, $O^{\cdot}$, and N_2^*, which take part in the conversion of cyclohexane and reactive intermediates in the plasma reaction. At 3.0 kJ/L, the removal efficiency of cyclohexane in humidified air plasma was higher than that in dry air and nitrogen. The results showed that humidity has a vital influence on the removal efficiency of cyclohexane in the non-thermal plasma DBD reactor process. It has been reported that the relative humidity of about 30% significantly increased the concentration of $OH^{\cdot}$ radical (Kim *et al.*, 2003). In addition to the

energetic electron-initiated decomposition of cyclohexane molecules, the formation of more reactive OH and O radicals at higher SIE creates new cyclohexane decomposition pathways through oxidation of cyclohexane and intermediates leading to higher removal efficiency and product selectivity.

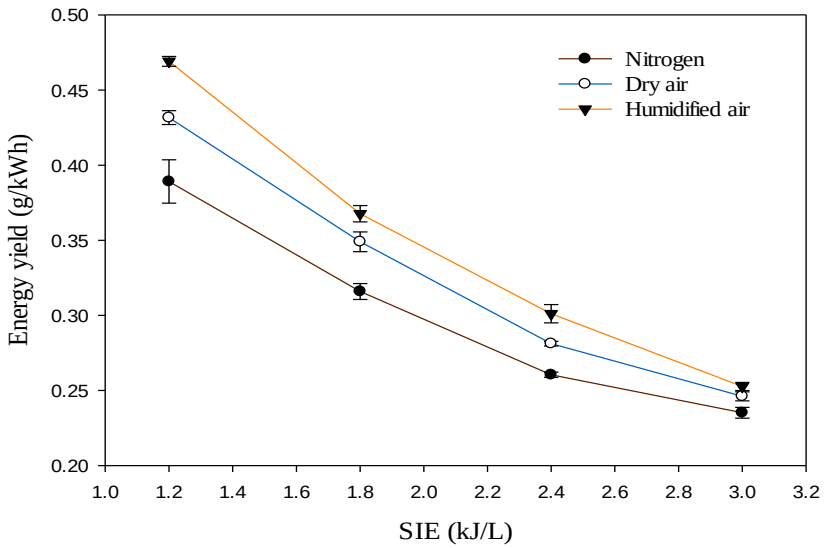

Figure 5.2 Effect of SIE on the energy yield of cyclohexane in nitrogen, dry and humidified air carrier gas (Reaction conditions: Temperature = ambient; Concentration = 220 ppm; Total flow rate = 100 ml/min; residence time = 2.3 s).

Figure 5.2 presents the energy yield of the system as a function of SIE. The energy yield was evaluated and compared at constant initial concentration and fixed residence time at ambient temperature and atmospheric pressure. The energy yield decreased with increasing SIE in all carrier gases. This may be partially due to energy loss to vibration and electronic excitation of carrier gas molecules, resulting in decreased input energy (Mustafa *et al.*, 2018). In addition, there are "diminishing returns" as the plasma input power increases (Saleem *et al.*, 2019f). In humidified air plasmas, the maximum energy yield obtained was 0.47 g/kWh at the SIE 1.2 kJ/L. At 3.0 kJ/L, the introduction of oxygen and water vapour in the DBD plasma not only increased the removal efficiency of cyclohexane but also enhanced the energy yield of the system. The energy yield of the DBD-plasma reactor for non-thermal plasma removal of cyclohexane followed a sequence of nitrogen plasma < dry air < humidified air carrier gas in the SIE range tested.

The main products from cyclohexane decomposition were H_2, C_1-C_4 "lower hydrocarbons", CO, CO_2, and solid residue. Figure 5.3 shows the effect of SIE on the selectivity to lower hydrocarbons (C_1-C_4).

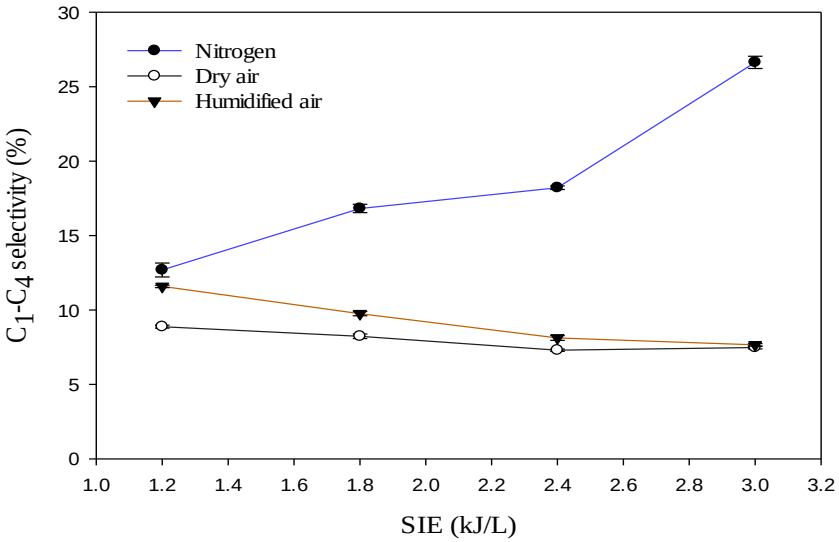

Figure 5.3 Effect of SIE on selectivity to LHC in nitrogen, dry and humidified air carrier gas (Reaction conditions: Temperature = ambient; Concentration = 220 ppm; Total flow rate = 100 ml/min; Residence time = 2.3 s).

The selectivity to lower hydrocarbons increased monotonically with increasing SIE in nitrogen plasma but decreased in dry and humidified air. The decrease in selectivity to lower hydrocarbons is due to oxygen and water vapour, which promotes the selectivity to CO and CO_2 in dry and humidified air plasmas.

The effect of SIE on the selectivity to H_2 yield is presented in Figure 5.4:

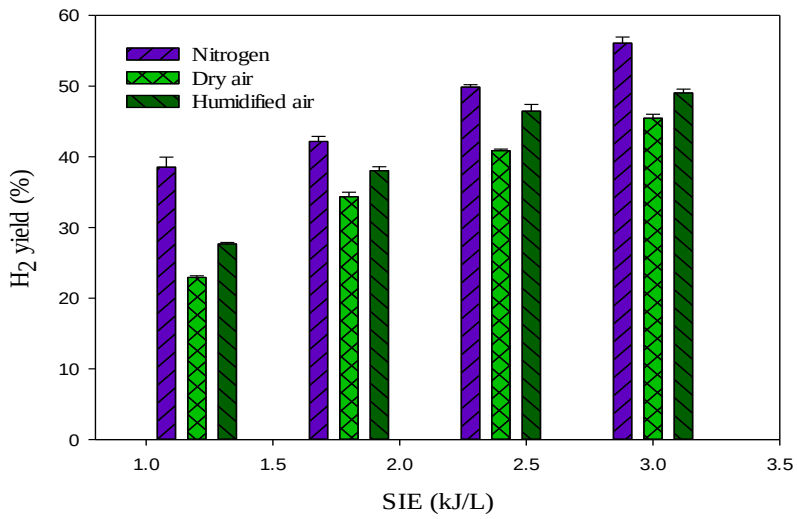

Figure 5.4 Effect of SIE on yield of H_2 in nitrogen, dry and humidified air carrier gas (Reaction conditions: Temperature = ambient; Concentration = 220 ppm; Total flow rate = 100 ml/min; Residence time = 2.3 s).

It can be observed that the H_2 yield significantly increased with SIE in all the carrier gases. This is because increasing SIE increased the number of energetic electrons and excited species that

could promote the ring-opening of cyclohexane to produce hydrogen and lower hydrocarbons (Karatum *et al.*, 2016; Saleem *et al.*, 2019g).

In pure nitrogen plasma, excited nitrogen $N_2(A^3\sum_u^+)$ and $N(^2D)$ can break the C-H and C-C bonds of VOC molecules**.** Therefore, N_2^* with 6.17 eV mean electron energy can efficiently break the C-H (4.32 eV) and C-C (3.59 eV) in cyclohexane molecules. It was observed that the absence of oxygen in nitrogen plasmas resulted in the higher formation of lighter hydrocarbons (C_1-C_4), H_2 and solid residue in the decomposition process.

Figure 5.5 shows the effect of SIE on the selectivity to CO and CO_2 in dry and humidified air. It can be observed that selectivity to CO_2 significantly increased with SIE, while selectivity to CO remains constant in dry air plasma. In humidified air plasma, the CO selectivity slightly increases when SIE increases from 1.2 to 1.8 kJ/L and remains constant when SIE increases to 2.4 -3.0 kJ/L. This is because the O and OH radicals generated from electron impacted dissociation of H_2O molecules can oxidise CO leading to higher selectivity to CO_2 at higher SIE. Clearly, the introduction of water vapour with a relative humidity of 25% (0.004 kg/m^3) at 20 ℃ could increase CO_2, which is a desirable non-harmful product and suppressed CO formation. In this study, the CO concentration at all SIE is well below the permissible exposure limit (PEL) of 50 ppm.

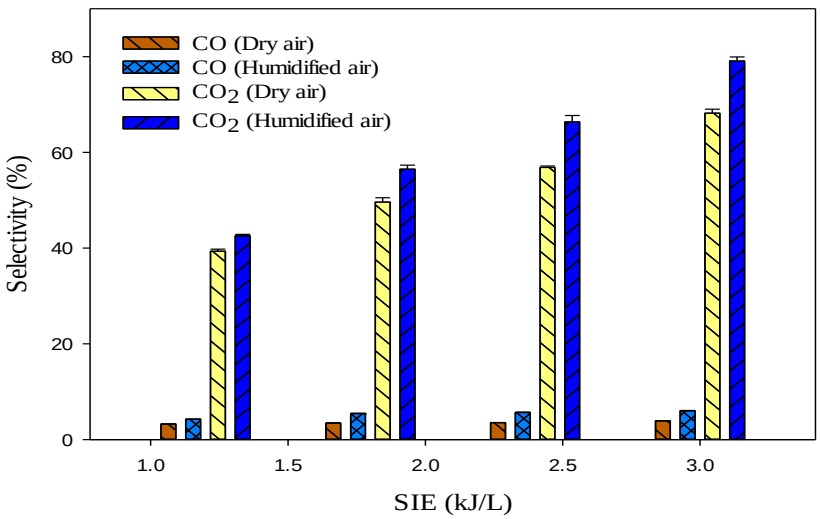

Figure 5.5 Effect of SIE on selectivity to CO and CO_2 in dry and humidified air carrier gas (Reaction conditions: Temperature = ambient; Concentration = 220 ppm; Total flow rate = 100 ml/min; Residence time = 2.3 s).

Similar findings were reported in plasma-catalytic removal of C_6H_{12} in a gliding discharge reactor (Młotek *et al.*, 2015). The maximum selectivity to CO_2 was achieved in humidified air carrier gas at 3.0 kJ/L. This is due to the increase in OH, H and O radicals which convert the fragments of cyclohexane to CO, CO_2 and H_2 at the expense of lower hydrocarbons. Trushkin

et al. (2013) reported that the presence of water vapour suppressed the selectivity to light hydrocarbons and promoted CO_2 selectivity during the NTP-assisted decomposition of toluene. The lower hydrocarbons are converted to H_2, and CO_2.

5.2.2 Effect of concentration

The effect of cyclohexane concentration on the removal efficiency in nitrogen, dry and humidified air carrier gas is shown in Figure 5.6. In this study, concentration was varied between 220-520 ppm at the total flow rate of 100 ml/min, residence time (2.3 s) and SIE (2.4 kJ/L) to evaluate the performance of the DBD reactor at a higher concentration of cyclohexane. Clearly, concentration is a significant parameter that influences the removal efficiency of cyclohexane regardless of the carrier gas: the removal efficiency of cyclohexane decreased significantly with increasing concentration. The maximum removal of cyclohexane was observed at 220 ppm (93.5%) in humidified air and decreased significantly when increasing the concentration up to 520 ppm (50.8%) at constant SIE and residence time.

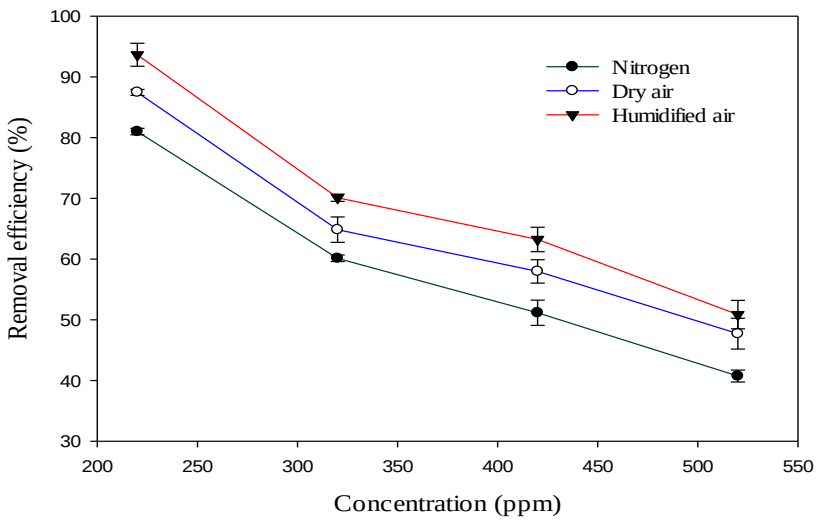

Figure 5.6 Effect of concentration on removal efficiency of cyclohexane in nitrogen, dry and humidified air carrier gas (Reaction conditions: Temperature = ambient; SIE = 2.4 kJ/L; Total flow rate = 100 ml/min; Residence time = 2.3 s).

The reduction in removal efficiency is due to the increase in the number of cyclohexane molecules flowing into the plasma reactor at constant plasma power and residence time. On average, each molecule will collide with fewer active species and electrons in the plasma reactor (Chen *et al.*, 2016). In addition, the number of molecules in the discharge region increases, although SIE, residence time, discharge gap and discharge length remain fixed. For this reason, the ability of undecomposed cyclohexane gas molecules to escape from the DBD reactor

discharge area increases. Similar findings have been observed in the plasma-assisted decomposition of benzene (Saleem *et al.*, 2019g).

The effects of concentration on selectivity to LHC (C_1-C_4), H_2, CO, and CO_2 in each carrier gas are presented in Figure 5.7, Figure 5.8 and Figure 5.9.

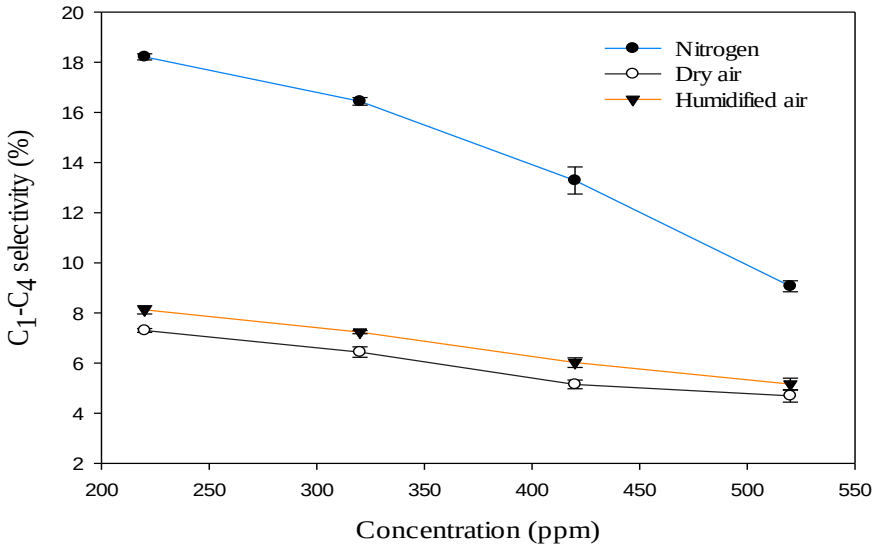

Figure 5.7 Effect of concentration on selectivity to LHC in nitrogen, dry and humidified air carrier gas (Reaction conditions: Temperature = ambient; SIE = 2.4 kJ/L; Total flow rate = 100 ml/min; Residence time = 2.3 s).

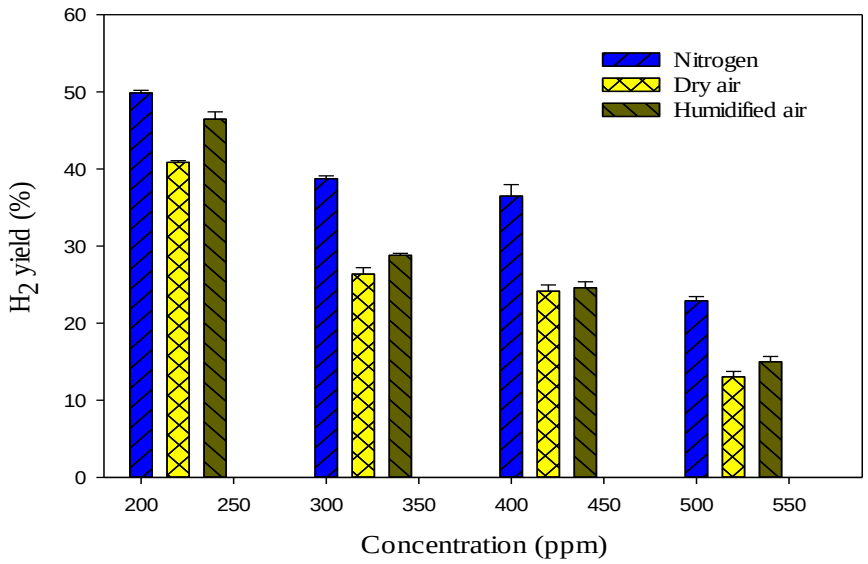

Figure 5.8 Effect of concentration on yield of H_2 in nitrogen, dry and humidified air carrier gas (Reaction conditions: Temperature = ambient; SIE = 2.4 kJ/L; Total flow rate = 100 ml/min; Residence time = 2.3 s).

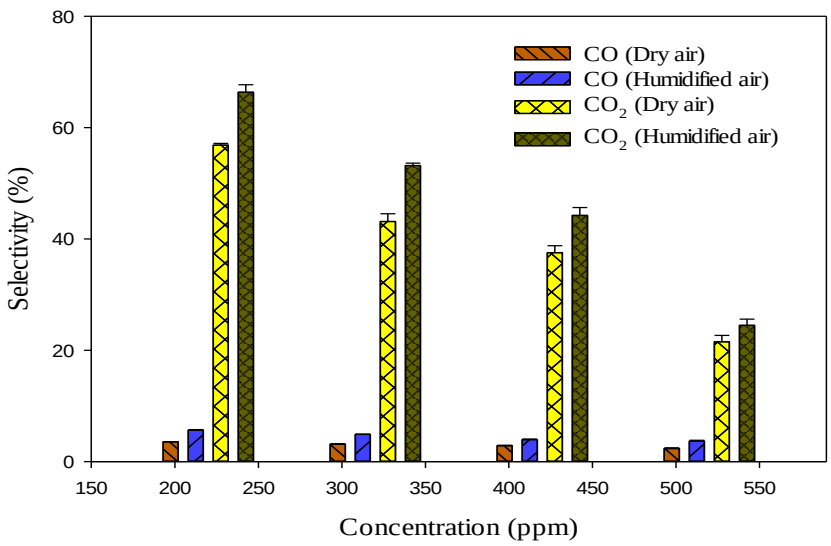

Figure 5.9 Effect of concentration on selectivity to CO and CO_2 in dry and humidified air carrier gas (Reaction conditions: Temperature = ambient; SIE = 2.4 kJ/L; Total flow rate = 100 ml/min; Residence time = 2.3 s).

It can be observed that selectivity to LHC, CO and CO_2 decreased with increasing cyclohexane inlet concentration at constant residence time and SIE. Furthermore, as the cyclohexane inlet concentration increases, H_2 yield decreases. This could be due to a decrease in the relative number of reactive species (N_2^*, e) when compared with cyclohexane molecules. At higher inlet concentrations, more cyclohexane entered the discharge zone (at fixed reaction conditions: SIE = 2.4 kJ/L, residence time = 2.3 s), which reduced the contribution of energetic electrons and excited background gas/carrier gas in the decomposition of cyclohexane to lower hydrocarbons and hydrogen, hence energy consumption increased. Similar findings were reported in the plasma-assisted decomposition of toluene (Saleem *et al.*, 2018).

The selectivity to CO_2 followed a similar pattern as that of H_2. For example, in dry and humidified air carrier gases, selectivity to CO_2 decreased from 56.9% and 66.4% (220 ppm) to 21.5 and 24.5% (520 ppm). This could be due to the constant number of energetic electrons and active radicals reacting with higher cyclohexane molecules at high concentrations. In summary, each VOC molecule shares fewer electrons and active species, resulting in decreased product selectivity (Wang *et al.*, 2017).

5.2.3 Effect of residence time

To investigate the effect of residence time on the removal efficiency of cyclohexane in nitrogen, dry and humidified air, the residence time was varied in the range of 1.2 to 2.3 s at constant concentration and fixed plasma power. The effect of residence time on the removal efficiency of cyclohexane is shown in Figure 5.10. It can be observed that the removal efficiency of

cyclohexane increased with residence time in all carrier gases. At 4 W, the removal efficiency of cyclohexane in dry and humidified air plasmas significantly increased from 59.9 and 70.9% (1.2 s) to 87.5 and 93.7% (2.3 s), respectively.

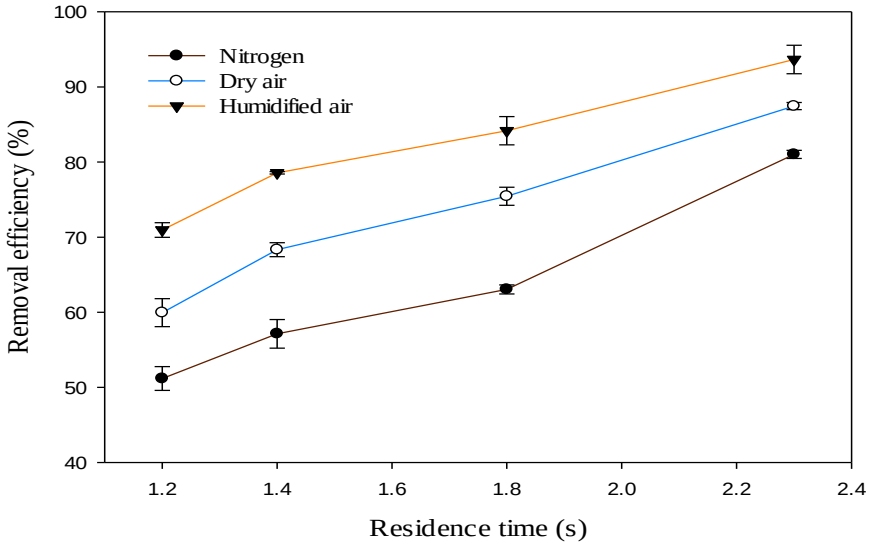

Figure 5.10 Effect of residence time on removal efficiency of cyclohexane in nitrogen, dry and humidified air carrier gas (Reaction conditions: Temperature = ambient; Concentration = 220 ppm; Flow rate = 100 -190 ml/min; Power = 4 W).

The residence time is controlled by changing the flow rate (Saleem *et al.*, 2019e). The SIE strongly affects the decomposition of the VOC compounds and depends on the power and flow rate used. Here, power was kept constant, so the SIE only depended on the flow rate. Therefore, at a lower flow rate, SIE increases, and a higher value of SIE contributes to increasing the decomposition of VOC compounds, as, at higher residence times, the cyclohexane molecules and carrier gas are subjected to the DBD reactor discharge zone for a longer time, leading to an increase in collisions with energetic electrons, and other active species. In humidified air plasma, the maximum removal efficiency obtained was 93.7% (2.3 s). Again, the humidified air environment exhibited the highest conversion due to the presence of $OH^{\cdot}$ radicals.

Figure 5.11, Figure 5.12, and Figure 5.13 show the selectivity to various products in nitrogen, dry and humidified air carrier gas. Lower hydrocarbons (C_1-C_4), H_2, CO, and CO_2 are the main products of the plasma decomposition of cyclohexane. It can be observed that selectivity to H_2 and CO_2 increased with increasing residence time.

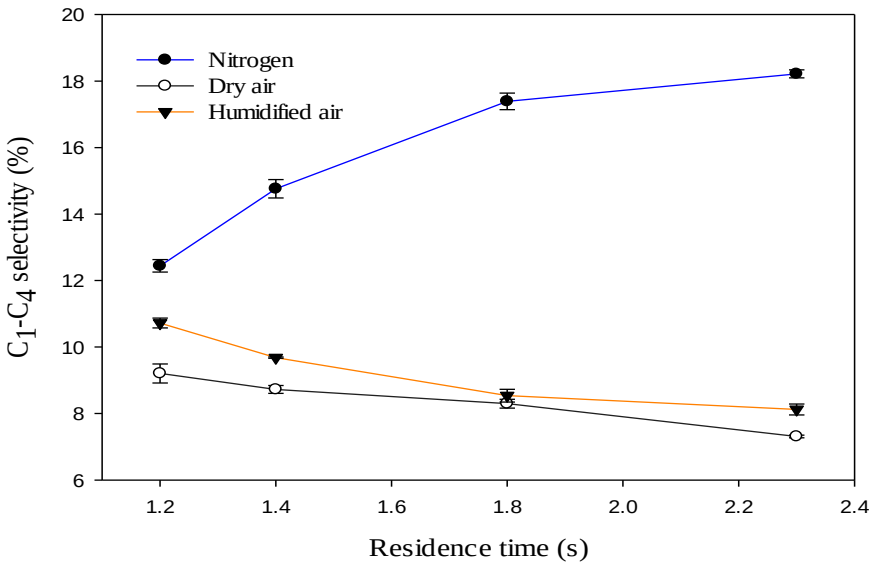

Figure 5.11 Effect of residence time on selectivity to LHC in nitrogen, dry and humidified air carrier gas (Reaction conditions: Temperature = ambient; Concentration = 220 ppm; Flow rate = 100 -190 ml/min; Power = 4 W).

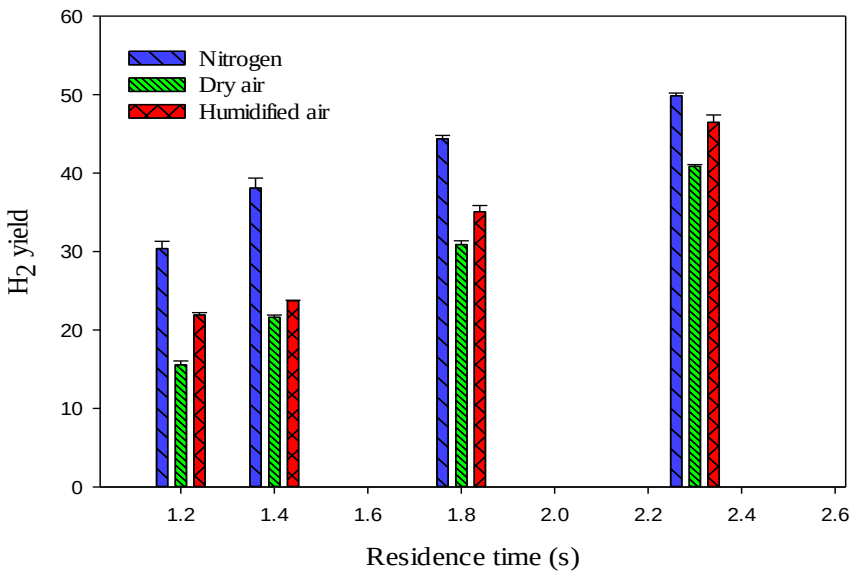

Figure 5.12 Effect of residence time on the yield of H_2 in nitrogen, dry and humidified air carrier gas (Reaction conditions: Temperature = ambient; Concentration = 220 ppm; Flow rate = 100 -190 ml/min; Power = 4 W).

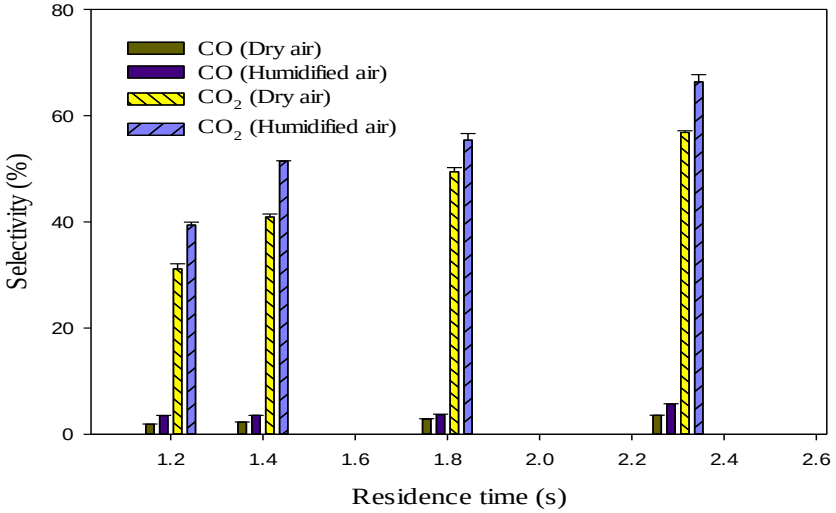

Figure 5.13 Effect of residence time on selectivity to CO_2 and CO in dry and humidified air carrier gas (Reaction conditions: Temperature = ambient; Concentration = 220 ppm; Flow rate = 100 -190 ml/min; Power = 4 W).

In humidified air plasma, the $OH^{\cdot}$ radicals are generated from the dissociation of H_2O in the DBD plasma reactor. They react with cyclohexane fragments to produce CO and CO_2, while the $H^{\cdot}$ radicals can react to produce H_2 through a combination reaction. Hydrogen is produced by H-abstraction from the C-H bond (4.32 eV) of cyclohexane molecule, while CO, CO_2 and LHC require breakage of C-C (3.82 eV) bonds. Cyclohexane is decomposed in DBD plasmas via two reaction pathways: (1) C-H bond cracking and subsequent steps for radical generation and (2) cracking of C-C bonds (Gong *et al.*, 2012). Most LHCs are produced by cracking the C-C bonds of cyclic VOCs with energy below 8 eV in the plasma process (Blin-Simiand *et al.*, 2008). However, selectivity to LHC increased with residence time only in nitrogen. This is probably due to the absence of oxygen, which would promote the formation of lower hydrocarbons and solid deposits. It was also observed that selectivity to CO slightly increased. Selectivity to CO_2 significantly increased due to the presence of $O^{\cdot}$ and $OH^{\cdot}$ radicals at all tested conditions, which is in agreement with previous experimental studies (Młotek *et al.*, 2015).

5.2.4 Mechanisms of cyclohexane decomposition

In a typical non-thermal plasma DBD system, the mean electron energy is in the range 1-10 eV (Petitpas *et al.*, 2007). In the Maxwellian electron energy distribution function (EEDF), the higher the average electron energy, the more electrons with higher energy will be produced. Highly energetic electrons can produce more active species via increased electron-impact dissociation, ionization and excitation of the carrier gases and cyclohexane molecules, which

can initiate cyclohexane decomposition, as shown in reactions (R5.1) - (R5.9). At higher SIEs, energetic electrons collide with the carrier gases, transform them into radicals, and react with cyclohexane molecules. In the carrier gases used here (nitrogen, dry and humidified air) the excited species include: N_2^*, $N_2(A), O_2^*$ and gas-phase radicals such as $O^{\cdot}$, $OH^{\cdot}$ and $H^{\cdot}$. The radicals are generated due to the collision of energetic electrons with $N_2(A)$ and on H_2O as shown in R (5.1) to R (5.8):

$$e + N_2 \rightarrow e + N + N \qquad \text{R (5.1)}$$

$$e + N_2 \rightarrow e + N_2^* \qquad \text{R (5.2)}$$

$$e + N_2 \rightarrow N_2(A) + e \qquad \text{R (5.3)}$$

$$e + O_2 \rightarrow e + O^{\cdot} + O^{\cdot} \qquad \text{R (5.4)}$$

$$e + H_2O \rightarrow H^{\cdot} + OH^{\cdot} + e \qquad \text{R (5.5)}$$

$$e + O_2 \rightarrow O(^1D) + O(^3P) + e \qquad \text{R (5.6)}$$

$$N_2(A) + H_2O \rightarrow N_2 + OH^{\cdot} + H^{\cdot} \qquad \text{R (5.7)}$$

$$O + H_2O \rightarrow 2OH^{\cdot} \qquad \text{R (5.8)}$$

The decomposition of cyclohexane can occur via three pathways, as shown in Figure 5.14.

(i) electron-impacted decomposition reactions e^*

(ii) collision-induced cyclohexane decomposition by excited species such as N_2^*

(iii) reactions with gas-phase radicals ($O^{\cdot}, OH^{\cdot}$),

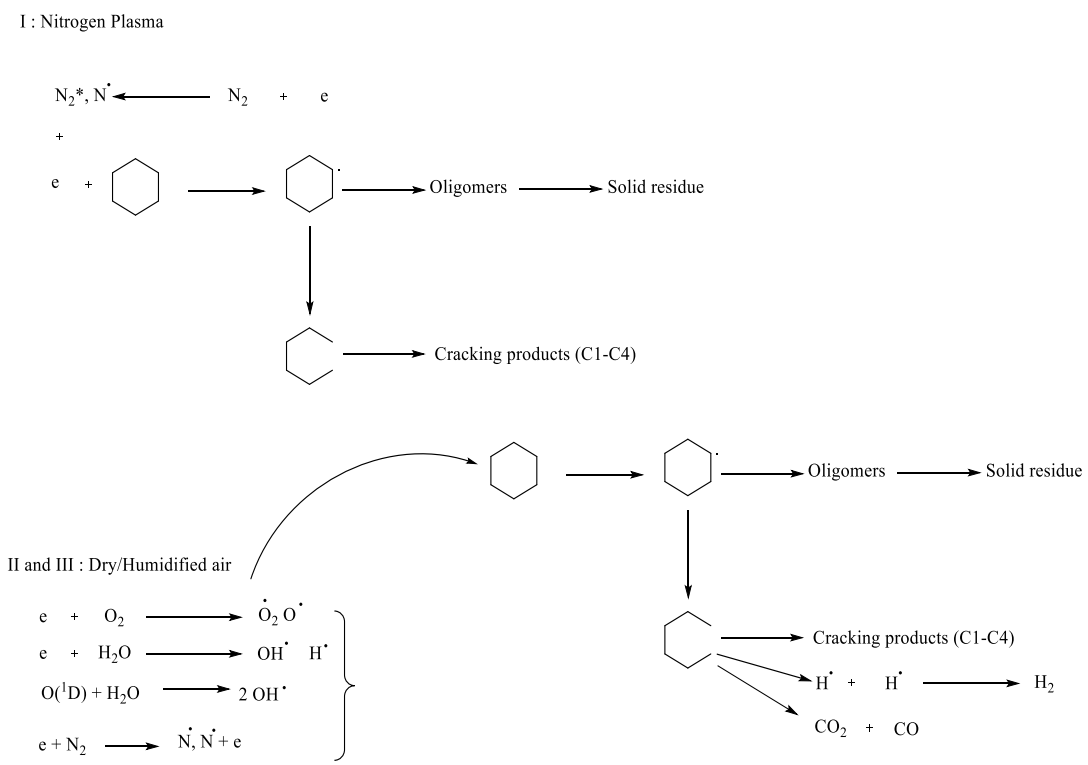

Figure 5.14 Proposed cyclohexane decomposition reaction route.

In cyclohexane, the bond dissociation energy for the C-H bond (4.32 eV) is higher than that for the C-C bond (3.59 eV) (Gong *et al.*, 2012). Therefore, the initial step of cyclohexane decomposition is more likely to take place through C-C bond breakage than the C-H bond. Excited species (N_2^*), gas − phase radicals $(O^{\cdot}, OH^{\cdot})$ and highly energetic electrons with energy greater than 3.59 eV can crack the cyclohexane ring to form products R (5.9)- R (5.17). The decomposition of cyclohexane is triggered by a direct collision between energetic electrons and cyclohexane molecules. In an electron-impacted decomposition reaction, there are two major decomposition pathways: (a) the ring-opening reaction of cyclohexane to create $C_6H_{11}^{\cdot}$ (b) the dehydrogenation reaction of cyclohexane to convert to $C_6H_{11}^{\cdot}$ R (5.9) -R (5.10).

$$C_6H_{12} + e \rightarrow C_6H_{11} + H + e \qquad \text{R (5.9)}$$

$$C_6H_{11} + H + e \rightarrow C_4H_6 + C_2H_4 + H_2 + e \qquad \text{R (5.10)}$$

In pure nitrogen carrier gas, the removal efficiency increased with SIE due to the high proportion of excited N_2 species. After the collision with highly energetic electrons, the N_2 molecules became excited and shifted to a higher energy state. The excited N_2 species can collide with cyclohexane molecules R (5.11), converting C_6H_{12} to $C_6H_{11}^{\cdot}$ and H, which further decomposes to lower hydrocarbons, an example of which is shown in R (5.12). It has been reported that excited species of N_2 play a significant role in the non-thermal plasma decomposition of volatile organic compounds (Bityurin *et al.*, 2009).

$$C_6H_{12} + N_2^* \rightarrow C_6H_{11} + H + N_2 \quad \text{R (5.11)}$$

$$C_6H_{11} + H + N_2 \rightarrow C_2H_4 + C_4H_6 + H_2 + N_2 \quad \text{R (5.12)}$$

In addition, metastable N_2 also contributes to higher removal efficiency. The decomposition of cyclohexane occurs through cracking of the cyclohexane ring due to collision with metastable N_2, resulting in energy transfer and subsequent decomposition of the cyclohexane molecules to lower hydrocarbons and hydrogen (Snoeckx *et al.*, 2013).

The presence of oxygen in dry air can lead to the formation of excited oxygen atoms and molecules and $O^{\cdot}$ radicals. These species will participate in the decomposition of cyclohexane and the formation of plasma products. A proposed reaction scheme for the decomposition of cyclohexane to main by-products can be summarized in R (5.13) -R (5.17).

$$C_6H_{12} + e \rightarrow C_4H_6 + C_2H_4 + H_2 + e \quad \text{R (5.13)}$$

$$C_4H_6 + H_2 + e \rightarrow 2C_2H_2 + 2H_2 + e \quad \text{R (5.14)}$$

$$C_2H_4 + 2O_2 \rightarrow 2CO + 2H_2O \quad \text{R (5.15)}$$

$$2C_2H_2 + 3O_2 \rightarrow 4CO + 2H_2O \quad \text{R (5.16)}$$

$$2CO + O_2 \leftrightarrow 2CO_2 \quad \text{R (5.17)}$$

The energetic electrons initiate the ring-opening reaction, converting the cyclohexane into lower hydrocarbons and hydrogen R (5.13)-R (5.14). The oxidation of C_2H_4 and C_2H_2 from R (5.15)- R (5.16) to form CO and H_2O by oxidative specie O_2 is possible. CO can further oxidize to form CO_2 by reaction with excited oxygen atoms or $OH^{\cdot}$ radicals.

The introduction of water vapour gave new insights into the cyclohexane decomposition pathway in non-thermal plasma DBD reactors. The electrons have enough energy to produce chemically reactive species, e.g., $O^{\cdot}, OH^{\cdot}$ in humidified air carrier gas via excitation, dissociation, and ionization. $OH^{\cdot}$, radical is one of the most reactive radicals for the decomposition of hydrocarbons. In humidified air plasmas, $OH^{\cdot}$ radicals can convert cyclohexane to lower hydrocarbons $(C_1 - C_4), H_2, CO, CO_2$ and H_2O. Traces of cyclohexanol were also observed as one of the products between 2.4 to 3.0 kJ/L SIE at a constant concentration (220 ppm) and residence time (2.3 s). The addition reaction of $C_6H_{11}^{\cdot}$ under the influence of $OH^{\cdot}$ radicals to decompose to $C_6H_{11}OH$ and the dehydrogenation reaction of $C_6H_{11}^{\cdot}$ under the influence of oxygen radicals to produce lower hydrocarbons (Jiang *et al.*, 2018).

5.3 **Cyclohexane by-products**

5.3.1 Solid deposit

Solid residues were deposited on the inner wall of the DBD reactor, as well as the surface of the inner electrode. Saleem *et al.* (2019g) similarly reported the formation of light yellow (in H_2 carrier gas) and dark brown (in CO_2 carrier gas) solid deposits inside the DBD reactor in the plasma-assisted decomposition of benzene. Similar findings were reported in the plasma-assisted decomposition of ethylbenzene (Karatum *et al.*, 2016). Guo *et al.* (2008) reported the formation of a yellow solid deposit after the plasma decomposition of toluene in the DBD reactor and expressed the deposit as an aromatic polymer.

In this study, it can be observed that solid residues were formed on the inner wall of the reactor as well as the external surface of the inner tube in nitrogen and dry air carrier gases, as shown in Figure 5.15.

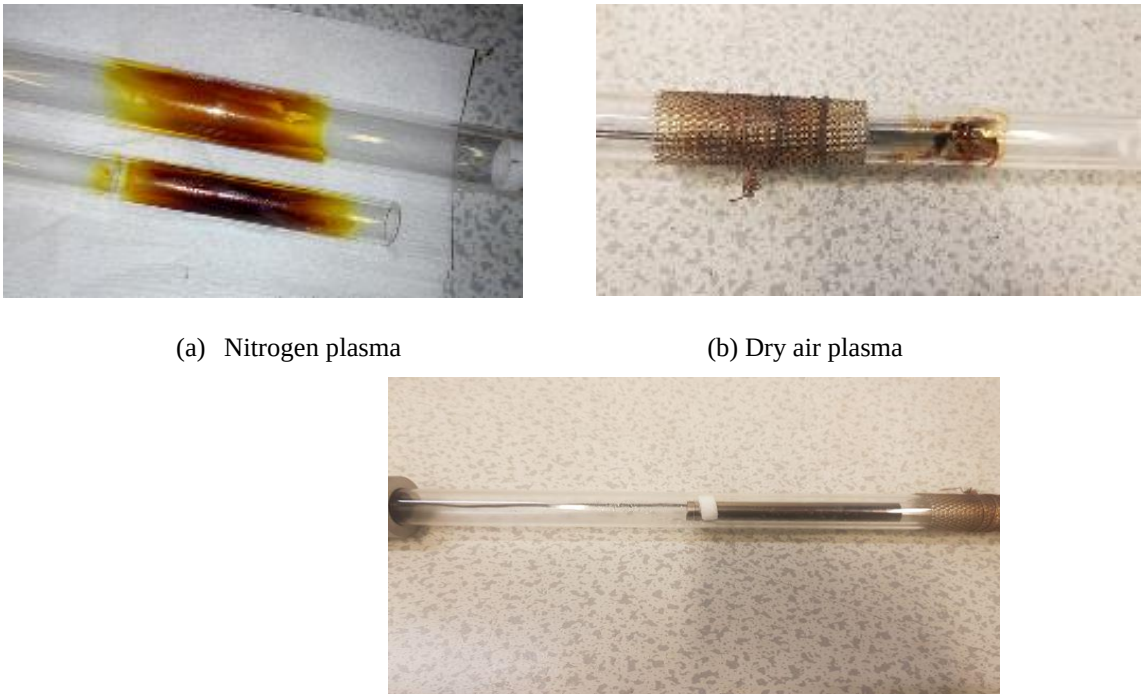

(a) Nitrogen plasma (b) Dry air plasma

(c) Humidified air plasma

Figure 5.15 DBD reactors after cyclohexane decomposition in (a) nitrogen, (b) dry air and (c) humidified air.

The deposit was dark brown in nitrogen, and dark brown with yellow viscous residue in dry air. Cyclohexane formed solid residue due to the oligomerisation of hydrocarbon radicals produced in the plasma system in pure nitrogen and dry air due to the absence of oxygen in nitrogen and low oxygen environment in a dry air carrier gas. Zheng *et al.* (2014) reported similar findings in plasma-assisted removal of acetone in a packed-bed DBD reactor. In a previous study, the

formation of yellow deposit inside the DBD reactor was also reported, and it is possible that the formation of yellow deposit was due to an oligomerization mechanism of monomers to produce macromolecular products (Saleem *et al.*, 2019b). Here, the solid deposits formed in nitrogen were evaluated by weighing the DBD reactor before and after the experiments at constant SIE (3.0 kJ/L), concentration (220 ppm) and residence time (2.3 s). The solid residue was found to account for about 53% of the carbon in the reaction and then analysed with a CHNS analyser. Some portion of the solid residue was dissolved in cyclohexane and analysed using GC-MS. It was found that the solid deposit consists of 62.4% carbon, 7.9% hydrogen and 15.8% nitrogen. The GC-MS analysis revealed that the solid residue consists of aromatic polymers and nitrogen containing compounds such as benzonitrile. Młotek *et al.* (2015) reported that solid deposits formed during the plasma decomposition of cyclohexane in a gliding discharge reactor using dry air were carbonaceous compounds, and their presence can cause a fouling problem to the reactor. The formation of a solid deposit would change the dielectric constant of the glass quartz and may lead to thermal energy build-up, which would break down the dielectric barrier (Chen *et al.*, 2009).

Therefore, to address this problem, solid deposit formation must be reduced or eliminated for novel DBD plasma technologies. To eliminate the formation of solid deposits in the DBD reactor, humidified air was used as a carrier gas under the same experimental conditions. It was observed that removal efficiency and product selectivity were enhanced. Furthermore, solid deposits were eliminated in humidified air. This was probably due to the presence of $OH^{\cdot}$ radicals. The $OH^{\cdot}$ radicals formed by dissociative electron collision with H_2O may lead to higher conversion rates and provide more oxygen to the system, which eliminates the solid residue in the humidified air environment, as shown in Figure 5.15(c). The formation of solid residues is directly associated with the absence of oxygen or low oxygen content in the carrier gas (Zheng *et al.*, 2014).

5.3.2 Ozone and NOx formation

Ozone is an unavoidable by-product in dry air plasmas. In this study, the effect of SIE on ozone formation was investigated at constant concentration and residence time at ambient temperature in dry air. Ozone concentrations at the outlet of the DBD reactor when operating at a steady-state were measured using Gastec detector tubes. Figure 5.16 shows the effect of SIE on ozone formation.

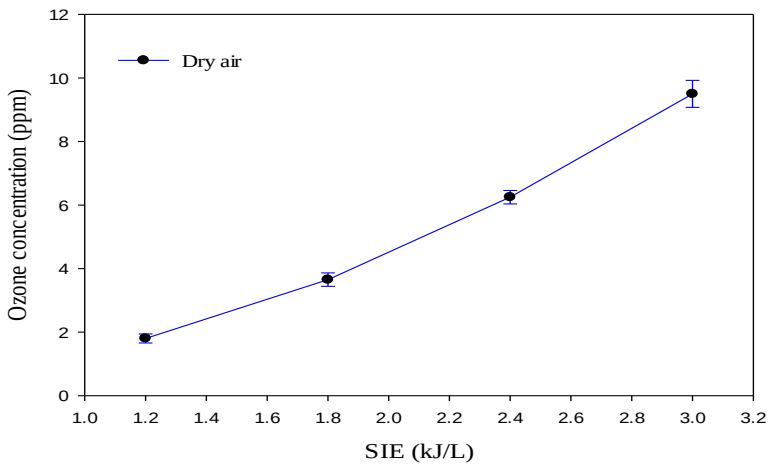

Figure 5.16 Ozone concentration as a function of SIE (Reaction conditions: Temperature = ambient; Concentration = 220 ppm; Total flow rate = 100 ml/min; Residence time = 2.3 s; Carrier gas = dry air).

It was observed that ozone concentrations increased with SIE. Similar findings were reported in the DBD plasma-assisted decomposition of acetone in dry air. Plasma generated in a dielectric barrier discharge (DBD) can produce O_3 via various routes. Ozone can be produced by a direct reaction between oxygen and highly energetic electrons (Hama Aziz *et al.*, 2017). The formation of ozone by this route is a two-step process: (1) Firstly, the atomic oxygen radicals are formed through dissociation of oxygen molecules by electron impact reaction, as shown in R (5.18).

$$O_2 + e \rightarrow O^{\cdot} + O^{\cdot} \qquad \text{R (5.18)}$$

(2) Finally, the atomic oxygen reacts with molecular oxygen via three-body collisions that lead to the formation of ozone according to reaction R(5.19).

$$O_2 + O + M \rightarrow O_3 + M \qquad \text{R (5.19)}$$

M represents nitrogen or oxygen molecules. In addition, NOx formation is a major factor of concern in the plasma-assisted decomposition of VOCs (Subrahmanyam *et al.*, 2006), and its formation reduce the energy efficiency of the treatment process (Karatum *et al.*, 2016). The dissociation of dry air may lead to N and O generation, which is the major source of NOx. However, the operating conditions, property of VOCs, SIE, humidity and reactor configuration can be important factors affecting the NOx formation (Harling *et al.*, 2009). NOx was not detected in the effluent in this study by using Gastec detector tubes. This could be due to the influence of lower flow rates, the nature of VOC, and reactor configuration during the cyclohexane decomposition. Similar findings have been reported in previous experimental studies (Harling *et al.*, 2009; Raju *et al.*, 2013). However, it is also possible to reduce the

formation of NOx in an air DBD plasma by optimizing the specific input energy (SIE), reactor design and operating conditions (Harling *et al.*, 2005; Harling *et al.*, 2008).

5.3.3 A semi-empirical model of cyclohexane decomposition

In NTP reactors, the actual reaction rate constant is a critical parameter to evaluate and predict the removal efficiency of VOCs. A previously published worked indicated that the decomposition of a compound in NTPs was energy-dependent. In this study, it was observed that the removal efficiency of cyclohexane in a non-thermal plasma DBD depended upon plasma power, concentration, and residence time. Most of the previous studies on VOCs evaluated the decomposition model as a function of SIE (Karatum *et al.*, 2016; Saleem *et al.*, 2019g). The reaction rate constant was evaluated based on residence time at fixed plasma power in nitrogen, dry and humidified air. A previously published work (Anderson *et al.*, 1999; Zhang *et al.*, 2011) based on a first-order kinetic model was employed. The model equation R(5.20 - R 5.23) are semi-empirical and does not explain the complex chemical reaction taking place in the DBD reactor. Instead, it combines all processes into a single equation, which frequently yields a satisfactory overall kinetic relationship.

$$X^{\cdot} + [C_6H_{12}] \xrightarrow{k} \text{Products} \qquad \text{R (5.20)}$$

$$r = f(\text{Power}, \text{Concentration}, \text{residence time}) \quad . \quad . \quad . \qquad \text{R (5.21)}$$

$$r = \frac{d[C_6H_{12}]}{dt} = k.[C_6H_{12}]^n \quad . \quad . \quad . \qquad \text{R (5.22)}$$

by integrating R (5.22) and assuming n=1, the cyclohexane outlet concentration at any given residence time can be written by the expression R (5.23).

$$[C_6H_{12}] = [C_6H_{12}]_0 \times e^{-kt} \quad . \quad . \quad . \qquad \text{R (5.23) (5.22)}$$

Where $X^{\cdot}$ is a "lumped" concentration of all radicals produced in the plasma discharge zone, $[C_6H_{12}]$ and $[C_6H_{12}]_0$ are the outlet and inlet concentration of cyclohexane in ppm, k is the reaction rate constant, and n is the reaction order. The natural logarithmic plots of the remaining fraction of cyclohexane with respect to residence time in a different type of carrier gas are presented in Figure 5.17. The plot exhibits a straight line in all the carrier gases. Therefore, the decomposition of cyclohexane in nitrogen, dry and humidified air carrier gases can be expressed as:

$$\ln\frac{[C_6H_{12}]}{[C_6H_{12}]_0} = -k_t \times t \quad . \quad . \quad . \qquad \text{R (5.24)}$$

The models are semi-empirical and summarize the non-thermal plasma decomposition of cyclohexane, which can be used to predict the removal efficiency of the DBD plasma system.

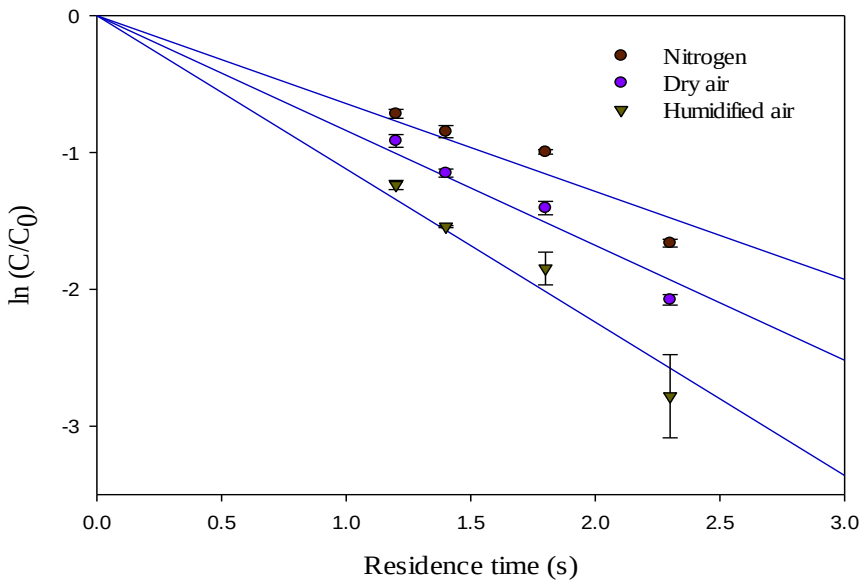

Figure 5.17 Effect of residence time on the remaining fraction of cyclohexane in nitrogen, dry and humidified air (Reaction conditions: Temperature = ambient, power = 4 W, Concentration = 220 ppm, Flow rate = 100 – 190 ml/min).

The reaction rate constants are 0.83, 1.02 and 1.3 s^{-1} for nitrogen, dry and humidified air, respectively. This shows that longer residence time provides more contact time between the energetic electrons and cyclohexane molecules in the DBD reactor. Therefore, residence time plays a significant role in the decomposition of VOCs.

5.4 **Summary**

A dielectric barrier discharge (DBD) reactor was used to remove cyclohexane from an ambient air gas stream as a function of carrier gas (nitrogen, dry and humidified air), specific input energy (1.2 - 3.0 kJ/L), concentration (220 - 520 ppm) and residence time (1.2 - 2.3 s) at ambient temperature and atmospheric pressure. The key findings were that in nitrogen, cyclohexane decomposed mainly to H_2, lower hydrocarbons (C_1-C_4) ("LHC") and solid residue. In dry air, CO, CO_2, and water were also formed. In humidified air, the water vapour had three effects:

(i) it reduced LHC whilst increasing the yields of H_2 and CO_2

(ii) prevention of solid residue formation, presumably due to the formation of $OH^{\cdot}$ radicals

(iii) increased conversion of the cyclohexane.

(iv) reduced CO formation

(v) eliminated O_3

Hence, the performance of DBD devices to remove cyclohexane, and perhaps other VOCs would improve when operating in humid conditions, or when the inlet gas stream is humidified. The maximum cyclohexane removal efficiency (98.2%) was achieved at specific input energy of 3 kJ/L and a residence time of 2.3 s in humidified air.

Chapter 6. Decomposition of benzene vapour using non-thermal plasmas: effect of moisture content on eliminating solid residue

6.1 Introduction

In this chapter, a dielectric barrier discharge (DBD) reactor was used to decompose benzene in dry and humidified air at ambient temperature and atmospheric pressure. The effect of process variables such as plasma power (2-10 W) and moisture content (relative humidity of 0 - 40% at 20°C) on the removal efficiency of benzene, product selectivity, and elimination of the solid residues in the reactor was investigated. Benzene was chosen as a model VOC compound because of its abundance and significant adverse health effect.

6.2 Results and discussion

6.2.1 Effect of power and carrier gases

Plasma power and carrier gases have a key role in the decomposition of VOCs in dielectric barrier discharge (DBD) systems. The effects of power and carrier gases were investigated on the removal of benzene (removal efficiency) and product selectivity. The effects of plasma power and carrier gases on the removal of benzene are presented in Figure 6.1. The plasma power varied in the range of 2 -10 W, and the carrier gases were dry and humidified. The inlet concentration of benzene was 350 ppm, and the residence time was 2.3 s.

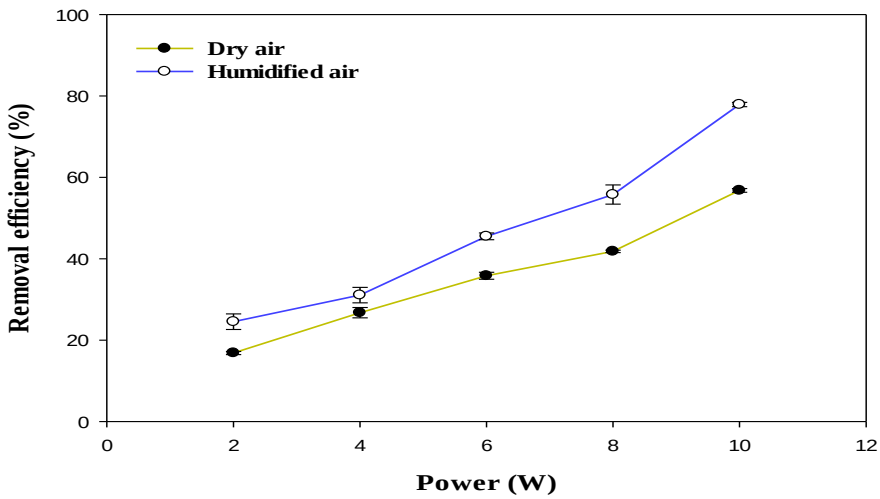

Figure 6.1 Effect of power on the removal efficiency of benzene (Reaction conditions: Temperature = ambient; Concentration = 350 ppm; Total flow rate = 100 ml/min; Residence time = 2.3 s, Relative humidity = 25% at 20°C, SIE = 1.2 – 6 kJ/L).

The benzene removal efficiency increased from 16.8% to 56.8% and 24.5% to 77.9% when the plasma power increased from 2 to 10 W in dry and humidified air. The plasma power increased the number of highly energetic electrons in the DBD reactor (Wu *et al.*, 2014; Zhu *et al.*, 2015); hence, the number of reactive species produced by the collisions between the energetic electrons and the carrier gas molecules significantly increased, leading to benzene higher decomposition.

Figure 6.1 also shows benzene's removal efficiency in humidified air plasma was significantly higher than in dry air. The hydroxyl radical ($OH^{\cdot}$) generated in humidified air plasma is a more potent oxidant than the O radical (formed in dry air plasma) and can oxidise the VOC molecules (Jiang *et al.*, 2015). Therefore, the formation of more OH and O radicals at higher plasma power increases the decomposition of benzene through oxidation of the benzene intermediates, resulting in a higher removal efficiency and CO_2 selectivity.

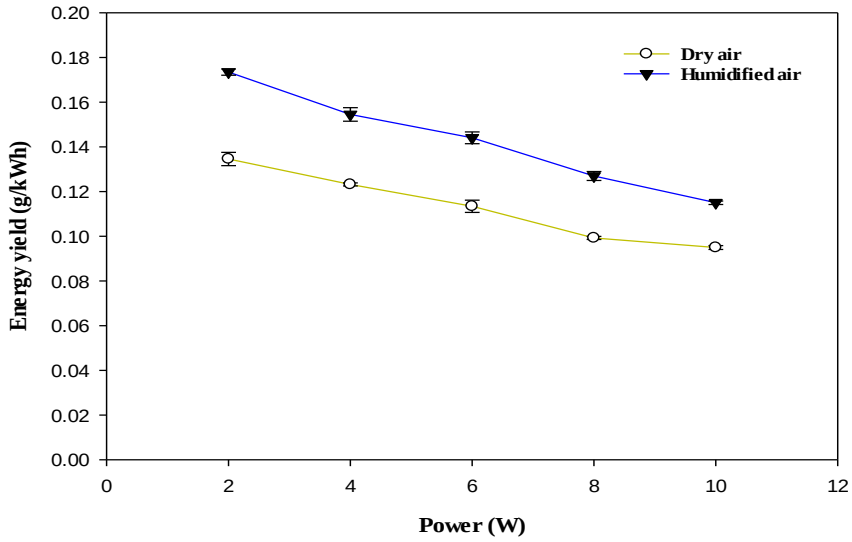

Figure 6.2 Effect of power on the energy yield of benzene decomposition (Reaction conditions: Temperature = ambient; Concentration = 350 ppm; Total flow rate = 100 ml/min; Residence time = 2.3 s, Relative humidity = 25% at 20℃, SIE = 1.2 – 6 kJ/L).

Figure 6.2 shows the effect of plasma power on the energy yield of the process. It was observed that as the plasma power and removal efficiency increased, the energy efficiency decreased. Similar observations were reported in Chapter 4 and Chapter 5 of this work. To improve the energy efficiency of the decomposition process, the plasma power needs to be optimized for the desired removal efficiency.

The products of benzene decomposition using dry and humidified air carrier gases were CO_2, CO and lower hydrocarbons (C_1-C_5). Solid residues and O_3 were also formed.

Figure 6.3 demonstrates plasma power's effect on the selectivity to CO_2 and CO in dry and humidified air.

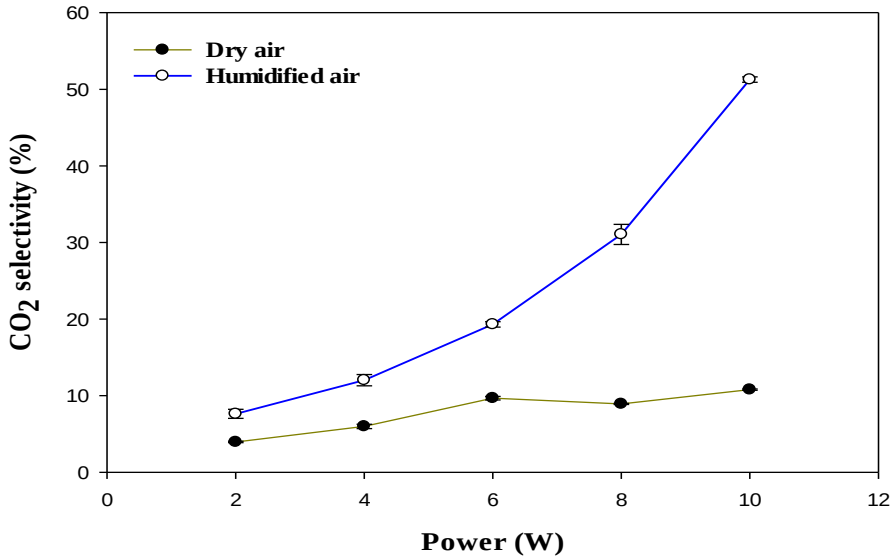

(a)

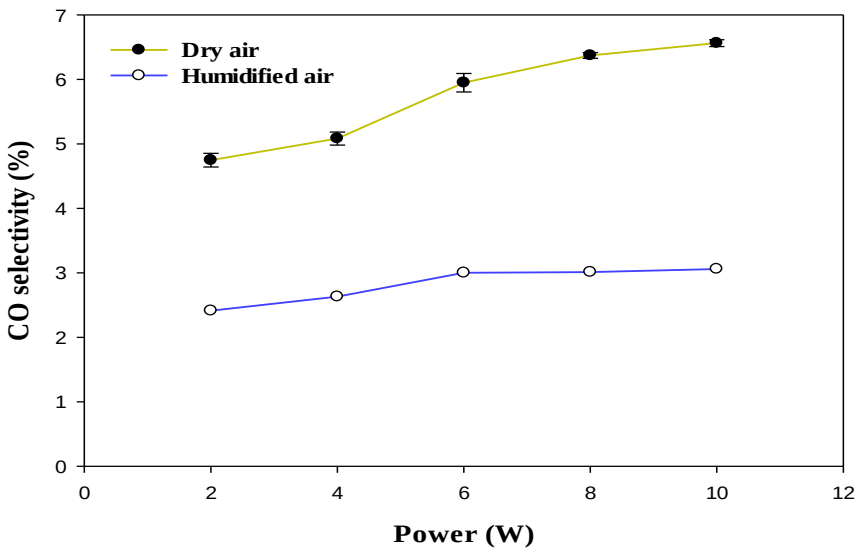

(b)

Figure 6.3 Effect of power on selectivity to (a) CO_2, and (b) CO, (Reaction conditions: Temperature = ambient; Concentration = 350 ppm; Total flow rate = 100 ml/min; Residence time = 2.3 s, Relative humidity = 25% at 20℃, SIE = 1.2 – 6 kJ/L).

As observed in Figure 6.3 (a) and Figure 6.3 (b), the selectivity to CO_2 and CO increases with increasing plasma power in both dry and humidified air. The selectivity to CO_2 and CO increased from 4.0% to 10.8% and from 4.7% to 6.7% when plasma power increased from 2 to

10 W in dry air, respectively. The selectivity to CO_2 was low because CO is rarely oxidised to CO_2 using dry air carrier gas in an NTP alone system (Ogata *et al.*, 1999).

From Figure 6.3 (a) and Figure 6.3 (b), it can be observed that humidified air plasma exhibits the highest selectivity to CO_2 (up to 51.3% at 10 W). In contrast, selectivity to CO remains constant as the power increases from 6-10 W. In addition, the maximum selectivity to CO in humidified air was around 3.1%. The humidified air plasma significantly reduced the production of CO and enhanced CO_2 selectivity as power increased. The O and OH radicals participated in the oxidation of the CO and the reaction intermediates produced during VOC decomposition (Vandenbroucke *et al.*, 2011). The introduction of water vapour to the non-thermal plasma DBD system increases the selectivity to CO_2 and decreases CO selectivity (Thevenet *et al.*, 2008).

The effect of plasma power on C_1–C_5 lower hydrocarbons selectivity in dry and humidified air plasmas is shown in Figure 6.4.

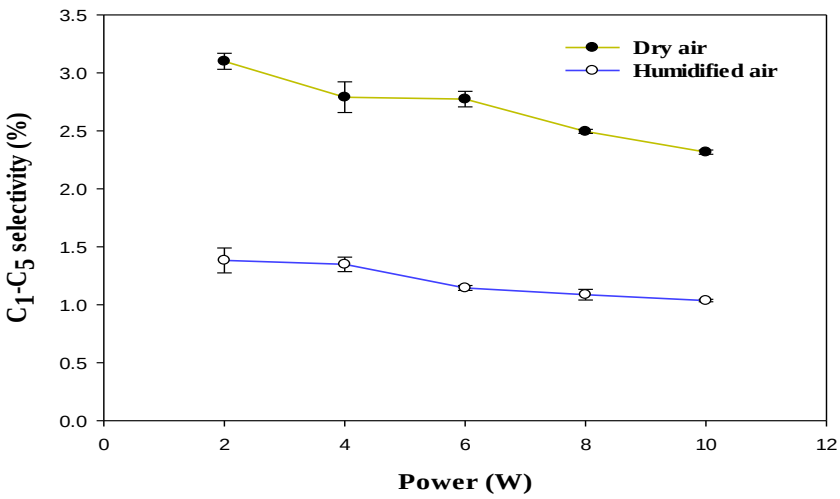

Figure 6.4 Effect of power on selectivity to C_1-C_5 (Reaction conditions: Temperature = ambient; Concentration = 350 ppm; Total flow rate = 100 ml/min; Residence time = 2.3 s, Relative humidity = 25% at 20℃, SIE = 1.2 – 6 kJ/L).

In dry and humidified air, the selectivity to C_1–C_5 lower hydrocarbons decreased as power increased. The presence of OH and O radicals, which increased the selectivity to CO and CO_2 in humidified air and dry air plasmas, could explain the decrease in selectivity to lower hydrocarbons. The OH and O radicals can oxidise the reaction intermediates to CO, CO_2, and H_2O, decreasing C_1-C_5 formation in humidified and dry air. As reported in the previous studies of the NTP decomposition of benzene (Ye *et al.*, 2008; Saleem *et al.*, 2019g), in this study, solid residues were also formed. Here, dark brown and yellowish-brown solid residues, which may foul the reactor over time, were deposited in the DBD reactor in dry and humidified air. In

addition, the solid residues formed in the reactor can change the dielectric constant of the quartz, resulting in the mechanical problem of the dielectric due to thermal energy built up in the NTP system (Ye *et al.*, 2008). The introduction of water vapour with RH of 25% (4.0 x 10^{-3} kg/m^3) at 20 °C reduced the mass of the solid residue from 37.1% in dry air to 18.6% in humidified air. Therefore, there may be an optimum moisture content that can help in reducing/eliminating the solid residue formation in the NTP-DBD system.

6.2.2 Effect of water vapour

The relative humidity was varied across the range of 0% - 40% at 20°C. Figure 6.5 shows the effect of relative humidity on the removal efficiency of benzene.

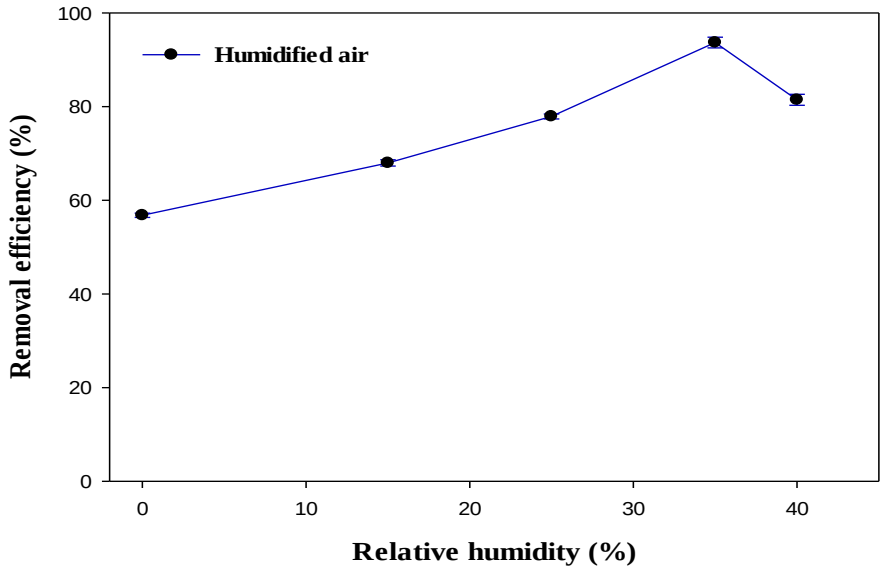

Figure 6.5 Effect of relative humidity on the removal efficiency of benzene (Reaction conditions: Power = 10 W; Temperature = ambient, Concentration = 350 ppm; Total flow rate = 100 ml/min; Residence time = 2.3 s, SIE = 6 kJ/L).

Clearly, the removal efficiency of benzene increased with increasing relative humidity. The benzene removal efficiency was 56.8% at RH of 0% at 20°C, which increased to 93.7% at RH of 35% at 20°C. The increased removal efficiency of benzene could be due to the formation of OH radicals in the humidified air. The water vapour plays a vital role as it provides H and OH radicals via the electron impact dissociation of H_2O molecules (Vandenbroucke *et al.*, 2011; Abdelaziz *et al.*, 2018):

$$e + H_2O \rightarrow e + OH^{\cdot} + H^{\cdot} \qquad R\ (6.1)$$

$$N_2(A^3\Sigma_u^{\ +}) + H_2O \rightarrow N_2 + OH^{\cdot} + H^{\cdot} \qquad R\ (6.2)$$

$$e + O_2 \rightarrow e + O(^1D) + O(^3P) \qquad R\ (6.3)$$

$$O(^1D) + H_2O \rightarrow 2OH^{\cdot} \qquad R\ (6.4)$$

As the relative humidity increases, the OH radical concentration will increase, which leads to higher removal efficiency of benzene and selectivity to CO_2. It has been reported that OH radicals generated in humidified air plasmas are much more potent oxidants than the oxygen atoms or peroxy radicals produced in the non-thermal plasma technique (Jiang *et al.*, 2015).

Figure 6.6 shows the effect of increasing humidity on the conversion to CO and CO_2.

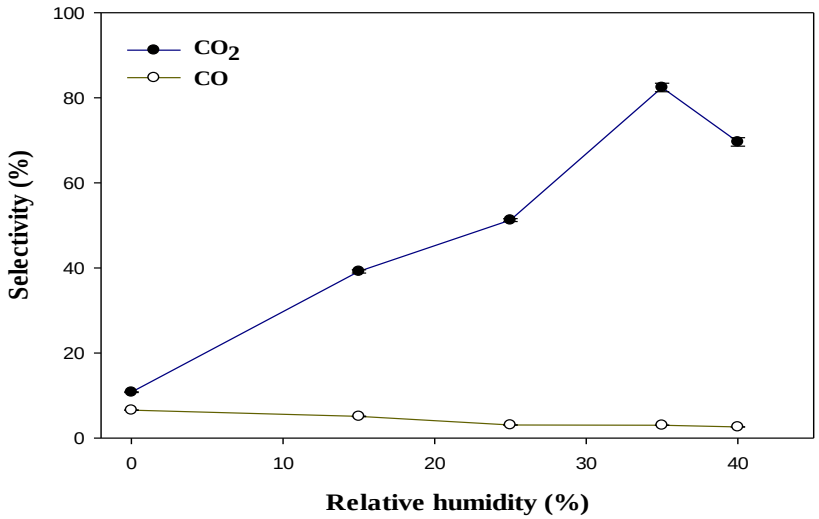

Figure 6.6 Effect of relative humidity on selectivity to CO and CO_2 (Reaction conditions: Power = 10 W; Temperature = ambient, Concentration = 350 ppm; Total flow rate = 100 ml/min; Residence time = 2.3 s, SIE = 6 kJ/L).

Clearly, increasing humidity is desirable here, as it increases CO_2, which is desirable as a non-toxic product, and decreases CO. Note that the CO level at all powers is well below the occupational exposure limit of 50ppm, as it is in the range of 3-18ppm. It was observed that selectivity to CO_2 increased from 18.6% to 82.4% when the relative humidity increased from 0% to 35% at 10 W, respectively. The formation of more radicals such as OH and O at higher relative humidity must account for the increase in selectivity to CO_2 (Raju. *et al.*, 2013; Ma *et al.*, 2016). However, increasing the relative humidity further (between 40% to 80%) may negatively affect the removal efficiency of alkanes and aromatic VOCs in NTPs.

The effect of increasing humidity on selectivity to C_1-C_5 is shown in Figure 6.7.

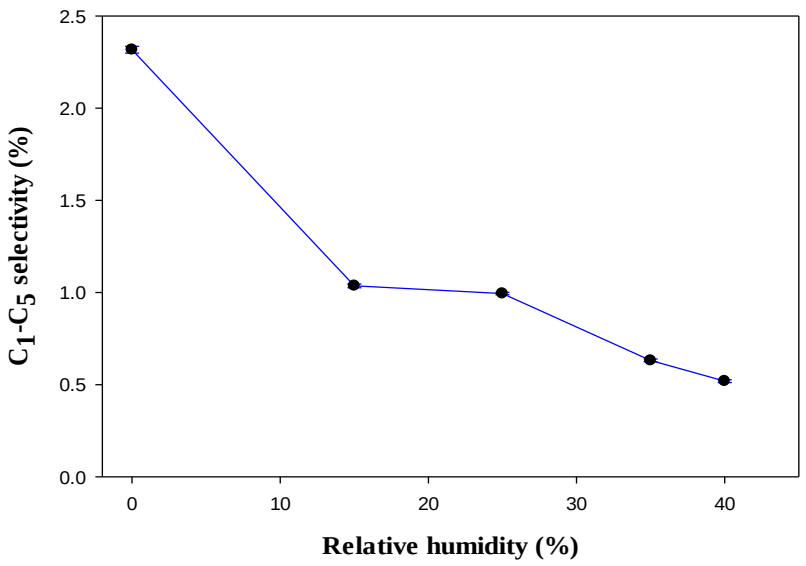

Figure 6.7 Effect of relative humidity on selectivity to C_1-C_5 (Reaction conditions: Power = 10 W; Temperature = ambient, Concentration = 350 ppm; Total flow rate = 100 ml/min; Residence time = 2.3 s; SIE = 6 kJ/L).

The selectivity to C_1-C_5 hydrocarbons decreased with increasing relative humidity, as shown in Figure 6.7. The presence of O and OH radicals in the plasma system suppressed LHC formation or oxidised the LHC intermediates to CO_2.

However, increasing the relative humidity further (between 40% to 80%) may negatively affect the removal efficiency of alkanes and aromatic VOCs in non-thermal plasmas. In this study, the influence of increasing relative humidity above 35% (i.e., relative humidity of 40% at 20 ℃ at 10 W) was investigated. The removal efficiency of benzene and CO_2 selectivity significantly decreased from 93.7% and 82.4% to 81.4% and 69.8% as the relative humidity increased from 35% to 40% at 10 W, as shown in Figure 6.5 and, Figure 6.6 respectively. This indicates the negative effect of excess water vapour on benzene decomposition. As the relative humidity increases, more energetic electrons may be quenched by electronegative water molecules, lowering the electron density and average energy in the discharge region, reducing active species generation, which decreases removal efficiency and CO_2 selectivity (Jiang *et al.*, 2016). At higher relative humidity, the presence of water vapour may also change the plasma characteristics, thereby reducing the total charge transferred in a micro-discharge of DBD plasma and, as a result, decreasing the volume of the reactive plasma zone (Falkenstein *et al.*, 1997). The selectivity to lower hydrocarbons also decreased with increasing relative humidity to 40%, as shown in Figure 6.7.

In this study, the maximum removal efficiency of benzene was about 93.7%, and the highest CO_2 selectivity (82.4%) was achieved at a relative humidity of 35% (absolute humidity = 0.006 kg/m^3) at 20℃ at 10 W. Hence, relative humidity of 35% at 20℃ appears to be the most suitable humidity in the range for the non-thermal plasma decomposition of benzene. Even though maximum removal efficiency, CO_2 selectivity and elimination of solid residue were achieved at 35% relative humidity, the carbon balance was the incomplete due possible formation of condensable products. Therefore, the ice cooling trap method collected the condensable products. The collected liquid phase sample was qualitatively analysed using GC-MS. The GC-MS analysis revealed that the liquid-phase products consist of oxygenates such as 2-hexanone, 3-hexanone and 3-hexanol, respectively.

Summary of benzene removal efficiency and product selectivities is presented in Table 6.1.

Table 6.1 Overview of benzene removal efficiency and product selectivities. (Conditions: Total flow rate = 100 ml/min, Power = 10 W, Concentration = 350 ppm, SIE = 6 kJ/L, Relative humidity = 35% at 20℃).

Compounds	**Removal efficiency (%)**	**Selectivity (%)**
Benzene	93.7	
CO_2	-	82.4
CO	-	3.0
C_1-C_5	-	0.7
Oxygenates	-	13.9

6.2.3 Ozone and NOx formation in the DBD reactor

In dry air, non-thermal plasma decomposition of VOCs unavoidably produces O_3. The generation of O_3 in the plasma DBD system is initiated through collisions between energetic electrons and the oxygen molecules, which convert O_2 into atomic oxygen:

$$\mathrm{e} + \mathrm{O_2} \rightarrow \mathrm{O}(^3\mathrm{P}) + \mathrm{O}(^3\mathrm{P}) + \mathrm{e}\ (6.1\ \mathrm{eV}) \qquad \mathrm{R}(6.5)$$ (Gudmundsson *et al.*, 2013)

$$\mathrm{e} + \mathrm{O_2} \rightarrow \mathrm{O}(^3\mathrm{P}) + \mathrm{O}(^1\mathrm{D}) + \mathrm{e}\ (8.4\ \mathrm{eV}) \qquad \mathrm{R}(6.6)$$ (Gudmundsson *et al.*, 2013)

Furthermore, the reaction between the excited state of nitrogen and oxygen can produce additional O radicals in the air, as shown in R (6.7) (Kogelschatz *et al.*, 1997).

$$\mathrm{N_2}\left(A^3\textstyle\sum_u^+ \mathrm{B}^3\Pi_g\right) + \mathrm{O_2} \rightarrow \mathrm{N_2} + \mathrm{O} + \mathrm{O} \qquad \mathrm{R}\ (6.7)$$

O_3 can be formed through a three-body recombination reaction of molecular oxygen and atomic oxygen, as shown in R (6.8).

$$\mathrm{O} + \mathrm{O_2} + \mathrm{M} \rightarrow \mathrm{O_3} + \mathrm{M} \qquad \mathrm{R}\ (6.8)$$ (Zhu *et al.*, 2014)

The third body, M, can be oxygen or nitrogen or the surface of the dielectric in the DBD reactor (Atkinson *et al.*, 1997; Zhu *et al.*, 2014). For a better understanding of the influence of water vapour on the O_3 concentration in benzene decomposition, it was evaluated across a range of relative humidities, from 0% to 35% at 20 ℃ at constant power at ambient conditions.

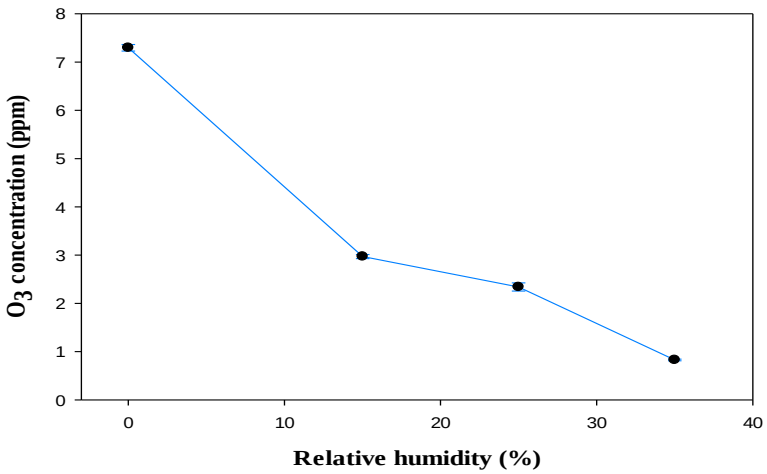

Figure 6.8 Ozone concentration as a function of relative humidity (Reaction conditions: Power = 10 W; Temperature = ambient; SIE = 6 kJ/L).

The introduction of water vapour significantly decreased the ozone concentration. The ozone concentration decreased from 7.3 ppm at 0% RH to 0.5 ppm at 35% RH at 20℃, as shown in Figure 6.8. The introduction of water vapour into the DBD system causes the production of hydroxyl radicals (OH), which would result in the rapid consumption of O atoms (Zhu *et al.*, 2014). The OH radical is the most desired reactive species since it is a powerful and non-selective oxidant. It can react with most organic contaminants by either removing hydrogen from alcohols and saturated aliphatic hydrocarbons or adding electrophilic H to unsaturated hydrocarbons (Lukes *et al.*; Hama Aziz *et al.*, 2017).

The addition of water vapour to the DBD suppressed ozone generation as a result of the consumption of $O(^1D)$ (Ma *et al.*, 2016). In addition, O_3 concentration decreased due to an increase in direct interactions between O_3 and gas-phase radicals, including OH and H radicals. The generation of OH and H radicals from electron impact dissociation of H_2O was described in R (6.1). Therefore, the O_3 destruction reactions can be summarised as (Zhu *et al.*, 2008; Karuppiah *et al.*, 2012):

$$O_3 + H^{\cdot} \rightarrow O_2 + OH^{\cdot} \qquad \text{R (6.9)}$$

$$O_3 + OH^{\cdot} \rightarrow O_2 + HO_2^{\cdot} \qquad \text{R (6.10)}$$

$$O_3 + HO_2^{\cdot} \rightarrow 2O_2 + OH^{\cdot} \qquad \text{R(6.11)}$$

NOx is a common undesired by-product in the NTP decomposition of volatile organic compounds, and its generation can cause severe environmental problems (Subrahmanyam *et al.*, 2006). NO_x can be generated through the electron impact dissociation of N_2/O_2 (dry air) as described in R (6.12)-R (6.16) (Zheng *et al.*, 2014; Zhu *et al.*, 2014). However, the OH radicals can oxidise NO to form HNO_2 as shown in R (6.17) (Zheng *et al.*, 2013).

$$N_2 + e \rightarrow N^{\cdot} + N^{\cdot} + e \qquad \text{R (6.12)}$$

$$O_2 + e \rightarrow O^{\cdot} + O^{\cdot} + e \qquad \text{R (6.13)}$$

$$N + O \rightarrow NO \qquad \text{R (6.14)}$$

$$NO + O \rightarrow NO_2 \qquad \text{R (6.15)}$$

$$O_3 + NO \rightarrow O_2 + NO_2 \qquad \text{R (6.16)}$$

$$OH + NO \rightarrow HNO_2 \qquad \text{R (6.17)}$$

NO_x concentrations were measured using Gastec Detector Tubes (detection limit = 0.1 ppm). In this study, no traces of NO_x were identified under all the experimental conditions. Similar findings have been reported in the plasma-assisted decomposition of alkanes and aromatic VOCs (Raju. *et al.*, 2013). This could be due to the presence of water vapour in the reaction, which provides more OH radicals in the plasma discharge, resulting in fast oxidation of the VOC molecules (Zhu *et al.*, 2014). In addition, OH radicals suppressed the formation of O_3 in the decomposition process, leading to the conversion of NO_x to HNO_2. In addition, OH radical shut down the O_3 containing route, as shown in R (6.10). Therefore, it is possible to eliminate or reduce NO_x concentrations below 0.1 ppm by controlling the amount of water vapour in the carrier gas and plasma power.

6.2.4 Solid residue formation in the dielectric barrier discharge reactor

The formation of solid residues in the plasma-assisted decomposition of volatile organic compounds is one of the major drawbacks limiting the full application of non-thermal plasmas DBD reactors. Previous researchers have observed the formation of dark-brown and light-yellow solid residues inside the dielectric barrier discharge reactor during benzene decomposition (Guo *et al.*, 2008; Saleem *et al.*, 2019g). In addition, the appearance of polymeric materials in the DBD reactor after benzene decomposition has been reported (Cal *et al.*, 2001; Ye *et al.*, 2008).

In this study, solid residues were formed on the inner wall of the DBD reactor and the surface of the inner tube in dry and humidified air carrier gases, as shown in Figure 6.9 (a) and Figure

6.9Figure 6.9 (b). It was observed that the colour of the residue was dark brown in dry air plasma and yellowish-brown in the humidified air carrier gas. Saleem *et al.* (2019g) reported similar findings in the plasma-assisted decomposition of benzene using H_2 and CO_2 carrier gases. Karatum *et al.* (2016) reported the formation of dark-brown solid residue in the plasma-assisted decomposition of ethylbenzene and toluene. However, Figure 6.9 (b) and Figure 6.9 (c) show how this deposition decreased with increasing humidity. The solid residue formation is undoubtedly due to the oligomerisation reactions of smaller monomers and benzene itself to oligomers (Saleem *et al.*, 2019a).

(a) Dry air plasma

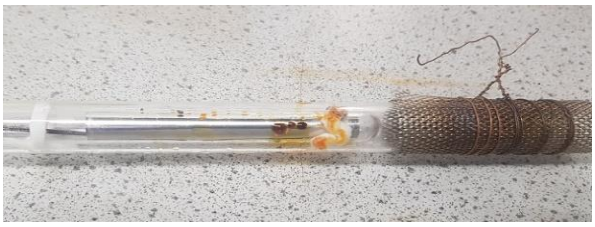

(b) Humidified air plasma (RH 25% at 20 ℃)

(c) Humidified air plasma (RH 35% at 20 ℃)

Figure 6.9 Plasma DBD reactors after benzene decomposition in nitrogen, dry and humidified air carrier gases. (a) Nitrogen plasma, (b) Dry air plasma, (c) Humidified air plasma.

The name of the compound, chemical formula, and chemical structure of the composition of the solid residues formed during the decomposition of benzene decomposition is presented in Table 6.2.

Table 6.2 Decomposition products identified by GC-MS in dry and humidified air

Name of compound	Chemical formula	Chemical structure	Dry air	Humidified air
3-Hexanone	$C_6H_{12}O$	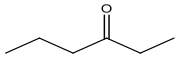	−	+
2-Hexanone	$C_6H_{12}O$	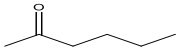	−	+
3-Hexanol	$C_6H_{14}O$	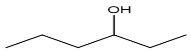	−	+
2,4-Dimethylheptane	C_9H_{20}	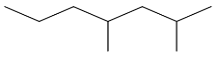	−	+
Ethylbenzene	C_6H_{10}	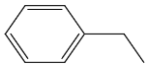	+	−
Ethynylbenzene	C_8H_6	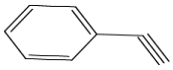	+	+
Styrene	C_8H_8	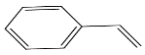	+	−
Hydroperoxide,1-ethylbutyl	$C_6H_{14}O_2$	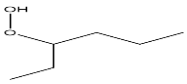	−	+
Hydroperoxide,1-methylpentyl	$C_6H_{14}O_2$	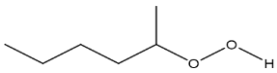	−	+
Pyridine, 3-methyl	C_6H_7N	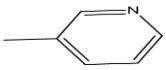	+	−
Benzonitrile	C_6H_5N	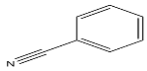	+	+
1,2-Propynylbenzene	C_9H_8	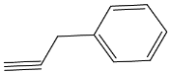	+	−
Nitrobenzene	$C_6H_5NO_2$	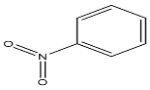	−	+
2-Nitrophenol	$C_6H_5NO_3$	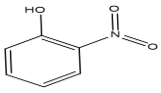	−	+

" − ": not detected and " + " : detected

In dry air plasma, the composition of the solid residue includes aromatics such as ethylbenzene, styrene, ethynylbenzene, benzonitrile, and 1,2-propenyl benzene. These are undesired products in the plasma decomposition of VOCs. The introduction of water vapour (relative humidity of 25% at 20℃) reduced the formation of aromatics products and promoted the formation of oxygenated products, including 3-hexanone and 2-hexanone, 3-hexanol, etc. The solid deposit accounted for 37.1% of the carbon in the decomposition process in dry air plasma and reduced to18.6% when water vapour with RH of 25% at 20℃ was introduced to the DBD system at 10 W, 350 ppm and 2.3 s. This was probably due to the formation of OH radicals in the plasma. It also implies that water vapour (relative humidity of 25% at 20℃) promotes the decomposition process towards increasing the removal efficiency of benzene. The detailed peaks of the products identified by the GC-MS are also shown in Appendix A-6.1 and A-6.2.

Previous work on the decomposition of VOCs using a non-catalytic and catalytic plasma system described the residues as carbonaceous or aromatic deposits (Chen *et al.*, 2009; Karatum *et al.*, 2016). The formation of solid residues during the decomposition process is a matter of concern because their production may foul the dielectric barrier discharge reactor over a long operation time and are undesirable by-products. Solid residue formation must be minimised or eliminated for DBD plasma techniques to be more effective and efficient.

Here, increasing the relative humidity to 35% at 20℃ removed the solid residue entirely, indicating that humidification of the input stream could be a straightforward solution to the problem, with various other benefits (reduction of ozone, CO, and lower HCs).

6.2.5 Benzene decomposition pathways in a DBD plasma system

Non-thermal plasmas consist of reactive species such as energetic electrons, atoms, ions, and molecules. The highly energetic electrons generate excited species and gas-phase radicals. The energetic electrons can react with VOCs to decompose them into various products such as LHCs, CO_2 and H_2O (Lee *et al.*, 2004; Hoseini *et al.*, 2019). The average electron energy in a typical non-thermal plasma DBD process is in the range of 1–10 eV (Yan *et al.*, 2002; Fridman, 2008). Benzene is very stable, with a π −bond system. The bond dissociation energy (BDE) of C-H and C=C bonds in benzene is 4.6 eV and 5.4 eV (Xu *et al.*, 2014). The average electron energy of the plasma system at 0%, 15%, 25% and 35% RH is 4.14, 4.49, 4.74 and 5.0 eV, respectively, as evaluated using BOLSIG+ (See Appendix A-6.5) (Hagelaar *et al.*, 2005). Note that 4.6 eV is required to break the C-H bond in the aromatic ring of benzene.

There is a range of possible benzene decomposition pathways in a non-thermal plasma DBD reactor. Ring-opening and subsequent dehydrogenation of benzene by highly energetic electrons to form the phenyl radical $C_6H_5^{\cdot}$ is a common initial step (Jiang *et al.*, 2018):

$$C_6H_6 + e \rightarrow H^{\cdot} + C_6H_5^{\cdot} + e \qquad \text{R (6.18)}$$

In addition to the direct benzene decomposition by energetic electron impact reactions, collision-induced benzene decomposition by excited species such as N_2^*, $N^{\cdot}$ can also lead to the formation of phenyl radical as demonstrated in R (6.19):

$$C_6H_6 + N_2^* \rightarrow H^{\cdot} + C_6H_5^{\cdot} + N_2^* \qquad \text{R (6.19)}$$

Furthermore, the electron impact dissociation of H_2O and O_2 in the DBD system produces H, OH and O radicals that can initiate the decomposition reaction through dehydrogenation of benzene to form phenyl radical ($C_6H_5^{\cdot}$) R (6.20) -R (6.22) (Jiang *et al.*, 2018):

$$C_6H_6 + O^{\cdot} \rightarrow OH^{\cdot} + C_6H_5^{\cdot} \qquad \text{R (6.20)}$$

$$C_6H_6 + OH^{\cdot} \rightarrow H_2O + C_6H_5^{\cdot} \qquad \text{R (6.21)}$$

$$C_6H_6 + H^{\cdot} \rightarrow H^{\cdot} + H^{\cdot} + C_6H_5^{\cdot} \qquad \text{R(6.22)}$$

The ring derivatives of benzene, such as phenol, nitrobenzene, and 2-nitrophenol, can be formed through the reaction between phenyl radicals and gas-phase radicals, as shown in R (6.23)-R (6.25) (Lee *et al.*, 2004; Ma *et al.*, 2016).

$$C_6H_5^{\cdot} + OH^{\cdot} \rightarrow C_6H_5OH \qquad \text{R (6.23)}$$

$$C_6H_5^{\cdot} + NO_2^{\cdot} \rightarrow C_6H_5NO_2 \qquad \text{R (6.24)}$$

$$C_6H_5^{\cdot} + O^{\cdot} + NO_2^{\cdot} \rightarrow C_6H_5NO_3 \qquad \text{R (6.25)}$$

The O and OH radicals can further oxidise the reaction intermediate to form C_5H_5OH, CO_2 and H_2O R (6.26) – R (6.30) (Jiang *et al.*, 2018).

$$C_6H_5^{\cdot} + O^{\cdot} \rightarrow CO + C_5H_5^{\cdot} \qquad \text{R (6.26)}$$

$$C_5H_5^{\cdot} + OH^{\cdot} \rightarrow C_5H_5OH \qquad \text{R (6.27)}$$

$$C_5H_5OH + OH^{\cdot} \rightarrow H_2O + C_5H_4OH \qquad \text{R (6.28)}$$

$$C_5H_4OH + O_2 \rightarrow HO_2 + C_5H_4O^{\cdot} \qquad \text{R(6.29)}$$

$$C_5H_4O^{\cdot} + O^{\cdot} \rightarrow CO_2 + C_4H_4^{\cdot} \qquad \text{R (6.30)}$$

However, apart from the oxygenated products, the reactive species can react with the fragments of model VOC and open a new pathway for the formation of lower hydrocarbons (C_1-C_4), CO and CO_2, as shown in R (6.31)-R (6.35) :

$$C_4H_4^{\cdot} + OH^{\cdot} \rightarrow CO + C_3H_5^{\cdot} \qquad \text{R (6.31)}$$

$$C_3H_5^{\cdot} + OH^{\cdot} \rightarrow CO + C_2H_6 \qquad \text{R (6.32)}$$

$$C_2H_6 + e \rightarrow CH_3^{\cdot} + CH_3^{\cdot} + e \qquad \text{R (6.33)}$$

$$2CH_3^{\cdot} + 2H^{\cdot} \rightarrow 2CH_4 \qquad \text{R (6.34)}$$

$$2CO + O_2^{*} \rightarrow 2CO_2 \qquad \text{R (6.35)}$$

Moreover, the reaction intermediates can form higher hydrocarbons such as benzonitrile, ethylbenzene, ethynylbenzene, 2, 4-dimethylheptane, 1, 2-propenyl benzene and pyridine, 3-methyl as identified in the GC-MS analysis.

6.3 Comparative decomposition of hexane, cyclohexane, and benzene in different carrier gases: understanding the effects of chemical structure

The removal efficiency of different C_6 VOCs (hexane, cyclohexane, benzene) in nitrogen, dry and humidified air carrier gases is presented in Figure 6.10.

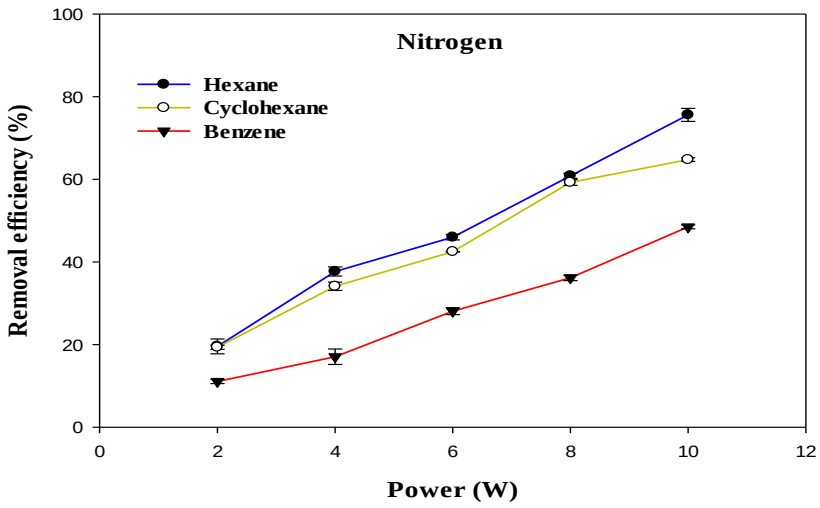

(a)

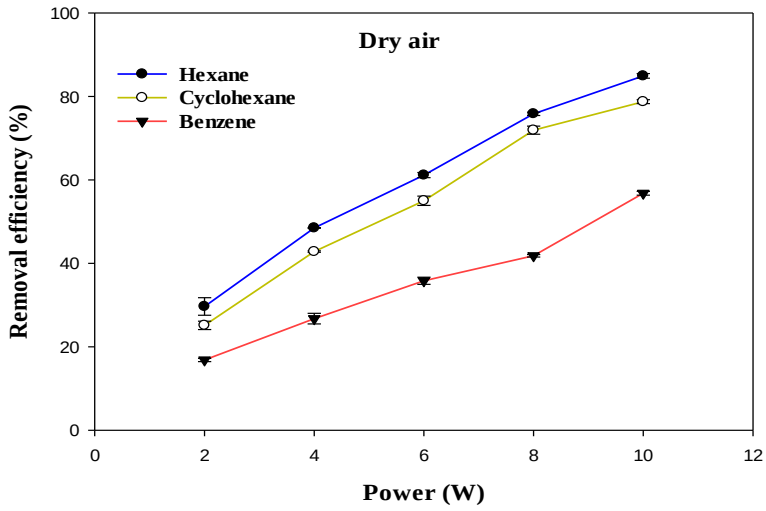

(b)

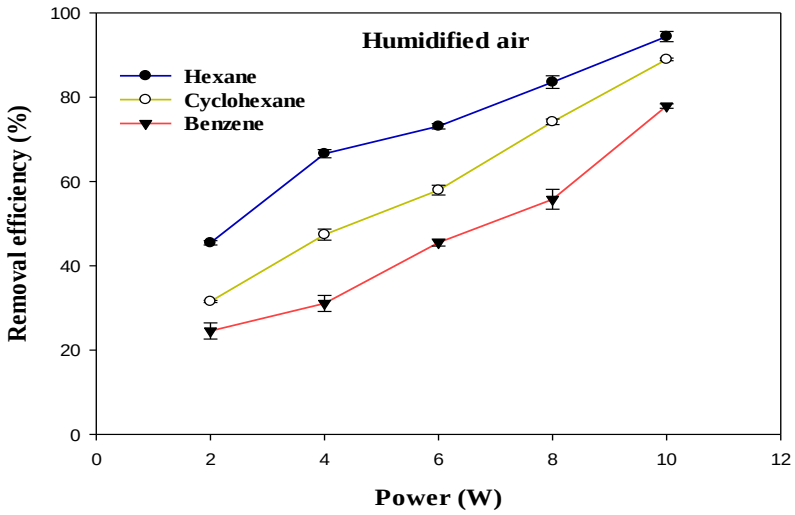

(c)

Figure 6.10 Effect of power and carrier gases on the removal efficiency of HCB (a) nitrogen, (b) dry air, and (c) humidified air (Reaction conditions: Temperature = ambient; Concentration = 350 ppm; Total flow rate = 100 ml/min; Residence time = 2.3 s, Relative humidity 25%).

It shows that the removal efficiency of hexane, cyclohexane and benzene increased with increasing power regardless of the carrier gas used. Increasing the plasma power at constant inlet concentration and residence time can increase the number of highly energetic electrons and chemically reactive species ($O^{\cdot}$, $OH^{\cdot}$, N_2^*) capable of initiating various reactions in the DBD reactor, increasing the removal efficiency of VOCs (Zhu *et al.*, 2015).

The order of the removal efficiency follows benzene < cyclohexane < hexane. The maximum removal efficiency was achieved in humidified air plasma. It was noted that the oxidation power of OH radicals is higher than excited O_2, O or N_2 species or other radicals generated in NTP

reactors (Sun *et al.*, 1997). The findings revealed that water vapour with a relative humidity of 25% at 20 ℃ significantly impacts the removal efficiency of the C_6 series in the NTP-DBD reactors. It has been reported that a relative humidity of about 30% increased the concentration of OH radicals during the NTP decomposition of benzene (Kim *et al.*, 2003). In addition to the energetic electron-initiated decomposition of hexane, cyclohexane and benzene, the formation of more reactive OH and O radicals at higher power opens new decomposition pathways via oxidation of model VOCs and intermediates resulting in higher removal efficiency and CO_2 selectivity in humidified air plasma. The enhanced average electron energy of the humidified air is another factor affecting the reaction (nitrogen (3.85 eV), dry air (4.14 eV) and humidified air (4.73 eV) as evaluated using BOLSIG+ (Appendix A-6.5) (Hagelaar *et al.*, 2005)). Therefore, the maximum removal efficiency obtained in humidified air plasma can be attributed to its highest average electron energy and the formation of more reactive species (i.e., OH, O) in the reactor.

Figure 6.10 shows that the removal efficiency is different in the decomposition of hexane, cyclohexane, and benzene, indicating that the chemical structure of the model VOCs does play an important role in the reaction under plasma conditions. As shown in Figure 6.10, hexane was more easily decomposed than cyclohexane and benzene in all the carrier gases. This is due to the differences in the chemical structure and bond dissociation energy of the model VOCs. The strength of the chemical bond of the VOC molecules is one of the main parameters affecting the removal efficiency of VOCs in the plasma system. The C-H and C-C bond dissociation energy in the model, VOCs, are summarized in Table 6.3.

Table 6.3 Bond dissociation energy of hexane, cyclohexane, and benzene.

Model VOC	**Bond dissociation energy (eV)**	
	C-H	**C-C**
Hexane	4.25	3.74
Cyclohexane	4.32	3.82
Benzene	4.60	5.40

Among the C_6 series of VOCs, the bond dissociation energy of the C-C bond in the benzene ring (5.4 eV) is the highest, followed by that in cyclohexane (3.82 eV), and that in hexane (3.74 eV). Therefore, simple hydrocarbons, e.g., alkanes, are easier to decompose than cyclic alkanes and aromatic VOCs. The carbon balance of some of the results of the plasma-assisted decomposition of hexane, cyclohexane and benzene are presented in Appendix A-6.6.

One of the key factors restricting the broad application of non-thermal plasma DBD reactors is the formation of solid residues in the plasma-assisted decomposition of VOCs. In this work,

solid residues formed in hexane, cyclohexane, and benzene decomposition due to the oligomerization of hydrocarbon radicals generated in the plasma reactor. Table 6.4 summarises the solid residue formation in different carrier gases.

Table 6.4 Formation of solid residue in different carrier gases.

Carrier gas	**Model VOC**		
	C_6H_{14}	**C_6H_{12}**	**C_6H_6**
Nitrogen	Yellow	Dark brown	Dark brown
Dry air	Yellow	Yellow	Dark brown
Humidified air (RH = 25% at 20 ℃)	Disappeared	Disappeared	Yellow and dark brown

The solid deposition would cause operational problems by fouling and eventually blocking pipework. Therefore, the solid residue must be eliminated in the plasma reactor to address this problem. It has been observed that the introduction of water vapour with a relative humidity of 25% at 20 ℃ eliminated the formation of solid residue during the decomposition of hexane and cyclohexane. The presence of OH radicals has probably caused this effect. However, solid residue is also formed during benzene decomposition in humidified air under the same experimental conditions. This may be due to the lower hydrogen weight fraction in the benzene compared to hexane and cyclohexane. When the relative humidity is increased to 35%, however, the solid residue was eliminated, indicating the amount of OH is important in the plasma process and that the solid residue formed by the benzene was more intransigent than that formed by the other species. Perhaps this indicates that it contained more aromatic bonds than the other species' solid residues, which seems likely. The $OH^{\cdot}$ and $H^{\cdot}$ generated through dissociative electron collision with H_2O can easily react with H abstracted from hexane or cyclohexane. VOC molecules with a large number of hydrogens tend to be more reactive with $OH^{\cdot}$ or $H^{\cdot}$.

6.4 **Summary**

The decomposition of benzene in a DBD reactor was studied as a function of power and air humidity at ambient temperature and atmospheric pressure. The removal efficiency of benzene increased with increasing plasma power in both dry and humidified air plasma but was always significantly higher in humidified air and was as high as 93.7% in 35% humidified air. The benzene decomposition products were CO_2, CO, lower hydrocarbons (C_1-C_5) and solid residue. As power increased, the selectivity to CO and CO_2 increased, whereas C_1-C_5 decreased. The presence of water vapour had a number of desirable effects:

a. Significantly increased the removal efficiency of benzene

b. Significantly reduced formation of C_1-C_5
c. Increased selectivity to CO_2 (up to 82.4%)
d. Eliminated solid residue formation
e. Reduced ozone formation

Proposed mechanisms for these effects are given within this paper in detail, but all centre on the formation of OH radicals. The OH radical is highly reactive than oxygen excited species, and its presence opens up various new reaction pathways for the decomposition of benzene into smaller molecules, most of which are less toxic.

Overall, DBD performance in benzene decomposition, and therefore perhaps other aromatic VOCs, can be greatly improved by optimising plasma power and carrier gas moisture content. In particular, the elimination of solid residue by operating at higher humidities in this study provides an effective solution to a problem limiting the full application of the DBD system for VOC removal.

Chapter 7. Plasma-assisted removal of methanol in N_2, dry and humidified air using a dielectric barrier discharge (DBD) reactor

7.1 Introduction

In this part of the research, a non-thermal plasma dielectric barrier discharge (DBD) was used to remove methanol from ambient air. The effects of carrier gases (N_2, dry and humidified air), power (2-10 W), inlet concentration (260-350 ppm), and residence time (1.2-3.3 s) were investigated to evaluate the performance of the plasma DBD reactor in terms of removal efficiency, product selectivity and elimination/reduction of unwanted by-products. Pathways for the decomposition of methanol in the NTP-alone system using different atmospheric gases have been explored.

7.2 Results and Discussion

7.2.1 Effect of carrier gases and power

The effect of power on the removal efficiency of methanol in N_2, dry, and humidified air is shown in Figure 7.1. The input power significantly affects the performance of the reaction regardless of the carrier gas used. In N_2 carrier gas, methanol decomposition increases from 27.6% to 71.3% when the input power is increased from 2 W to 10 W (SIE = 1.7 – 8.6 kJ/L). This is generally expected because as the input power increases, the number of the energetic electrons increases, increasing the number of excited species, ions, and free radicals due to the collision between these energetic electrons and gas molecules (Saleem *et al.*, 2019d). Therefore, the reaction probability between the reactive species and CH_3OH molecules in the discharge zone increased (Wang *et al.*, 2019).

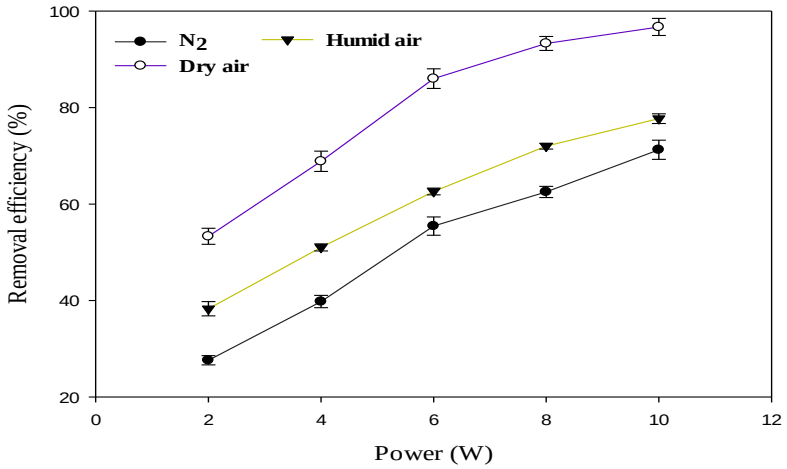

Figure 7.1 Effect of power in different carrier gases as a function of removal efficiency of methanol (Reaction conditions: Temperature = ambient; Concentration = 260 ppm; Total flow rate = 70 ml/min; Residence time = 3.3 s, SIE = 1.7 – 8.6 kJ/L, Relative humidity = 24%, Error bars represent the standard deviation ± σ for 3 measurement results).

The maximum methanol removal efficiency of 96.7% was achieved in dry air, followed by humidified air (77.7%) and N_2 (71.3%) at 10 W and 3.3 s. This was due to the action of the O radical in dry air, which dominates the plasma system's decomposition process. The average electron temperature of dry air is 4.14 eV, which is higher than the 3.85 eV mean electron energy of pure nitrogen (Luo, 2004). It is well known that the decomposition of dilute volatile organic compounds in dry air plasmas is initiated by the direct electron impact dissociation of N_2 and O_2 to form chemically reactive species such as N, $N_2(A^3\sum_u{}^+)$, O, and $O(^1D)$ for the conversion of VOCs and intermediates into H_2O, CO, CO_2, and other by-products (Zhu *et al.*, 2016b). Therefore, the generation of higher discharges in dry air plasma can lead to the formation of excited species such as O-radicals, excited N_2 and metastable $N_2(A^3\sum_u{}^+)$ (Sato *et al.*, 2005). This resulted in a more significant increase in the conversion of methanol.

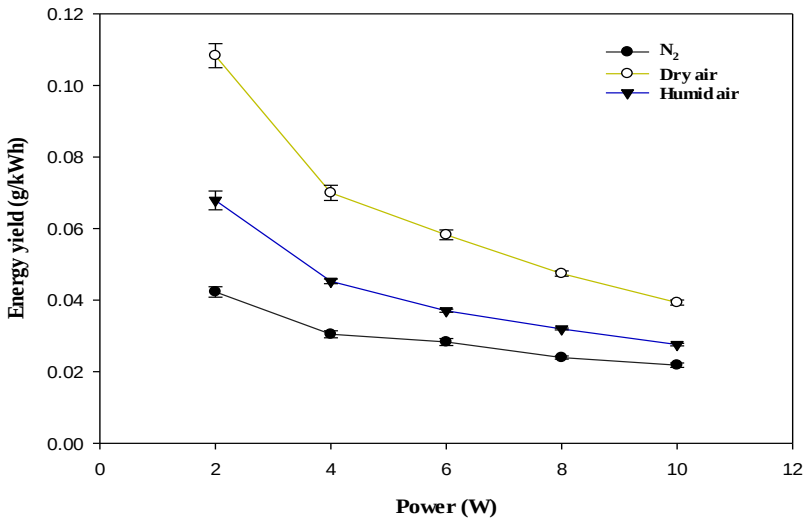

Figure 7.2 Effect of power and carrier gases on the energy yield (Reaction conditions: Temperature = ambient; Concentration = 260 ppm; Total flow rate = 70 ml/min; Residence time = 3.3 s, SIE = 1.7 – 8.6 kJ/L, Relative humidity = 24%, Error bars represent the standard deviation ± σ for 3 measurement results).

Figure 7.2 shows the effect of power and carrier gases on the energy yield of the plasma reaction process. The energy yield significantly decreased as the power increased from 2 to 10 W in all the carrier gases. For example, the energy yield decreased from 0.11 to 0.04 (g/kWh) with increased plasma power from 2 to 10 W in dry air plasma, which was inconsistent with previous results in Chapters 4-6. Previous studies have reported similar findings (Wang *et al.*, 2016; Saleem *et al.*, 2021a).

Carbon dioxide, carbon monoxide, methane, ethane, n-butane, butene, and hydrogen were produced in all carrier gases. Previous investigations reported only the production of CO, CO_2 and H_2 as the major products formed in dry or humid air carrier plasma (Shuji Tanabe, 2000).

The effect of power in different carrier gases as a function of selectivity to CO_2, CO, C_2-C_4, CH_4, and H_2 yield is presented in Figure 7.3 - Figure 7.4.

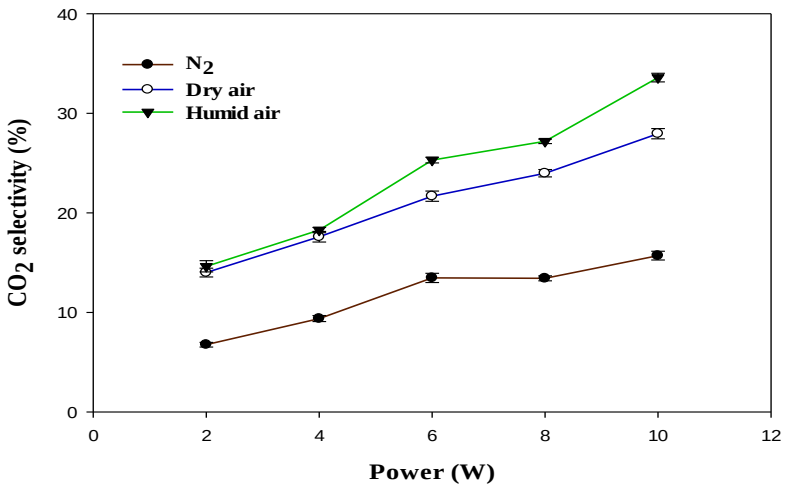

Figure 7.3 Effect of power in different carrier gases as a function of selectivity to CO_2 (Reaction conditions: Temperature = ambient; Concentration = 260 ppm; Total flow rate = 70 ml/min; Residence time = 3.3 s, SIE = 1.7 – 8.6 kJ/L, Relative humidity = 24%, Error bars represent the standard deviation ± σ for 3 measurement results).

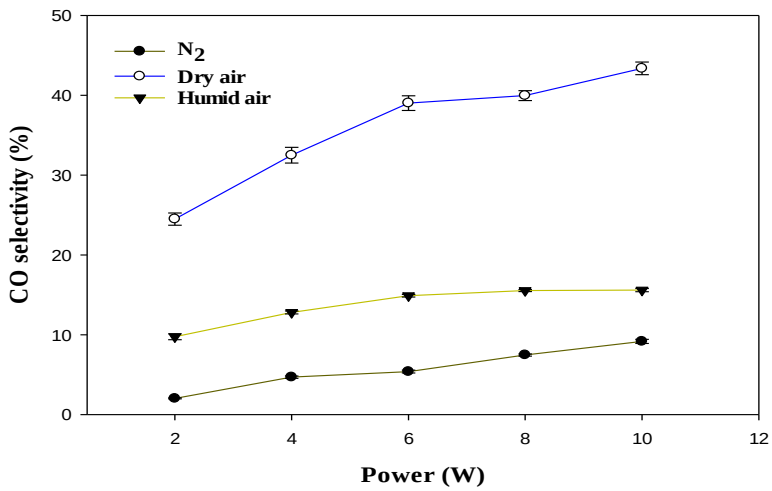

Figure 7.4 Effect of power in different carrier gases as a function of selectivity to CO (Reaction conditions: Temperature = ambient; Concentration = 260 ppm; Total flow rate = 70 ml/min; Residence time = 3.3 s, SIE = 1.7 – 8.6 kJ/L, Relative humidity = 24%, Relative humidity = 24%, Error bars represent the standard deviation ± σ for 3 measurement results).

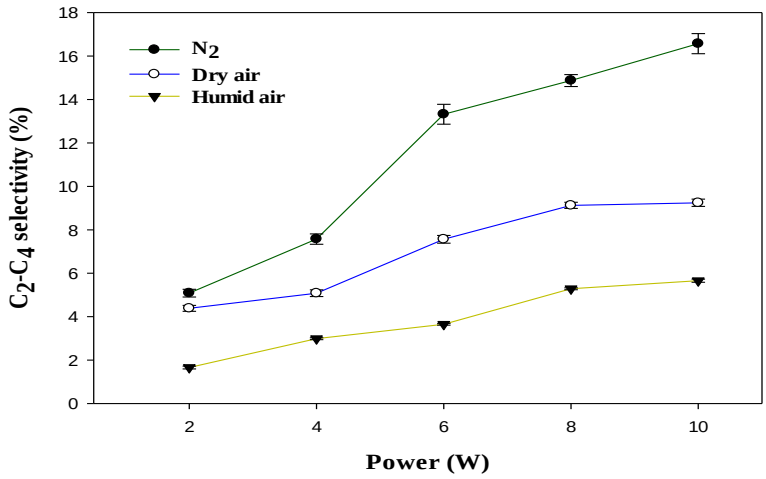

Figure 7.5 Effect of power in different carrier gases as a function of selectivity to C_2-C_4 (Reaction conditions: Temperature = ambient; Concentration = 260 ppm; Total flow rate = 70 ml/min; Residence time = 3.3 s, SIE = 1.7 – 8.6 kJ/L, Relative humidity = 24%, Error bars represent the standard deviation ± σ for 3 measurement results).

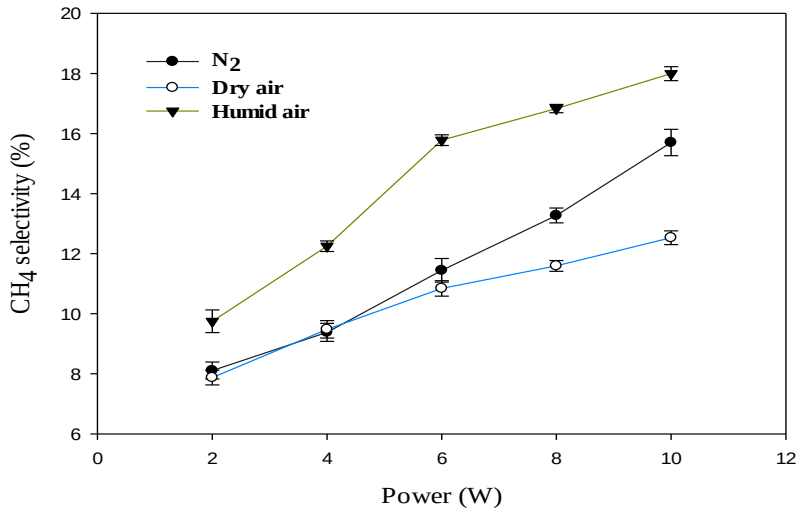

Figure 7.6 Effect of power in different carrier gases as a function of selectivity to CH_4 (Reaction conditions: Temperature = ambient; Concentration = 260 ppm; Total flow rate = 70 ml/min; Residence time = 3.3 s, SIE = 1.7 – 8.6 kJ/L, Relative humidity = 24%, Error bars represent the standard deviation ± σ for 3 measurement results).

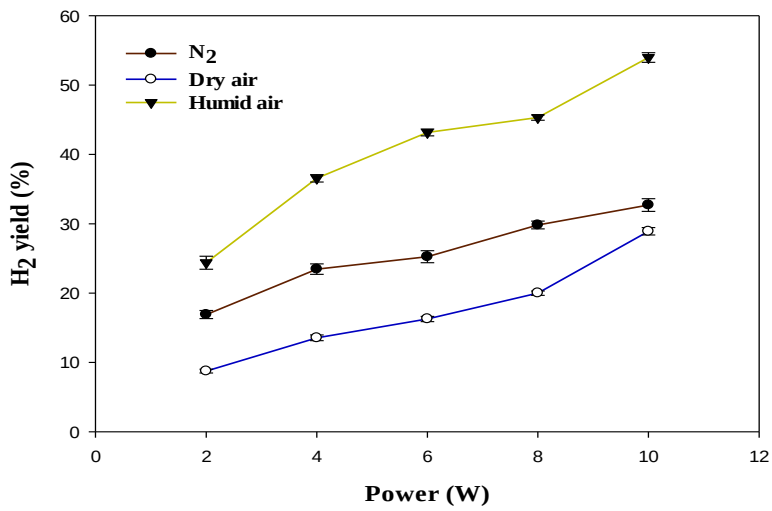

Figure 7.7 Effect of carrier gases and power on yield of H_2 (Reaction conditions: Temperature = ambient; Concentration = 260 ppm; Total flow rate = 70 ml/min; Residence time = 3.3 s, SIE = 1.7 – 8.6 kJ/L, Relative humidity = 24%, Error bars represent the standard deviation ± σ for 3 measurement results).

As presented in Figure 7.3 - Figure 7.4, increasing the input power increases product selectivity, indicating that the high input power directly enhances the product selectivity due to the high number of energetic electrons. The relationship between electron energy distribution function (EEDF) and electron energy indicates that the higher the mean electron energy is, the more electrons with higher energy will be generated (Michelmore *et al.*, 2013). Electron impact dissociation has been reported to play a significant role in decomposing VOCs to produce CH_3 radicals, which recombine to produce higher hydrocarbons (Saleem *et al.*, 2019a). These findings indicate that the presence of $O^{\cdot}$ in dry air favoured the formation of CO and suppressed hydrocarbon formation.

Figure 7.5 and Figure 7.6 also show that higher input power resulted in higher selectivity to C_2-C_4 and CH_4 in all the carrier gases. For instance, C_2-C_4 selectivity increased from 5.1% to 16.6% in N_2, and CH_4 selectivity increased from 9.7% to 17.9% in dry air. The selectivity to C_2-C_4 (C_2H_6, C_4H_{10} and C_4H_8) is higher in N_2 plasma than in dry and humidified air, especially at higher input power. This is because the presence of the O radical in dry air opens up routes to CO formation instead. The maximum selectivity to C_2-C_4 was observed in N_2 plasmas. This was due to enrichment in CH_3 radicals compared to other carrier gases tested here, which can be converted to CH_4, C_2H_6, C_2H_5, C_4H_8, and C_4H_{10} (see section **7.2.4**). In N_2 plasma, the probability of collision between CH_3OH and various excited N_2 species (e.g. metastable state nitrogen $N_2(A^3\sum_u{}^+)$) are higher, leading to more CH_3 radicals at higher residence time. The CH_3 can be dimerised to form C_2H_6, and CH_4 can be generated through the hydrogenation

reaction of CH_3, as shown in R (4)-R (5) (Kim *et al.*, 2014b). However, the selectivity to C_2-C_4 is lower in dry and humidified air when compared with N_2 plasma. This is because the presence of O and OH radicals in dry and humidified air oxidises the intermediate species to CO and CO_2 (Zhu *et al.*, 2016b). At the same time, the excited N_2, metastable N_2, can be quenched/consumed by oxygen species to form ground state N_2 and NOx (NO + NO_2). It is significant to note that NOx was not detected in the present study. Furthermore, as the input power increases, methanol decomposition leads to a higher yield of H_2 through recombination reaction of H-radicals or dissociation of CH_3OH (Kim *et al.*, 2014a; Zhang *et al.*, 2015b).

In humid air, this route is joined by other routes based on the OH radical formed from the dissociation of H_2O, which promotes CO_2 formation. In addition, O and OH radicals can also oxidise hydrocarbon species and CO leading to higher CO_2 selectivity (Trushkin *et al.*, 2013). The presence of water vapour reduces the methanol removal efficiency. This is probably due to the opening up of the reverse reaction OH + CH_3 to CH_3OH. Also, greater humidity reduces the transfer of charges between the electrodes, leading to a decrease in effective plasma volume, (Petitpas *et al.*, 2007) which leads to a higher reduction of the plasma electric field (Van Durme *et al.*, 2009), which would also decrease the removal efficiency.

However, water addition increased the selectivity to CO_2 and CH_4 and the yield of H_2, rather than CO and longer hydrocarbons. The increase in CO_2 selectivity is due to the more rapid oxidation of CO to CO_2 by the OH radical than by the $O^{\cdot}$ (dry air) or N_2* (in nitrogen only). Clearly, introducing water vapour to the NTP-alone system could (i) reduce CO generation, (ii) reduce O_3 concentration, (iii) increase the yield of H_2, and (iv) increase CO_2 selectivity. Detailed mechanisms of the methanol decomposition pathways are presented in **7.2.4**.

The formation of solid residues during the decomposition process is a source of concern because they can foul the DBD reactor over time and are undesirable by-products. Solid residue formation must be reduced or eliminated for DBD plasma techniques to be more effective and efficient (Saleem *et al.*, 2019c; Saleem *et al.*, 2020). In this work, no solid residue was formed in the DBD reactor in all the tested carrier gases. This could be due to the influence of operating conditions, reactor configuration and nature of the model VOC (i.e., CH_3OH), which produced more $OH^{\cdot}$ radicals through the dissociation of methanol during the decomposition process. In the NTP decomposition of VOCs, reactive species such as OH, O and H radicals can be generated due to the impact of energetic electrons on the VOC molecules and the carrier gases. The electrons have mean energies in the range 1-10 eV (Petitpas *et al.*, 2007). Therefore, in methanol decomposition, OH radicals can easily be generated from the electron impact dissociation of CH_3OH. It has been reported that OH and O radicals are potent oxidants

produced in the non-thermal plasma technique (Jiang *et al.*, 2015). The OH, H and O radicals generated in the plasma reactor can convert methanol and its intermediates to CO, CO_2, H_2 and H_2O. In addition, the methanol produces OH radicals that can break down C and more complex hydrocarbons that form the solid deposits. Another reason for the elimination of solid residue is the shorter discharge gap used in this study compared with the larger discharge gap from previous studies. The shorter discharge gap can significantly increase the electric field strength, which could increase the number of energetic electrons the energy in the plasma discharge zone (Ma *et al.*, 2015). The shorter discharge gap (1.5 mm) can facilitate the generation of more OH radicals from electron impact dissociation of CH_3OH, increasing the removal efficiency and fast oxidation of carbon species to CO and CO_2.

7.2.2 Effect of CH_3OH concentration

Figure 7.8 shows the effect of CH_3OH concentration on the removal efficiency in N_2, dry, and humidified air. The inlet concentration of CH_3OH was varied over the range of 260-350 ppm with a total gas flow rate of 70 ml/min (residence time of 3.3 s) and input power of 6 W at ambient temperature and atmospheric pressure. It was observed that the removal efficiency of methanol decreased with increasing the inlet concentration of CH_3OH regardless of the carrier gas used.

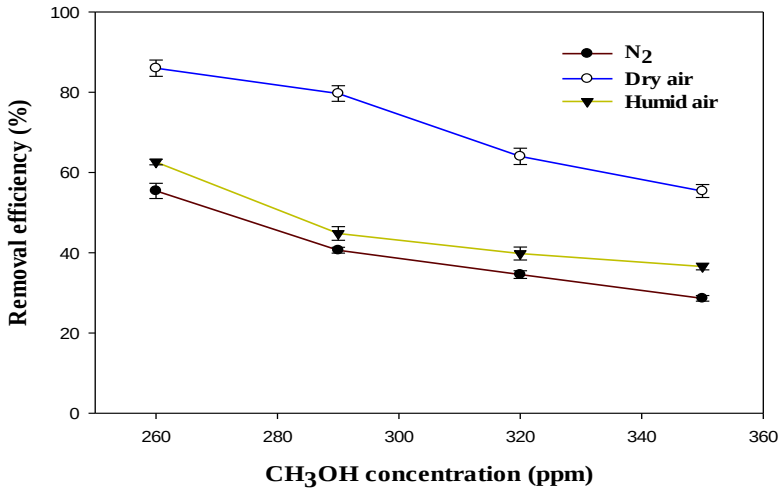

Figure 7.8 Effect of concentration on removal efficiency of methanol in N_2, dry and humidified air (Reaction conditions: Temperature = ambient; Power = 6 W; Total flow rate = 70 ml/min; Residence time = 3.3 s, SIE = 5.1 kJ/L, Relative humidity = 24%, Error bars represent the standard deviation ± σ for 3 measurement results).

For instance, the removal efficiency of methanol in N_2, dry and humidified air plasmas are 55.4%, 86.0% and 62.6% at an inlet concentration of 260 ppm, respectively. However, these

values decreased to 28.6%, 55.4% and 36.5% when the inlet concentration increased to 350 ppm. This is because the number of methanol molecules flowing into the DBD reactor increases while discharge length, input power, and residence time remain fixed. As a result, the undecomposed VOC molecules have a greater probability of leaving the DBD reactor discharge area unreacted.

The effect of CH_3OH inlet concentration on selectivity to CO_2, CO, C_2-C_4, CH_4, and H_2 yield in different carrier gases is presented in Figure 7.9 -Figure 7.13.

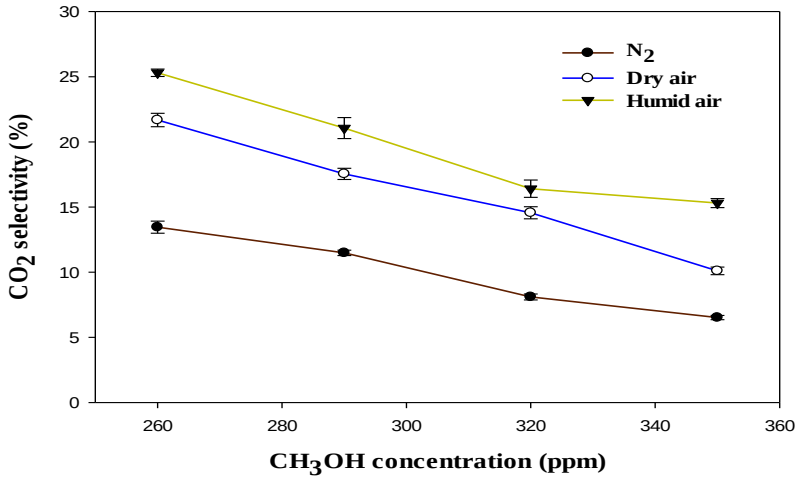

Figure 7.9 Effect of concentration on selectivity to CO_2 in N_2, dry and humidified air (Reaction conditions: Temperature = ambient; Power = 6 W; Total flow rate = 70 ml/min; Residence time = 3.3 s, SIE = 5.1 kJ/L, Relative humidity = 24%, Error bars represent the standard deviation ± σ for 3 measurement results).

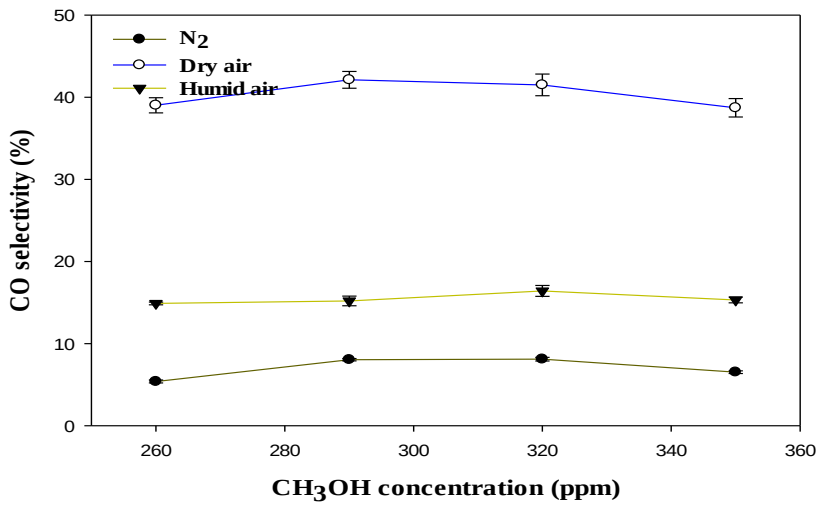

Figure 7.10 Effect of concentration on selectivity to CO in N_2, dry and humidified air (Reaction conditions: Temperature = ambient; Power = 6 W; Total flow rate = 70 ml/min; Residence time = 3.3 s, SIE = 5.1 kJ/L, Relative humidity = 24%, Error bars represent the standard deviation ± σ for 3 measurement results).

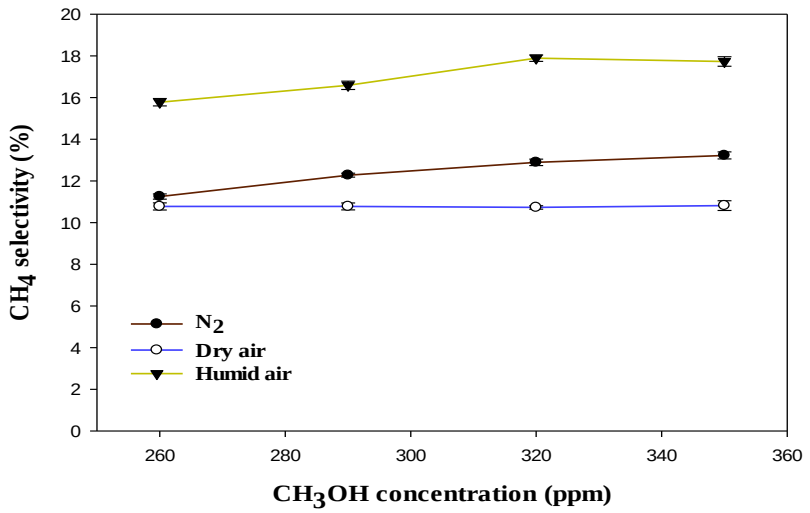

Figure 7.11 Effect of concentration on selectivity to CH_4 in N_2, dry and humidified air (Reaction conditions: Temperature = ambient; Power = 6 W; Total flow rate = 70 ml/min; Residence time = 3.3 s, SIE = 5.1 kJ/L, Relative humidity = 24%, Relative humidity = 24%, Error bars represent the standard deviation ± σ for 3 measurement results).

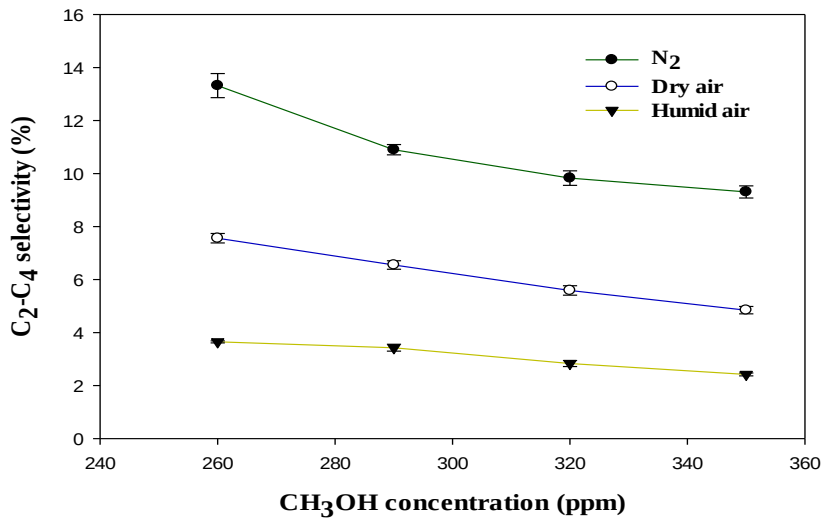

Figure 7.12 Effect of concentration on selectivity to C_2-C_4 in N_2, dry and humidified air (Reaction conditions: Temperature = ambient; Power = 6 W; Total flow rate = 70 ml/min; Residence time = 3.3 s, SIE = 5.1 kJ/L, Relative humidity = 24%, Error bars represent the standard deviation ± σ for 3 measurement results).

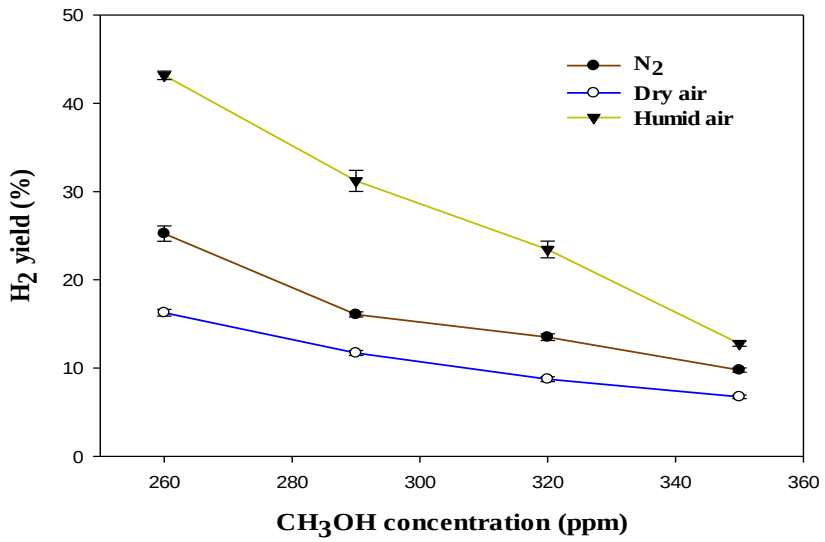

Figure 7.13 Effect of concentration on yield of H_2 in N_2, dry and humidified air (Reaction conditions: Temperature = ambient; Power = 6 W; Total flow rate = 70 ml/min; Residence time = 3.3 s, SIE = 5.1 kJ/L, Relative humidity = 24%, Error bars represent the standard deviation ± σ for 3 measurement results).

The selectivity to CO_2 decreased with increasing CH_3OH inlet concentration. For example, increasing CH_3OH inlet concentration from 260 ppm to 350 ppm resulted in a considerable decrease in CO_2 selectivity from 25.3% and 10.1% in dry air plasma. The selectivity to CO increased as the CH_3OH inlet concentration increased from 260 ppm to 320 ppm in all the carrier gases and then decreased when methanol concentration increased to 350 ppm. In humidified air plasma, an increase in CH_4 selectivity from 15.8 to 17.9% was observed when methanol concentration increased from 260 to 320 ppm, as shown in Figure 7.11. The selectivity to C_2-C_4 decreases as the CH_3OH inlet concentration increases, as more CH_3 radicals are produced, which react with H-radicals to form CH_4 (see mechanisms in section **7.2.4**).

The H_2 yield decreases as the CH_3OH inlet concentration increases from 260 to 350 ppm. This is because, at higher concentrations, the number of energetic electrons, excited species, and gas-phase radicals is reduced per methanol molecule, resulting in a more significant reduction in the yield of H_2 in the decomposition process. Furthermore, more VOC molecules were subjected to the discharge zone at higher concentrations, while the concentration of energetic electrons, excited species, and gas-phase radicals remained constant (Chen *et al.*, 2014; Norsic *et al.*, 2018).

7.2.3 Effect of residence time

Figure 7.14 shows the effect of residence time on the removal efficiency of methanol in N_2, dry, and humidified air carrier gases. The removal efficiency of methanol significantly

increased from 29.6%, 32.4%, 50.8% at 1.4 s to 55.4%, 62.6%, and 86.1% at 3.3 s in N_2, humidified and dry air carrier gases, respectively. Clearly, the removal efficiency of methanol significantly increases with increasing residence time in all carrier gases.

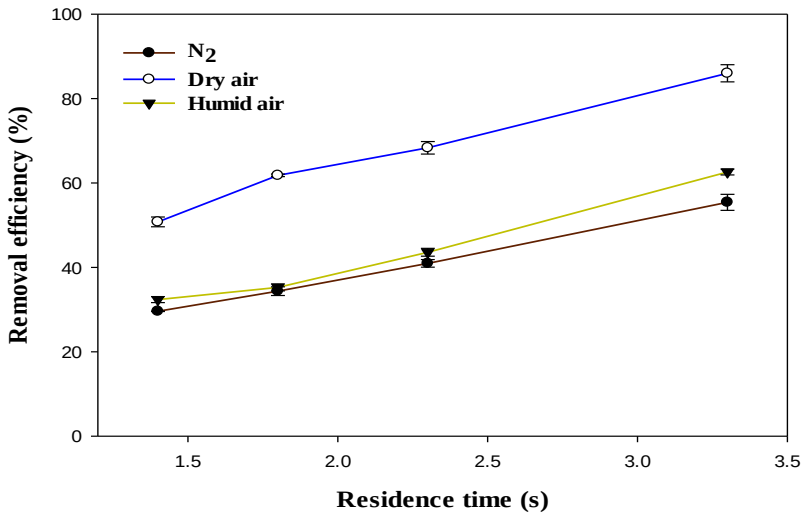

Figure 7.14 Effect of residence time on the removal efficiency of methanol in N_2, dry and humidified air (Reaction conditions: Temperature = ambient; Concentration = 260 ppm; Flow rate = 70 -160 ml/min; Power = 6 W, SIE = 2.3 - 5.1 kJ/L, Relative humidity = 24%, Error bars represent the standard deviation ± σ for 3 measurement results).

The VOC molecules have more time to interact with the reactive plasma-generated species at higher residence times, increasing removal efficiency(Saleem *et al.*, 2018). The maximum removal efficiency of methanol achieved was 86.1% at 3.3 s in dry air plasma.

The effect of residence time on selectivity to CO_2, CO, C_2-C_4, CH_4, and H_2 yield in different carrier gases is presented in Figure 7.15 - Figure 7.19.

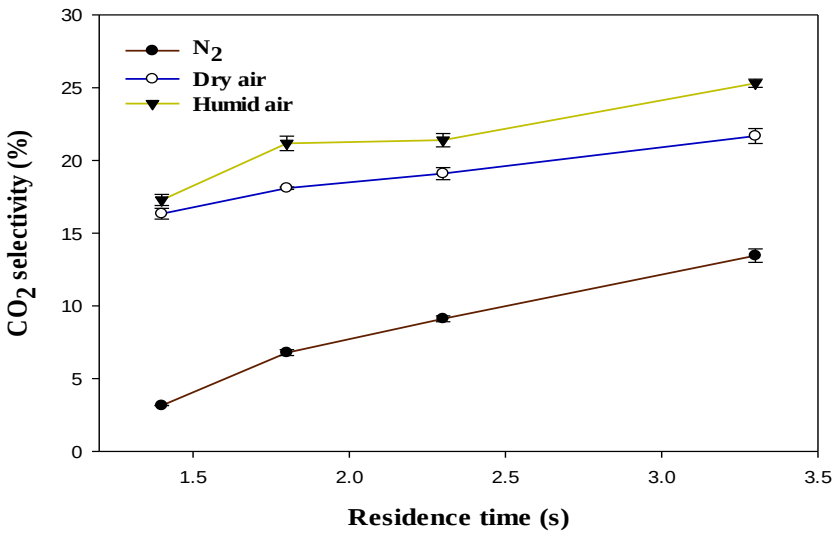

Figure 7.15 Effect of residence time on selectivity to CO_2 in N_2, dry and humidified air (Reaction conditions: Temperature = ambient; Concentration = 260 ppm; Flow rate = 70 -160 ml/min; Power = 6 W, SIE = 2.3 - 5.1 kJ/L, Relative humidity = 24%, Error bars represent the standard deviation ± σ for 3 measurement results).

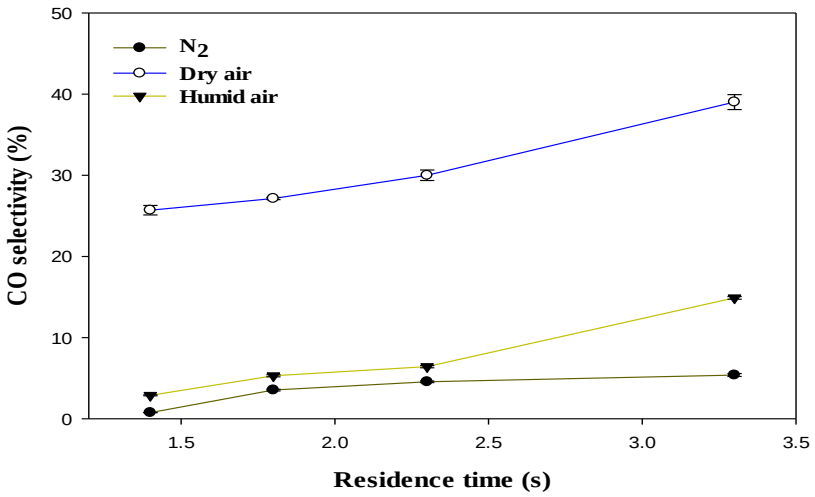

Figure 7.16 Effect of residence time on selectivity to CO in N_2, dry and humidified air (Reaction conditions: Temperature = ambient; Concentration = 260 ppm; Flow rate = 70 -160 ml/min; Power = 6 W, SIE = 2.3 - 5.1 kJ/L, Relative humidity = 24%, Error bars represent the standard deviation ± σ for 3 measurement results).

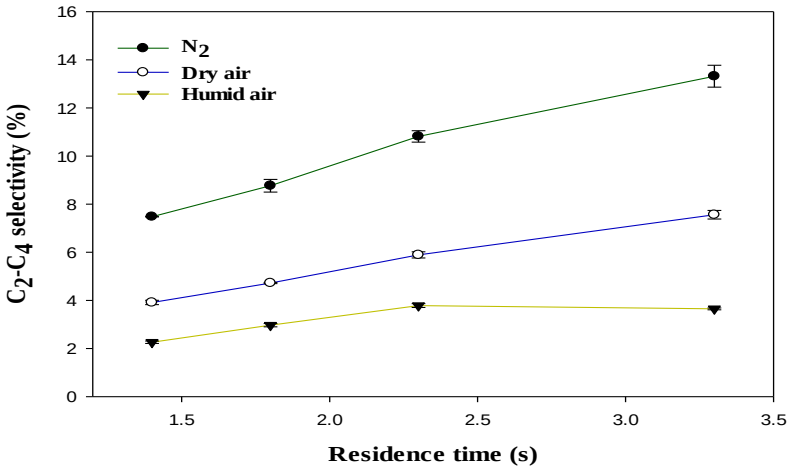

Figure 7.17 Effect of residence time on selectivity to C_2-C_4 in N_2, dry and humidified air (Reaction conditions: Temperature = ambient; Concentration = 260 ppm; Flow rate = 70 -160 ml/min; Power = 6 W, SIE = 2.3 - 5.1 kJ/L, Relative humidity = 24%, Error bars represent the standard deviation ± σ for 3 measurement results).

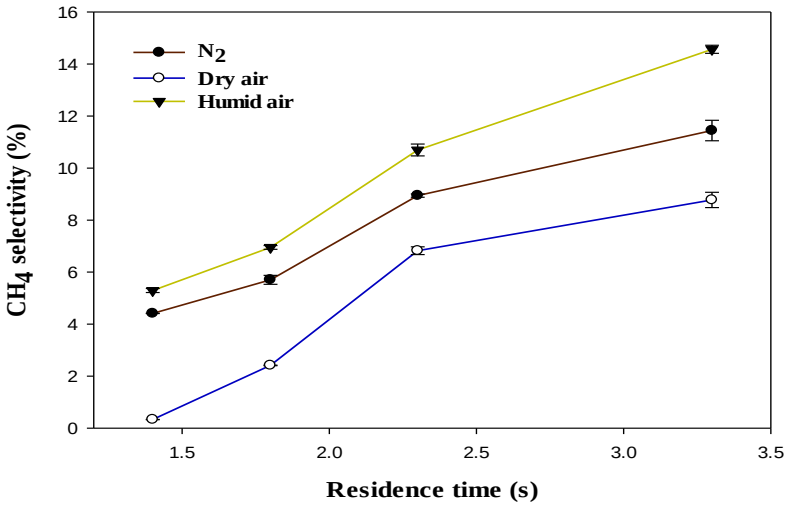

Figure 7.18 Effect of residence time on selectivity to CH_4 in N_2, dry and humidified air (Reaction conditions: Temperature = ambient; Concentration = 260 ppm; Flow rate = 70 -160 ml/min; Power = 6 W, SIE = 2.3 - 5.1 kJ/L, Relative humidity = 24%, Error bars represent the standard deviation ± σ for 3 measurement results).

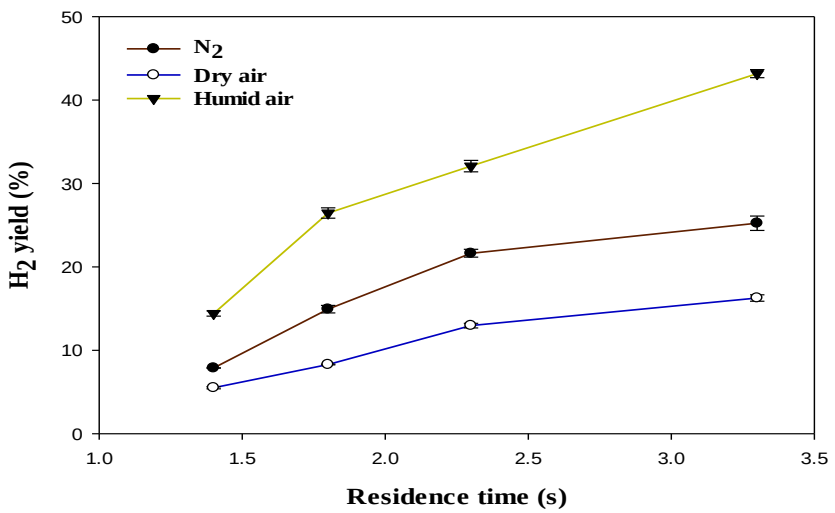

Figure 7.19 Effect of residence time on selectivity to C_2-C_4 in N_2, dry and humidified air (Reaction conditions: Temperature = ambient; Concentration = 260 ppm; Flow rate = 70 -160 ml/min; Power = 6 W, SIE = 2.3 - 5.1 kJ/L, Relative humidity = 24%, Error bars represent the standard deviation ± σ for 3 measurement results).

The product selectivity and H_2 yield increased with residence time. The CO_2 selectivity and H_2 yield increased from 17.3%, 14.4% to 25%, and 43.2% as the residence time increased from 1.4 to 3.3 s in humidified air. The selectivity to CO_2 and yield of H_2 increased due to more reaction/collision time between the energetic electrons, gas-phase radicals ($OH^{\cdot}$, $O^{\cdot}$ and $H^{\cdot}$) and the methanol molecules in the plasma zone.

7.2.4 Mechanisms of methanol decomposition using NTP-plasma

In a dielectric barrier discharge (DBD) plasma, discharge occurs in three stages: breakdown, quasi-equilibrium, and non-equilibrium (Kogelschatz, 2003). Non-equilibrium plasmas cause the formation of excited species, ions, and radicals. The average electron energy in the DBD system is between 1 and 10 eV (Petitpas *et al.*, 2007). The excited species such as N_2, $N_2(A)$, $N_2(A^3\sum_u^+)$, O_2 and radicals (O, H and OH) could be generated through continuous collision with the energetic electrons produced in the DBD plasma reactor as reported in Chapter 5. The plasma-assisted decomposition of VOCs in N_2, dry and humidified air carrier gases can be initiated in three pathways: electron-impact decomposition reactions e^*, collisions with excited species such as N_2 and O_2, and reactions with gas-phase radicals, such as O, H or OH. The C-O, C-H, and O-H bond dissociation energies of CH_3OH are 3.638 eV, 4.291 eV, and 4.768 eV, respectively (Qi *et al.*, 2019). Therefore, electrons, excited species, and gas-phase radicals with energies above 3.638 eV could break the strong C-O bond in methanol, generating

intermediates that are further converted to gaseous products such as CO_2, CO, CH_4, H_2, and C_2-C_4 hydrocarbons.

Methanol decomposes to species such as $CH_3^{\cdot}$, CH_2OH, and CHOH through electron-impacted reaction as shown in R(7.1)-R(7.3) (Han *et al.*, 2006).

$$CH_3OH + e \rightarrow CH_3^{\cdot} + OH^{\cdot} + e \qquad R(7.1)$$

$$CH_3OH + e \rightarrow CH_2OH + H + e \qquad R(7.2)$$

$$CH_3OH + e \rightarrow CHOH + H_2 + e \qquad R(7.3)$$

Once produced, CH_3 can easily react with H radicals to form CH_4 through hydrogenation reaction R(7.4) (Kim *et al.*, 2014a). CH_3 can also dimerise to form longer hydrocarbons such as C_2H_6, C_2H_5, C_4H_8, and C_4H_{10} through hydrogenation and coupling reactions between the C_mH_n species at low temperatures, as shown between R(7.4)- R(7.8).

$$CH_3 + H \rightarrow CH_4 \qquad R(7.4)$$

$$CH_3 + CH_3 \rightarrow C_2H_6 \qquad R(7.5)$$

$$C_2H_6 + H \rightarrow C_2H_5 + H_2 \qquad R(7.6)$$

$$C_2H_5 + C_2H_5 \rightarrow C_4H_{10} \qquad R(7.7)$$

$$C_2H_{10} + e \rightarrow C_4H_8 + H_2 + e \qquad R(7.8)$$

CH_2O is unstable in NTPs, (Zhang *et al.*, 2015b) and can be converted to CO and H_2 via electron impact dissociation reaction, as shown in R(7.9) (Han *et al.*, 2006).

$$CHOH + e \rightarrow CO + H_2 + e \qquad R(7.9)$$

It has been proposed that the direct collision of methanol molecules with excited species and gas-phase radicals could open up a new decomposition pathway, as shown in R(7.10)-R(7.14) (Lee *et al.*, 2013).

$$CH_3OH + N, N_2(A) \rightarrow CH_3^{\cdot} + OH^{\cdot} + N, N_2 \qquad R(7.10)$$

$$CH_3OH + N, N_2(A) \rightarrow CH_3O^{\cdot} + H + N, N_2 \qquad R(7.11)$$

$$CH_3OH + N, N_2(A) \rightarrow CH_2OH^{\cdot} + H + N, N_2 \qquad R(7.12)$$

$$CH_3OH + O, O(^1D) \rightarrow CH_2OH^{\cdot} + OH^{\cdot} \qquad R(7.13)$$

$$CH_3OH + O, O(^1D) \rightarrow CH_3O^{\cdot} + OH^{\cdot} \qquad R(7.14)$$

The addition of water vapour to non-thermal plasma DBD reactors provided new insights into the methanol decomposition pathway. Here, the radicals $H^{\cdot}$ and $OH^{\cdot}$ are generated through the

electron impact dissociation and excitation reaction of H_2O molecules as shown in R(7.15) – R(7.18) (Vandenbroucke *et al.*, 2011; Abdelaziz *et al.*, 2018).

$$H_2O + e \rightarrow OH^{\cdot} + H^{\cdot} + e \qquad R(7.15)$$

$$N_2(A^3\sum_u{}^+) + H_2O \rightarrow N_2 + OH^{\cdot} + H^{\cdot} \qquad R(7.16)$$

$$e + O_2 \rightarrow e + O(^1D) + O(^3P) \qquad R(7.17)$$

$$O(^1D) + H_2O \rightarrow 2OH^{\cdot} \qquad R(7.18)$$

The OH, O and H radicals generated can convert methanol to CO_2, H_2 and H_2O as shown in R(7.19) – R(7.22). It is important to note that the introduction of water vapour with a relative humidity of 24% at 20 ℃ increased CO_2, CH_4 and H_2 and decreased CO and longer hydrocarbon selectivities.

$$CH_3OH + OH^{\cdot} \rightarrow CH_2OH^{\cdot} + H_2O \qquad R(7.19)$$

$$CH_3OH + OH^{\cdot} \rightarrow CH_3O^{\cdot} + H_2O \qquad R(7.20)$$

$$CH_3OH \rightarrow 2H_2 + CO \qquad R\ (7.21)$$

$$CO + H_2O \rightarrow H_2 + CO_2 \qquad R(7.22)$$

The CH_3OH decomposition pathway R(7.21) is followed by H_2O gas shift reaction R(7.22) when water vapour is added to the DBD process, leading to increased CO_2 selectivity and H_2 yield (Zhang *et al.*, 2016). The H radical produced through the dissociation of CH_3OH can recombined with the H radical generated from the dissociation of H_2O to form more H_2, as shown in R(7.23).

$$H^{\cdot} + H^{\cdot} \rightarrow H_2 \qquad R(7.23)$$

$$CHOH + H^{\cdot} \rightarrow HCO + H_2 \qquad R(7.24)$$

$$H^{\cdot} + HCO^{\cdot} + e \rightarrow H_2 + CO \qquad R(7.25)$$

Another reason for the increased H_2 is that during methanol conversion using non-thermal plasma, H_2 is also produced through the reaction of CH_2O with H radicals as in R(7.24), and HCO can further react with H radical to form H_2 and CO, as in R(7.25) (Kim *et al.*, 2014a). This agrees with the experimental findings that H_2 yield increased and CO decreased with plasma power when water vapour was introduced.

The interaction of H_2O with CH_3OH is also known to be a significant pathway for the production of H_2 and CO_2 R(7.26) (Zhang *et al.*, 2016).

$$CH_3OH + H_2O \rightarrow 3H_2 + CO_2 \qquad R(7.26)$$

Shuji Tanabe (2000) also reported that, apart from methanol decomposition to H_2 and CO, as shown in R(7.21), there was another reaction pathway: that between H_2O and CH_3OH, leading to CO_2 and H_2 (see R(7.26)). In addition, water vapour increased the selectivity to CO_2 (Thevenet *et al.*, 2008). The O and OH radicals can oxidise CO to CO_2, as shown in R(7.27) and R(7.28) (Atkinson *et al.*, 1997), and hydrogen radicals can recombine to form H_2 (R7.29) (Panda *et al.*, 2020).

$$CO + OH^{\cdot} \rightarrow CO_2 + H \qquad R(7.27)$$

$$CO + O^{\cdot} \rightarrow CO_2 \qquad R(7.28)$$

$$H^{\cdot} + H^{\cdot} \rightarrow H_2 \qquad R(7.29)$$

Based on the analyses above, the methanol decomposition pathways are summarised in Figure 7.20.

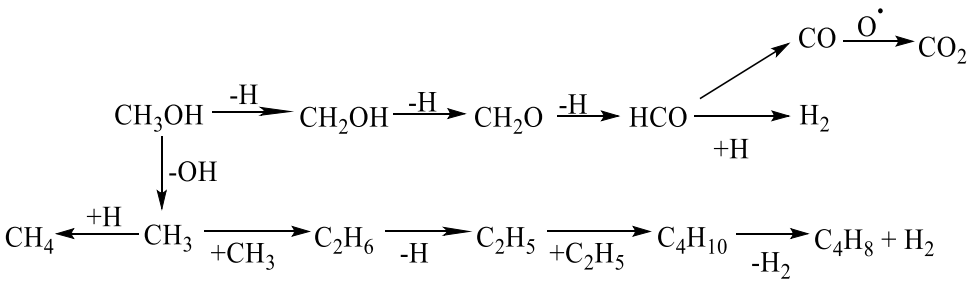

Figure 7.20 Decomposition pathways of methanol.

7.2.5 Ozone and NOx formation

Ozone is one of the main by-products formed in non-thermal plasma DBD abatement of VOCs using dry air. O_3 formation can be initiated in a DBD plasma via collisions between energetic electrons and oxygen molecules, as shown in R(7.30) -R(7.31) (Gudmundsson *et al.*, 2013).

$$e + O_2 \rightarrow O(^3P) + O(^3P) + e\ (6.1\ eV) \qquad R(7.30)$$

$$e + O_2 \rightarrow O(^3P) + O(^1D) + e\ (8.4\ eV) \qquad R(7.31)$$

Furthermore, O_3 can also be generated through a three-body recombination reaction of atomic oxygen O and molecular oxygen, as shown in R(32). (Zhu *et al.*, 2014) The third body M can be oxygen or nitrogen molecules in the dry air carrier gas.

$$O + O_2 + M \rightarrow O_3 + M \qquad R(7.32)$$

Here, the influence of input power on ozone formation at constant CH_3OH concentration (260 ppm) and residence time (3.3 s) in dry and humidified air carrier gases were studied. The O_3 concentrations from the outlet of the DBD reactor were measured using the standard KI solution

method as described by Yulianto *et al.* (2019). The O_3 concentration as a function of input power using dry and humidified air carrier gases is presented in Figure 7.21.

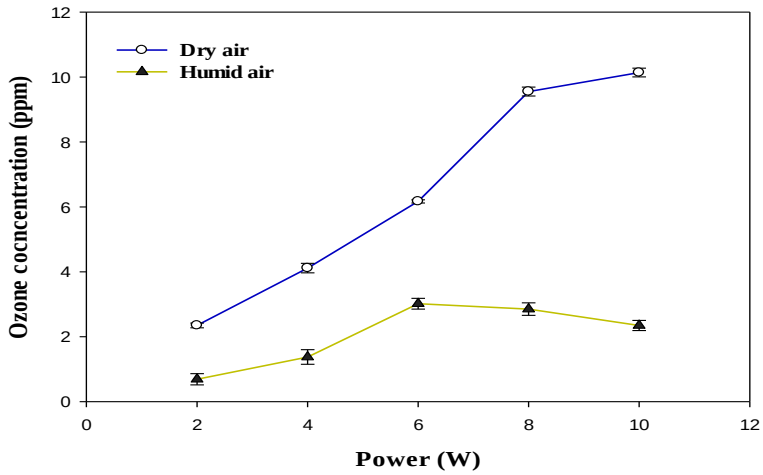

Figure 7.21 Ozone concentration as a function of input power (Reaction conditions: Temperature = ambient; Concentration = 260 ppm; Total flow rate = 70 ml/min; Residence time = 3.3 s; SIE = 1.7 – 8.6 kJ/L; Carrier gas = dry and humidified air, Relative humidity = 24%, Error bars represent the standard deviation ± σ for 3 measurement results).

The ozone concentration increased with input power in dry air. The O_3 concentration increased from 2.4 ppm (2 W) to 10.2 ppm (10 W) at constant inlet methanol concentration (260 ppm) and residence time (3.3 s) in dry air. However, ozone concentration initially increases when the plasma power increases from 2 to 6 W and decreases when plasma power increases (8- 10 W) in humid air plasma.

The introduction of water vapour significantly reduced the ozone concentration at every point and kept it below 3 ppm. Water addition reduces the production of ozone due to the utilisation of $O(^1D)$ by H_2O, the primary source of ozone formation (Zhu *et al.*, 2008). H_2O decreased the O_3 concentration by quenching the energetic electrons (Huang *et al.*, 2011). On the other hand, the O_3 concentration decreased due to an increase in direct interactions between O_3 and gas-phase radicals such as OH, H and $HO_2^{\cdot}$ radicals. As a result, the O_3 destruction reactions can be summarised as follows: R(7.33)-R(7.35) (Zhu *et al.*, 2008; Karuppiah *et al.*, 2012).

$$O_3 + H^{\cdot} \rightarrow O_2 + OH^{\cdot} \qquad R(7.33)$$

$$O_3 + OH^{\cdot} \rightarrow O_2 + HO_2^{\cdot} \qquad R(7.34)$$

$$O_3 + HO_2^{\cdot} \rightarrow 2O_2 + OH^{\cdot} \qquad R(7.35)$$

In the plasma-assisted decomposition of VOCs, the formation of NOx is a significant health and environmental concern (Subrahmanyam *et al.*, 2006) and decreases the efficiency of the

abatement process (Karatum *et al.*, 2016). In dry air plasma, NO_x can be formed via the electron impacted dissociation reaction of N_2/O_2 as shown in R(7.36)-R(7.40) (Zheng *et al.*, 2014; Zhu *et al.*, 2014).

$$O_2 + e \rightarrow O^{\cdot} + O^{\cdot} + e \qquad R(7.36)$$

$$N_2 + e \rightarrow N^{\cdot} + N^{\cdot} + e \qquad R(7.37)$$

$$O + N \rightarrow NO \qquad R(7.38)$$

$$O + NO \rightarrow NO_2 \qquad R(7.39)$$

$$NO + O_3 \rightarrow O_2 + NO_2 \qquad R(7.40)$$

The excited N_2 or metastable N_2 species can be quenched/consumed by oxygen species to form ground state N_2 and NOx ($NO + NO_2$) (Harling *et al.*, 2009). In this work, the DBD outlet NOx concentrations at a steady-state were measured using Gastec detector tubes (detection limit =0.1 ppm). NOx was not detected in any of the tested experimental conditions; hence, it is below 0.1 ppm and is therefore not at problematic levels. This could be due to more OH radicals in the decomposition process generated from the electron impact dissociation reaction of CH_3OH and H_2O, which provides more OH radicals in the plasma discharge, resulting in the conversion of VOC intermediates to CO_2, H_2O and H_2 (Zhu *et al.*, 2014). Furthermore, the OH radicals can oxidise NO to form HNO_2 as shown in R(7.41) (Zheng *et al.*, 2013).

$$NO + OH \rightarrow HNO_2 \qquad R(7.41)$$

Since OH and H radicals can shut down the ozone pathway, as shown R(7.33-7.34), it is possible to eliminate or reduce NOx concentrations to below 0.1 ppm by preventing reducing ozone formation either by operating the DBD reactor at low flow rates and low plasma power, or by the introduction of water vapour with a relative humidity of 24%. It is important to note that operating a DBD reactor at very flow rates and low plasma power can increase the specific input energy and residence time, which can affect the product distribution. The carbon balance analysis is presented in Appendix A-7.1.

7.3 **Summary**

A dielectric barrier discharge (DBD) plasma system was used to remove methanol from gas streams at ambient temperature and pressure. The system was studied with carrier gases of dry air, humidified air and nitrogen to determine the respective roles of N_2, O_2 and H_2O. The plasma power (2-10 W), CH_3OH inlet concentration (260-350 ppm), and residence time (1.4-3.3 s) were varied for each gas. The removal efficiency of methanol increased with input power and

residence time regardless of the carrier gas used and decreased with increasing CH_3OH inlet concentration. The maximum removal efficiency of methanol (96.7%) was achieved at 10 W and a residence time of 3.3 s in dry air plasma. The methanol removal efficiency increased in the series: $N_2 <$ humidified air $<$ dry air. In dry air plasma, the findings suggest that the action of O radicals dominates the methanol decomposition. Methanol was converted to CO_2, H_2, and various hydrocarbons (CH_4, C_2H_6, C_4H_{10} and C_4H_8). The N_2 carrier gas exhibited the highest selectivity to C_2-C_4 hydrocarbons due to the absence of O and OH, which could decompose hydrocarbons. CO_2 and CO production was lower in N_2 than the other carrier gases, again because of the absence of O and OH radicals, which resulted in higher selectivity to hydrocarbons. The introduction of H_2O (RH= 24% at 20℃) into the carrier gas reduced the removal efficiency but significantly improved selectivity toward CO_2 and H_2. There were various other benefits to the presence of H_2O, including significant reductions in both O_3 and CO.

The reaction mechanisms for the various decomposition pathways of methanol have been hypothesised, including electron impact decomposition reaction, direct collision with excited species, and reaction with gas-phase radicals such as O, H or OH. The role of the OH radical can largely explain the effects of H_2O inclusion. Furthermore, no solid residue was formed in the DBD reactor in all the carrier gases. Overall, the dry air plasma exhibited the highest removal efficiency, but the humidification, although it decreased the removal efficiency, significantly reduced various typically unwanted species, including CO and O_3, whilst increasing the more desired (less toxic) species, such as CO_2 and H_2.

7.4 **Analysis of the overall performance of the DBD reactor**

Table 7.1 provide the overall assessment of the performance of the developed DBD reactor compared with the conventional methods of VOC decomposition in terms of removal efficiency and the formation of unwanted by-products.

Table 7.1 Overall assessment of the performance of the developed DBD reactor compared with other conventional methods

Treatment technique	**Removal efficiency %**	**Secondary by-products**	**Comments**	**References**
NTP-DBD	77-98	Solid residue Ozone	• Flexible and simple reactor design • Low energy consumption • Work with mixture of gases (VOC and carrier gases) • Higher removal efficiency and product selectivity have been achieved at low plasma power (10 W) • The reactor operates close to room temperature • Convert toxic VOCs to environmentally friendly product • Solid deposition and ozone formation were eliminated in the presence of humid air • NOx was below the detection limit	This study
Biofiltration	60-95	Biomass	• Selective and slow decomposition process • Longer retention time • No recovery of materials	(Steinberg *et al.*, 2005)
Thermal oxidation	95-99	Combustion products	• Require additional control of process equipment • Re-emission of VOC after treatment • High energy consumption • Produce high NOx and ozone	(Choi *et al.*, 2000)

Condensation	70-85	Condensate	• Requires post treatment and frequent turn around maintenance • Require extensive cooling (not economical) • Good product recovery • Only applicable for VOCs with boiling points above 33 ℃	(Belaissaoui *et al.*, 2016; Uria-Tellaetxe *et al.*, 2016)
Catalytic oxidation	90-98	Ozone and NOx Solid residue	• Catalyst deactivation • High cost of catalyst replacement • Some compounds can poison the catalyst	(Azalim *et al.*, 2011)
Adsorption	80-90	Spent carbon	• Susceptible to moisture • Blockage of the pores, thereby decreasing treatment efficiency	(Tian *et al.*, 2016)

In addition, the selected results of this work are summarized and compared with previous studies of the plasma-assisted decomposition of VOCs, as shown in Table 7.2

Table 7.2 Comparison of selected removal efficiency (RE) and energy yield (EY) for this study with previous studies.

VOCs	Type of NTP reactor	Carrier gas	C_{in} (ppm)	RE (%)	Energy yield (g/kWh)	References
Hexane	DBD	Nitrogen	350	75.6	0.57	This study
		Dry air	350	84.9	0.64	
		Humid air	350	94.4	0.71	
Hexane	DBD	Air 15% O_2 (N_2 balance)	367	78.0	0.80	(Jin *et al.*, 2016)
Hexane	CD	Air	500	57.0	ND	(Marotta *et al.*, 2007)
Hexane	GAD	Air	968	81.0	ND	(Yan *et al.*, 2007)
		Nitrogen	968	57.0	ND	
		Argon	968	56.0	ND	
Cyclohexane	DBD	Nitrogen	220	91.4	0.28	This study
		Dry air	220	95.7	0.32	
		Humid air	220	98.2	0.47	
Cyclohexane	GAD	Air	0.5, 1% vol.	92.5	ND	(Młotek *et al.*, 2015)
Benzene	DBD	Dry air	350	56.8	0.12	This study
		Humid air	350	77.9	0.15	
Benzene	DBD	Humid air (RH =70%)	276	45	3.90	(Ye *et al.*, 2008)
Benzene	DBD	Dry air (5% O_2)	200	75	5.70	(Kim *et al.*, 2008)
Benzene	DBD	Air (RH = 0-90%)	500-2700	>99.9	ND	(Cal *et al.*, 2001)
Benzene	DBD	Dry air	100	90	1.50	(Lee *et al.*, 2004)
Benzene	DBD	Air	95	58	0.50	(Karatum *et al.*, 2016)
Benzene	DBD	Humid air	500	75	15.2	(Ma *et al.*, 2016)
Methanol	DBD	Nitrogen	260	71.3	0.02	This study
		Dry air	260	96.7	0.04	
		Humid air	260	77.7	0.03	
Methanol	DBD	Nitrogen	18 mol%	74	5.00	(Wang *et al.*, 2016)
Methanol	DBD	Nitrogen/Air	446	44	1.30	(Wang *et al.*, 2019)
Methanol	SDBD	Dry air	50	60	0.16	(Norsic *et al.*, 2018)
		Humid air (RH= 35%)	50	43	0.12	

The developed DBD reactor in this study enhanced the removal efficiency of VOCs such as cyclohexane (98.2%), methanol (96.7%), hexane (94.4%), benzene (77.9%) and improved product selectivity at low plasma power (10 W), and low energy consumption close to room temperature at atmospheric pressure in the presence of humid air. Furthermore, the developed DBD reactor in this study improved technology for the reduction of VOCs in gaseous effluents based on a low-cost, low energy non-thermal plasma technology, so pertains to indoor and outdoor air quality control.

Chapter 8. Conclusions and recommendations

8.1 Conclusions

The decomposition of a sequence of three 6-carbon hydrocarbons, hexane (as a model linear alkane), cyclohexane (as a model cycloalkane) and benzene (as a model aromatic), was studied in a non-thermal plasma dielectric barrier discharge (DBD) reactor, at ambient temperature and atmospheric pressure. Because alkanes (including cycloalkanes), aromatics, and alcohol are the most common anthropogenic hydrocarbon VOCs in the atmosphere, they were chosen as the model VOCs. Hexane, cyclohexane, and benzene are prominent representatives of alkanes, cycloalkanes and aromatics and are classified as highly volatile organic compounds. Methanol was also studied as a common VOC pollutant. Methanol is odorous volatile alcohol that has been mainly used industrially as a solvent, alternative source of fuel and pesticide. The process parameters studied were: plasma power, specific input energy, carrier gases (nitrogen, dry air and humidified air), oxygen concentration, inlet VOC concentration, residence time, and moisture content. The output variables were VOC removal efficiency, product selectivity and elimination/reduction of unwanted by-products.

Broadly, this study demonstrated that in an NTP-assisted VOC decomposition, in addition to the energetic electron impact causing direct VOC molecule decomposition, the excited state of carrier gas molecules (i.e. N, $N_2(A^3\sum_u{}^+)$, O, and $O(^1D)$, and OH species) has a significant effect on the VOC removal efficiency and product selectivity.

In hexane decomposition, the removal efficiency increased with increasing plasma power/specific input energy (SIE) and O_2 concentration. Hexane mainly decomposed to lower hydrocarbons (C_1-C_5), CO, CO_2, and solid/viscous residues. The removal efficiency in air and humidified air was higher than N_2 due to the formation of O and OH radicals. N_2 plasmas exhibited the lowest removal efficiency of hexane due to the absence of oxygen in the background gas. The maximum removal efficiency, of 94.4%, and CO_2 selectivity, of 84.7% were achieved in humidified air. This was due to the presence of potent OH radicals which has higher oxidation power than the O and nitrogen excited species.

Increasing the O_2 concentration increased both the removal efficiency and CO_2 selectivity. This is probably due to the generation of more oxygen radicals. As O_2 concentration increased from 5 to 21%, the proportion of CO_2 in the product gas increased, and the selectivity to lower hydrocarbons decreased.

A simple first-order reaction model was developed, which was consistent with the NTP decomposition of hexane in all three atmospheres. Rate constants ("energy constants") were derived for all three atmospheres. This would be vital information for reactor design and scale-up of this technology.

In the case of cyclohexane decomposition, the removal of cyclohexane increased with residence time and specific input energy in all the carrier gases. However, the removal efficiency of cyclohexane decreased with increasing inlet concentration at constant residence time and SIE. The maximum removal efficiency (98.2%) was achieved at an SIE of 3 kJ/L and a residence time of 2.3 s in humidified air. The key findings were that cyclohexane decomposed mostly into H_2, lower hydrocarbons (C_1–C_4) ("LHC"), and solid residue in nitrogen. Other species, including CO, CO_2, and water, were generated when dry air was used as the carrier gas. When humidified air was used, there were further effects due to the water vapour, which had three effects:

(i) it lowered LHC while increasing CO_2 and H_2 yields.

(ii) it prevented solid residue formation in the DBD reactor, probably due to the production of OH radicals in the plasma reactor.

(iii) it increased the removal of cyclohexane.

The maximum O_3 concentrations (< 10ppm) were observed at 3.0 kJ/L SIE in dry air. NO_X was not detected in any carrier gas.

The benzene removal efficiency and the selectivity to CO_2 increased with plasma power/SIE in both dry and humidified air. In contrast, the selectivity to LHC decreased. The most important finding of this study was that the formation of solid residue in the plasma reactor was removed by operating in humidified air. As the amount of water vapour increased from 0 to 35% at 20℃, the benzene removal efficiency and CO_2 selectivity increased; O_3 decreased from 7.3 ppm to 0.5 ppm; NO_x and solid residue were eliminated. These effects are due to OH radicals. Mechanisms for the various effects are proposed in Chapter 7. The maximum benzene removal efficiency was 93.7%, and the maximum selectivity to CO_2 was 82.4% (both at a relative humidity of 35% at 20℃ and 10 W).

The chemical bond energy of the VOC molecules are one of the main parameters that can determine the removal efficiency of VOCs in the plasma system. Under NTP conditions, the removal efficiency depends on VOCs' chemical structures. The bond dissociation energy of the C-C bond in the benzene ring is the highest among the C_6 series of VOCs evaluated in this study, followed by the C-C bond in cyclohexane, then benzene. In these results, it can be

observed that alkanes hydrocarbons, break down faster than cycloalkanes, which break down faster than aromatics. The increasing order of the removal efficiency follows the sequence benzene < cyclohexane < hexane.

In methanol decomposition, the conversion of methanol increased with power/SIE and residence time regardless of the carrier gas used. However, the removal efficiency decreased with the increasing concentration of CH_3OH. The removal efficiency of methanol followed a sequence of dry air > humidified air >N_2 carrier gas. The O radical in dry air dominates the decomposition process of the plasma system. This is because in the presence of water vapour, the OH from CH_3OH may be consumed by the OH radical formed from the dissociation of water, leading to decreased removal efficiency. The introduction of water vapour into the DBD system decreased the removal efficiency but had a number of significant advantages: increased CO_2 selectivity and yield of H_2 and significantly reduced formation of O_3, CO and higher hydrocarbons. These effects are due to the presence of potent OH radicals. Overall, this research indicates that methanol can be almost completely removed with the correct operating parameters (96.7% removal; 10W; 3.3s in dry air plasma) and shows that humidification of the gas stream is beneficial.

The reactive species such as the OH radicals responsible for the decomposition of VOCs are highly dependent on the composition/nature of the model compound. The OH radicals can easily oxidise reaction intermediates to CO_2 and H_2O. The OH radicals can also oxidise the carbon species, thereby eliminating solid residue. The VOCs without OH groups in their structure, e.g., hexane, cyclohexane, and benzene, are better decomposed using humidified air plasma due to OH radicals, which have high oxidation power at a certain amount of water vapour (RH of 25% for hexane and cyclohexane, and RH of 35% for benzene). However, the removal efficiency of CH_3OH decreased in humidified air plasma, because the energetic electrons could be quenched by electronegative properties of H_2O molecules (the OH from CH_3OH may be consumed by OH from H_2O).

The synergistic effect of the plasma and water vapour was studied to determine whether it would reduce the formation of unwanted by-products such as O_3, NO_X and solid residue in the DBD reactor. The introduction of water vapour with RH= 25% at 20 ℃ for hexane and cyclohexane, and RH= 35% for benzene, significantly increased the removal efficiency and the CO_2 selectivity while wholly eliminating solid residue and NO_X in the NTP-decomposition of VOCs. Again, this is due to the presence of potent OH radicals. In the gas phase reaction, the OH radicals can oxidise the reaction intermediates of VOC to CO_2 and H_2O faster than oxygen atoms, thereby increasing removal efficiency, CO_2 selectivity, and elimination of solid residue

and NOx. The OH radicals can convert NO to HNO_2, and, further, oxidise it to NO_2 and H_2O. In addition, OH radicals can remove solid residue through the reaction OH + C → CO + H (gas/solid-phase reaction). Humidification improved the removal efficiency and increased the yield of H_2 and CO_2 selectivity. These results imply that the decomposition of VOCs by non-thermal plasma DBDs is dominated by the effect of OH and O radicals. Furthermore, the addition of water to the process suppressed O_3 formation and reduced CO formation in all the tested conditions. NOx was not detected (<0.1 ppm) in any of the tested experimental conditions in this research.

Overall, the performance of DBD plasmas in the decomposition of hexane, cyclohexane, benzene, and perhaps other alkanes and aromatic VOCs can be greatly improved by optimizing plasma power and carrier gas moisture content. Furthermore, the performance of the DBD would improve when operating in humid conditions or when the inlet gas stream is humidified at low powers (10W or less)/SIE, as it can eliminate the formation of solid residues, NOx and ozone.

8.2 **Future work**

8.2.1 Advanced plasma diagnosis of the VOC decomposition process

The measurement of the plasma properties during the decomposition of the VOCs process is the major area where more research is needed. *In situ*, measurements are critical for detecting and quantifying the actions of the reactive species generated in the plasma. This knowledge would help develop a better understanding of the chemical reactions that occur in the plasma zone of the DBD reactor. They would also aid in the optimization of the plasma technique and conditions for efficient VOC decomposition using non-thermal plasmas. The diagnosis technique of the plasma parameters such as electron temperature, electron density and reactive radical density (with FTIR and OES (optical emission spectrum)) should be evaluated further to understand the NTP decomposition pathways in the DBD reactor.

8.2.2 Kinetic simulations and scale-up investigation of VOCs decomposition using NTP reactors

Another area that has to be developed is kinetic simulation. It is important to model the decomposition of alkanes (hexane and cyclohexane), aromatics (benzene), alcohols (methanol), and mixtures of different VOCs to back up the experimental findings and better comprehend the decomposition pathways of VOCs in the plasma system. The semi-empirical models developed in chapters 4 & 5 would be vital for reactor design and scale-up of this technology. In addition, these semi-empirical models could serve as the basis for kinetic modelling and can be used in predicting the removal efficiency of the DBD plasma system. The kinetic data could be used as an input in chemical reaction engineering design challenges like scale-up studies. Applying suitable chemical kinetic models would allow the development of an efficient dielectric barrier discharge system to achieve maximum removal efficiency of VOCs at least expense. Process scaling-up remains a significant challenge for environmental applications of NTPs. Therefore, understanding the effect of reactor hydrodynamics on process performance is a critical step toward overcoming this challenge. The concepts of chemical engineering could be used to evaluate the effect of DBD reactor configurations, plasma properties, process operating parameters, and flow regimes, e.g., laminar or turbulent flow, on a DBD system's performance.

References

Abdelaziz, A., Ishijima, T. and Seto, T. (2018) 'Humidity effects on surface dielectric barrier discharge for gaseous naphthalene decomposition', *Physics of Plasmas*, 25, p. 043512.

Ağıral, A., Boyadjian, C., Seshan, K., Lefferts, L. and Gardeniers, J.G.E. (2010) 'Pathway Study on Dielectric Barrier Discharge Plasma Conversion of Hexane', *The Journal of Physical Chemistry C*, 114(44), pp. 18903-18910.

Anderson, G.K., Snyder, H. and Coogan, J. (1999) 'Oxidation of Styrene in a Silent Discharge Plasma', *Plasma Chemistry and Plasma Processing*, 19(1), pp. 131-151.

Arno, J., Bevan, J.W. and Moisan, M. (1995) 'Acetone conversion in a low-pressure oxygen-surface wave plasma', *Environmental Science and Technology*, 29(8), pp. 1961-1965.

Atkinson, R., Baulch, D.L., Cox, R.A., Hampson, R.F., Kerr, J.A., Rossi, M.J. and Troe, J. (1997) 'Evaluated Kinetic and Photochemical Data for Atmospheric Chemistry: Supplement VI. IUPAC Subcommittee on Gas Kinetic Data Evaluation for Atmospheric Chemistry', *Journal of Physical and Chemical Reference Data*, 26(6), pp. 1329-1499.

Azalim, S., Franco, M., Brahmi, R., Giraudon, J.-M. and Lamonier, J.-F. (2011) 'Removal of oxygenated volatile organic compounds by catalytic oxidation over Zr–Ce–Mn catalysts', *Journal of Hazardous Materials*, 188(1), pp. 422-427.

Bahri, M., Haghighat, F., Rohani, S. and Kazemian, H. (2016) 'Impact of design parameters on the performance of non-thermal plasma air purification system', *Chemical Engineering Journal*, 302, pp. 204-212.

Ban, J.-Y., Son, Y.-H., Kang, M. and Choung, S.-J. (2006) 'Highly concentrated toluene decomposition on the dielectric barrier discharge (DBD) plasma–photocatalytic hybrid system with Mn-Ti-incorporated mesoporous silicate photocatalyst (Mn-Ti-MPS)', *Applied Surface Science*, 253(2), pp. 535-542.

Baránková, H. and Bárdos, L. (2010) 'Effect of the electrode material on the atmospheric plasma conversion of NO in air mixtures', *Vacuum*, 84(12), pp. 1385-1388.

Bay, K., Wanko, H. and Ulrich, J. (2006) 'Absorption of Volatile Organic Compounds in Biodiesel: Determination of Infinite Dilution Activity Coefficients by Headspace Gas Chromatography', *Chemical Engineering Research and Design*, 84(1), pp. 22-28.

Belaissaoui, B., Le Moullec, Y. and Favre, E. (2016) 'Energy efficiency of a hybrid membrane/condensation process for VOC (Volatile Organic Compounds) recovery from air: A generic approach', *Energy*, 95, pp. 291-302.

Bityurin, V.A., Filimonova, E.A. and Naidis, G.V. (2009) 'Simulation of Naphthalene Conversion in Biogas Initiated by Pulsed Corona Discharges', *IEEE Transactions on Plasma Science*, 37(6), pp. 911-919.

Blin-Simiand, N., Jorand, F., Magne, L., Pasquiers, S., Postel, C. and Vacher, J.-R. (2008) 'Plasma Reactivity and Plasma-Surface Interactions During Treatment of Toluene by a Dielectric Barrier Discharge', *Plasma Chemistry and Plasma Processing*, 28(4), pp. 429-466.

Bodar, C.W.M., Berthault, F., de Bruijn, J.H.M., van Leeuwen, C.J., Pronk, M.E.J. and Vermeire, T.G. (2003) 'Evaluation of EU risk assessments existing chemicals (EC Regulation 793/93)', *Chemosphere*, 53(8), pp. 1039-1047.

Boeglin, M.L., Wessels, D. and Henshel, D. (2006) 'An investigation of the relationship between air emissions of volatile organic compounds and the incidence of cancer in Indiana counties', *Environmental Research*, 100(2), pp. 242-254.

Bogaerts, A. and Neyts, E.C. (2018) 'Plasma Technology: An Emerging Technology for Energy Storage', *ACS Energy Letters*, 3(4), pp. 1013-1027.

Bouchaala (2012) 'Volatile Organic Compounds Removal Methods: A Review', *American Journal of Biochemistry and Biotechnology*, 8(4), pp. 220-229.

Bouchard, D., Höhener, P. and Hunkeler, D. (2008) 'Carbon Isotope Fractionation During Volatilization of Petroleum Hydrocarbons and Diffusion Across a Porous Medium: A Column Experiment', *Environmental Science & Technology*, 42(21), pp. 7801-7806.

Bunn, W., W Hesterberg, T., Valberg, P., Slavin, T., Hart, G. and Lapin, C. (2005) *A Reevaluation of the Literature Regarding the Health Assessment of Diesel Engine Exhaust*.

Byeon, J.H., Park, J.H., Jo, Y.S., Yoon, K.Y. and Hwang, J. (2010) 'Removal of gaseous toluene and submicron aerosol particles using a dielectric barrier discharge reactor', *Journal of Hazardous Materials*, 175(1), pp. 417-422.

Cal, M.P. and Schluep, M. (2001) 'Destruction of benzene with non-thermal plasma in dielectric barrier discharge reactors', *Environmental Progress*, 20(3), pp. 151-156.

Chen, F., Huang, X., Cheng, D.-g. and Zhan, X. (2014) 'Hydrogen production from alcohols and ethers via cold plasma: A review', *International Journal of Hydrogen Energy*, 39(17), pp. 9036-9046.

Chen, H.L., Lee, H.M., Chen, S.H., chang, M.B., Yu, S.J. and Li, S.N. (2009) 'Removal of Volatile Organic Compounds by Single-Stage and Two-Stage Plasma Catalysis Systems: A Review of the Performance Enhancement Mechanisms, Current Status, and Suitable Applications', *Environmental Science and Technology*, 43(43), pp. 2216–2227.

Chen, J., Xie, Z., Tang, J., Zhou, J., Lu, X. and Zhao, H. (2016) 'Oxidation of toluene by dielectric barrier discharge with photo-catalytic electrode', *Chemical Engineering Journal*, 284, pp. 166-173.

Choi, B.S. and Yi, J. (2000) 'Simulation and optimization on the regenerative thermal oxidation of volatile organic compounds', *Chemical Engineering Journal*, 76(2), pp. 103-114.

DEFRA (2022) *Emissions of air pollutants in the UK – Non-methane volatile organic compounds (NMVOCs)*. UK: Department for Environment Food and Rural Affairs, National Statistics. [Online]. Available at: https://www.gov.uk/government/statistics (Accessed: 18 March 2022).

Derwent, R.G. (1995) 'Sources, distributions, and fates of VOCs in the atmosphere', in *Volatile Organic Compounds in the Atmosphere*. pp. 1-16.

Deshusses, M.A. and Johnson, C.T. (2000) 'Development and Validation of a Simple Protocol To Rapidly Determine the Performance of Biofilters for VOC Treatment', *Environmental Science & Technology*, 34(3), pp. 461-467.

Devinny, J.S., Deshusses, M.A. and Todd, S.W. (1999) 'Biofiltration for air pollution control'.

Dewulf, J. and Van Langenhove, H. (1999) *Anthropogenic volatile organic compounds in ambient air and natural waters: a review on recent developments of analytical methodology, performance and interpretation of field measurements*.

Einaga, H. and Ogata, A. (2008) 'Benzene oxidation with ozone over supported manganese oxide catalysts: effect of catalyst support and reaction conditions', *Journal of hazardous materials*, 164(2-3), pp. 1236-41.

Eliasson, B. and Kogelschatz, U. (1991) 'Nonequilibrium volume plasma chemical processing', *IEEE Transactions on Plasma Science*, 19(6), pp. 1063-1077.

EPA (1990) 'U.S. EPA. Initial list of hazardous air pollutants with modifications; https://www.epa.gov/haps/

initial-list-hazardous-air-pollutants-modifications.'.

Fabry, F., Rehmet, C., Rohani, V. and Fulcheri, L. (2013) 'Waste Gasification by Thermal Plasma: A Review', *Waste and Biomass Valorization*, 4(3), pp. 421-439.

Falkenstein, Z. and Coogan, J.J. (1997) 'Microdischarge behaviour in the silent discharge of nitrogen-oxygen and water-air mixtures', *Journal of Physics D: Applied Physics*, 30(5), pp. 817-825.

Fridman, A. (2004) *The 31st IEEE International Conference on Plasma Science, 2004. ICOPS 2004. IEEE Conference Record - Abstracts.*, 1-1 July 2004.

Fridman, A. (2008) *Plasma Chemistry*. Cambridge University Press, Cambrige, Cambridge.

Fridman, A. and Lawrence, K. (2004) *Plasma Physics and Engineering, CRC Press*

Fridman. A (2008) *Plasma Chemistry*. Cambridge University Press.

Futamura, S. and Kabashima, H. (2004) 'Effects of Reactor Type and Voltage Properties in Methanol Reforming With Nonthermal Plasma', *IEEE Transactions on Industry Applications*, 40(6), pp. 1459-1466.

Gaens, W.V. and Bogaerts, A. (2013) 'Kinetic modelling for an atmospheric pressure argon plasma jet in humid air', *Journal of Physics D*, 46, p. 275201.

Gong, C.-M., Li, Z.-R. and Li, X.-Y. (2012) 'Theoretical Kinetic Study of Thermal Decomposition of Cyclohexane', *Energy & Fuels*, 26(5), pp. 2811-2820.

Gudmundsson, J.T., Kawamura, E. and Lieberman, M.A. (2013) 'A benchmark study of a capacitively coupled oxygen discharge of the oopd1 particle-in-cell Monte Carlo code', *Plasma Sources Science and Technology*, 22(3), p. 035011.

Guo, T., Bai, Z., Wu, C. and Zhu, T. (2008) 'Influence of environmental temperature and relative humidity on photocatalytic oxidation of toluene on activated carbon fibers coated TiO2', *Frontiers of Environmental Science & Engineering in China*, 2(2), pp. 224-229.

Guo, T., Du, X., Peng, Z., Xu, L., Dong, J., Li, J., Cheng, P. and Zhou, Z. (2017) 'Quantification and risk assessment of organic products resulting from non-thermal plasma removal of toluene in nitrogen', *Rapid Commun Mass Spectrom*, 31(17), pp. 1424-1430.

Hagelaar, G.J.M. and Pitchford, L.C. (2005) 'Solving the Boltzmann equation to obtain electron transport coefficients and rate coefficients for fluid models', *Plasma Sources Science and Technology*, 14(4), pp. 722-733.

Hakoda, T., Hashimoto, S., Fujiyama, Y. and Mizuno, A. (2000) 'Decomposition Mechanism for Electron Beam Irradiation of Vaporized Trichloroethylene−Air Mixtures', *The Journal of Physical Chemistry A*, 104(1), pp. 59-66.

Hama Aziz, K.H., Miessner, H., Mueller, S., Kalass, D., Moeller, D., Khorshid, I. and Rashid, M.A.M. (2017) 'Degradation of pharmaceutical diclofenac and ibuprofen in aqueous solution, a direct comparison of ozonation, photocatalysis, and non-thermal plasma', *Chemical Engineering Journal*, 313, pp. 1033-1041.

Han, Y., Wang, J.-g., Cheng, D.-g. and Liu, C.-j. (2006) 'Density Functional Theory Study of Methanol Conversion via Cold Plasmas', *Industrial & Engineering Chemistry Research*, 45(10), pp. 3460-3467.

Hanna, S.R., Paine, R., Heinold, D., Kintigh, E. and Baker, D. (2007) 'Uncertainties in Air Toxics Calculated by the Dispersion Models AERMOD and ISCST3 in the Houston Ship Channel Area', *Journal of Applied Meteorology and Climatology*, 46(9), pp. 1372-1382.

Harling, A.M., Glover, D.J., Whitehead, J.C. and Zhang, K. (2008) 'Novel Method for Enhancing the Destruction of Environmental Pollutants by the Combination of Multiple Plasma Discharges', *Environ. Sci. Technol.* , 42(12), pp. 4546–4550.

Harling, A.M., Glover, D.J., Whitehead, J.C. and Zhang, K. (2009) 'The role of ozone in the plasma-catalytic destruction of environmental pollutants', *Applied Catalysis B: Environmental*, 90(1-2), pp. 157-161.

Harling, A.M., Whitehead, J.C. and Zhang, K. (2005) 'NOx Formation in the Plasma Treatment of Halomethanes', *J. Phys. Chem. A* 109(49), pp. 11255-11260.

Helmig, D., J, B., Galbally, I.E., A, L., Milton, M.J.T., S, P., -Duelmer, C.P., Reimann, S. and P. Tans, a.S.T. (2009) 'Volatile Organic Compounds in the Global Atmosphere', *EOS, Transactions, American Geo physical Union*, 90 (52), pp. 513-520.

Hill, S.L., Whitehead, J.C. and Zhang, K. (2007) 'Plasma Processing of Propane at Hyper-Atmospheric Pressure: Experiment and Modelling', *Plasma Processes and Polymers*, 4(7-8), pp. 710-718.

Hirota, K., Sakai, H., Washio, M. and Kojima, T. (2004) 'Application of Electron Beams for the Treatment of VOC Streams', *Industrial & Engineering Chemistry Research*, 43(5), pp. 1185-1191.

Hoseini, S., Rahemi, N., Allahyari, S. and Tasbihi, M. (2019) 'Application of plasma technology in the removal of volatile organic compounds (BTX) using manganese oxide nano-catalysts synthesized from spent batteries', *Journal of Cleaner Production*, 232, pp. 1134-1147.

Hu, Q.-y., Wang, C. and Huang, K.-x. (2015) 'Biofiltration performance and characteristics of high-temperature gaseous benzene, hexane and toluene', *Chemical Engineering Journal*, 279, pp. 689-695.

Huang, H., Ye, D. and Leung, D.Y.C. (2011) 'Plasma-Driven Catalysis Process for Toluene Abatement: Effect of Water Vapor', *IEEE Transactions on Plasma Science*, 39(1), pp. 576-580.

IARC (2017) 'IARC Monograph on the Evaluation of Carcinogenic Risks to Humans. 2017. http://monographs.iarc.fr/ENG/Classification/latest_classif.php. Accessed 03 October 2019.', *World Health Organization, International Agency for Research on Cancer.*, 1-117.

Irena and methanol institute (2021) *Innovation Outlook: Renewable Methanol,*. International Renewable Energy Agency, (Accessed: 08/12/2021).

Jarrige, J. and Vervisch, P. (2006) 'Decomposition of three volatile organic compounds by nanosecond pulsed corona discharge: Study of by-product formation and influence of high voltage pulse parameters', *Journal of Applied Physics*, 99(11), p. 113303.

Jeon, E.C., Kim, K.J., Kim, J.C., Kim, K.H., Chung, S.G., Sunwoo, Y. and Park, Y.K. (2008) 'Novel hybrid technology for VOC control using an electron beam and catalyst', *Research on Chemical Intermediates*, 34(8-9), pp. 863-870.

Jiang, B., Fei, X., Yao, S., Wang, Q., Yao, X., Xu, K. and Chen, Z. (2020) 'Decomposition of a gas mixture of four n-alkanes using a DBD reactor', *Plasma Science and Technology*, 22(11).

Jiang, B., Wen, Y., Li, Z., Xia, D. and Liu, X. (2018) 'Theoretical Analysis on the Removal of Cyclic Volatile Organic Compounds by Non-thermal Plasma', *Water, Air, & Soil Pollution*, 229(2).

Jiang, L., Zhu, R., Mao, Y., Chen, J. and Zhang, L. (2015) 'Conversion characteristics and production evaluation of styrene/o-xylene mixtures removed by DBD pretreatment', *Int J Environ Res Public Health*, 12(2), pp. 1334-50.

Jiang, N., Hu, J., Li, J., Shang, K., Lu, N. and Wu, Y. (2016) 'Plasma-catalytic degradation of benzene over Ag–Ce bimetallic oxide catalysts using hybrid surface/packed-bed discharge plasmas', *Applied Catalysis B: Environmental*, 184, pp. 355-363.

Jin, Q., Jiang, B., Han, J. and Yao, S. (2016) 'Hexane decomposition without particle emission using a novel dielectric barrier discharge reactor filled with porous dielectric balls', *Chemical Engineering Journal*, 286, pp. 300-310.

Karatum, O. and Deshusses, M.A. (2016) 'A comparative study of dilute VOCs treatment in a non-thermal plasma reactor', *Chemical Engineering Journal*, 294, pp. 308-315.

Karuppiah, J., Manoj Kumar Reddy, P., Linga Reddy, E. and Subrahmanyam, C. (2013) 'Catalytic Non-Thermal Plasma Reactor for Decomposition of Dilute Chlorobenzene', *Plasma Processes and Polymers*, 10(12), pp. 1074-1080.

Karuppiah, J., Reddy, E.L., Reddy, P.M., Ramaraju, B., Karvembu, R. and Subrahmanyam, C. (2012) 'Abatement of mixture of volatile organic compounds (VOCs) in a catalytic non-thermal plasma reactor', *J Hazard Mater*, 237-238, pp. 283-9.

Khan, F.I. and Ghoshal, A.K. (2000) 'Removal of Volatile Organic Compounds from polluted air', *Journal of Loss Prevention in the Process Industries*, 13, pp. 527-545.

Khoja, A.H., Tahir, M. and Amin, N.A.S. (2017) 'Dry reforming of methane using different dielectric materials and DBD plasma reactor configurations', *Energy Conversion and Management*, 144, pp. 262-274.

Kim, D.H., Mok, Y.S. and Lee, S. (2011) 'Effect of temperature on the decomposition of trifluoromethane in a dielectric barrier discharge reactor', *Thin Solid Films*, 519, pp. 6960-6963.

Kim, H.-H. (2004) *Nonthermal Plasma Processing for Air-Pollution Control: A Historical Review, Current Issues, and Future Prospects*.

Kim, H.-H., Lee, Y.-H., Ogata, A. and Futamura, S. (2003) 'Plasma-driven catalyst processing packed with photocatalyst for gas-phase benzene decomposition', *Catalysis Communications*, 4(7), pp. 347-351.

Kim, H.-H., Ogata, A. and Futamura, S. (2008) 'Oxygen Partial Pressure-Dependent Behavior of Various Catalysts for the Total Oxidation of VOCs Using Cycled System of Adsorption and Oxygen Plasma', *Applied Catalysis B-environmental - APPL CATAL B-ENVIRON*, 79, pp. 356-367.

Kim, H.-H., Oh, S.-M., Ogata, A. and Futamura, S. (2004) 'Decomposition of Benzene Using Ag/TiO2 Packed Plasma-Driven Catalyst Reactor: Influence of Electrode Configuration and Ag-Loading Amount', *Catalysis Letters*, 96(3), pp. 189-194.

Kim, K.H., Szulejko, J.E., Kumar, P., Kwon, E.E., Adelodun, A.A. and Reddy, P.A.K. (2017) 'Air ionization as a control technology for off-gas emissions of volatile organic compounds', *Environ Pollut*, 225, pp. 729-743.

Kim, T., Jo, S., Song, Y.-H. and Lee, D.H. (2014a) 'Synergetic mechanism of methanol–steam reforming reaction in a catalytic reactor with electric discharges', *Applied Energy*, 113, pp. 1692-1699.

Kim, T., Jo, S., Song, Y.-H. and Lee, D.H. (2014b) 'Synergetic mechanism of methanol steam reforming reaction in a catalytic reactor with electric discharges', *Applied Energy*, 113, pp. 1692-1699.

Kogelschatz, U. (2003) 'Dielectric-barrier Discharges Their History, Discharge Physics, and Industrial Applications.', *Plasma Chemistry and Plasma Processing*, , 23(1), p. 46.

Kogelschatz, U., Eliasson, B. and Egli, W. (1997) 'Dielectric-Barrier Discharges. Principle and Applications', *Le Journal de Physique IV*, 07(C4), pp. C4-47-C4-66.

Kudryashov, S.V., Ryabov, A.Y., Ochered'ko, A.N. and Sirotkina, E.E. (2018) 'Synthesis of propylene oxide in a barrier discharge plasma', *AIP Conference Proceedings*, 2051(1), p. 020159.

Kundu, S.K., Kennedy, E.M., Gaikwad, V.V., Molloy, T.S. and Dlugogorski, B.Z. (2012) 'Experimental investigation of alumina and quartz as dielectrics for a cylindrical double dielectric barrier discharge reactor in argon diluted methane plasma', *Chemical Engineering Journal*, 180, pp. 178-189.

Kuo, C.-H. and Arunachalam, S. (2014) 'One-pot room-temperature conversion of cyclohexane to adipic acid by ozone and UV light', *Photochemistry Research*, 346(6216), pp. 1495-1497.

Langmuir, I. (1928) 'Oscillations in ionized gases', *Proc. Nat. Acad. Sci. U.S.* , 14, p. 628.

Lee, B.-Y., Park, S.-H., Lee, S.-C., Kang, M. and Choung, S.-J. (2004) 'Decomposition of benzene by using a discharge plasma–photocatalyst hybrid system', *Catalysis Today*, 93-95, pp. 769-776.

Lee, E.H., Kim, J., Cho, K.S., Ahn, Y.G. and Hwang, G.S. (2010) 'Degradation of hexane and other recalcitrant hydrocarbons by a novel isolate, Rhodococcus sp. EH831', *Environ Sci Pollut Res Int*, 17(1), pp. 64-77.

Lee, P.-F., Matsui, H., Xu, D.-W. and Wang, N.-S. (2013) 'Thermal Decomposition and Oxidation of CH3OH', *The Journal of Physical Chemistry A*, 117(3), pp. 525-534.

Li, S., Dang, X., Yu, X., Abbas, G., Zhang, Q. and Cao, L. (2020) 'The application of dielectric barrier discharge non-thermal plasma in VOCs abatement: A review', *Chemical Engineering Journal*, 388.

Liang, W., Li, J., Li, J. and Jin, Y. (2009) 'Abatement of toluene from gas streams via ferro-electric packed bed dielectric barrier discharge plasma', *Journal of Hazardous Materials*, 170(2), pp. 633-638.

Liang, W.J., Ma, L., Liu, H. and Li, J. (2013) 'Toluene degradation by non-thermal plasma combined with a ferroelectric catalyst', *Chemosphere*, 92(10), pp. 1390-5.

Liang, Y., Li, J., Xue, Y., Tan, T., Jiang, Z., He, Y., Shangguan, W., Yang, J. and Pan, Y. (2021) 'Benzene decomposition by non-thermal plasma: A detailed mechanism study by synchrotron radiation photoionization mass spectrometry and theoretical calculations', *J Hazard Mater*, 420, p. 126584.

Liotta, L. (2010) *Catalytic oxidation of volatile organic compounds on supported noble metals*.

Liu, S., Mei, D., Wang, L. and Tu, X. (2017a) 'Steam reforming of toluene as biomass tar model compound in a gliding arc discharge reactor', *Chemical Engineering Journal*, 307, pp. 793-802.

Liu, S.Y., Mei, D.H., Nahil, M.A., Gadkari, S., Gu, S., Williams, P.T. and Tu, X. (2017b) 'Hybrid plasma-catalytic steam reforming of toluene as a biomass tar model compound over Ni/Al2O3 catalysts', *Fuel Processing Technology*, 166, pp. 269-275.

Lu, M., Huang, R., Wu, J., Fu, M., Chen, L. and Ye, D. (2015) 'On the performance and mechanisms of toluene removal by FeOx/SBA-15-assisted non-thermal plasma at atmospheric pressure and room temperature', *Catalysis Today*, 242, pp. 274-286.

Lukes, P., Locke, B.R. and Brisset, J.-L. 'Aqueous-Phase Chemistry of Electrical Discharge Plasma in Water and in Gas–Liquid Environments', in *Plasma Chemistry and Catalysis in Gases and Liquids*. pp. 243-308.

Luo, Y.-R. (2004) 'Handbook of Bond Dissociation Energies in Organic Compounds', *Journal of the American Chemical Society*, 126(3), pp. 982-982.

Ma, T., Zhao, Q., Liu, J. and Zhong, F. (2016) 'Study of Humidity Effect on Benzene Decomposition by the Dielectric Barrier Discharge Nonthermal Plasma Reactor', *Plasma Science and Technology*, 18(6), pp. 686-692.

Ma, T.J. and Lan, W.S. (2015) 'Ethylene decomposition with a wire-plate dielectric barrier discharge reactor: parameters and kinetic study', *International Journal of Environmental Science and Technology*, 12(12), pp. 3951-3956.

Magureanu, M., Mandache, N.B., Parvulescu, V.I., Subrahmanyam, C., Renken, A. and Kiwi-Minsker, L. (2007) 'Improved performance of non-thermal plasma reactor during decomposition of trichloroethylene: Optimization of the reactor geometry and introduction of catalytic electrode', *Applied Catalysis B: Environmental*, 74(3-4), pp. 270-277.

Marotta, E., Callea, A., Rea, M. and Paradisi, C. (2007) 'DC Corona Electric Discharges for Air Pollution Control. Part 1. Efficiency and Products of Hydrocarbon Processing', *Environmental Science & Technology*, 41(16), pp. 5862-5868.

McAdams, R. (2001) 'Prospects for non-thermal atmospheric plasmas for pollution abatement', *Journal of Physics D: Applied Physics*, 34(18), p. 2810.

Mei, D. and Tu, X. (2017) 'Conversion of CO 2 in a cylindrical dielectric barrier discharge reactor: Effects of plasma processing parameters and reactor design', *Journal of CO2 Utilization*, 19, pp. 68-78.

Michelmore, A., Steele, D.A., Whittle, J.D., Bradley, J.W. and Short, R.D. (2013) 'Nanoscale deposition of chemically functionalised films via plasma polymerisation', *RSC Advances*, 3(33).

Młotek, M., Reda, E., Jóźwik, P., Krawczyk, K. and Bojar, Z. (2015) 'Plasma-catalytic decomposition of cyclohexane in gliding discharge reactor', *Applied Catalysis A: General*, 505, pp. 150-158.

Mustafa, M.F., Fu, X., Liu, Y., Abbas, Y., Wang, H. and Lu, W. (2018) 'Volatile organic compounds (VOCs) removal in non-thermal plasma double dielectric barrier discharge reactor', *J Hazard Mater*, 347, pp. 317-324.

Mustafa, M.F., Liu, Y., Duan, Z., Guo, H., Xu, S., Wang, H. and Lu, W. (2017) 'Volatile compounds emission and health risk assessment during composting of organic fraction of municipal solid waste', *J Hazard Mater*, 327, pp. 35-43.

Mutaf-Yardimci, O., Saveliev, A.V., Fridman, A.A. and Kennedy, L.A. (2000) 'Thermal and nonthermal regimes of gliding arc discharge in air flow', *Journal of Applied Physics*, 87(4), pp. 1632-1641.

Norsic, C., Tatibouët, J.-M., Batiot-Dupeyrat, C. and Fourré, E. (2018) 'Methanol oxidation in dry and humid air by dielectric barrier discharge plasma combined with MnO2–CuO based catalysts', *Chemical Engineering Journal*, 347, pp. 944-952.

Nörtemann, B. (1999) 'Biodegradation of EDTA', *Applied Microbiology and Biotechnology*, 51(6), pp. 751-759.

Ogata, A., Shintani, N., Mizuno, K., Kushiyama, S. and Yamamoto, T. (1997) *IAS '97. Conference Record of the 1997 IEEE Industry Applications Conference Thirty-Second IAS Annual Meeting*. 5-9 Oct. 1997.

Ogata, A., Shintani, N., Mizuno, K., Kushiyama, S. and Yamamoto, T. (1999) 'Decomposition of benzene using a nonthermal plasma reactor packed with ferroelectric pellets', *IEEE Transactions on Industry Applications*, 35(4), pp. 753-759.

Ognier, S., Cavadias, S. and Amouroux, J. (2007) 'Aromatic VOC Removal by Formation of Microparticles in Pure Nitrogen Discharge Barrier Discharge', *Plasma Processes and Polymers*, 4(5), pp. 528-536.

Panda, N.R. and Sahu, D. (2020) 'Enhanced hydrogen generation efficiency of methanol using dielectric barrier discharge plasma methodology and conducting sea water as an electrode', *Heliyon*, 6(9), p. e04717.

Papaefthimiou, P., Ioannides, T. and Verykios, X.E. (1998) 'Performance of doped Pt/TiO2 (W6+) catalysts for combustion of volatile organic compounds (VOCs)', *Applied Catalysis B: Environmental*, 15(1), pp. 75-92.

Parmar, G.R. and Rao, N.N. (2008) 'Emerging Control Technologies for Volatile Organic Compounds', *Critical Reviews in Environmental Science and Technology*, 39(1), pp. 41-78.

Penetrante, B.M., Hsiao, M.C., Bardsley, J.N., Merritt, B.T., Vogtlin, G.E., Wallman, P.H., Kuthi, A., Burkhart, C.P. and Bayless, J.R. (1996) 'Electron beam and pulsed corona processing of volatile organic compounds in gas streams', *Pure and Applied Chemistry*, 68(5), pp. 1083-1087.

Petitpas, G., Rollier, J., Darmon, A., Gonzalezaguilar, J., Metkemeijer, R. and Fulcheri, L. (2007) 'A comparative study of non-thermal plasma assisted reforming technologies', *International Journal of Hydrogen Energy*, 32(14), pp. 2848-2867.

Qi, Z., Yang, L., Lin, X., Zhao, Y., Niu, J., Liu, D., Ding, Z., Xia, Y., Ji, L. and Zhao, Z. (2019) 'Interaction of Plasma Jet With Methanol as Fundamental Processes in Solution', *IEEE Transactions on Plasma Science*, 47(11), pp. 4802-4810.

Raju, B.R., Reddy, E.L., Karuppiah, J., Reddy, P.M.K. and Subrahmanyam, C. (2013) 'Catalytic non-thermal plasma reactor for the decomposition of a mixture of volatile organic compounds', *Journal of Chemical Sciences*, 125(3), pp. 673-678.

Raju., B.R., E Linga, R., J, K., Manoj., P., Kumar, R. and and Ch, S. (2013) 'Catalytic non-thermal plasma reactor for the decomposition of a mixture of volatile organic compounds.', *Journal of Chemical Sciences*, 125 (3), pp. 673-678.

Ruddy, E.N. and Carroll, L.A. (1993) 'SELECT THE BEST VOC CONTROL STRATEGY', *Chemical Engineering Progress*, 89(7), pp. 28-35.

Salamanca, D., Dobslaw, D. and Engesser, K.H. (2017) 'Removal of cyclohexane gaseous emissions using a biotrickling filter system', *Chemosphere*, 176, pp. 97-107.

Saleem, F., Kennedy, J., Dahiru, U.H., Zhang, K. and Harvey, A. (2019a) 'Methane conversion to H2 and higher hydrocarbons using non-thermal plasma dielectric barrier discharge reactor', *Chemical Engineering and Processing - Process Intensification*, 142, p. 107557.

Saleem, F., Kennedy, J., Dahiru, U.H., Zhang, K. and Harvey, A. (2019b) 'Methane conversion to H2 and higher hydrocarbons using non-thermal plasma dielectric barrier discharge reactor', *Chemical Engineering and Processing - Process Intensification*, 142.

Saleem, F., Khoja, A.H., Umer, J., Ahmad, F., Abbas, S.Z., Zhang, K. and Harvey, A. (2021a) 'Removal of benzene as a tar model compound from a gas mixture using non-thermal plasma dielectric barrier discharge reactor', *Journal of the Energy Institute*, 96, pp. 97-105.

Saleem, F., Rehman, A., Ahmad, F., Khoja, A.H., Javed, F., Zhang, K. and Harvey, A. (2021b) 'Removal of toluene as a toxic VOC from methane gas using a non-thermal plasma dielectric barrier discharge reactor', *RSC Advances*, 11(44), pp. 27583-27588.

Saleem, F., Umer, J., Rehman, A., Zhang, K. and Harvey, A. (2020) 'Effect of Methane as an Additive in the Product Gas toward the Formation of Lower Hydrocarbons during the Decomposition of a Tar Analogue', *Energy & Fuels*, 34(2), pp. 1744-1749.

Saleem, F., Zhang, K. and Harvey, A. (2018) 'Role of CO2 in the Conversion of Toluene as a Tar Surrogate in a Nonthermal Plasma Dielectric Barrier Discharge Reactor', *Energy & Fuels*.

Saleem, F., Zhang, K. and Harvey, A. (2019c) 'Direct Conversion of Benzene as a Tar Analogue to Methane Using Non-thermal Plasma', *Energy & Fuels*, 33(3), pp. 2598-2601.

Saleem, F., Zhang, K. and Harvey, A. (2019d) 'Plasma-assisted decomposition of a biomass gasification tar analogue into lower hydrocarbons in a synthetic product gas using a dielectric barrier discharge reactor', *Fuel*, 235, pp. 1412-1419.

Saleem, F., Zhang, K. and Harvey, A. (2019e) 'Removal of Toluene as a Tar Analogue in a N2 Carrier Gas Using a Non-thermal Plasma Dielectric Barrier Discharge Reactor', *Energy & Fuels*, 33(1), pp. 389-396.

Saleem, F., Zhang, K. and Harvey, A. (2019f) 'Temperature dependence of non-thermal plasma assisted hydrocracking of toluene to lower hydrocarbons in a dielectric barrier discharge reactor', *Chemical Engineering Journal*, 356, pp. 1062-1069.

Saleem, F., Zhang, K. and Harvey, A.P. (2019g) 'Decomposition of benzene as a tar analogue in CO2 and H2 carrier gases, using a non-thermal plasma', *Chemical Engineering Journal*, 360, pp. 714-720.

Samal, S. (2017) 'Thermal plasma technology: The prospective future in material processing', *Journal of Cleaner Production*, 142, pp. 3131-3150.

Sarigiannis, D.A., Karakitsios, S.P., Gotti, A., Liakos, I.L. and Katsoyiannis, A. (2011) 'Exposure to major volatile organic compounds and carbonyls in European indoor environments and associated health risk', *Environ Int*, 37(4), pp. 743-65.

Sato, T., Kambe, M. and Nishiyama, H. (2005) 'Analysis of a Methanol Decomposition Process by a Nonthermal Plasma Flow', *JSME International Journal Series B Fluids and Thermal Engineering*, 48(3), pp. 432-439.

Schiavon, M., Schiorlin, M., Torretta, V., Brandenburg, R. and Ragazzi, M. (2017) 'Non-thermal plasma assisting the biofiltration of volatile organic compounds', *Journal of Cleaner Production*, 148, pp. 498-508.

Schiavon, M., Schiorlin, M., Torretta, V., Ragazzi, M. and Rada, E.C. (2016) 'Biofiltration combined with non-thermal plasma for air pollution control: a preliminary investigation', *International Journal of Sustainable Development and Planning*, 11(4), pp. 627-635.

Schiorlin, M., Marotta, E., Rea, M. and Paradisi, C. (2009) 'Comparison of Toluene Removal in Air at Atmospheric Conditions by Different Corona Discharges', *Environmental Science & Technology*, 43(24), pp. 9386-9392.

Shang, K., Wang, M., Peng, B., Li, J., Lu, N., Jiang, N. and Wu, Y. (2020) 'Characterization of a novel volume-surface DBD reactor: discharge characteristics, ozone production and benzene degradation', *Journal of Physics D: Applied Physics*, 53(6:065201).

Shuji Tanabe, H.M., Kenji Okitsu, and Hiroshige Matsumoto (2000) 'Generation of Hydrogen from Methanol in a Dielectric-Barrier Discharge-Plasma System', *Chemistry Letters*, 29(10), pp. 1116-7.

Siemens, W. (1857) 'Ueber die elektrostatische Induction und die Verzögerung des Stroms in Flaschendrähten', *Annalen der Physik*, 178(9), pp. 66-122.

Sivachandiran, L. and Subrahmanyam, C. (2012) 'DBD plasma reactor for oxidative decomposition of Chlorobenzene', *International Journal of Chemical Reactor Engineering*, 10, pp. 1542-6580.

Snoeckx, R., Setareh, M., Aerts, R., Simon, P., Maghari, A. and Bogaerts, A. (2013) 'Influence of N2 concentration in a CH4/N2 dielectric barrier discharge used for CH4 conversion into H2', *International Journal of Hydrogen Energy*, 38(36), pp. 16098-16120.

Son, Y.S., Kim, J., Choi, I.Y. and Kim, J.C. (2021) 'Decomposition of n-hexane using a dielectric barrier discharge plasma', *Environ Technol*, 42(13), pp. 2067-2076.

Spigno, G. and De Faveri, D.M. (2005) 'Modeling of a vapor-phase fungi bioreactor for the abatement of hexane: Fluid dynamics and kinetic aspects', *Biotechnology and Bioengineering*, 89(3), pp. 319-328.

Steinberg, I., Rohde, C., Bockreis, A. and Jager, J. (2005) 'Increase of the purification efficiency of biofilters by the use of a complementary ionisation step', *Waste Management*, 25(4), pp. 375-381.

Subrahmanyam, C., Magureanu, M., Renken, A. and Kiwi-Minsker, L. (2006) 'Catalytic abatement of volatile organic compounds assisted by non-thermal plasma: Part 1. A novel dielectric barrier discharge reactor containing catalytic electrode', *Applied Catalysis B: Environmental*, 65(1), pp. 150-156.

Subrahmanyam, C., Renken, A. and Kiwi-Minsker, L. (2007) 'Novel catalytic non-thermal plasma reactor for the abatement of VOCs', *Chemical Engineering Journal*, 134(1-3), pp. 78-83.

Sultana, S., Vandenbroucke, A., Leys, C., De Geyter, N. and Morent, R. (2015) 'Abatement of VOCs with Alternate Adsorption and Plasma-Assisted Regeneration: A Review', *Catalysts*, 5(2), pp. 718-746.

Sun, B., Sato, M. and Sid Clements, J. (1997) 'Optical study of active species produced by a pulsed streamer corona discharge in water', *Journal of Electrostatics*, 39(3), pp. 189-202.

Teplý, J., Dressler, M., Janča, J. and Tesa>r, C. (1995) 'Destruction of Organic Compounds in a High-Frequency Discharge Plasma at Reduced Pressure', *Plasma Chemistry and Plasma Processing*, 15(3), pp. 465-479.

Thevenet, F., Guaitella, O., Puzenat, E., Guillard, C. and Rousseau, A. (2008) 'Influence of water vapour on plasma/photocatalytic oxidation efficiency of acetylene', *Applied Catalysis B: Environmental*, 84(3-4), pp. 813-820.

Thevenet, F., Sivachandiran, L., Guaitella, O., Barakat, C. and Rousseau, A. (2014) 'Plasma–catalyst coupling for volatile organic compound removal and indoor air treatment: a review', *Journal of Physics D: Applied Physics*, 47(22).

Tian, F., Zhang, X. and Chen, Y. (2016) 'Highly selective adsorption and separation of dichloromethane/trichloromethane on a copper-based metal–organic framework', *RSC Advances*, 6(37), pp. 31214-31224.

Trushkin, A.N., Grushin, M.E., Kochetov, I.V., Trushkin, N.I. and Akishev, Y.S. (2013) 'Decomposition of toluene in a steady-state atmospheric-pressure glow discharge', *Plasma Physics Reports*, 39(2), pp. 167-182.

U Chasanah, E.Y., A Z Zain, E Sasmita, M Restiwijaya, A W Kinandana, F Arianto, M Nur (2019) 'Evaluation of Titration Method on Determination of Ozone Concentration produced by Dielectric Barrier Discharge Plasma (DBDP) Technology', *Journal of Physics: Conference Series*, 1153.

Urashima, K. and Chang, J.-S. (2000) 'Removal of Volatile Organic Compounds from Air Streams and Industrial Flue Gases by Non-Thermal Plasma Technology', *Dielectrics and Electrical Insulation, IEEE Transactions on*, 7, pp. 602-614.

Uria-Tellaetxe, I., Navazo, M., de Blas, M., Durana, N., Alonso, L. and Iza, J. (2016) 'Gas-phase naphthalene concentration data recovery in ambient air and its relevance as a tracer of sources of volatile organic compounds', *Atmospheric Environment*, 131, pp. 279-288.

Van Durme, J., Dewulf, J., Demeestere, K., Leys, C. and Van Langenhove, H. (2009) 'Post-plasma catalytic technology for the removal of toluene from indoor air: Effect of humidity', *Applied Catalysis B: Environmental*, 87(1-2), pp. 78-83.

Vandenbroucke, A.M., Mora, M., Jiménez-Sanchidrián, C., Romero-Salguero, F.J., De Geyter, N., Leys, C. and Morent, R. (2014) 'TCE abatement with a plasma-catalytic combined system using MnO2 as catalyst', *Applied Catalysis B: Environmental*, 156-157, pp. 94-100.

Vandenbroucke, A.M., Morent, R., De Geyter, N. and Leys, C. (2011) 'Non-thermal plasmas for non-catalytic and catalytic VOC abatement', *Journal of Hazardous Materials*, 195, pp. 30-54.

Wang, B., Chi, C., Xu, M., Wang, C. and Meng, D. (2017) 'Plasma-catalytic removal of toluene over CeO 2 -MnO x catalysts in an atmosphere dielectric barrier discharge', *Chemical Engineering Journal*, 322, pp. 679-692.

Wang, B., Yan, W., Ge, W. and Duan, X. (2013) 'Methane conversion into higher hydrocarbons with dielectric barrier discharge micro-plasma reactor', *Journal of Energy Chemistry*, 22(6), pp. 876-882.

Wang, L., Liu, S.Y., Xu, C. and Tu, X. (2016) 'Direct conversion of methanol to n-C4H10 and H2 in a dielectric barrier discharge reactor', *Green Chemistry*, 18(20), pp. 5658-5666.

Wang, Q., Fan, X.-R., Cui, L., Wang, P., Wu, J. and Chen, J. (2009) 'Plasma-Aided Cotton Bioscouring: Dielectric Barrier Discharge Versus Low-Pressure Oxygen Plasma', *Plasma Chemistry and Plasma Processing*, 29(5), pp. 399-409.

Wang, T., Sun, B.-M., Xiao, H.-P., Zeng, J.-y., Duan, E.-p., Xin, J. and Li, C. (2012) 'Effect of Reactor Structure in DBD for Nonthermal Plasma Processing of NO in N2 at Ambient Temperature', *Plasma Chemistry and Plasma Processing*, 32(6), pp. 1189-1201.

Wang, X., Wu, J., Wang, J., Xiao, H., Chen, B., Peng, R., Fu, M., Chen, L., Ye, D. and Wen, W. (2019) 'Methanol plasma-catalytic oxidation over CeO2 catalysts: Effect of ceria morphology and reaction mechanism', *Chemical Engineering Journal*, 369, pp. 233-244.

Wei, W., Wang, S.X. and Hao, J.M. (2011) '[Uncertainty analysis of emission inventory for volatile organic compounds from anthropogenic sources in China]', *Huan Jing Ke Xue*, 32(2), pp. 305-12.

Wenjing Lu, Y.A., Muhammad Farooq Mustafa, Chao Pan, Hongtao Wang (2019) 'A review on application of dielectric barrier discharge plasma technology on the abatement of volatile organic compounds', *Front. Environ. Sci. Eng.*, 13(2), pp. 30-.

WHO (1989) 'Volatile organic compounds in air analysis'.

William, J.C. and Lead, P.E. (1997) *VOC Control Strategies in Plant Design, In: Chemical Processing: Project Engineering Annual*, p. 44.

Wu, J., Xia, Q., Wang, H. and Li, Z. (2014) 'Catalytic performance of plasma catalysis system with nickel oxide catalysts on different supports for toluene removal: Effect of water vapor', *Applied Catalysis B: Environmental*, 156-157, pp. 265-272.

Xiao, G., Xu, W., Wu, R., Ni, M., Du, C., Gao, X., Luo, Z. and Cen, K. (2014) 'Non-Thermal Plasmas for VOCs Abatement', *Plasma Chemistry and Plasma Processing*, 34(5), pp. 1033-1065.

Xu, N., Fu, W., He, C., Cao, L., Liu, X., Zhao, J. and Pan, H. (2014) 'Benzene Removal Using Non-thermal Plasma with CuO/AC Catalyst: Reaction Condition Optimization and Decomposition Mechanism', *Plasma Chemistry and Plasma Processing*, 34(6), pp. 1387-1402.

Yan, J.H., Bo, Z., Li, X.D., Du, C.M., Cen, K.F. and Chéron, B.G. (2007) 'Study of Mechanism for Hexane Decomposition with Gliding Arc Gas Discharge', *Plasma Chemistry and Plasma Processing*, 27(2), pp. 115-126.

Yan, K., van Heesch, E.J.M., Pemen, A.J.M., Huijbrechts, P.A.H.J., van Gompel, F.M., van Leuken, H. and Matyas, Z. (2002) 'A high-voltage pulse generator for corona plasma generation', *IEEE Transactions on Industry Applications*, 38(3), pp. 866-872.

Yang, C., Xu, Y.R., Teo, K.C., Goh, N.K., Chia, L.S. and Xie, R.J. (2005) 'Destruction of organic pollutants in reusable wastewater using advanced oxidation technology', *Chemosphere*, 59(3), pp. 441-5.

Yao, S., Wu, Z., Han, J., Tang, X., Jiang, B., Lu, H., Yamamoto, S. and Kodama, S. (2015) 'Study of ozone generation in an atmospheric dielectric barrier discharge reactor', *Journal of Electrostatics*, 75, pp. 35-42.

Ye, Z., Zhang, Y., Li, P., Yang, L., Zhang, R. and Hou, H. (2008) 'Feasibility of destruction of gaseous benzene with dielectric barrier discharge', *J Hazard Mater*, 156(1-3), pp. 356-64.

Yehia, D.A. (2016) *The electrical characteristics of the dielectric barrier discharges*.

Yu, Q., Kong, M., Liu, T., Fei, J. and Zheng, X. (2012) 'Characteristics of the Decomposition of CO2 in a Dielectric Packed-Bed Plasma Reactor', *Plasma Chemistry and Plasma Processing*, 32(1), pp. 153-163.

Yulianto, E., Restiwijaya, M., Sasmita, E., Arianto, F., Kinandana, A.W. and Nur, M. (2019) 'Power analysis of ozone generator for high capacity production', *Journal of Physics: Conference Series*, 1170.

Zhang, H., Li, K., Sun, T., Jia, J., Lou, Z. and Feng, L. (2014) 'Removal of styrene using dielectric barrier discharge plasmas combined with sol–gel prepared TiO2 coated γ-Al2O3', *Chemical Engineering Journal*, 241, pp. 92-102.

Zhang, H., Li, K., Sun, T., Jia, J., Lou, Z., Yao, S. and Wang, G. (2015a) 'The combination effect of dielectric barrier discharge (DBD) and TiO2 catalytic process on styrene removal and the analysis of the by-products and intermediates', *Research on Chemical Intermediates*, 41(1), pp. 175-189.

Zhang, H., Li, X., Zhu, F., Bo, Z., Cen, K. and Tu, X. (2015b) 'Non-oxidative decomposition of methanol into hydrogen in a rotating gliding arc plasma reactor', *International Journal of Hydrogen Energy*, 40(46), pp. 15901-15912.

Zhang, H., Zhu, F., Li, X., Cen, K., Du, C. and Tu, X. (2016) 'Enhanced hydrogen production by methanol decomposition using a novel rotating gliding arc discharge plasma', *RSC Advances*, 6(16), pp. 12770-12781.

Zhang, T., Li, Q., Liu, Y., Duan, Y. and Zhang, W. (2011) 'Equilibrium and kinetics studies of fluoride ions adsorption on CeO2/Al2O3 composites pretreated with non-thermal plasma', *Chemical Engineering Journal*, 168(2), pp. 665-671.

Zhang, X., Zhu, A., Li, X. and Gong, W. (2004) 'Oxidative dehydrogenation of ethane with CO2 over catalyst under pulse corona plasma', *Catalysis Today*, 89(1), pp. 97-102.

Zheng, C., Shen, X., Gao, X., Li, Z., Zhu, X., Luo, Z. and Cen, K. (2013) 'Planar Laser-Induced Fluorescence Diagnostics for Spatiotemporal OH Evolution in Pulsed Corona Discharge', *IEEE Transactions on Plasma Science*, 41(3), pp. 485-493.

Zheng, C., Zhu, X., Gao, X., Liu, L., Chang, Q., Luo, Z. and Cen, K. (2014) 'Experimental study of acetone removal by packed-bed dielectric barrier discharge reactor', *Journal of Industrial and Engineering Chemistry*, 20(5), pp. 2761-2768.

Zheng, M., Yu, D., Duan, L., Yu, W. and Huang, L. (2017) 'In-situ fabricated CuO nanowires/Cu foam as a monolithic catalyst for plasma-catalytic oxidation of toluene', *Catalysis Communications*, 100, pp. 187-190.

Zhu, M., Tong, Z., Zhao, Z., Jiang, Y. and Zhao, Z. (2016a) 'A Microporous Graphitized Biocarbon with High Adsorption Capacity toward Benzene Volatile Organic Compounds (VOCs) from Humid Air at Ultralow Pressures', *Industrial & Engineering Chemistry Research*, 55(13), pp. 3765-3774.

Zhu, T., Li, J., Jin, Y., Liang, Y. and Ma, G. (2008) 'Decomposition of benzene by non-thermal plasma processing: Photocatalyst and ozone effect', *International Journal of Environmental Science & Technology*, 5(3), pp. 375-384.

Zhu, X., Gao, X., Yu, X., Zheng, C. and Tu, X. (2015) 'Catalyst screening for acetone removal in a single-stage plasma-catalysis system', *Catalysis Today*, 256, pp. 108-114.

Zhu, X., Gao, X., Zheng, C., Wang, Z., Ni, M. and Tu, X. (2014) 'Plasma-catalytic removal of a low concentration of acetone in humid conditions', *RSC Adv.*, 4(71), pp. 37796-37805.

Zhu, X., Liu, S., Cai, Y., Gao, X., Zhou, J., Zheng, C. and Tu, X. (2016b) 'Post-plasma catalytic removal of methanol over Mn–Ce catalysts in an atmospheric dielectric barrier discharge', *Applied Catalysis B: Environmental*, 183, pp. 124-132.

Appendices

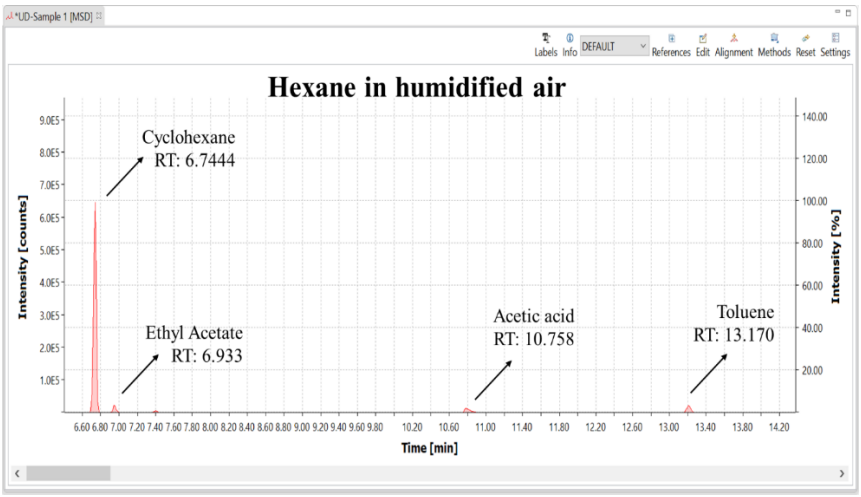

Appendix A-4.1: GC-MS analysis of the hexane decomposition in humidified air carrier gas.

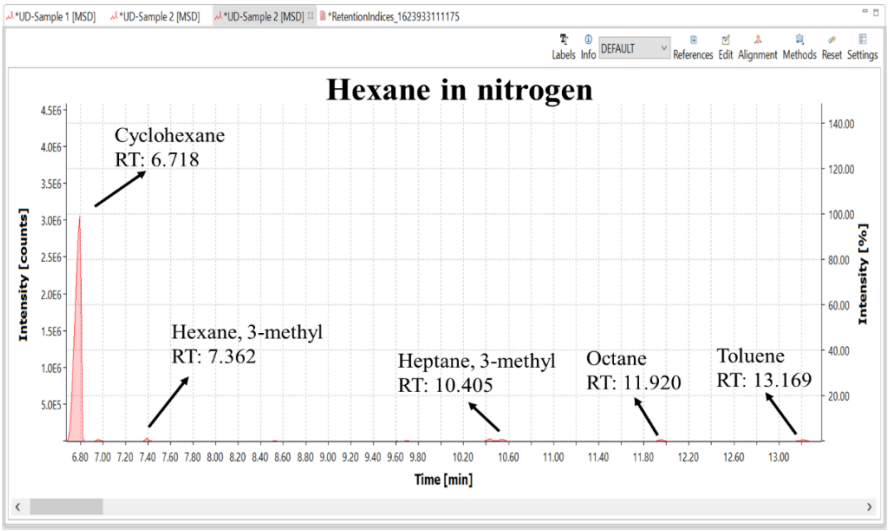

Appendix A-4.2: GC-MS analysis of the hexane decomposition in nitrogen carrier gas.

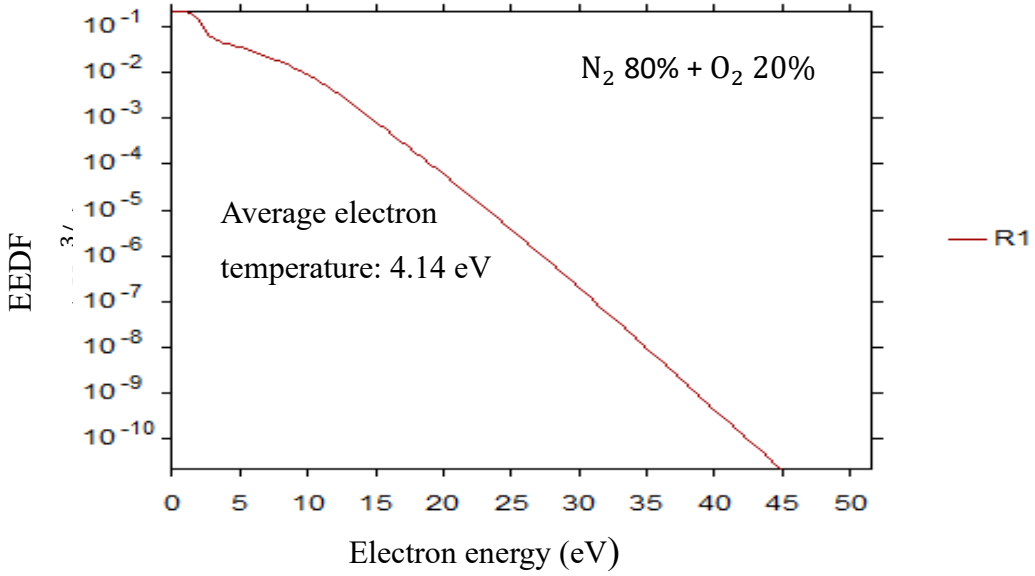

Appendix A-4.3: EEDF of N_2 and O_2

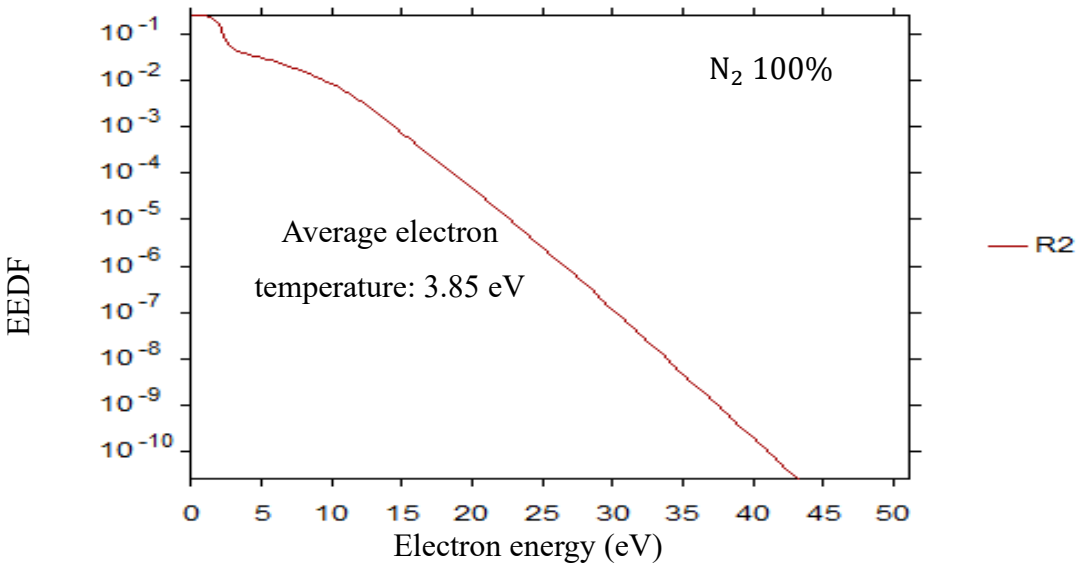

Appendix A-4.4: EEDF of N_2

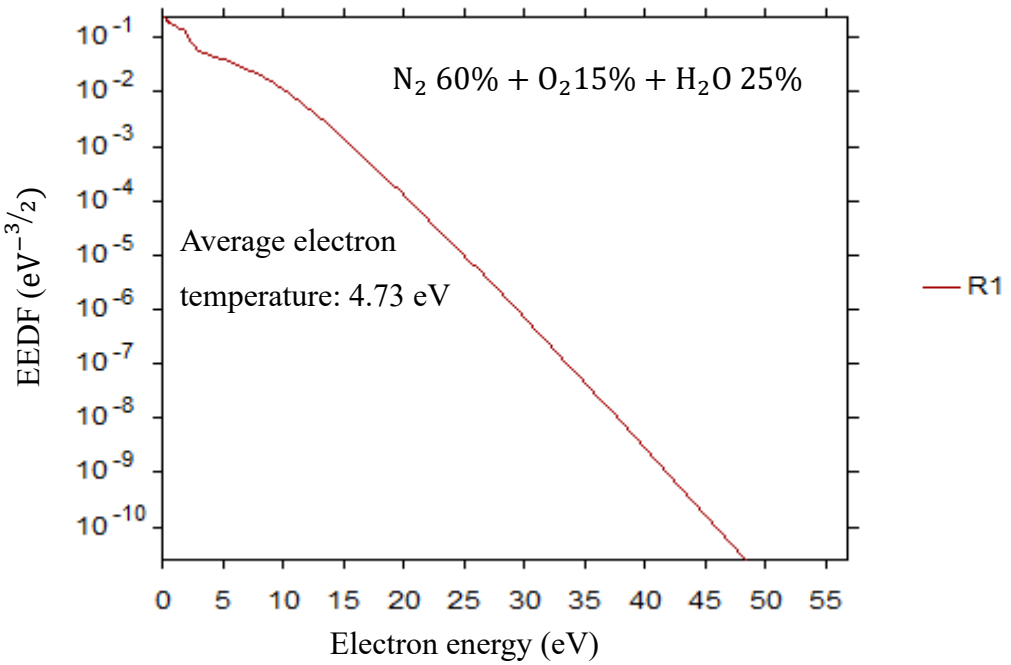

Appendix A-4.5: EEDF of N_2 60% + $O_2$15% + H_2O 25%

Appendix A-4.6 Decomposition products identified by GC-MS in Nitrogen, dry and humidified air

Name of compound	Chemical formula	Chemical structure	Nitrogen	Dry air	Humidified air
Cyclohexane	C_6H_{12}		+	−	+
Hexane, 3-methyl	C_7H_{16}	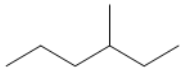	+	−	+
Heptane, 3-methyl	C_8H_{18}	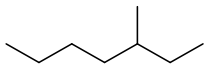	+	−	+
Octane	C_8H_{18}	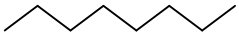	+	−	+
Toluene	C_7H_8	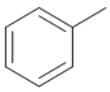	+	−	+
Ethyl acetate	$C_4H_8O_2$	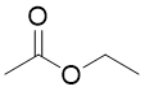	−	−	+
Acetic acid	CH_3COOH	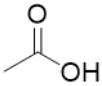	−	−	+

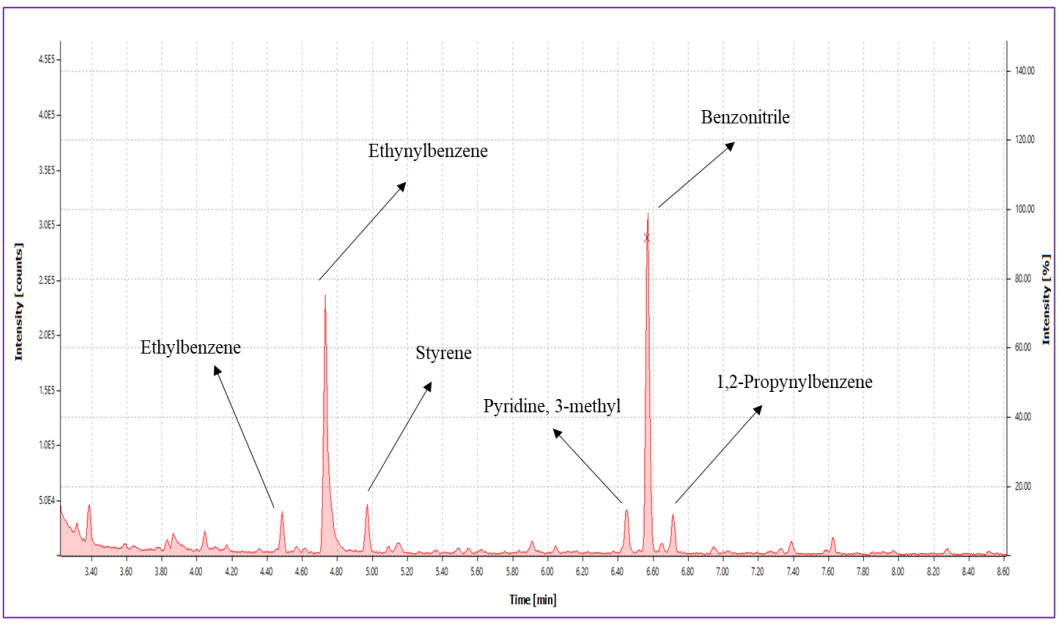

Appendix A-6.1: GC-MS analysis of the benzene decomposition in a dry air plasma.

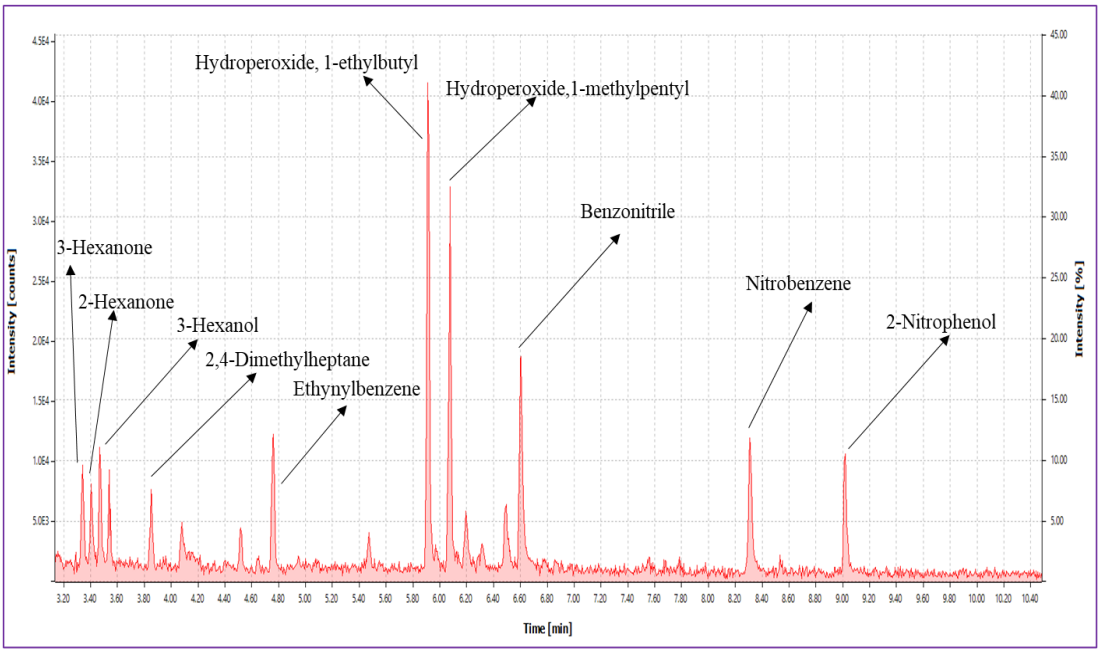

Appendix A-6.2 : GC-MS analysis of the benzene decomposition in a humidified air carrier gas.

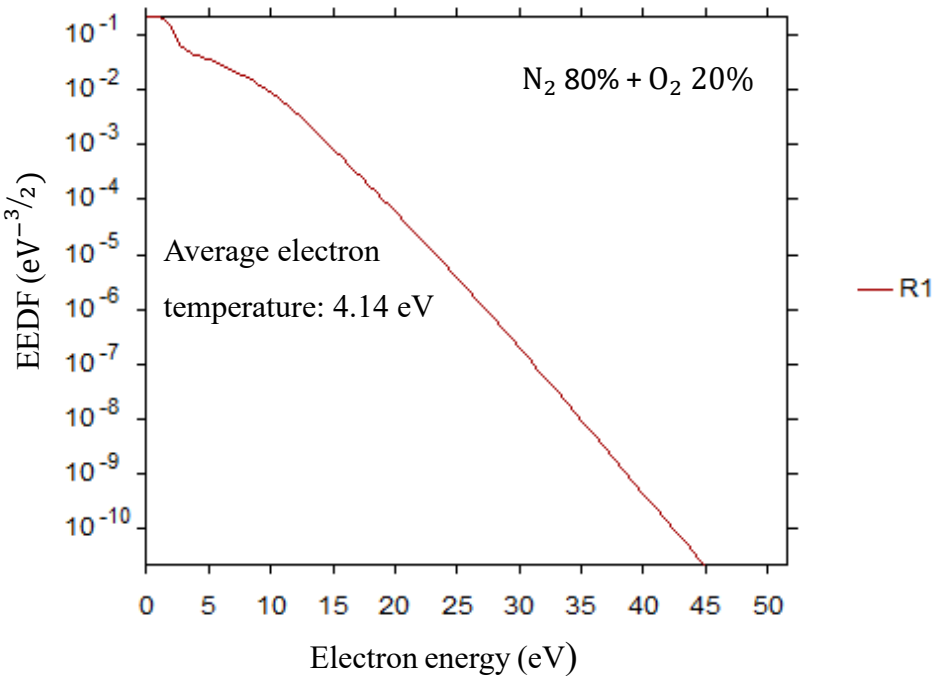

Appendix A-6.3：EEDF as a function of electron energy/eV in dry air.

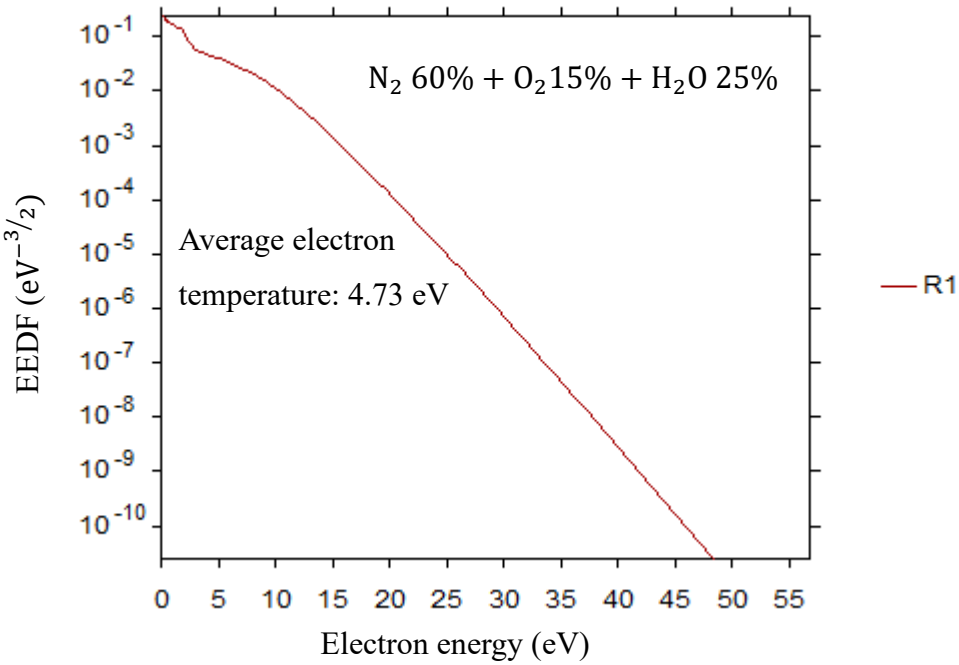

Appendix A-6.4: EEDF of N_2 60% + $O_2$15% + H_2O 25%.

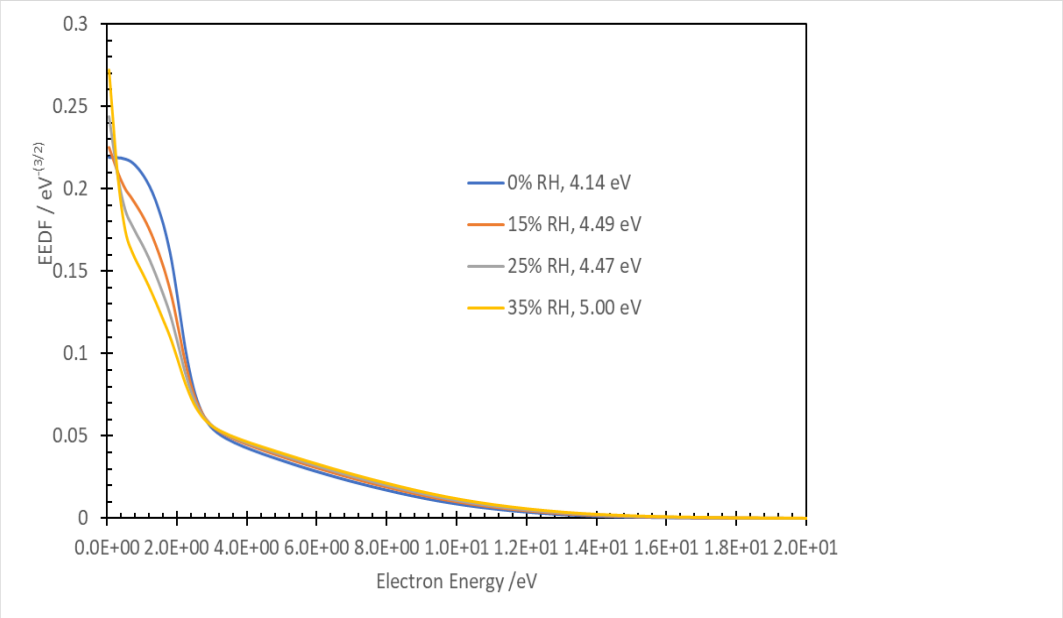

Appendix A-6.5: EEDF as a function of electron energy/eV.

Appendix A-6.6 Carbon balance of hexane, cyclohexane, and benzene decomposition.

A. Hexane decomposition carbon balance (Reaction conditions: temperature = ambient; Inlet concentration of hexane = 350 ppm; Total flow rate = 100 ml/min; Residence time = 2.3 s; Plasma power = 10 W, SIE = 6 kJ/L).

Carrier gas	**Nitrogen**		**Dry air**		**Humid air**	
Compounds	Inlet (mol%)	Outlet (mol%)	Inlet (mol%)	Outlet (mol%)	Inlet (mol%)	Outlet (mol%)
Hexane	100	24.4	100	15.1	100	5.60
CO_2	0.00	0.00	0.00	40.7	0.00	84.6
CO	0.00	0.00	0.00	2.20	0.00	4.79
C_1-C_5	0.00	38.9	0.00	5.77	0.00	2.68
Solid/viscous residue	0.00	36.7	0.00	36.2	0.00	0.00
Missing Carbon	0.00	0.00	0.00	0.03	0.00	2.33
Total	100	100	100	100	100	100

B. Cyclohexane decomposition carbon balance (comparative study section: Reaction conditions: temperature = ambient; Inlet concentration of hexane = 350 ppm; Total flow rate = 100 ml/min; Residence time = 2.3 s; Plasma power = 10 W, SIE = 6 kJ/L).

Carrier gas	**Nitrogen**		**Dry air**		**Humid air**	
Compounds	Inlet (mol%)	Outlet (mol%)	Inlet (mol%)	Outlet (mol%)	Inlet (mol%)	Outlet (mol%)
Hexane	100	35.2	100	21.2	100	11.0
CO_2	0.00	0.00	0.00	16.2	0.00	74.8
CO	0.00	0.00	0.00	21.2	0.00	3.89
C_1-C_4	0.00	31.9	0.00	3.71	0.00	1.23
Solid/viscous residue	0.00	32.8	0.00	36.1	0.00	9.01
Missing Carbon	0.00	0.1	0.00	1.59	0.00	0.07
Total	100	100	100	100	100	100

C. Benzene decomposition carbon balance (Reaction conditions: Temperature = ambient; Concentration = 350 ppm; Total flow rate = 100 ml/min; Residence time = 2.3 s, Relative humidity = 25% at 20℃, Plasma power = 10 W, SIE = 6 kJ/L).

Carrier gas	**Dry air**		**Humid air**	
Compounds	Inlet (mol%)	Outlet (mol%)	Inlet (mol%)	Outlet (mol%)
Benzene	100	43.1	100	22.1
CO_2	0.00	10.7	0.00	51.2
CO	0.00	6.56	0.00	3.07
C_1-C_5	0.00	2.32	0.00	1.00
Solid/viscous residue	0.00	37.2	0.00	22.5
Missing Carbon	0.00	0.12	0.00	0.13
Total	100	100	100	100

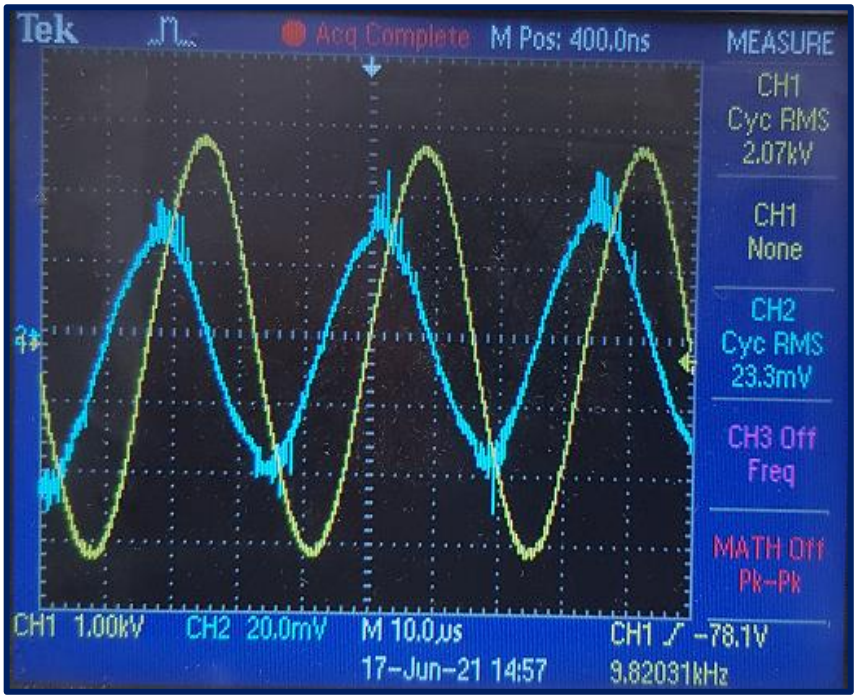

Appendix A-6.7: Typical voltage/current waveform at the plasma power of 10 W in dry air.

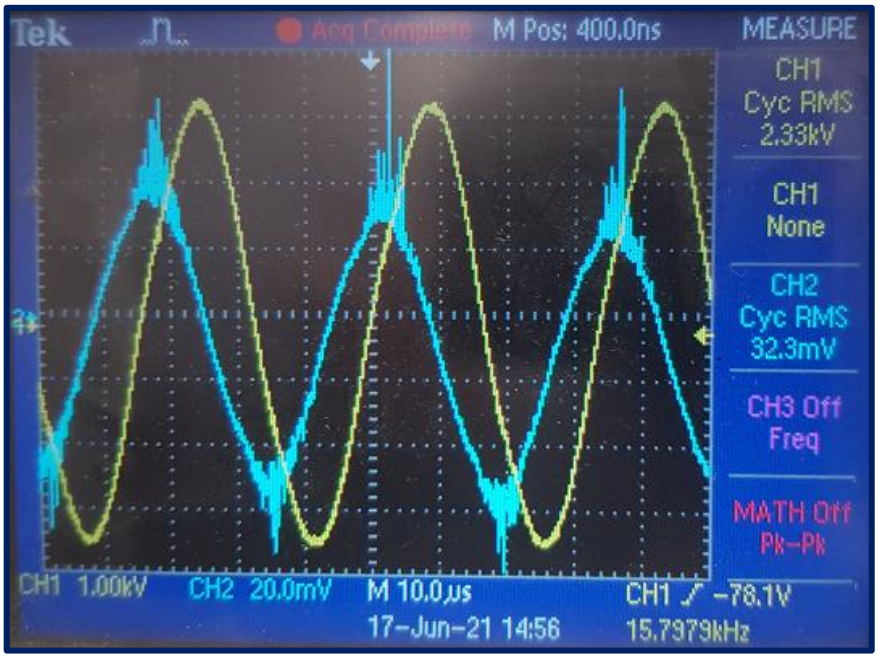

Appendix A-6.8: Typical voltage/current waveform at the plasma power of 10 W humidified air.

Appendix A-7.1 Carbon balance of methanol decomposition.

Methanol decomposition carbon balance ((Reaction conditions: Temperature = ambient; Concentration = 260 ppm; Total flow rate = 70 ml/min; Residence time = 3.3 s, Plasma power = 10 W, SIE = 8.6 kJ/L, Relative humidity = 24%).

Carrier gas	**Nitrogen**		**Dry air**		**Humid air**	
Compounds	Inlet (mol%)	Outlet (mol%)	Inlet (mol%)	Outlet (mol%)	Inlet (mol%)	Outlet (mol%)
Methanol	100	28.7	100	3.3	100	22.3
CO_2	0.00	15.7	0.00	27.9	0.00	33.5
CO	0.00	9.15	0.00	43.3	0.00	15.5
C_2-C_5	0.00	16.5	0.00	9.24	0.00	5.65
CH_4	0.00	15.7	0.00	12.5	0.00	17.9
Oxygenates	0.00	6.78	0.00	3.60	0.00	4.80
Missing Carbon	0.00	7.35	0.00	0.16	0.00	0.35
Total	100	100	100	100	100	100

Appendix A-8 The standard error calculated for ozone measurement

A table showing the accuracy of each ozone measurement has been provided in Appendix A-8. Example of error measurement for ozone has been presented.

The standard error gives the accuracy of a sample mean by measuring the sample-to-sample variability of the sample means. The Standard error of the mean (SEM) describes how precise the mean of the sample is as an estimate of the true mean of the population.

SEM is calculated simply by taking the standard deviation and dividing it by the square root of the sample size, as shown in the Equation below.

$$\mathrm{SEM} = \sqrt{\frac{\sum_i^N (x_i - \overline{x})^2}{N(N-1)}}$$

where:

- xi is the ith measure;
- $\bar{x}$ (x-bar) stands for the mean value of our dataset; and
- N is the number of data points.

The standard error was determined using the following steps:

1. The mean value ($\bar{x}$) was evaluated. It's usually the arithmetic average.

2. The differences $\bar{x}i-x$ for every point were determined.
3. Square the differences for each point separately, $(xi-\bar{x})^2$.
4. All of the squared differences $\sum(xi-\bar{x})^2$ were added up.
5. Divide the sum by the product $N(N-1)$.
6. Finally, the square root of this ratio was worked out.

The standard error gives the accuracy of a sample mean by measuring the sample-to-sample variability of the sample means.

The standard error calculated for ozone measurement

Plasma power (W)	**Ozone 1 (ppm)**	**Ozone 2 (ppm)**	**SEM**
2	2.88	2.94	0.021213
4	4.344	4.416	0.025456
6	4.812	4.968	0.055154
8	5.76	5.808	0.023037
10	6.804	7.032	0.08061